Postnatal Development and Functional Connectivity of the Subiculum

Fabio Ribeiro Rodrigues

Thesis submitted to University College London in consideration for the Degree of Doctor of Philosophy Neuroscience

Declaration

I, Fabio Ribeiro Rodrigues, confirm that the work presented in this thesis is my own. Where information has been derived from other sources, I confirm that this has been indicated in the thesis.

Acknowledgements

First of all, I have to thank my supervisor, Francesca Cacucci, for her guidance, support, and for fueling my interest and passion in neuroscience. I have become a better scientist by learning from her over the past 4 years.

I would also like to thank the Wellcome Trust for funding my PhD, particularly Prof David Attwell, Prof Patricia Salinas, Prof Sarah-Jayne Blakemore, and Prof Alasdair Gibb, for granting me the opportunity of being part of the Neuroscience Programme.

I also want to thank Tom Wills, for his support over the years in data analysis, surgery, data collection, and thesis writing.

The entire Cacucci Lab needs to be thanked, not just for putting up with me, but also for teaching me and helping me whenever I needed. In particular, I would like to thank Joshua for taking the time to teach me about head direction cells and attractors, but also for the general support. Yi and Eleonora, for the words of encouragement, the wisdom parted, and laughs we shared. I especially want to thank Laurenz Muessig. Laurenz was, alongside Francesca (but not officially), my primary supervisor. He taught me how to build drives, do surgeries, run behavioral experiments, cut data, analyze it, the list goes on. Without his coaching and support through the years, I definitely would not have made it this far.

I also would like to thank everyone at the CDN in KCL that brightened up my days in this last year: Rita, Antoine, Alina M, Sînzi, Connor, Hanya, Paola, Tristan, Vicky, Andy, Sara, and Celia. I especially need to thank Alina Letzel, for her wisdom and support which got me through some bad times.

I also need to thank my friends, Renato, Claudia, and Elina for their continued friendship and support, and Misun Kim, for her relentless care and faith in capabilities as a scientist.

I also need to thank my boyfriend Darryl Hayward, for caring for me and helping me find confidence in myself in these last months, couldn't have made it without you.

I especially need thank Dot Overington, whom I had the pleasure to meet 4 years ago when I was starting this adventure. Thank you for the chats, proofreads, post-surgery Wahaca dinners, but most importantly, for helping me overcome my 'inner-saboteur'.

Finally, I would also like to thank my grandmother, my parents and my sisters, for believing in me and reminding me that I was able to do anything that I set my mind to.

Thank you all!

Abstract

The ability to navigate through an environment and build mental representations of the space we visit, is an essential skill for many living creatures. In the hippocampus, space is represented through the activity of different spatial cell types, such as place cells, head-direction cells, and grid cells. In young animals, spatial cell types emerge at different ages: head-direction cells emerge in adult-like form at postnatal day (P) 16, but can be recorded before this age; grid cells emerge abruptly at P21; and place cells can first be recorded at age P16, but they gradually improve their firing characteristics. An also important spatial cell type, but often not talked about, are boundary encoding neurons in subiculum. Their physiology in the adult is well understood, but not much is known about their early postnatal features and how boundary information affects the firing of other spatial cell types.

The work in this thesis aims to understand the postnatal development of subicular Boundary-Vector Cells (BVCs) as well as their functional relationship with entorhinal grid cells. The work here presented demonstrates that BVCs can be recorded from as early as P16, and like place cells, this spatial cell type gradually improves its firing characteristics until the animal reaches adulthood.

Impact Statement

The work featured in this thesis has deepened our understanding of the postnatal maturation of neuronal networks involved in spatial navigation. Through the comparison current and new methods for spatial cell selection, we demonstrate that boundary-coding neurons in the Subiculum can be recorded in rats as early as postnatal day 16. The novel selection method described in this thesis may be of benefit in future research into boundary-tuned neurons within the hippocampal formation. Furthermore, the results outlined in Chapter 5 of this thesis hint at the existence of two types of boundary-tuned neurons, one found in Subiculum and one in the Medial Entorhinal Cortex. This set of results will result in a publication in a scientific journal.

Table of Contents

Acknowledgements **3**

Abstract **4**

Impact Statement **5**

Table of Figures **9**

Table of Tables **12**

Abbreviations **13**

Chapter 1 The Spatial Cognitive Map **15**

1.1 Tolman and the Cognitive Map **15**

1.1.1 – Looking for the Cognitive Map 16

1.1.2 – Beyond Place Cells 17

1.2 Anatomy of a Cognitive Map **19**

1.2.1 – The Hippocampal Formation 21

1.2.2 – The Parahippocampal Region 35

1.2.3 – Embryonic development and postnatal maturation of hippocampal fields 43

Chapter 2 Physiology of the Spatial Cognitive Map **46**

2.1 Electrophysiology at the population level **46**

2.2 Single-Unit Activity **47**

2.2.1 – Spatially Modulated Neurons – Place Cells 48

2.2.2 – Spatially Modulated Neurons – Head-Direction Cells 51

2.2.3 – Spatially Modulated Neurons – Boundary Vector Cells 54

2.2.4 – Spatially Modulated Neurons – Grid Cells 57

2.2.5 – Other spatial cell types without spatial correlates 60

Chapter 3 General aspects of rodent postnatal development **61**

3.1 General behavior and locomotion **61**

3.2 Olfaction. **64**

3.3 Somatosensation **64**

3.4 Auditory perception **64**

3.5 Vision **64**

3.6 Vestibular functions **65**

3.7 Hippocampal Associated Spatial Behaviors **65**

3.7.1 – Exploratory Behavior 65

3.7.2 – Path Integration 66

3.7.3 – Maze Solving 66

Preamble Summary and Thesis Goals 68

Chapter 4 General Methodology 69

4.1 Animal Husbandry 69

4.2 Microdrive Preparation 70

4.3 Surgeries 71

4.3.1 – Rat pup surgeries 71

4.3.2 – Adult Rat Surgeries 72

4.4 Data Collection 73

4.4.1 – General aspects of recording environments 73

4.4.1 – Acquisition of electrical signals and positional information 73

4.4.2 – Cell screening procedures 74

4.5 Data Analysis 75

4.5.1 – Spike cluster separation 75

4.5.2 – Rate maps 75

4.5.3 – Spike shuffling procedure to determine cell inclusion criteria 78

4.5.4 – Individual cell properties 79

4.6 Histology and Imaging 81

4.6.1 – Fixation of brain tissue 81

4.6.2 – Slicing 81

4.6.3 – Nissl Staining for implant tracking 82

4.6.4 – Immunohistochemistry 82

4.6.5 – Imaging 83

4.7 Statistical Tests 83

Chapter 5 The development of Subicular Boundary Representation 85

5.1 Brief Introduction 85

5.1.1 – Goals of the Experiment 86

5.2 General Methodology and Analysis 86

5.2.1 – Behavioral Paradigm 86

5.3 Data Analysis 88

5.3.1 – Detecting BVCs 89

5.3.2 – Analyzed features 96

5.3.3 – Statistical tests 97

5.4 Histology 97

5.5 – Performance of the BVC Selection Methods 101

5.5.1 – Putative BVCs according to the Border Score method 101
5.5.2 – Putative BVCs according to the Response Model method 104
5.5.3 – The preferred distance, but not angular tuning of selected cells varies between detection methods 108
5.5.4 – Both selection methods detect high numbers of the same cells in the adult dataset 110
5.6 BVCs develop gradually, like their place cell 'neighbors' 111
5.6.1 – The percentage of recorded BVCs increases with age 111
5.6.2 – The peak firing rate of BVCs increases throughout postnatal development 116
5.6.4 – Stability of BVC firing fields also increases with age 117
5.6.5 – Barrier-triggered changes in firing rate 119
5.6.6 – Subicular cells selected with the BS method also show protracted maturation 121
5.7 Chapter Discussion 123
5.7.1 – Boundary coding in the MEC of young rats 123
5.7.2 – Postnatal maturation of boundary coding in the Sub appears to mirror that of hippocampal place cells 124
5.7.3 – Comparing entorhinal and subicular boundary coding 125
Chapter 6 General Discussion 127
6.1 Subicular BVCs can be recorded from P16 onwards and gradually attain adult-like firing characteristics 127
6.1.1 – Border Score vs Response Model Score 128
6.1.2 – Spatial cells within the HF obtain adult-like firing characteristics throughout a protracted period 129
6.2 – Fitting BVCs in the spatial cognitive map 131
6.3 – Boundaries and navigation 132
References 134

Table of Figures

Figure 1.1 – The Tolman Sunburst Maze environments. 15
Figure 1.2 – Spatially tuned cells recorded in the hippocampus and associated hippocampal areas. 18
Figure 1.3 – Location and axes of the rat HF and PHR in the brain. 22
Figure 1.4 – Layer organization of the HF and PHR..... **Error! Bookmark not defined.**
Figure 1.5 – Location of the rhinal cortices in the rat brain. 37
Figure 1.6 – Summary of connectivity of the different rhinal cortices. 42
Figure 2.1 – Example of a place cell of the dorsal CA1. 48
Figure 2.2 – Example of a HDC recorded in the ADN. 52
Figure 2.3 – Effect of boundary extension on place cell firing and the boundary-vector model. 54
Figure 2.4 – Examples of boundary coding neurons. 55
Figure 2.5 – Example of a MEC grid cell. 57
Figure 3.1 – Summary of postnatal developmental milestones of sensory and motor systems, spatial and hippocampus-dependent behaviors, as well as the emergence of spatially tuned neurons. 63
Figure 4.1 – Schematic of tetrode carrying microdrives and photographs of adult ‘poor-lady’ and pup ‘omnetic’ microdrives. 70
Figure 4.2 – Average path length and coverage of the testing arena across the tested ages. 77
Figure 4.3 – Example of a spike shuffling procedure. The 78
Figure 5.1 – Cell Screening Paradigm for BVC detection. 87
Figure 5.2 – Age-specific cell distribution and respective 95th percentile ranks of the BS (and spatial information) of shuffled rate maps. 91
Figure 5.3 – Examples of model maps oriented towards the East wall with varying preferred tuning distances. 93
Figure 5.4 – Example of how the Response Model Score works. 94
Figure 5.5 – Age-specific cell distribution and respective 99th percentile ranks of the maximum RM scores of shuffled rate maps. 95
Figure 5.6– Example of region definition for barrier-related firing analysis. 96
Figure 5.7 – Histological images of the recorded rat pup brains. 98
Figure 5.8 – Histological images of the recorded rat pup brains II. 99
Figure 5.9 – Histological images of the recorded rat pup and adult rat brains. 100

Figure 5.10 – Percentages of selected BVCs using the 95th percentile rank of the BS and spatial information of age matched population shuffled rate maps as a threshold. 101
Figure 5.11 – Examples of neurons selected with the Border Score method in the P16-P18 age group. 102
Figure 5.12 – Examples of neurons selected with the Border Score method in the P19-P21 age group. 103
Figure 5.13 – Examples of neurons selected with the Border Score method in the P22-P25 age group. 103
Figure 5.14 – Examples of neurons selected with the Border Score method in adult rats. 104
Figure 5.15 – Percentages of selected BVCs using the 99.7th percentile rank of the BVC Model Score of age matched population shuffled rate maps as a threshold. 105
Figure 5.16 – Examples of neurons selected with the Response Model method in the P16-P18 age group. 106
Figure 5.17 – Examples of neurons selected with the Response Model method in the P19-P21 age group. 106
Figure 5.18 – Examples of neurons selected with the Response Model method in the P22-P25 age group. 107
Figure 5.19 – Examples of neurons selected with the Response Model method in the Adult age group. 107
Figure 5.20 – Tuning distance distributions of boundary-coding cells selected by the BS or RM methods across age groups. 108
Figure 5.21 – Tuning angle distributions of boundary-coding cells selected by the BS or RM methods across age groups. 109
Figure 5.22 – Percentage of cells selected using the BS method, RM method, or both and examples. 110
Figure 5.23 – Rate maps of putative BVCs in the P16-P18 age group. 112
Figure 5.24 – Rate maps of putative BVCs in P19-P21 age group. 113
Figure 5.25 – Rate maps of putative BVCs in P22-P25 age group. 114
Figure 5.26 – Rate maps of putative BVCs in the Adult dataset. 115
Figure 5.27 – Mean and peak firing rates for selected BVCs across the different age groups. 116
Figure 5.28 – Spatial information of selected BVCs across development. 117
Figure 5.29 – Stability of BVC within and between baseline trials throughout development. 118

Figure 5.30 – Firing rate in barrier-defined proximal and distal regions across baseline and barrier trials per age group. 119
Figure 5.31 – Subicular cells selected with the BS method also show protracted maturation of their spatial tuning, firing, and stability. 121

Table of Tables

Table 5.1 – Breakdown table of cells excluded from further analyses. 88
Table 5.2 – Number of cells that pass the cell-matched percentile for BS, SI, and Both, with examples. 90
Table 5.3 – Table of means and standard deviations for the mean firing rate per age group. 116
Table 5.4 – Table of means and standard deviations for the stability of BVCs both within and across trials across the different age groups. 118
Table 5.5 – Table of means and standard deviations for the firing rate of BVCs in the distal region across the different age groups and trials. 120
Table 5.6 – Table of means and standard deviations for the firing rate of BVCs in the distal region across the different age groups and trials. 120

Abbreviations

AAV – Adeno-Associated Virus

AB – Anti-Body

ADN – Anterodorsal Nucleus

AP – Anterior-Posterior

BS – Border Score

BVC – Boundary Vector Cell

CA – Cornu Ammonis

CaMKIIa – Ca2+/calmodulin-dependent protein kinase II a

cAMP – Cyclic Adenosine Monophosphate

CCE – Cue-Controlled Environment

CNO – Clozapine-N-Oxide

CR – Cajal-Retzius

DAPI – 4',6-diamidino-2-phenylindole

DG – Dentate Gyrus

DREADD – Designer Receptor Exclusively Activated by Designer Drug

DV – Dorso-Ventral

E – Embryonic Day

EC – Entorhinal Cortex

EEG – Electroencephalogram

ERK – Extracellular signal-Regulated Kinase

GABA – γ-Aminobutyric Acid

GAD – Glutamic Acid Decarboxylase

GC – Grid Cell

GFP – Green Fluorescent Protein

GIRK – G-protein Inwardly Rectifying Potassium Channel

h – Hour

HD – Head-Direction

HDC – Head Direction Cell

HICAP – Hilar Commisural-Associational Pathway-related (cell)

HIPP - Hilar Perforant Path-associated (cell)

hM4DGi – Gi-coupled human M4 DREADD

IP – Intraperitoneal

L – Layer

LEC – Lateral Entorhinal Cortex

LED - Light-Emitting Diode

LFP – Local Field Potential

LIA – Large Irregular Amplitude (activity)

MAPK – Mitogen-Activated Protein Kinase

MEC – Medial Entorhinal Cortex

min – Minutes

ML – Medio-Lateral

MOPP – Molecular Layer Perforant Path-associated (cell)

NS – North-South

OCT – Optimum Cutting Temperature compound

O-LM – Oriens Lacunosum-Moleculare Associated (cell)

P – Postnatal Day

PaS – Parasubiculum

PBS – Phosphate-Buffered Saline

PER – Perirhinal Cortex

PHR – Parahippocampal Region

POR – Postrhinal Cortex

PP – Perforant Path

PrS – Presubiculum

RM – Response Model

RV – Rayleigh Vector

SEM – Standard Error of the Mean

SIA – Small Irregular Amplitude (activity)

SPW – Sharp Wave

Sub – Subiculum

V1 – Primary Visual Cortex

VIP – Vasoactive Intestinal Peptide

WE – West-East

Chapter 1 The Spatial Cognitive Map

'*What I am going to say must be considered, therefore, simply as* … rat*iocinations offered free*.' (Tolman, 1948, p.207)

Knowing where one is and where one needs to go is an essential instinct that allows animals to survive. From ants to bees, fish to birds, rats to elephants, navigation is essential. Understanding its neural basis constitutes a significant challenge for Neuroscientific research, which can allow a better understanding of how complex brain structures can give rise to complex behaviors. Moreover, given the universality of this animal behavior, understanding its mechanisms can help us better understand the evolution of neuronal circuits underlying it.

1.1 Tolman and the Cognitive Map

Whatever task an animal undertakes – foraging, migrating, or escaping a predator –, its brain passively gathers information about the animal's environment, allowing it to create an internal representation of its whereabouts. This idea was first posited in 1946 by Tolman and colleagues, through an experiment that demonstrated that, when it comes to spatial navigation, an animal does not just create 'stimulus-response' associations (Tolman et al., 1946a). This classic experiment was performed in an elevated maze, the 'Sunburst Maze' (Tolman et al., 1946b). Rats were trained to run from a starting platform along a single path to a goal location and, on the way, cross a circular walled enclosure (Figure 1.1A). On test days, the rats would have to choose from several paths radiating

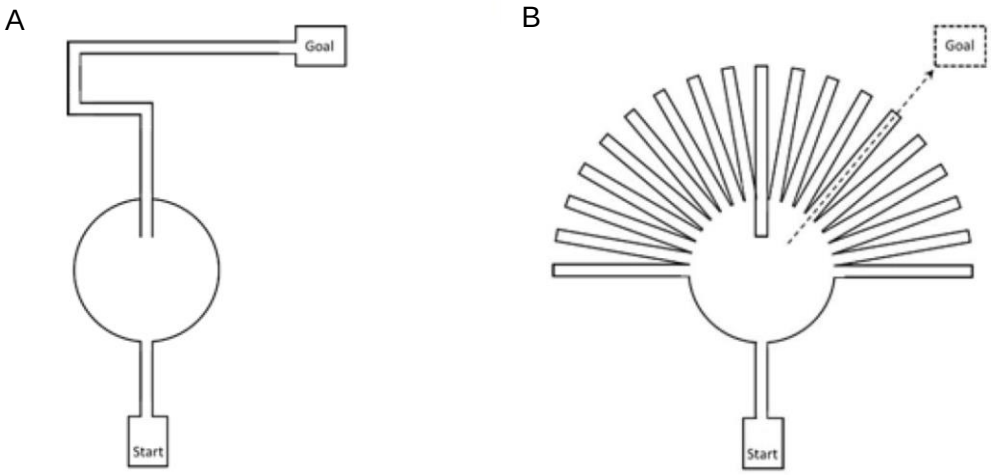

Figure 1.1 – The Tolman Sunburst Maze environments. The animals were first trained to enter the circular arena and then follow a linear track into the goal location (A). After the training sessions, the animals were then presented with several paths radiating from the circular arena (B) and had to choose one of the paths that would lead them straight to the goal location (indicated with the arrow). The animals most tended to choose paths that lied in the direction of the goal location. Figure was adapted from(Overington, 2017)

from the circular enclosure the one that led them to the same goal location (Figure 1.1B). When exposed to this environment, the majority of rats chose the path that lied in the direction of the goal platform. Tolman thus concluded that navigation is not composed of strict strategies, as expected by simple stimulus-association responses. The results obtained indicated the presence of an internal representation of the environment the rats were trained on, which allowed them to opt for the shortest path to the goal, even if this had never been experienced during training (Tolman et al., 1946b).

Tolman's whole body of work supports the idea of the existence of a neuronal network that supports internal representations of our surroundings. By training rats in an environment consisting of 14 interconnected T Mazes without using a reward, *i.e.*, the animals were just allowed to explore the environment without any specific (shaped) response, Tolman showed that once a reward was introduced in particular locations, trained rats took less time to get to the goal than non-trained ones. Therefore, the 'passive exploration' of an environment accounts for shorter latencies in place learning tasks in trained rats compared to naïve controls (Tolman and Honzik, 1930). With this in mind, Tolman suggested that incoming sensory input from the exploration of a given environment is 'usually worked over and elaborated in the central control room into a tentative, cognitive-like map of the environment … indicating routes and paths and environmental relationships, which finally determines what responses, if any, the animal will finally release' (Tolman, 1948). The search for this spatial cognitive map and its central control room became the focus of scientific research that lasts until this day.

1.1.1 – Looking for the Cognitive Map

The study and description of strange and medical cases has been fundamental in proving or disproving scientific and philosophical theories about the self and the brain – like Phineas Gage, whose left frontal lobe was damaged by a blasting powder propelled tamping iron, thus resulting in abrupt personality changes and opened a debate on cerebral localization of personality aspects (Damásio, 1994). Another famous case is that of Henry Molaison, also known as Patient H.M. H.M., an epileptic from young age, underwent bilateral medial temporal lobe aspiration in 1953, a procedure performed by Dr William Beecher Scoville in an attempt to reduce HM's epileptic episodes (Scoville and Milner, 1957). The procedure resulted in the removal of medial temporal brain regions, namely the hippocampal formation, amygdala and entorhinal cortex (Corkin et al., 1997). As a result, HM's epilepsy symptoms ceased almost entirely, but instead he lost the ability to form new memories (anterograde amnesia) as well as a temporally graded memory loss of events prior to the surgery (retrograde amnesia) (Scoville and Milner, 1957). Brenda Milner's description and testing of HM and other patients that had

medial temporal lobe lesions, allowed her to pinpoint the hippocampus as a key player in memory formation and storage (Milner and Penfield, 1955, Scoville and Milner, 1957).

The existence of a cognitive map, and its relationship with the hippocampus became more evident with the seminal work of John O'Keefe and Jonathan Dostrovsky in 1971. Through *in vivo* electrophysiology, activity of single neurons in the hippocampus was recorded, and the authors described the presence of cells with directional and locational preferences. These cells' firing would cease with sufficient changes in the environment, which was accompanied by increasing exploratory behaviors like rearing (O'Keefe and Dostrovsky, 1971). The suppression of place learning by fornix lesions (a major afferent/efferent pathway of the hippocampus) (O'Keefe et al., 1975) and, more importantly, the first comprehensive description of place specific units (Figure 1.2A) also in the *Cornu Ammonis* (CA) 1 region of the hippocampus (O'Keefe, 1976) further reinforced the authors' hypothesis of the hippocampus being the 'control room' for spatial cognition and the putative location of the spatial cognitive map. The discovery of 'place cells' in the hippocampus, together with the review of behavioral deficits displayed by animals and humans whose hippocampi had sustained lesions, led O'Keefe and Nadel to posit that the hippocampus is the neural substrate of the Spatial Cognitive Map (O'Keefe and Nadel, 1978).

1.1.2 – Beyond Place Cells

Further work on the place cell system demonstrated that these cells create a higher-order representation of space based on a variety of sensory stimuli. When these stimuli are stable, so is the map. Manipulations of the environment – olfactory, visual, or tactile – lead to changes in the place cell activity pattern, resulting in the same physical space being represented by different ensembles of CA1 cells (O'Keefe and Conway, 1978, Save et al., 2000, Bostock et al., 1991). Attesting to the universality of the cognitive map, besides rodents, place cells have also been described in pigeons (Bingman et al., 2006), bats (Ulanovsky and Moss, 2007, Yartsev and Ulanovsky, 2013), and humans (Ekstrom et al., 2003). Since then, other spatially tuned neurons have been found in other brain structures: animal orientation related neurons known as head direction cells (HDCs, Figure 1.2B) (Ranck Jr, 1984, Taube et al., 1990a, Taube et al., 1990b); neurons which fire multiple, discrete, and equidistant areas in the environment, resulting in a tessellating structure of equilateral triangles, known as grid cells (GCs, Figure 1.2C) (Fyhn et al., 2004); and neurons which respond maximally to borders or boundaries in an environment (Figure 1.2D), known as border neurons (Solstad et al., 2008) or boundary vector cells (BVCs) (Lever et al., 2009). All these cells are anchored to external

cues in the environment, and thus code for position and/or direction based on relative location of the animal from those cues and not based on the animal's self-position – and are thus allocentric in opposition to egocentric. Together, these spatially tuned neurons are thought to be the substrate with which the brain can represent positional, directional, odometrical and boundary information, respectively.

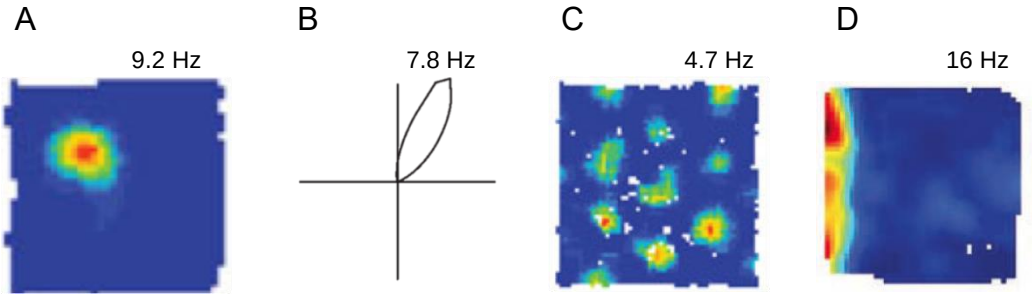

Figure 1.2 – Spatially tuned cells recorded in the hippocampus and associated hippocampal areas. (A) Place cell recorded from dorsal CA1 of the rat hippocampus. The plot shows the location where the cell was most active by color-coding the cell's firing rate (number of action potentials by dwell time). Thus the peak firing rate (located in the top right corner), corresponds to the red color, while blue colors represent lower firing rates. These cells have well-defined receptive fields which correspond to locations in the environment where the cells fire maximally. (B) Head-direction cell recorded from the entorhinal cortex. The polar plot represents the cell's firing rate by animals' heading direction, i.e. the animal orientation to which the cell responded maximally to. These cells fire maximally whenever the animal's heading direction is aligned with the cell's directional tuning preference. (C) Firing rate map of a GC. An individual GC has multiple firing peaks that create a triangular lattice with each field at approximately the same distance and angle from another field, thus creating a grid-like pattern. These cells are thought to combine positional, directional and odometrical input to create a metric of space. The rate maps in A to C are all taken from Wills et al. (2014). (D) Firing rate map of an entorhinal border cell. These cells code for the presence of boundaries that are in a specific allocentric direction. Examples taken from (Solstad et al., 2008).

More recent studies have also looked at the post-natal maturation of neurons in the hippocampal formation and associated brain regions through *in vivo* electrophysiological recordings (Langston et al., 2010, Wills et al., 2010). Recordings from young animals (from 2 to 4 weeks of age) have shown that place cells are present and functioning, but their stability and precision keeps maturing through juvenility (Langston et al., 2010, Wills et al., 2010). HDCs can also be recorded from a young age, with adult-like stability (Wills et al., 2010), especially after eye opening (around post-natal age, P15), when HDCs become stable and coherent (Tan et al., 2015, Bjerknes et al., 2015). GCs on the other hand, are not detectable until 3 weeks of age (P20-P21) and mature to adult-like levels throughout the 4th postnatal week (Wills et al., 2010, Bjerknes et al., 2014). Moreover, boundary representation by border neurons is also detectable from P17 onwards in the medial entorhinal cortex (MEC) (Bjerknes et al., 2014). From the postnatal standpoint, not much is known about the subiculum and its BVCs.

Understanding the functional relationship between the elements of the cognitive map is also of paramount importance. With this in mind, several researchers have looked at the functional connectivity and hierarchic influences of these spatial-cells. For instance, HDC

activity is necessary for grid cell firing, as shown by the inactivation of the anterodorsal nucleus of the thalamus (a component of the HDC circuit) with lidocaine, which significantly disrupts grid cell firing in the MEC (Winter et al., 2015). The absence of HDC input is not necessary to drive place cell firing, but lesions to areas that convey the HDC signal may cause spatial firing instability (Calton et al., 2003). Additionally, reversible inactivations of CA1 and, consequently, of place cell firing, lead to the disruption of grid cell firing (Bonnevie et al., 2013). Not much is known about how BVCs affect place or grid cell firing.

The work presented in this thesis aims to fill in the gaps pointed out previously, namely with regards to BVCs. Therefore, the experiments in Chapter 5 aim to answer when BVCs in Subiculum (Sub) are first detected and how their postnatal maturation proceeds. Chapters 6 and 7 detail the experiments performed to understand the functional aspects of the Sub to MEC projections, as well as the potential relationship between BVCs and GCs.

Before delving into these questions, the following section will detail some aspects of the anatomy of the cognitive map as well as the neural mechanisms that underlie spatial navigation.

1.2 Anatomy of a Cognitive Map

Having established that the hippocampus is necessary in both memory formation/storage and spatial navigation, the neural bases of the spatial cognitive map had been discovered. However, as Yadin Dudai wrote on the potential role of the hippocampus in memory, hippocampal neuronal ensembles may act ‘as an index for neocortical neurons that attend the information, and binds them into a coherent representation’ (Dudai, 2012). The same can be true for spatial navigation, meaning that, even though the hippocampal formation is the core of the spatial cognitive map, the output of this brain region to other associated areas may be necessary for accurate and flexible spatial representations (O'Keefe and Nadel, 1978). In fact, data from patients with hippocampal lesions demonstrate that although the hippocampus is not vital for day-to-day navigation, it is required to create malleable and accessible representations of the external world (Corkin et al., 1997, Corkin, 2002, Corkin, 2013, Maguire et al., 2006). Thus, understanding the form and connectivity of the hippocampus and associated hippocampal areas is vital to understand how the cognitive map functions.

Hippocampal neuroanatomy has been a subject of interest for over a century. Thanks to the pioneering silver staining techniques, Camillo Golgi initiated the description of this structure to understand the relationship between fibers and neuron aggregates. This was

indeed possible due to the well-defined cell layer structures present in this brain region (Golgi, 1885, Golgi et al., 2001). Following on the footsteps of Golgi, Santiago Ramón y Cajal made the famous drawings of the hippocampal formation, minutely describing the cells and afferents to and from each layer (Ramón y Cajal, 1893). With this work, Ramón y Cajal foresaw not just the vast influence of this structure throughout the brain due to its connectivity, but based on the dynamic polarization principle – action potentials in a neuron flow from dendrites to axons – proposed a direction for the flow of information within this brain area (Andersen et al., 2007). Another great hippocampal anatomist worth mentioning is Rafael Lorente de Nó. Lorente de Nó extended the analysis of the many hippocampal neurons, described interconnections between them and, on the basis of their dendritic tree and connections, divided the hippocampus into defined sub-regions, from CA4 to CA1 (Lorente De Nó, 1934, Andersen et al., 2007). Some contemporary hippocampal neuroanatomists include Larry Swanson and Menno Witter, whose work has heavily influenced modern hippocampal research.

Before continuing with the anatomical description of these brain structures, a few aspects need to be considered. Regarding nomenclature, and focusing particularly on the rodent brain, the work here presented follows the logic used by Lavenex and Amaral in 'The Hippocampus Book' (Chapter 3, Andersen et al. (2007)) and Cappaert, van Strien and Witter in 'The Rat Nervous System' (Chapter 20, Cappaert et al. (2015)). Therefore:

- The hippocampal formation (HF) is a C-shaped structure comprised by adjoining regions: the dentate gyrus (DG), the hippocampus proper (composed by the CA fields CA3, CA2 and CA1), and subiculum (Sub).
- The parahippocampal region (PHR) constitutes the cortical mantle areas that border the caudal and ventral HF. This includes the presubiculum (PrS), parasubiculum (PaS), entorhinal cortex (EC), perirhinal cortex (PER), and postrhinal cortex.

The nomenclature used to describe the three-dimensional positioning of both formations in the brain derives from the proximity of the structure with other brain areas. As such, the three axes are:

- For the HF and part of the PHR, the long axis extends from the septal nuclei – starting thus medially in the rostrodorsal portion of the rodent brain –, over the diencephalon, expanding laterally into the caudoventral portion of the hemisphere, where it borders the amygdaloid complex. The long axis is therefore called the 'septotemporal axis'.

- The transverse axis is orthogonal to the septotemporal axis. When describing the location along the transverse axis, the DG is used as a proximal extreme, *i.e.*, a particular region of a hippocampal field can be proximal (closer) or distal (far) to DG. For instance, the CA1 portion that borders CA2 is considered proximal, whereas the one closest to Sub is distal CA1.
- The superficial-to-deep or radial axis runs orthogonally to the layers in each HF or PHR field. Also, due to the inward bending of the HF and part of the PHR (PrS and PaS), this axis is oriented in the opposite direction of the brain's dorso-ventral axis. Therefore, dorsal layers of these inward bending fields are considered deep, while ventrally located layers are, in hippocampal radial axis terms, superficial.

The cortical areas of the PHR, namely the EC, PER and POR are not characterized by the same axes as the remaining fields areas. The EC is described as having dorso-ventral (running from the top of the animal's brain to the bottom side) and medial-lateral (going from the brain's midline to the sides of the head) axes, whereas PER and POR have a rostral-caudal (nose-to-neck) axis. All three cortical areas have a superficial-to-deep axis as well, where layers closest to the pial surface are superficial, and those closer to the ventricle are deep.

1.2.1 – The Hippocampal Formation

All areas belonging to the HF are part of the allocortex (from greek 'other' cortex), and as such, do not display the typical six-layered structure. In fact, all HF subfields are triple layered, containing a deep polymorphic layer, a pyramidal cell layer and a superficial layer containing mostly white matter, called molecular layer (Andersen et al., 2007). The information flow was thought to be unidirectional across the so-called tri/poly-synaptic loop of the hippocampus (Andersen et al., 1971): information arrives at the EC and gets carried into the (1) DG via the perforant pathway, which then projects to (2) CA3 via the mossy fibers, in turn activating (3) CA1 via the Schaffer Collaterals, and out of CA1 via the alveus (Andersen et al., 1971). Further studies showed that input from CA1 arrives in Sub, which then projects back into the EC, closing the hippocampal information loop (Swanson and Cowan, 1975, Andersen et al., 2007). Better tracing and imaging techniques have then demonstrated that sparser back-projections sometimes occur between these subfields (Sun et al., 2014, Finch et al., 1983), but the main flow of information is still the one described.

In terms of the fiber systems associated with the HF, three major ones can be distinguished. Carrying information from the EC into all fields of the HF is the angular bundle, which travels from caudal to rostral levels in the rat brain. Afferent and efferent signals from and to subcortical targets, like the thalamus, hypothalamus, and brain stem, travel along the fimbria-fornix pathway, present on the rostral end of dorsal HF. Lastly, communication between the HF of both hemispheres is achieved through dorsal and ventral hippocampal commissures (Andersen et al., 2007).

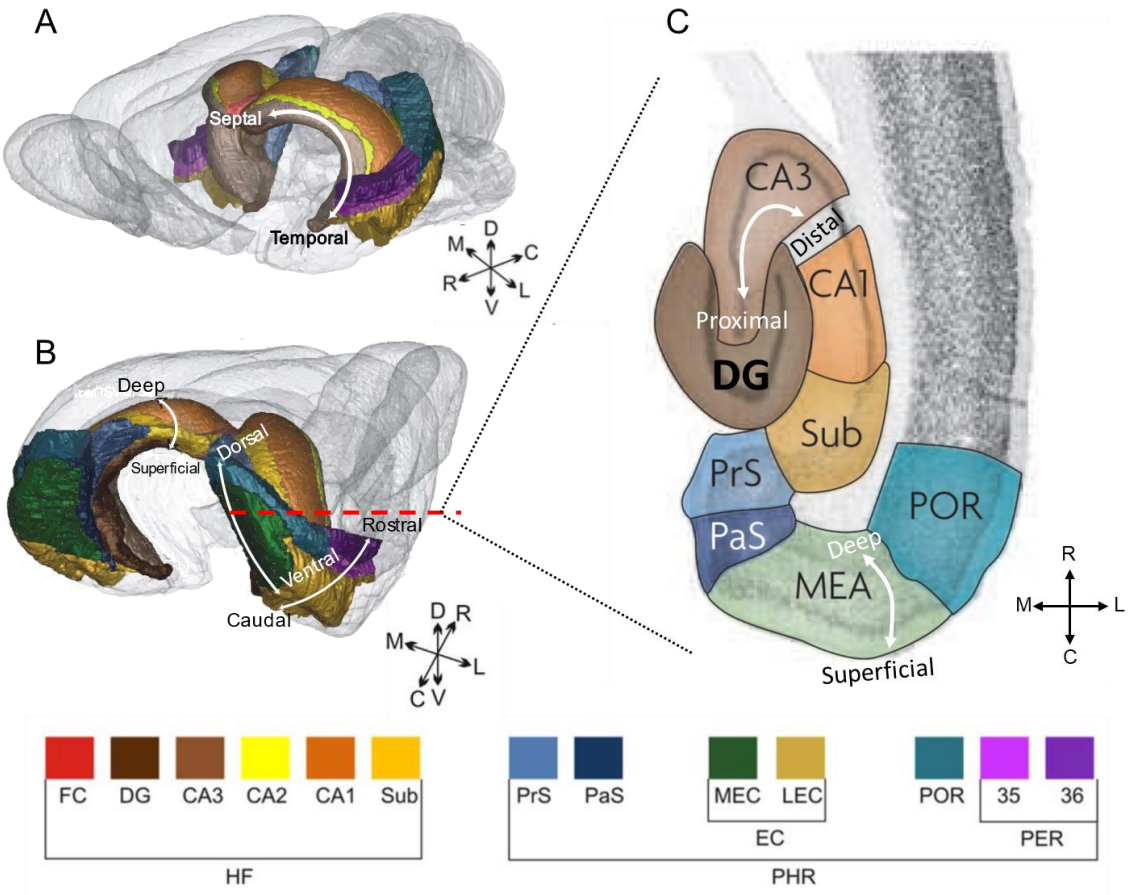

Figure 1.3 – Location and axes of the rat HF and PHR in the brain. This figure shows the rat HF and PHR from different perspectives as well as a horizontal section to illustrate the different axes. All figures have the different brain axes on the bottom right corner (D, dorsal; V, ventral; R, rostral; C, caudal; M, medial; L, lateral. The different areas within both the HF and PHR are color-coded according to the legend in the bottom of the figure. (A) Rostro-lateral view of the rat brain and underlying hippocampus. The long axis of the HF is indicated with the white arrow, and it runs from the septal (dorsal-medial positions) to temporal regions (ventral-lateral brain areas). (B) Caudal-lateral view of the PHR and septal HF. The white arrow on the left HF demonstrates the radial axis of the hippocampus, which runs from deep to superficial layers. On the right hemisphere, the two arrows highlight the dorsal-ventral and caudal-rostral axes of the PHR. The red dashed line represents the section plane of the slice view of (C). (C) Horizontal section of the rat brain showing the different regions within the HF and PHR. Besides highlighting the position of the different areas within the brain, the figure also shows the radial axis on the MEA (equivalent to MEC). Also, the figure exemplifies the HF transverse axis, which is defined as the relative distance to the DG. Regions of the different HF areas closer to the DG are considered proximal, while regions further from it are distal. Images are adapted from van Strien et al. (2009), Cappaert et al. (2015), and Boccara et al. (2015).

1.2.1.1 – Dentate Gyrus

Regarding its layer organization, the most superficial layer in the DG is relatively cell-free, the molecular layer. Deeper to it lies the granule cell layer, the principal cell layer, and it is made up by densely grouped granule cells. These two layers are often called *fascia dentata and* form a 'V' or 'U' shape along the septotemporal axis, enclosing the deepest layer of the DG, the hilus (see Figure 1.4). Lorente De Nó (1934) designated the hilus as CA4. In the standard rat brain atlas nomenclature, this polymorphic layer is labelled as hilus and the reasons are explained below (Andersen et al., 2007, Cappaert et al., 2015).

Molecular Layer. This layer consists mainly of the dendrites of granule cells, basket cells and the several polymorphic cells. Terminal axonal plexuses from several brain regions are present in this area as well. Despite its low abundance, three types of interneurons can be found in this layer. Basket cells are vasoactive intestinal peptide (VIP) positive interneurons located deep in the molecular layer. Typically, basket cells have triangular or multipolar somas, axons with terminals in the granule cell layer, and aspiny dendrites in the molecular layer (Hazlett and Farkas, 1978, Ribak and Seress, 1983, Cappaert et al., 2015). Chandelier cells are axo-axonic cells, meaning that their axons descend from the molecular layer into the granule cell layer, collateralize and terminate on the axon initial segment of granule cells. These parvalbumin positive interneurons have a dendritic tree that spans the width of the molecular layer, suggesting that their main inputs are excitatory perforant path (projections from the EC), and associational/commissural (projections from the contralateral hilus) inputs. Due to their morphology, these cells are thought to control the output of granule cells (Ribak and Shapiro, 2007, Cappaert et al., 2015, Andersen et al., 2007). The other cell type, named molecular layer perforant path-associated cell (MOPP cell), has its triangular or multipolar soma deep in the molecular layer. Both its axon terminal and aspiny dendritic tree remain within the molecular layer (Han et al., 1993, Andersen et al., 2007, Cappaert et al., 2015).

Granule Cell Layer. Granule cells, the principal cells of the DG, have elliptical cell bodies, and a cone-shaped, spiny, dendritic tree that protrudes towards the superficial portion of the molecular layer. Granule cell density varies along the septotemporal axis of the HF, being much higher towards the septal pole (Andersen et al., 2007, Cappaert et al., 2015, Gaarskjaer, 1978). Basket cells also exist along the deeper regions of the granule cell layer, in-between granule cells and the hilus. These parvalbumin positive interneurons have a pyramidal soma and a single aspiny dendrite that ascends to the

molecular layer, where it branches, and several basal dendrites that ramify into the hilus. The axons of these basket cells form complex axonal plexuses around granule cell somas, hence their name (Ribak and Seress, 1983, Andersen et al., 2007, Cappaert et al., 2015). Also deep in the granular cell layer, there are a variety of glutamic acid decarboxylase (GAD) positive neurons of different morphologies (multipolar or fusiform-shaped with several aspiny dendrites in the molecular layer and hilus) (Ribak and Seress, 1983) which are thought to provide additional modulation of granule cell activity (Andersen et al., 2007, Cappaert et al., 2015).

Hilus. It was originally named CA4 by Lorente De Nó, as he thought it to be an extension of the hippocampus. Further characterization of this field revealed that this was not the case. The hillus is thought to contain more than 20 morphologically distinguishable cell types, thus being considered to arise from the merging of the polymorphic zones of both the DG and the hippocampus, but more closely related to the DG (Amaral, 1978). The most common cell type is the so-called mossy cell. These have large triangular or multipolar somas, with three or more dendrites emanating from the cell body and extending into the hilus, with fewer branches extending into the granule cell layer or molecular layer. Mossy cell dendrites contain complex spines also found in CA3, named 'thorny excrescences', which correspond to the termination sites of mossy fiber axons (projections from granule cells). The density of these spines is much higher in mossy cells that in pyramidal CA3 neurons. These cells are glutamatergic and give rise to the associational/commisural projection, which terminates deep in the molecular layer of the DG. Fusiform type cells have varying numbers and density of spines. One type first described by Amaral (1978), now called hilar perforant path-associated cell (HIPP cell), has a long multipolar soma, reacts positively to somatostatin, and has two or three principal dendrites that run parallel to the granule cell layer. They have a high number and density of spines and their axons ascend to superficial areas of the molecular layer, where both the perforant path axon terminals and granule cell dendrites are found. Another fusiform type cell is also triangular or multipolar in shape, with aspiny dendrites in both the hilus and molecular layer, and axons that terminate deep in the molecular layer. These are called hilar commissural-associational pathway-related cells (HICAP) (Andersen et al., 2007). Lastly, hilar chandelier cells have also been described, and these appear to have a dendritic tree just in the hilus, receive mossy fiber inputs, and terminate on the axon initial segments of mossy cells (Martinez et al., 1996, Cappaert et al., 2015).

Inhibitory connectivity in the DG. The variety of interneurons present in DG exerts a large influence on the excitatory network of this field. Not only the plexuses of some cell

types over large extensions of the granule cell layer (like basket cells), but the interconnectivity of interneurons within and across layers creates a complex inhibitory and disinhibitory control over granule cell activity. A clear example of this are the HIPP cells. Given that they receive mossy fiber inputs and have axon terminals in the superficial area of the molecular layer, synapsing onto granule cell dendrites, thus creating a local inhibitory feedback loop (Andersen et al., 2007).

Mossy Fibers. Besides the associational/commissural projection, the mossy fiber projection is the main efferent coming from the DG. They correspond to the unmyelinated axonal and excitatory projections from granule cells that terminate in CA3, although a distinct set of collaterals innervates hilar mossy cells. These fibers travel along the transverse axis into CA3, where they form synapses with the pyramidal neurons and, especially at septal levels, make an abrupt turn as they approach the CA2 field and travel temporally (Swanson et al., 1978, Amaral and Witter, 1989).

DG Afferents. The main input to the DG is the EC via the perforant pathway (Ramón y Cajal, 1893). This projection arises mainly from layer II neurons in the EC, with a smaller proportion of fibers arising from layers V/VI (Steward and Scoville, 1976), PrS, and PaS (Köhler, 1985) and takes its name because it 'perforates' the subiculum and hippocampal fissure on its way to the DG. The terminals of the perforant pathway (PP) terminate exclusively on the superficial molecular layer of the DG and form asymmetrical synapses onto granule cell dendrites (Nafstad, 1967) and a smaller part targets interneurons (Zipp et al., 1989). Furthermore, the PP can also be subdivided into lateral PP and medial PP, originating from the lateral EC (LEC) or medial EC (MEC), respectively. PP fibers originating in the LEC terminate in the most superficial third of the molecular layer, while those from MEC terminate in the middle third (Hjorth-Simonsen and Jeune, 1972).

The DG also receives input from the septal nuclei, namely from the medial septal nucleus and the diagonal band of Broca, arriving at the HF via the fimbria, dorsal fornix, supracallosal stria, and, temporally, through and around the amygdaloid complex (Mosko et al., 1973, Swanson et al., 1978, Amaral and Kurz, 1985a). The septal fibers innervate hilar cells and granule cells, and the fibers that innervate the former target tend to be γ-aminobutyric acid (GABA) positive and therefore inhibitory, while fibers that innervate the latter are mainly cholinergic (Kohler et al., 1984, Nyakas et al., 1987).

Additionally, the DG receives input from a variety hypothalamic nuclei, and from the brainstem (Wyss et al., 1979). From the brainstem, the DG receives a major adrenergic afferent from the pontine nucleus locus coeruleus, which terminates mostly in the hilus and extend to CA3, where mossy fibers can be detected (Pickel et al., 1974). Moreover,

the hilus receives a modest dopaminergic innervation from the VTA, while hilar GABAergic interneurons located close to granule cells receive significant serotonergic inputs from the raphe nuclei (Andersen et al., 2007, Conrad et al., 1974, Vertes et al.,

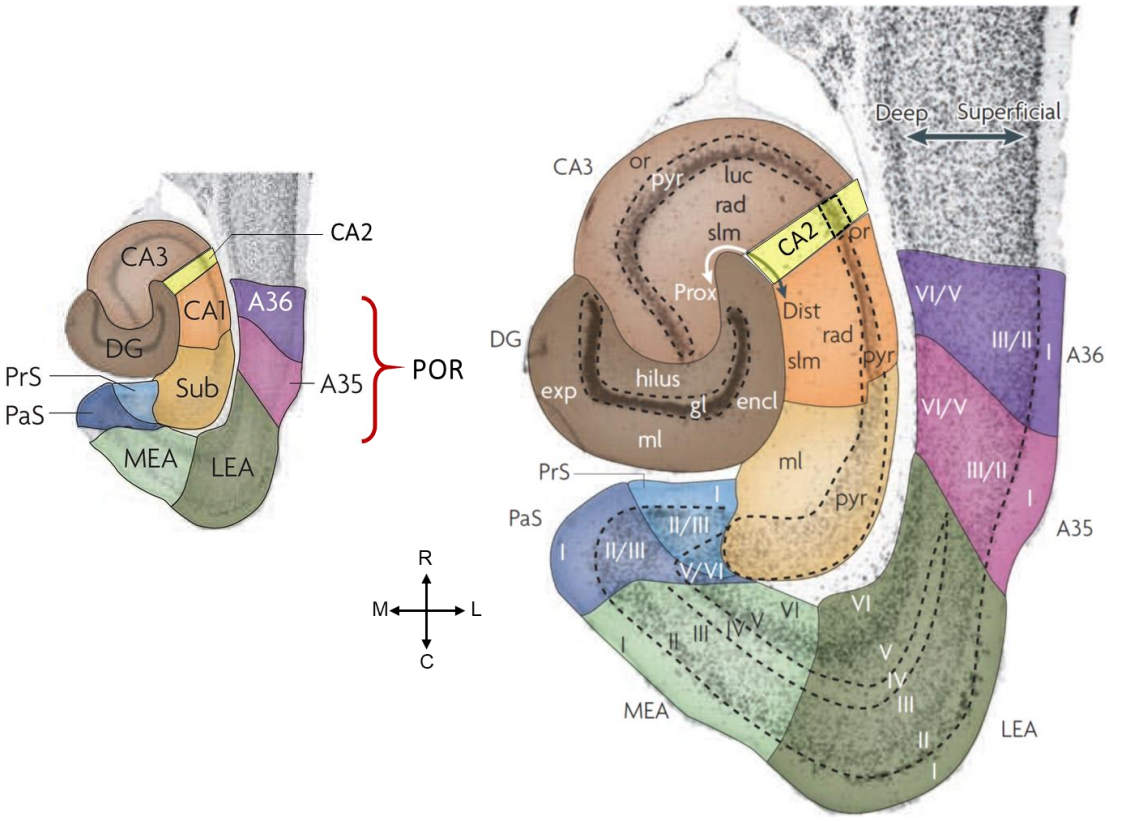

Figure 1.4 – Layer organization of the HF and PHR. The figure demonstrates the layer organization of the different areas within the HF and PHR. On the left, the figure shows the overall areas within each region, while on the right the same figure focuses on the different layers within each region. The Roman numerals indicate cortical layers; encl, enclosed blade of the DG, the portion of the DG that is in direct contact with the CA regions; exp, exposed blade of the DG, portion of the DG adjacent to the brain ventricle; gl, granule cell layer; luc, stratum lucidum; ml, molecular layer; or, stratum oriens; prox, proximal; pyr, pyramidal cell layer; rad, stratum radiatum; slm, stratum lacunosum-moleculare; R, rostral; C, caudal; M, medial; L, lateral. The abbrevations MEA and LEA are equivalent to MEC and LEC, respectively. Figures adapted from van Strien et al. (2009).

1999) .

1.2.1.2 – Hippocampus Proper

The hippocampus, as defined by Lorente De Nó (1934), is subdivided into three fields which are, from proximal to distal location from the DG: CA3, CA2, and CA1 (see Figure 1.4). All three sub-regions are characterized by displaying a principal cell layer, *stratum pyramidale*, tightly packed with pyramidal cells in CA1, and more loosely arranged in CA2 and CA3. Deeper to the pyramidal cell layer lies the relatively acellular layer, *stratum oriens*, containing mostly the basal dendrites of pyramidal neurons of the layer above along with some interneurons and axonal projections. Deeper to the *oriens* lies the alveus, which contains solely axonal projections. Uniquely in the CA3 field, above the

principal cell layer, lies the *stratum lucidum*, mostly comprised of mossy fibers. At the CA3/CA2 border, where the mossy fibers turn temporally, this layer thickens, marking the border between one field and the other. Superficial to the *stratum pyramidale* in CA2 and CA1, and above the *stratum lucidum* in CA3, lies the *stratum radiatum*. Here lie CA3 to CA3 associational connections, as well as the CA3 to CA1 projections – the Schaffer collaterals. The most superficial layer of the hippocampus is the *stratum lacunosum-moleculare*, where several afferents, including those from the EC, terminate (Andersen et al., 2007, Cappaert et al., 2015).

The pyramidal cells make up the vast majority of neurons in the hippocampus. These neurons have basal dendrites that protrude in to the *stratum oriens*, while their apical dendrites extend towards the hippocampal fissure, thus crossing the superficial layers. In CA3, the size of the dendritic tree varies along the transverse axis, with proximal CA3 pyramidal neurons having smaller sized dendritic trees than distal neurons. Distal CA3 pyramidal neurons have smaller apical dendrites which do not reach the *lacunosum-moleculare* (and do not get input from the EC for instance), while the proximal neurons possess larger basal and apical dendrites (Ishizuka et al., 1995). CA2 neurons do not receive mossy fiber input and their somas vary in dimension along the transverse axis, proximal ones being larger like CA3 neurons, and distal ones being smaller and more similar to CA1 ones(Ishizuka et al., 1995). CA1 pyramidal neurons are smaller and more homogenous than CA3 and proximal CA2 cells. Their dendritic trees are also smaller comparatively to CA3 (Ishizuka et al., 1995).

The interneuron types in the hippocampus, similarly to the DG, are quite heterogenous and scattered throughout the layers (Gulyas and Freund, 1996). Basket and chandelier cells exist throughout all CA fields, being located along the *stratum pyramidale*. Bistratified cells are another type of parvalbumin-positive interneuron whose axonal plexus extends to the *radiatum* and *oriens*, innervating the dendrites of pyramidal neurons (Gulyas and Freund, 1996). Another class of interneurons has been termed oriens lacunosum-moleculare (associated) cell (O-LM cell), featuring a dense axonal arbor solely in the *stratum lacunosum-moleculare* (Lacaille et al., 1987). Their dendrites and somas on the other hand, are located in zones containing pyramidal neuron recurrent collaterals, forming symmetrical synapses with distal apical dendrites (Lacaille et al., 1987, Andersen et al., 2007). Interneuron specific/selective neurons are a type of interneuron that innervates exclusively other interneurons (Gulyas and Freund, 1996, Andersen et al., 2007, Cappaert et al., 2015). Examples of this group of neurons are the hippocampo-septal cells, interneurons that project to other areas of the HF, like CA1, CA3 and the hilus of the DG (Somogyi and Klausberger, 2005).

CA3 Connectivity. CA3 is innervated by axons of their own collaterals – the associational projection –, by axons from contralateral CA3 – commissural projection –, and by the DG granule cells (Swanson et al., 1978). Interestingly, the associational innervation seems to vary along the transverse axis, with proximal CA3 cells connecting mostly with other proximal neurons in the same septotemporal region, while distal CA3 neurons project to other septotemporal regions along the whole proximal-distal axis (Ishizuka et al., 1990). It also receives PP fibers which arrive at the *stratum lacunosum-moleculare*, with the number of synaptic contacts and origin of fibers being similar to that of the DG. Additionally, and similarly to the DG, CA3 receives afferents from the septal nuclei – medial septal nucleus and diagonal band of Broca (Nyakas et al., 1987, Gulyas et al., 1990). At temporal levels, CA3 receives amygdalar afferents in the *oriens* and *radiatum* (Pikkarainen et al., 1999), and some weak inputs from the endopiriform nucleus (Behan and Haberly, 1999). Similarly to DG, CA3 also receives serotonergic input from raphe nuclei (Vertes et al., 1999) which, similarly to the DG, preferentially terminate onto GABAergic neurons (Freund et al., 1990). Also like the DG, CA3 contains few dopaminergic fibers (Andersen et al., 2007, Cappaert et al., 2015), but receives substantial adrenergic input (Pickel et al., 1974).

Within the hippocampus, and besides its recurrent collaterals, CA3 projects both to the molecular layer and hilus of the DG (Li et al., 1994), and CA2 (Lorente De Nó, 1934). But the most notable projection is that which targets CA1, the Schaffer collaterals. All portions of CA3 project to CA1, but these projections are organized differently along the transverse axis. Proximal CA3 cells tend to project towards more septal levels of distal CA1, and their axons terminate superficially in the *stratum radiatum*. Distal CA3 projects more densely to temporal portions of proximal CA1 and their axons terminate deeper in the *radiatum* and in the *stratum oriens* (Andersen et al., 2007, Ishizuka et al., 1990). Commissural projections from CA3 to contralateral CA3, CA2 and CA1 also occur (Swanson et al., 1980, Blackstad, 1956). The major subcortical efferent target of CA3 is the topographical projection to the septal complex – septal CA3 projects dorsally to the lateral septal nucleus, and the temporal portion of CA3 projects more ventrally (Swanson and Cowan, 1977). This projection arises both from CA3 pyramidal neurons (Swanson et al., 1980) and a sub-population of GABAergic neurons (Tóth and Freund, 1992, Cappaert et al., 2015).

CA2 Connectivity. Recent years have brought renewed interest in region CA2 (Jones and McHugh, 2011). Besides receiving input from CA3 (Lorente De Nó, 1934), recent reports also demonstrate projections from DG granule cells to CA2, whose pyramidal neurons subsequently project to CA1 (Kohara et al., 2014). The only other way to

differentiate this region other than through genetic markers (Lein et al., 2005), is through the selective afferents it receives from subcortical regions, specifically from the hypothalamic supramammillary area (Haglund et al., 1984).

CA1 Connectivity. As previously mentioned, CA1 is heavily innervated by ipsilateral Schaffer collaterals, as well as receiving contralateral CA3 projections. Additionally, CA1 receives afferents from a variety of cortical and subcortical areas. It receives a minor intrahippocampal projection from Sub (Finch et al., 1983, Sun et al., 2014) and is also weakly innervated by PrS and PaS (Köhler, 1985). Unlike the EC projection to DG, EC fibers that innervate CA1 originate in layer (L) III and not in LII (Steward and Scoville, 1976). The fibers terminate in the *stratum lacunosum-moleculare*, the majority of which are excitatory (Desmond et al., 1994). Fibers from MEC tend to innervate proximal CA1, while LEC fibers innervate distally (Steward and Scoville, 1976). Innervation from PER and POR follows a similar topographical arrangement, with fibers from the former targeting distal CA1 and those from the latter reaching proximal areas (Naber et al.). Subcortically, CA1 receives lighter septal inputs than CA3 (Nyakas et al., 1987) and few endopiriform collaterals (Behan and Haberly, 1999). In temporal regions, distal CA1 receives substantial input from the amygdaloid complex, terminating mostly in *strata oriens* and *radiatum* (Krettek and Price, 1977, Pitkanen et al., 2000). In terms of monoaminergic projections, CA1 receives little adrenergic, serotonergic and dopaminergic inputs (Pickel et al., 1974, Conrad et al., 1974, Vertes et al., 1999). The most prominent projections to CA1 are of thalamic origin. It receives substantial projections from the nucleus reuniens to the *lacunosum-moleculare* (Herkenham, 1978), which supports long-range contact between the hippocampus and prefrontal cortex (Ito et al., 2015).

CA1 interneurons are known to project to other HF areas, namely CA3 and DG (Gulyas and Freund, 1996). But the major CA1 efferent is the one targeted at Sub. The axons that contribute to the latter projection travel from the *oriens* or alveus, bend in Sub, and innervate its pyramidal cell layer (Swanson and Cowan, 1975, Finch et al., 1983). Along the transverse axis, CA1 afferents innervate Sub along a topographical gradient, with proximal CA1 projecting to distal Sub, and distal CA1 projecting to proximal Sub (Amaral et al., 1991, Witter, 2006). CA1 also reciprocates the EC connections with efferents directed mostly to MEC rather than LEC, which terminate predominantly in LV (Swanson and Cowan, 1977, Finch et al., 1983, Naber et al., 2001). This projection is also topographically arranged along both the transverse and long axis: proximal CA1 projects exclusively to MEC, while distal CA1 projects mainly to LEC (Witter et al., 2000, Naber et al., 2001); septal CA1 projects more heavily to dorsolateral MEC and LEC, while more

temporal CA1 regions target ventromedial regions of both the LEC and MEC (Naber and Witter, 1998, Kloosterman et al., 2003). Regarding PER or POR, CA1 projects more heavily to the latter, and projections to PER are mostly of septal origin, whereas those to POR tend to be more temporal (Cappaert et al., 2015). Additionally, CA1 projects to restrosplenial cortex (van Groen and Wyss, 1990b), medial prefrontal cortex (Swanson, 1981, Verwer et al., 1997), and infralimbic cortex (Jay and Witter, 1991). Subcortically, CA1 also projects to septal nuclei, much like CA3 (Naber and Witter, 1998). Furthermore, CA1 also projects to the nucleus accumbens, and temporally, to the anterior olfactory nucleus, hypothalamus, thalamic preoptic areas (Cenquizca and Swanson, 2006), and to the basal nucleus of the amygdala (Pitkanen et al., 2000).

1.2.1.3 – Subiculum

In comparison with other hippocampal and parahippocampal structures, the Sub remains relatively understudied. It was named by German physiologist Karl Friedrich Burdach (1826) and anatomically described by Ramón y Cajal (1909) who distinguished it from both CA1 and PrS due to its cytoarchitectonic structure. Collectively, the Subicular complex comprises the Sub, PrS, and PaS. Lorente De Nó (1934) also defined the transition zone between CA1 and Sub as prosubiculum, although this region in the rat is just considered a transitional zone.

Cytoarchitectonically, the Sub is comprised by two layers. Superficially in Sub and continuous with the *stratum radiatum* and *stratum lacunosum-moleculare*, lies the molecular layer (*stratum moleculare*) of Sub, which is largely acellular. Deeper to it, lies the pyramidal cell layer (*stratum pyramidale*), populated by loosely packed, large, spiny pyramidal neurons (Köhler, 1985, Witter et al., 1990). According to O'Mara et al. (2001), at the deepest levels of Sub and just above the alveus, lies a polymorphic layer, populated with neurons of smaller sizes. The pyramidal cell layer is easily distinguishable from that of CA1 due to is larger width. It is composed mainly of pyramidal neurons whose apical dendrites extend to the molecular layer and is continuous with LII of the PrS. Cells with smaller somas can be found scattered throughout the layer, representing putative interneurons of similar type to those of the hippocampus and DG. This classical anatomical characterization of Sub has been more recently challenged by the work of Bienkowski et al. (2018), where gene expression patterns in the mouse hippocampus were evaluated. This study not only genetically identified a subpopulation of subicular/CA1 cells that may represent a prosubiculum, but also identified 4 layers. Each of these layers was then associated with potentially different functions, as each of these was found to have different projection targets.

Pyramidal cell type distinctions have been made on the basis of their *in vitro* response to depolarizing pulses. Thus, subicular pyramidal cells can be either bursting or regular spiking neurons (Taube, 1993). Subsequent studies have then shown that cells in the superficial principal cell layer tend to be regular spiking, while neurons deeper in the layer tend to be of the bursting type (Greene and Totterdell, 1997, Harris et al., 2001a). Other works have also shown that, while CA1 is mostly comprised of regular spiking principal cells, there appears to be a gradient of increasing numbers of bursting neurons along the transverse axis Sub and not along the subicular radial axis (Kim and Spruston, 2012). This means that subicular regions closer to CA1 have a higher proportion of regular spiking neurons, while distal subicular regions have higher numbers of bursting cells (Jarsky et al., 2008). The difference between the output patterns of each of these subicular neurons is due to the presence of slowly deactivating calcium channels that allow the occurrence of afterdepolarizations. But the ionic current flow balance required to elicit subicular bursting is quite different from that observed CA1. In Sub, an initial Sodium-dependent spike is necessary to increase Calcium conductance into the cell, which then allows the generation of further Sodium-dependent action potentials. The inflow of calcium is also responsible for activating potassium currents which terminate the burst (Jung et al., 2001). In CA1 however, dendritic calcium currents derived from synaptic activation are sufficient to generate somatic burst responses (Golding et al., 1999). Further electrophysiological studies then demonstrated that regular-spiking neurons also respond in a bursting fashion in an activity-modulated manner, but later in the spike train (Graves et al., 2012). In addition, bursting neurons have been associated with increased sensitivity to somatostatin (Greene and Mason, 1996), while regular spiking cells appear to express nicotinamide adenine dinucleotide phosphate-diaphorase and neuronal isoform of nitric oxide synthase, meaning that these are potential nitric oxide producing neurons (Greene et al., 1997). Also, both neuronal populations are inversely affected by brain-derived neurotrophic factor: this signaling molecule is necessary for intrinsic plasticity of subicular neurons, but reduces the excitability of regular spiking cells, while increasing it in bursting ones (Graves et al., 2016).

Connectivity of Sub. The Sub gives rise to longitudinal associational projections from septal to temporal regions of the pyramidal cell layer, a relationship which is largely unidirectional (Köhler, 1985). Subicular intrinsic connectivity is thus strictly local – as there are several axonal terminations in the apical dendrites of local pyramidal cells both in the pyramidal and molecular layers (Harris et al., 2001a) – or associational, as

subicular pyramidal cells do not give rise to commissural projections (Swanson and Cowan, 1977).

Besides receiving projections from CA1, Sub also receives afferents from the retrosplenial cortex areas A29a, A29b, A29c, and A30 (Köhler, 1985). It also receives projections from both PrS, and PaS (Köhler, 1985, van Groen and Wyss, 1990b). The EC to Sub projection arises mainly from LIII, although some collaterals from PP arising from LII, and LV/VI also terminate in this area (Steward and Scoville, 1976, Tamamaki and Nojyo, 1993, Naber et al., 2000). These fibers mostly terminate in the molecular layer, and approximately 80% of these synapses are asymmetrical. Similarly to other hippocampal fields, the PP terminals are topographically organized along both the transverse and long axis of Sub: from proximal to distal areas, Sub receives input from increasingly medial regions of the EC, while from septal to temporal Sub, EC collaterals arise from increasingly ventral portions of the EC (Naber et al., 2000, Naber et al., 2001, Witter, 2006). Sub also receives afferents from both PER and POR, with the latter fibers terminating mostly in proximal Sub, whereas collaterals from the former cortical area terminate preferentially in distal Sub (Naber et al., 1999).

As Sub sends projections to a variety of cortical and subcortical areas, it is considered the output structure of the hippocampus (Swanson and Cowan, 1975). Inside the HF, Sub was thought to give to rise to a minor CA1 projection (Finch et al., 1983, Köhler, 1985, Sun et al., 2014). However, further work has then showed that this projection is more complex than previously thought. Further tracing studies demonstrated that in dorsal Sub the feedforward projection arising from CA1 appears to be mirrored by a back-projection (Sun et al., 2018). Both excitatory and inhibitory neurons appear to originate this back-projection. Moreover, the distal portion of CA1 appears to be more strongly innervated than proximal portion. This innervation also seems to be functional, as stimulation of proximal Sub reliably increases activity in distal CA1 (Sun et al., 2018). These data seem to agree with recent work suggesting that input from Sub back into the CA areas is also required for theta-based activity synchronization (Jackson et al., 2014). These data altogether provide further evidence that the information flow within the hippocampus is not strictly one directional.

Distal Sub also projects to LI of PrS and LI of PaS, but the densest projection is directed to LV of septal PrS. These projections are organized so that increasingly septal subicular areas project to increasingly dorsal locations of the PrS and PaS (Köhler, 1985, van Groen and Wyss, 1990b). The Sub also projects to ipsilateral EC, with subicular axonal terminals being located in LV/VI and a minor portion innervating LIII (Swanson and

Cowan, 1977, Beckstead, 1978, Köhler, 1985, Naber and Witter, 1998, Naber et al., 2001, Kloosterman et al., 2003). Regarding its topological arrangement, Sub-EC projections along the transverse axis are arranged in the opposite way of CA1-EC, *i.e.*, proximal Sub projections tend to innervate LEC, while distal Sub axonal terminals are mostly found in the MEC, such that the afferents and efferents from EC are in register. Along the septotemporal axis, the topographical arrangement of Sub-EC fibers is identical to CA1-EC, *i.e.*, the projections of neurons along the septo-temporal axis of Sub are topographically mapped onto the dorsolateral to ventromedial axis of both LEC of the MEC. (Witter et al., 2000, Naber et al., 2000, Naber et al., 2001). Layers V and VI of the PER and POR are also targets of subicular projections. The majority of fibers targeted to PER and POR arise from septal Sub, with proximal Sub innervating PER (adjacent to the LEC, also innervated by proximal Sub), while distal Sub preferentially innervates POR (Swanson and Cowan, 1977, Amaral and Witter, 1989, Kloosterman et al., 2003). Other prominent cortical targets include parts of the medial prefrontal cortex, anterior olfactory nucleus and agranular insular cortex (Jay et al., 1989, Witter et al., 1989, Witter et al., 1990, Verwer et al., 1997), as well as anterior cingulate cortex (White et al., 1990). The Sub also has substantial projections to the retrosplenial cortex, which originate predominantly in septal regions (Köhler, 1985, Witter et al., 1990, Witter et al., 1989). Subcortically, Sub projects to the septal complex (Swanson and Cowan, 1977), mammillary nuclei (Shibata, 1989), as well as several other hypothalamic nuclei (Swanson and Cowan, 1977, Witter et al., 1989, Witter et al., 1990). In the thalamus, subicular fibers terminate in the nucleus reuniens, nucleus interanteromedialis, paraventricular nucleus, nucleus gelatinosus (submedius), the bed nucleus of the stria terminalis, endopiriform nucleus (Swanson and Cowan, 1977, Canteras and Swanson, 1992), and accessory olfactory bulb (de la Rosa-Prieto et al., 2009). The Sub also sends substantial and topographically arranged efferents to the nucleus accumbens and olfactory tubercle (Groenewegen et al., 1987). The temporal region of Sub also gives rise to a significant projection to several amygdalar nuclei (Pitkanen et al., 2000).

The projection arrangement along the transverse axis of Sub also appears to be correlated with the distribution of bursting and regular spiking pyramidal cells. Thus, the distal region of Sub contains a higher proportion of bursting pyramidal cells (Jarsky et al., 2008), which project to more strongly to the ventromedial hypothalamic nucleus, MEC, retrosplenial cortex, and PrS (Kim and Spruston, 2012). The proximal region on the other hand, contains more regular spiking neurons which project mostly to the amygdala, LEC, orbitofrontal cortex, and nucleus accumbens (Jarsky et al., 2008, Kim and Spruston, 2012).

The number of subicular targets and afferents it receives make this hippocampal region an important hub of information. The organization of inputs and outputs is organized along the several subicular axes, as briefly touched upon in previous paragraphs. Besides the already mentioned back-projection to CA1, subicular outputs can be organized along the transverse axes in terms of function. Cembrowski et al. (2018) reported on the distinctive role of distal Sub in working memory. Through pharmacogenetic inhibition, the authors demonstrated that distal Sub is involved in working memory encoding, but not retrieval. These observations are in line with theories regarding the dual role of Sub in the encoding of both local and global, with proximal Sub thought to be involved in the encoding local cues, and distal Sub with global cues (Knierim et al., 2014). Moreover, considering the different subicular outputs along the transverse axis, it is not surprising that these compartments may play different roles in spatially guided behavior. But this requires further testing.

Along its longitudinal axis, the Sub also projects to substantially different and anatomically distinct brain regions. The dorsal subicular regions appear to mostly target other cortical areas (Swanson and Cowan, 1977, Amaral and Witter, 1989, Kloosterman et al., 2003), while ventral Sub projects more to thalamic, amygdalar, and ventral cortical areas (Swanson and Cowan, 1977, Canteras and Swanson, 1992). Further work has since demonstrated that projection patterns between layers within Sub also have different targets, but that this division of outputs across the radial axis still follows a dorsal to ventral (septal to temporal) gradient in function of these outputs (Bienkowski et al., 2018). The targets of dorsal Sub, which include PrS, PaS, EC, retrosplenial cortex, and some thalamic nuclei, appear to be associated with higher cognitive functions or with navigation. More ventral/temporal regions of Sub, which include a variety of thalamic and hypothalamic nuclei, as well as the amygdala and olfactory areas, appear to be more strongly associated with limbic functions (Bienkowski et al., 2018).

In summary, the complexity of subicular outputs can be observed at various levels of its organization: along the radial axis, different layers of subicular pyramidal cells will have different firing properties and/or different efferents; along the transverse axis, proximal and distal regions will have also different inputs and outputs, which may results in the recruitment of different subicular compartments into different aspects of spatial behavior; and the organization of the afferents and efferents of Sub across its long axis (septal to temporal) also indicates that subicular neurons may integrate different aspects of cognitive and limbic information – with the hypothetical prosubiculum being at the center of this integration (Bienkowski et al., 2018).

1.2.2 – The Parahippocampal Region

The regions comprising the PHR, unlike the HF, have an increased laminar organization. All of the PHR fields have been defined as being six-layer structures. However, because these layers are not easily discernible for the PrS, PaS and EC, these fields are considered part of the periallocortex, a transition zone from the three-layered HF to the neocortex. The PER and POR are considered part of the neocortex, presenting the classical six-layered structure (Stephan, 1975).

1.2.2.1 – Presubiculum

The PrS is distal to Sub and is bordered caudally by the EC and PaS. It is also subdivided into septal and dorsal (see Figure 1.4). Some work suggests that the septal portion of the PrS is in fact a separate subicular area (Brodmann, 1909, van Groen and Wyss, 1990c), termed postsubiculum. Different efferent targets and afferent inputs constitute the main reason for this division (van Groen and Wyss, 1990c), but both postsubiculum and septal/dorsal PrS refer to the same area. Radially, the mostly cell-free LI is continuous with the molecular layer of Sub, and deeper to it there's a the densely packed superficial layers (layers II and III) are separated from the deep layers by another cell-free layer, named *lamina dissecans*, continuous with the cell free layer in the EC (LIV, which has the same name). The deep layers of PrS (layers V and VI) are continuous with those of the EC and the principal layer of Sub. This structure contains both pyramidal and stellate cells in layers II and III, which are not easily distinguishable (Funahashi and Stewart, 1997). The deep layers are made up of two layers of large pyramidal neurons (LV and LVI), and deeper to it a layer containing a mix of both pyramidal and polymorphic cells.

Connectivity. The PrS contains both associational and commissural connections, the former existing throughout the whole septotemporal extent of the PrS. Commissural presubicular connectivity is found mostly in the temporal region (Funahashi and Stewart, 1997, van Groen and Wyss, 1990a). Other afferents besides Sub include: retrosplenial cortex (Sugar and Witter, 2016), axons from LV of visual area 18b (Vogt and Miller, 1983), posterior parietal cortex (Olsen et al., 2017), prelimbic and medial prefrontal cortices (Beckstead, 1978, van Groen and Wyss, 1990a). Subcortically, the PrS receives input from the medial septum, endopiriform nucleus, hypothalamus, raphe nuclei and locus coeruleus (van Groen and Wyss, 1990a). The main subcortical afferent comes from the dorsal thalamic nuclei, mainly both the anterodorsal, anteroventral nuclei, and

minor projections from laterodorsal nucleus and medial thalamic nucleus (Shibata, 1993, van Groen and Wyss, 1990a, van Groen and Wyss, 1990c).

PrS sends projections to the molecular layer and hilus of DG, the molecular layer of CA fields and Sub and to PaS (Köhler, 1985, van Groen and Wyss, 1990a). A prominent and dense projection to ipsi- and contralateral EC also occurs. Projections from superficial PrS cells terminate exclusively in LI and LIII of the EC, and to a lesser extent in LV/VI (Köhler, 1985, van Groen and Wyss, 1990a, van Groen and Wyss, 1990c), while projections from deep PrS layers terminate on ipsilateral deep layers of the EC and fewer of them in superficial layers (Honda and Ishizuka, 2004, van Groen and Wyss, 1990a, van Groen and Wyss, 1990c). PrS also project to PER and POR (van Groen and Wyss, 1990c), and retrosplenial cortex (Honda et al., 2011, van Groen and Wyss, 1990a). The septal PrS has a substantial bilateral efferent directed at the anterodorsal, and laterodorsal nuclei of the thalamus (Seki and Zyo, 1984, van Groen and Wyss, 1990b). Finally, PrS also sends projections to the hypothalamus, namely the medial and lateral nuclei of the mammillary complex (Swanson and Cowan, 1977).

1.2.2.2 – Parasubiculum

The PaS is bordered by the PrS rostro-proximally and MEC caudo-distally (see Figure 1.4). Similarly to the PrS, the PaS has almost indistinguishable layers II and III, which consist of large and densely packed pyramidal and stellate cells, and its deep layers are continuous with the deep EC layers (Boccara et al., 2015).

Connectivity. The PaS receives a prominent input from the amygdala (Krettek and Price, 1977, Pitkanen et al., 2000), but also from other subcortical regions such as the nucleus reuniens (Wouterlood et al., 1990), supramammillary nucleus (Haglund et al., 1984), serotonergic input from the raphe (Köhler et al., 1981). Besides having associational, and medial septal input (Alonso and Kohler, 1984) the PaS also receives minor projections from retrosplenial cortex, anterior cingulate area, posterior parietal cortex and visual cortex (Vogt and Miller, 1983, van Groen and Wyss, 1990a, Olsen et al., 2017).

Regarding its efferent connectivity, PaS innervates the molecular layer of the DG and the *stratum lacunosum-moleculare* of temporal CA1 and Sub (Köhler, 1985, van Groen and Wyss, 1990a). It also projects to PrS, the anterodorsal nucleus of the thalamus and the lateral portion of the mammillary bodies (van Groen and Wyss, 1990a, Wright et al., 2010). The most prominent PaS efferents are those that selectively innervate LII of both

the LEC and MEC, a projection which is mostly ipsilateral (Köhler, 1985, van Groen and Wyss, 1990a).

1.2.2.3 – Entorhinal Cortex

The EC plays a key role in information processing and flow in the hippocampal system. It represents the information gateway to the HF – via the PP – through which sensory and other cortical information arrives. Moreover, given the extensive projections it receives from HF fields (like CA1 and Sub), it is thought to act as a relay station through which hippocampal information is transferred to the neocortex – even though lighter direct neocortical projections from the HF also occur.

The EC in the rat lies ventrally in the caudal convexity of the cerebral cortex, bordering the PaS and PrS anteriorly (see Figure 1.4), the pyriform cortex and amygdalar complex rostro-ventrally, the PER and POR rostro-laterally (see Figure 1.5), V2 dorsolaterally,

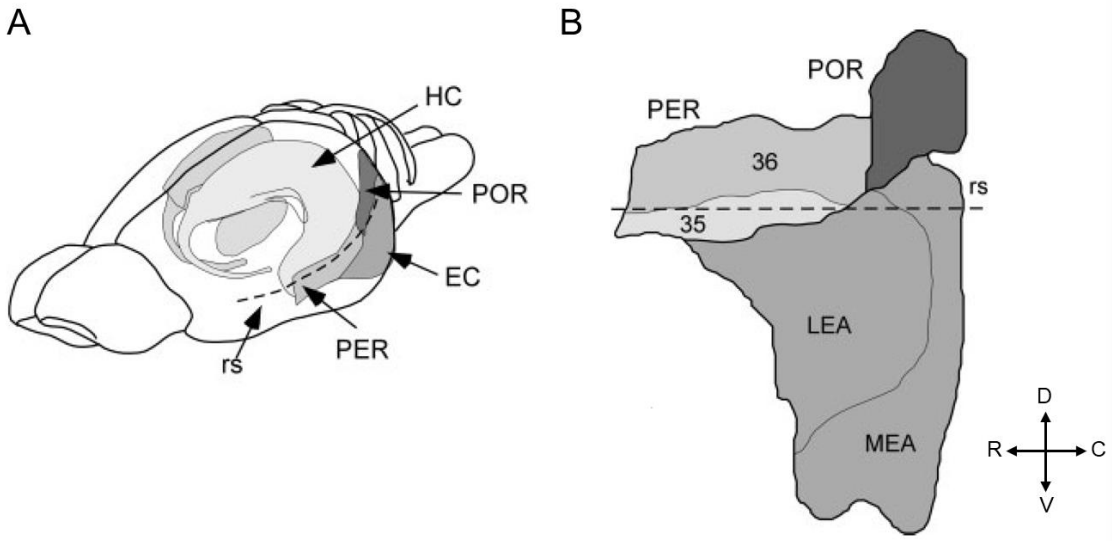

Figure 1.5 – Location of the rhinal cortices in the rat brain. (A) Rostrolateral view of the HF (denominated as HC) and the rhinal cortices. POR, postrhinal cortex; EC, entorhinal cortex; PER, perirhinal cortex; rs, rhinal sulcus. (B) Two-dimensional unfolded of the back of the entorhinal cortices. Areas 36 and 35 of the perirhinal cortex are indicated as the regions above and below the rhinal sulcus, respectively. D, dorsal; V, ventral; R, rostral; C, caudal. The LEA (equivalent to LEC) and MEA (equivalent to MEC) make up the EC. Image adapted from Furtak et al. (2007b).

and retrosplenial cortex dorsomedially.

Following the nomenclature established by Ramón y Cajal (1909), the EC is subdivided into six layers, four cellular layers (LII, III, V and VI) and two acellular (LI, and LIV, the latter being also called *lamina dissecans*). LI is the most superficial layer, closest to the pial surface, whereas LVI is the deepest. As previously mentioned, the EC is also divided into LEC and MEC (Brodmann, 1909, Insausti et al., 1997). The LEC lies in the rostrolateral part of the EC, while the MEC occupies the caudo-medial area. The cellular

laminae are easily distinguishable in both areas. Moreover, LIV boundaries are sharper in the MEC than LEC (Insausti et al., 1997).

Cytoarchitecture of the EC. Layer I of the EC, closest to the pial surface, is mostly acellular, containing the apical dendrites of pyramidal cells present in LII. The few cells it does contain are inhibitory, being multipolar or horizontal neurons (Miettinen et al., 1997, Wouterlood and Pothuizen, 2000). Layer II is mostly comprised of principal cells, (Lorente De Nó, 1934). These neurons' axons travel through the angular bundle, with some collaterals remaining in layers II and III. Stellate cells are only found in the MEC and correspond to about 50% of all principal cells found in this area. These cells, as well as other principal neurons, contribute to the PP, with their axons reaching the HF, particularly the DG and CA3 traveling via the angular bundle (Klink and Alonso, 1997, Dugladze et al., 2001, Gatome et al., 2010, Canto and Witter, 2012b). The LEC LII also has a variety of fan and multiform cells, spiny neurons whose axons also contribute to the PP (Tahvildari and Alonso, 2005, Canto and Witter, 2012a). This layer also contains multipolar, basket and chandelier cells, mediating local inhibitory interactions, while spiny horizontal bipolar cells project to the HF (Miettinen et al., 1997). Layer III is predominantly made up of pyramidal neurons whose axons travel through the angular bundle to innervate CA1 and Sub (Dugladze et al., 2001). A large network of inhibitory neurons with a variety of shapes can also be found in this layer (Miettinen et al., 1997). Layer IV, like LI, is mostly acellular, but it contains few pyramidal, fusiform and bipolar cells (Lingenhohl and Finch, 1991) whose dendrites reach superficial layers and some of which are also inhibitory (Wouterlood and Pothuizen, 2000). Layer V is a relatively large layer with several principal neuron cell types. Pyramidal neurons are the most common in this layer, whose axons provide inputs to deeper and superficial layers of the EC, as well as the HF through the angular bundle. Horizontal and multipolar cells make up the rest of the principal neuron types in this layer, with the former cells spreading their dendrites across the layer and having projection targets similar to pyramidal neurons (*i.e.* projecting to the HF via the angular bundle). Multipolar cells' axonal terminals exclusively innervate deep layers of the EC (Hamam et al., 2000, Gloveli et al., 2001, van Haeften et al., 2003). Interneuron-wise, parvalbumin positive cells are found in this layer as well as LVI, although in lower numbers compared to superficial EC layers (Wouterlood et al., 1995). Layer VI contains pyramidal cells and multipolar cells. The former cells project to the angular bundle and superficial layers, while the latter ones collateralize extensively in the deep layers of EC (Canto and Witter, 2012b, Dugladze et al., 2001).

Connectivity within the EC. The EC has an extensive associational and commissural network. Along the longitudinal axis (dorsolateral to ventromedial positions), the MEC and LEC projections starting from a particular longitudinal band remain in that same band. This organization relates to the longitudinal organization of PP fibers as well. There is also some reciprocal connectivity between LEC and MEC. Dorsolateral LEC areas projections are confined to this region, while ventromedial levels of LEC innervate both the ventromedial LEC and MEC. Projections starting in a particular longitudinal band of MEC project to the same band of the MEC and LEC (Dolorfo and Amaral, 1998). Along the radial axis, both deep and superficial layers of the MEC have axonal terminals in the superficial layers of the same regions. In the LEC, deep layer cells also target themselves (Dolorfo and Amaral, 1998). In the MEC, axons from LV cells create mostly excitatory synapses with principal cells and interneurons of layers I through III (van Haeften et al., 2003). Commissural connections also occur between superficial layers of all EC regions, with these projections terminating in homotopic regions of LI and II of the contralateral EC (Kohler, 1986, Kohler, 1988).

Connectivity with HF and other PHR fields. The EC projects to all HF fields via the PP(Steward and Scoville, 1976), but at septal levels some entorhinal fibers reach CA1 via the alvear pathway (Deller et al., 1996). The PP fibers arise mainly from LII and LIII neurons, with a smaller percentage coming from deep layer neurons. The projecting cells are mostly principal cells, but other cell types, including GABAergic cells, contribute with fibers (Steward and Scoville, 1976, Witter et al., 1989, Melzer et al., 2012).

The ipsilateral projection to DG is mostly made up of fibers from LII stellate cells of the EC (Steward and Scoville, 1976), with a smaller component coming from pyramidal and bipolar cells (Dugladze et al., 2001). These projections are radially organized (as discussed in the DG section) and longitudinally – fibers from dorsal EC areas project septally to DG, while the ventromedial EC projects more temporally (Ruth et al., 1982, Ruth et al., 1988, Dolorfo and Amaral, 1998). Similarly to DG, the PP fibers that innervate CA3 are mostly from stellate cells in LII (which also innervate DG) and show an identical radial and longitudinal innervation pattern (with the terminals being located in the *stratum lacunosum-moleculare*) (Steward and Scoville, 1976, Ruth et al., 1982, Ruth et al., 1988, Tamamaki and Nojyo, 1993). Information regarding projections to CA2 in rat are lacking, but the mouse CA2 receives direct EC innervation exclusively from LII neurons of both the MEC and LEC (Kohara et al., 2014). As previously discussed, CA1 is innervated solely by LIII pyramidal EC neurons, the majority of which is glutamatergic (Steward and Scoville, 1976, Desmond et al., 1994). The PP terminals in Sub are mainly found in the

outer molecular layer of Sub. Longitudinally, the EC projection to both CA1 and Sub follows that of the DG/CA3 (Naber et al., 2001). Layer II neurons of the EC also give rise to a contralateral projection to all fields of the HF, mainly directed at DG (Steward and Scoville, 1976). It is most prominent at septal levels of the HF and travels to contralateral HF via the alveus. Besides the already discussed innervation of PrS and PaS by the EC, it additionally sends efferents to all layers of the PER – most of which arise from the LEC – and to some areas of LVI of POR (Burwell and Amaral, 1998a, Burwell and Amaral, 1998b).

Extra-Hippocampal Connectivity. As the EC is viewed as the hippocampal information gateway center, it receives inputs from a variety of cortical areas. Therefore, the EC provides other hippocampal neurons with information arriving from primary sensory or higher-order cortical areas. It also receives input from relevant poli-sensory cortical areas, namely the PER and POR (which will be discussed in the next section). Briefly, the EC receives afferents from:

- Olfactory areas, namely the olfactory bulb (Kosel et al., 1981), anterior olfactory nucleus, and piriform cortex (Haberly and Price, 1978). Subcortically, the LEC receives olfactory information from the endopiriform nucleus, and the MEC, with exception of the dorsocaudal portion, receives only from the endopiriform nuclei (Behan and Haberly, 1999, Kerr et al., 2007).
- Frontal cortical areas, all of which project evenly to LEC, but the secondary motor area predominantly innervates MEC (Burwell and Amaral, 1998a, Kerr et al., 2007). Additionally, the prefrontal areas also project to the EC, more heavily to its lateral portion (Beckstead, 1979, Burwell and Amaral, 1998a, Kerr et al., 2007).
- Insular and Cingulate areas, the latter one having a strong projection from retrosplenial cortex to MEC (Burwell and Amaral, 1998a, Kerr et al., 2007).
- Parietal and Occipital cortices, both of which provide weak inputs. From the Parietal area, the LEC receives more somatosensory input than MEC, while MEC is innervated by more collaterals from the posterior parietal cortex than LEC. From the occipital area, visual association cortices provide inputs to LEC and dorsolateral MEC (Burwell and Amaral, 1998a, Kerr et al., 2007).

- Septal Complex, providing cholinergic input to LIV of both the LEC and MEC (Beckstead, 1978)
- Dense inputs from the amygdala (Beckstead, 1978, Pitkanen et al., 2000) and claustrum (Krettek and Price, 1977)
- Several thalamic and hypothalamic nuclei (see Cappaert et al. (2015) for an extensive review on this subject). The anterodorsal and anteroventral thalamic nuclei (Shibata, 1993, Van Groen and Wyss, 1995), for instance, project to deep layers of the EC.
- Brainstem areas, including dopaminergic input from the VTA (Beckstead, 1978), serotonergic input from raphe nuclei (Köhler et al., 1981), and noradrenergic input from the locus coeruleus (Fallon et al., 1978).

The EC also projects to several subcortical and cortical areas. The cortical projections are not as substantial as the PP (Insausti et al., 1997). The LEC sends comparatively stronger projections to piriform, frontal, temporal, insular and somatosensory areas than MEC, and both project equally to visual occipital areas (Agster and Burwell, 2009). Subcortically, the EC projects to: olfactory areas (endopiriform nucleus, olfactory tubercle and peduncle) (Haberly and Price, 1978, Kerr et al., 2007); septal complex (Swanson and Cowan, 1977); claustrum (Kerr et al., 2007); amygdala (Pitkanen et al., 2000, Kerr et al., 2007); basal ganglia; thalamus, and hypothalamus (Kerr et al., 2007). For a summary of the connectivity of the EC see Figure 1.6 A and B.

1.2.2.4 – Perirhinal and Postrhinal Cortices

Both the PER and POR take their names from their position regarding the rhinal fissure (see Figure 1.5). The PER is located rostrally, along the posterior half of the rhinal fissure. The POR, on the other hand, is located above and in the caudally in the rhinal sulcus. The PER can be subdivided into two regions: A35, inside the rhinal fissure; A36, dorsal to A35. A35 has poorer laminar differentiation than A36. POR, is mostly dysgranular and with a bilaminar appearance (Burwell et al., 1995, Burwell, 2001, Cappaert et al., 2015). Pyramidal and multipolar cells are the most abundant cell type in both PER and POR, although other cell types can be found in both areas (Sills et al., 2012, Furtak et al., 2007a).

Connectivity. Besides the associational connections within each field, both PER and POR receive afferents from CA1, Sub, PrS, PaS and EC (Furtak et al., 2007b). Additionally, the PER receives input from the medial prefrontal cortex, visual cortical areas, auditory cortex, and olfactory input from the piriform cortex (Furtak et al., 2007b,

Burwell and Amaral, 1998a). The POR on the other hand receives most of its input from visual areas, while getting moderate afferents from auditory, cingulate and parietal cortical areas (Furtak et al., 2007b). Subcortically, the PER is innervated by a variety of thalamic nuclei (Wouterlood et al., 1990, Shibata, 1993), hypothalamus (Canteras et al., 1994) and amygdala (Pitkanen et al., 2000). All subcortical projections to POR represent less than 15% of the total afferents, and most of these originate in the dorsal thalamic nuclei, and a smaller portion coming from the basal ganglia and amygdala (Furtak et al., 2007b, Pitkanen et al., 2000).

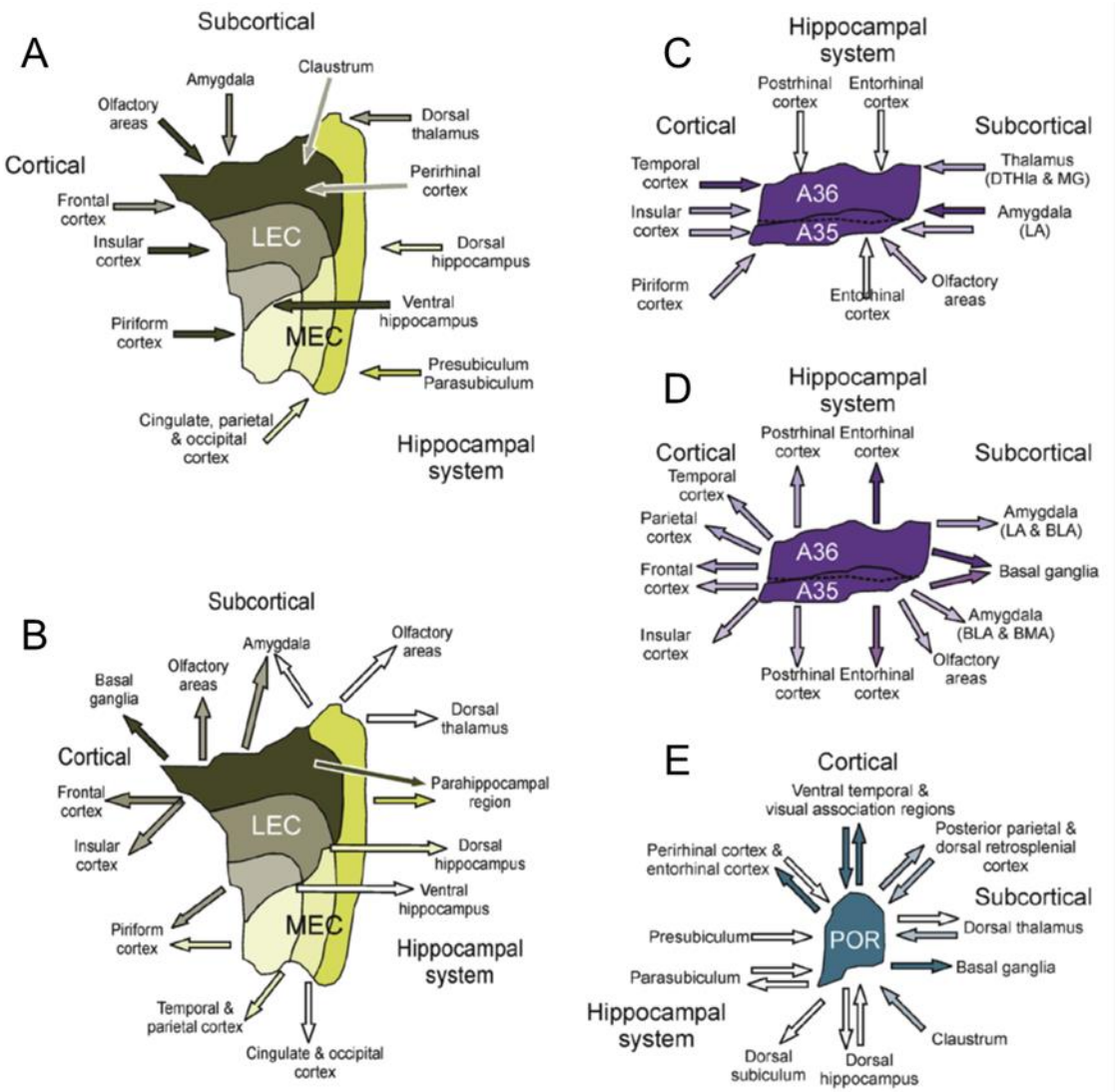

Figure 1.6 – Summary of connectivity of the different rhinal cortices. All images correspond to two dimensional unfolded maps of the different rhinal areas. All images are oriented in the same fashion: dorsal is towards the top of the page, and rostral is towards the left of the page. (A) Entorhinal cortex inputs to both the LEC (dark green bands and arrows) and MEC (light green bands arrows). (B) Entorhinal cortex efferents to the different brain regions. (C) and (D) represent the afferent sources and efferent targets, respectively, of the perirhinal cortex. (E) Afferent and efferent connectivity of the postrhinal cortex. Image adapted from (Cappaert et al., 2015).

Efferent-wise, both the PER and POR inter-innervate each other (Burwell and Amaral, 1998a, Burwell and Amaral, 1998b), as well as CA1, Sub, PrS and Pas (Naber et al.,

1999, Witter, 2006, Furtak et al., 2007b). Additionally, both areas send strong projections to the EC (Burwell and Amaral, 1998b, Furtak et al., 2007b). The PER also sends projections to medial prefrontal, insular, auditory, visual, piriform and cingulate cortices (Agster and Burwell, 2009). The thalamus, basal ganglia, and amygdala also receive axonal terminals from the PER (Furtak et al., 2007b, Pitkanen et al., 2000). The major efferent targets of the POR are the retrosplenial, posterior parietal, occipital, and temporal cortical regions. The POR also sends with weaker projections to frontal cortex, piriform cortex and insular cortex (Furtak et al., 2007b, Agster and Burwell, 2009). The POR also innervates the caudate-putamen, dorsal and ventral thalamus (Furtak et al., 2007b) and the amygdala (Pitkanen et al., 2000). See also Figure 1.6 (C through D) for a summary of PER and POR connectivity.

1.2.3 – Embryonic development and postnatal maturation of hippocampal fields

The embryonic development of HF and PHR fields, with the exception of the DG, is similar to that of the cortex: neural progenitor cells present in the ventricular (deep) zone of all hippocampal fields (except the DG) give rise to post-mitotic principal cells that migrate radially towards the marginal zone (superficial areas) to their final target region (Altman and Bayer, 1990a, Altman and Bayer, 1990b). CA3 pyramidal neuron migration differs slightly from this because this region does not lie close to the ventricular germinative layer. Thus, besides migrating radially, CA3 pyramidal neurons also migrate along the transverse axis to more proximal regions (Altman and Bayer, 1990b). Pyramidal neurons of the HF fields are generated between embryonic day (E) 16 and E21 in the rat (Bayer, 1980b), with peak proliferation of CA3 neurons occurring earlier (E17) than that of CA1 and Sub cells (E18/E19) (Bayer, 1980b). In the PHR, a maturation gradient occurs from lateral to medial brain areas, with the EC, PaS and PrS showing adult-like lamination at E22 (Bayer, 1980b). The DG morphogenesis happens in quite a different way.

DG granule cells, like other HF pyramidal neurons, are also born in the ventricular germinative layer but one day later than other principal cells (E17 instead of E16) (Angevine Jr, 1965) and, similarly to CA3 pyramidal neurons, migrate transversally along the future *stratum oriens*/*alveus* to the prospective DG area (Bayer, 1980a, Bayer, 1980b). These neurons establish a secondary proliferation area in the hilus of the DG which persists in the area during the entire granule cell neurogenesis period (Altman and Das, 1966, Altman and Bayer, 1990a). Rat pups are born with around 15% of the total amount of granule cells (Altman, 1966), and granule cell neurogenesis carries on after birth. In fact, it is one of the two brain areas with persistent neurogenesis in adulthood in

both rodents (Kempermann et al., 1997) and humans (Eriksson et al., 1998). At postnatal day (P) 5 in rodents, the DG contains 50% of normal adult granule cells, 5-10% of which is generated after P18 (Bayer, 1980b). This increase in number of granule cells is accompanied by a proportional decrease in cell number in the hilar region (Seress, 1977). This results in the DG lamination occurring from superficial/marginal area (the hilus) towards radially deeper areas (the ventricular area, prospective molecular layer).

Before the neurogenesis of hippocampal principal neurons (before E16), the prospective HF and PHR, like the rest of the brain, is invaded by migrating neurons arising from both the medial and lateral ganglionic eminences of the brain (Anderson, 1997). Neurons arising from both eminences will give rise to all types of interneurons found in these areas (for reviews on this subject see Marin and Rubenstein (2001) and Wonders and Anderson (2006)). Interneurons reach the prospective HF and EC areas between E13 and E18 (Amaral and Kurz, 1985b, Pleasure et al., 2000). The proper morphological development of neuronal dendrites in all hippocampal-related fields can terminate at various ages – for instance, interneurons develop their dendrites up to P20 (Lang and Frotscher, 1990), whereas CA1 dendritic arborization is fully mature only at P90 (Pokorný and Yamamoto, 1981).

Neuronal migration and axonal pathfinding for both pyramidal cells and interneurons, is a process heavily reliant on a panoply of signaling pathways. Some of these include semaphorin, ephrin, and Slit/Robo signaling pathways (Skutella and Nitsch, 2001) as well as extracellular matrix components (Forster et al., 1998). Another very important morphogenic agent in cortical development are the Cajal-Retzius (CR) cells. These reelin producing and secreting neurons serve various functions during hippocampal morphogenesis. They exist in higher quantities in the DG's molecular layer, as well as the *lacunosum-moleculare* and molecular layer of CA fields and Sub, respectively, thus creating a reelin gradient along these fields (Stanfield and Cowan, 1979) – this is also true for the neocortex, where the plexiform LI is reelin-rich (Frotscher, 1997). As a result, cells being generated at the opposite end of this reelin gradient, migrate radially and arrest their translocation as the reelin concentration increases, creating the lamination observed in both HF, PHR and other cortical areas (Frotscher, 1997, Frotscher, 1998). The CR cells thus play a critical role in late embryonic hippocampal morphogenesis (Stanfield and Cowan, 1979, D'Arcangelo et al., 1995, Hirotsune et al., 1995).

These same developmental signaling pathways and CR cells are also responsible for axon guidance. Once the axon is directed to its target region, axon terminals need to recognize the appropriate neuronal targets, and then generate synaptic contacts. The

combination of the attractive and repulsive signals in the target regions allow for appropriate axon guidance across considerable distances in the brain. In the mouse, PP axons coming from the EC arrive in the hippocampus at E15, and at the molecular layer of the DG at E17 (Super and Soriano, 1994). Studies in rat have shown that this is achieved by an early-formed CR cell projection from this layer to EC, which acts as a scaffold through which EC axons travel (Ceranik et al., 1999). Also in the rat, EC axon terminals in the DG demonstrate adult-like layer-specific termination patterns around P3, while spines are only observed at significant levels at around P12 (Loy et al., 1977, Fricke and Cowan, 1977). Given the late development of granule cells, mossy fiber axons are only observed in the *stratum lucidum* of CA3 at P3 (Amaral and Dent, 1981). At P9, CA3 neurons present fully developed synaptic contacts, but only at P21 do these fibers seem adult-like (Amaral and Dent, 1981). Schaffer collateral projections from CA3 to CA1 can be observed in the presumptive *radiatum* at E18, but spine maturation is only observed in the early postnatal days (Super et al., 1998). Commissural projections inside the HF appear to develop later, starting in the early postnatal days when previous connections have been established (Super and Soriano, 1994). Lastly, studies characterizing early postnatal features of subicular projections are lacking. The earliest study regarding Sub connectivity is that of O'Reilly et al. (2013), where projections from Sub to other PHR regions was assessed from P7 onwards. This study found that the topography of Sub projections to EC was already established by P7, but that both pyramidal neuron dendritic and axonal densities were underdeveloped, with axonal terminals still showing growth cones. Throughout the early postnatal period, subicular efferent fibers and terminal arborizations in PrS, PaS and EC increase in density, reaching adult-like levels by P19.

Chapter 2 Physiology of the Spatial Cognitive Map

Understanding the anatomy of the regions involved in spatial cognition is a first step into understanding how the cognitive map works. This following chapter will be devoted to detailing the electrophysiological aspects hippocampal regions and of the different spatially-tuned neurons they harbor.

2.1 Electrophysiology at the population level

Extracellularly placed electrodes can record voltage differences in their vicinity caused by current flowing in and out of dendrites and or somas. In this way, the electrodes record what is called a Local Field Potential (LFP), or its spatiotemporally smoothed version, the Electroencephalogram (EEG) (Buzsaki et al., 2012). This method has been used to characterize the population activity of neurons within and outside of the HF and PHR. It was using this method that Vanderwolf (1969) described three EEG patterns in the rat hippocampus: cyclic theta activity, large irregular amplitude (LIA) activity and small irregular amplitude (SIA) activity. Further work, has shown that six distinct EEG patterns can be observed in the hippocampus of behaving rats: theta (6-10 Hz), beta (12-30 Hz), gamma (30-100 Hz), and ripple (100-200 Hz) rhythmic waves; LIA and SIA as non-rhythmic waves. Some patterns do co-occur, but theta, LIA, and SIA are mutually exclusive, and they represent different hippocampal states. Rhythmic waves, with the exception of ripples, are associated with voluntary movement, while LIA, SIA, and ripples are associated with resting states (Whishaw and Vanderwolf, 1973, Buzsaki, 1986, Buzsaki et al., 1992).

Theta is the highest amplitude oscillation that can be recorded throughout the whole of the HF and PHR (Vanderwolf, 1969, Mitchell and Ranck Jr, 1980, Buzsaki, 2002, Anderson and O'Mara, 2004). The oscillation frequency ranges between 4-12 Hz and depends on several factors such as behavioral state (Whishaw and Vanderwolf, 1973), running speed (Sławińska and Kasicki, 1998) or age (Leblanc and Bland, 1979, Wills et al., 2010). This rhythm is generated in the medial septum/diagonal band of Broca (Lawson and Bland, 1993) and is fed to the hippocampal areas via the septohippocampal projections. It is though that the cholinergic projection depolarizes both principal and inhibitory cells throughout the hippocampal fields, while the septohippocampal GABAergic projections are responsible for rhythmic inhibition of hippocampal interneurons (Buzsaki, 2002, Freund and Antal, 1988).

Other types of population activity can have different roles at the network level. Sharp Wave (SPW) oscillations are a type of LIA which occurs during rest periods or immobility (Buzsaki et al., 1983). These are generated in CA3 in restfulness and CA2 in immobility periods, and are thought to entrain the activity of other hippocampal pyramidal neurons assemblies were active while the animal was engaged in a behavior (Buzsaki et al., 1983, Oliva et al., 2016). As a consequence, CA1 neurons fire a volley of action potentials at 150-200 Hz frequency, creating the ripple EEG pattern (Buzsaki et al., 1992). Up until P7, SPWs represent the most common type of oscillatory activity in the HF, already being quite similar to adult ones as well (Leinekugel et al., 2002, Karlsson et al., 2006, Mohns et al., 2007). These events increase in amplitude and decrease in width, reaching adult-like levels at P18 (Mohns et al., 2007). Ripples on the other hand, can only be observed with adult-like consistency at P14 (Mohns et al., 2007).

2.2 Single-Unit Activity

Extracellular single-unit recordings have also been used to characterize the behavioral correlates of the firing of single neurons. The development of multiple microelectrode recordings allowed the isolation specific neurons in the extracellular space surrounding the tip of these electrodes (Mcnaughton et al., 1983). As a result, the physiology of hippocampal neurons and their roles within the spatial cognitive map could be better understood.

One of the issues with this type of recording, is the inability to distinguish between principal and inhibitory action potentials. Thus, examining recorded neuronal waveforms has become a long-standing method to differentiate between both excitatory and inhibitory recorded cells. CA1 pyramidal neurons' action potentials can cluster into complex burst spikes, comprising 2-6 action potentials with decreasing amplitude and inter-spike intervals of less than 6ms (Ranck, 1973, Fox and Ranck, 1975, Harris et al., 2001b). Compared to interneurons, pyramidal neurons also tend to show wider waveforms – measured from the peak to the trough of the spike – than interneurons (the latter ones having a duration of 0.2-0.4ms, while the former neurons have 0.4-1ms duration) (Somogyi and Klausberger). Additionally, interneurons tend to have much higher firing rates (30-100 Hz) than pyramidal neurons (<20 Hz) (Ranck, 1973).

2.2.1 – Spatially Modulated Neurons – Place Cells

As discussed earlier in this chapter, the breakthrough discovery of place cells forever changed our view of the hippocampal-associated areas. The name attributed to these neurons derives from the observation that these fire volleys of action potentials whenever the animal (a rat in the case of O'Keefe's experiments) occupied a particular location in the environment (see Figure 2.1) and not anywhere else (O'Keefe and Dostrovsky, 1971, O'Keefe, 1976). The unique firing location that corresponded to the cell's receptive field was thus named 'place field', and the neuron 'place cell' (O'Keefe, 1976). Since then, and even though they are more commonly found in CA1 (O'Keefe and Dostrovsky, 1971), place cells have also been described in the DG (Jung and McNaughton, 1993), CA3 (Muller and Kubie, 1987), Sub (Sharp and Green, 1994), and EC (Quirk et al., 1992). Due to their complex spike firing pattern (O'Keefe, 1976, Henze et al., 2000) and through 2-photon microscopy calcium imaging studies (Ziv et al., 2013), there is reasonable evidence that place cells are pyramidal neurons. Place fields tend to vary with the shape and size of the environment the animal is in, with fields being randomly scattered throughout the recording environment (Muller and Kubie, 1987). Other reports have shown that place cells tend to cluster nearer to walls (Hetherington and Shapiro, 1997) or in goal locations (Hollup et al., 2001).

Generally, place cells do no exhibit more than one place field in environments smaller than $1m^2$ (Muller and Kubie, 1987, Muller et al., 1987), although for larger environments place cells can display multiple place fields (Fenton et al., 2008). Peak place cell firing

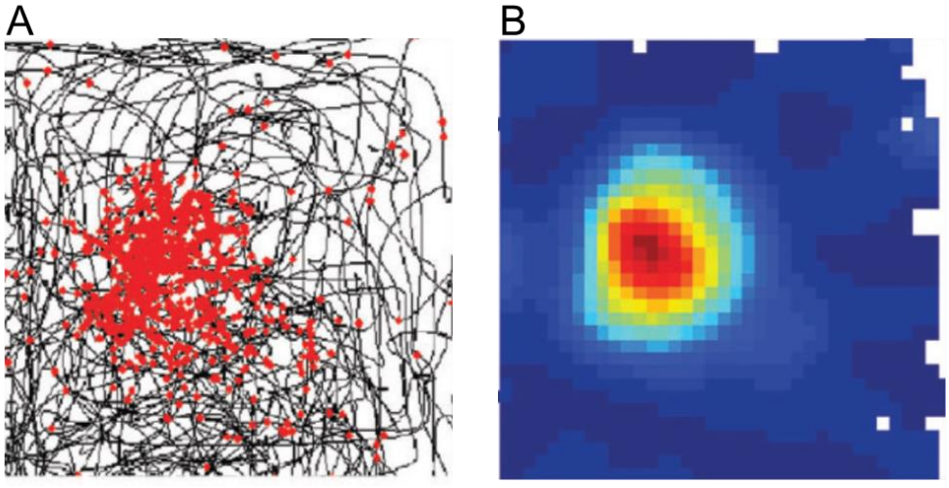

Figure 2.1 – Example of a place cell of the dorsal CA1. (A) The trajectory of the rat is highlighted with the black trace, and the red circles represent spikes fired along the rat's path. By binning the environment into bins of specific sizes and calculating the number of spikes fired and the animal's dwell time in each bin, firing rate maps like the one in (B) are obtained. (B) Color-coded rate map of the cell showed in (A), where red colours indicate higher firing rates, and blue colours lower or absent firing. Image adapted from Moser et al. (2015).

rates (calculated as the average of spikes fired in a spatial bin and dividing this by the time spent in that bin) range from ~40 Hz for a strongly firing cell to 1 Hz for weaker ones (Muller, 1996). However, as the place field is thought of as a two-dimensional Gaussian tuning curve, the firing rate is not uniform throughout the place field. Instead, peak rates are usually observed in the center of the field, while its edges have lower firing rates (O'Keefe and Burgess, 1996). The observed firing rates do not show heading direction dependence in open field mazes, but changes in the geometric properties of the environment can change this omnidirectional aspect. When animals run along linear tracks (narrow corridors), place cell firing becomes dependent on the animals' running direction (Muller et al., 1994, O'Keefe and Recce, 1993).

Linear track place cell recordings also showed that place cells code for location not just through changes in their firing rate, but also through temporal relationship of the cells spike timing and the phase of theta. As the animal crosses the place cell's receptive field, the cell fires at progressively earlier phases of the ongoing local theta cycle (O'Keefe and Recce, 1993), a phenomenon called phase precession. In this way, place cells can code for location both by increasing their firing rate and by phase precessing (Huxter et al., 2003).

Place cell firing can be affected by a host of stimuli, either environmental (sensory stimuli) or internally generated (path integration). It is well established that visual stimuli can and do modulate the activity of place cells (Quirk et al., 1990, Markus et al., 1994, Save et al., 2000), while olfactory cues do not exert such a strong influence (Save et al., 2000). These cues serve as allocentric anchors for place cell firing, meaning that the receptive field of place cells will rely on the stability of sensory landmarks. Several experiments have tested the influence of local (proximal) and global (distal/extra-maze) cues – most commonly, extra-maze cues consist of large white or black cards, as well as the room itself, while local cues correspond to the intra-maze visual patterns, odors, textures and the geometry of the maze. Work by O'Keefe and Conway (1978) has demonstrated that cue configurations of two and more cues the essential determinants of place cell firing. In this work, the authors demonstrated that cue mismatch (achieved by removal) up to a certain threshold (removal of 2 of the total 4 cues) was sufficient to maintain the activity of place cells. But cue mismatch beyond that, lead to more profound changes in place cell firing: changes in the preferred firing location and/or firing rate of the cells (O'Keefe and Conway, 1978). Overall, visual cues tend to exert the strongest influence on place cell activity(Fenton et al., 2000). As observed in subsequent studies, place cells rely on the stability of both local and global cues (Bostock et al., 1991, Hetherington and Shapiro, 1997, Renaudineau et al., 2007). Mismatches between local and global cue

configurations lead to changes in the firing pattern of place cells. Changes to place cell firing pattern include switching on and off, shifts in place field location – both of which are called field remapping (Bostock et al., 1991) – or even changes in firing rate – termed rate remapping (Hayman et al., 2003). How a place cell ensemble remaps depends on the extent of environmental change. Therefore, smaller or less complex changes to cues can lead to 'partial remapping', whereby a subset of place cells remap (Skaggs and McNaughton, 1998, Moita et al., 2004, Knierim, 2002), or with sufficient change to both local and global cues, the recorded ensemble can remap as a whole, causing what has been named 'global remapping' (Leutgeb et al., 2005).

The remapping process observed in CA1 is thought to reflect two neuronal computing processes: pattern completion and pattern separation. Due to the extensive collateralization of CA3 pyramidal neurons, David Marr (1971) proposed that this region could be able to fill-in degraded or incomplete representations (either spatial or mnemonic) and transmit that information to CA1 neurons – pattern completion. On the other hand, with sufficiently different input (sensory or otherwise) transmitted via the PP pathway, EC excitatory input can drive both DG granule cells and CA3 neurons to perform pattern separation, allowing the distinction between two representations (Marr, 1971, Rolls, 1996, Leutgeb et al., 2007, Leutgeb and Leutgeb, 2007, Yassa and Stark, 2011, Hunsaker and Kesner, 2013). Studies in rodents have since demonstrated that place cell networks possess characteristics common to auto-associative networks. Wills et al. (2005) showed that place cells coherently responded as a whole by remapping between two differently shaped environments (a circle and square). When presented with environments whose shape changed gradually from one form to another, the place cell network always responded as if the environment was a circle or a square, not changing its firing patterns for intermediate forms. These results suggest that CA1 networks transition from one state of activation, representing one environment, to another state as the environment changes, *i.e.* CA1 acts like an attractor network (Marr, 1971, Wills et al., 2005). Attractor network is a concept derived from mathematical models that describes dynamic systems in which all interacting units (neurons in this case) evolve to stable states, with transient perturbations (inputs) momentarily altering the system and driving it towards another stable state (Wang, 2009).

Place cells can be recorded in young rat pups as early as P16 (Wills et al., 2010, Langston et al., 2010). In such young animals, place cell stability and spatial information tend to be lower compared to adult place cells (Wills et al., 2010, Langston et al., 2010). In loose terms, spatial information represents how well we can predict the animal's location in an environment based on the cell's firing, therefore a cell that fires in more

than one location in the environment will have a lower spatial information index (Skaggs et al., 1993). Throughout postnatal development, place cell spatial tuning steadily improves, particularly when GCs mature (which happens around P21) (Wills et al., 2010, Langston et al., 2010, Wills and Cacucci, 2014, Muessig et al., 2015). Additional work also suggests that in pre-weaning animals, place cell accuracy is also positively correlated with the distance of the place field to environmental boundaries (Muessig et al., 2015). These results show that physical boundaries can act as relevant anchoring landmarks for place cell formation and stability. Even though some differences exist between young and adult place cells, from the day place cells emerge it is clear that the hippocampus is able to generate new place codes for novel spatial contexts (akin to pattern separation) and also reactivate familiar place codes with an incomplete set of sensory cues (akin to pattern completion) (Muessig et al., 2016). In conclusion, the place cell system appears to come online at around P16, and with continued growth, it continuously improves its spatial tuning.

Proper place cell firing, as previously discussed, relies on several environmental cues and sensory input. However, a particular type of proprioceptive input provides stability to place maps, namely the animal's orientation. Representation of the animal's heading direction is an essential aspect of the spatial cognitive map, and head-direction cells (HDCs) are responsible for relaying this information to both the HF and PHR.

2.2.2 – Spatially Modulated Neurons – Head-Direction Cells

HDCs, as the name indicates, are cells that fire maximally when the animal is facing a certain direction (Taube et al., 1990a). This preferred firing direction changes from cell to cell, and the whole HDC network therefore covers the whole range of possible head orientations. These cells were firstly discovered by Ranck Jr (1984), and their properties formally described in later publications (Taube et al., 1990b, Taube et al., 1990a). By recording from the dorsal PrS, the authors understood that these cells' preferred firing direction, much like place cells, relies on allocentric cues, *i.e.* a cell will fire when the animal faces a specific direction relative to a configuration of cues, meaning that the cell's preferred firing direction will 'remap' in a different environment (Taube et al., 1990b). Additionally, rotations of a salient visual cue in a cue-controlled environment (CCE) – which is acting like an anchoring landmark – will trigger HDC firing direction rotation proportional to that of the cue (Taube et al., 1990b). In a stable environment, the directional response, peak firing rate and directional firing range can be stable over weeks or months (Taube, 2007).

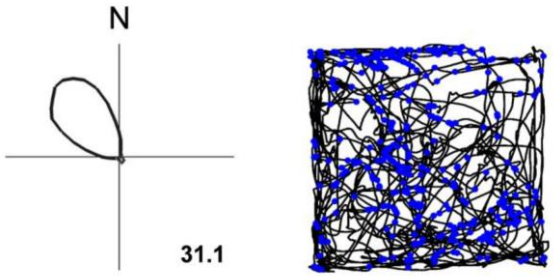

Figure 2.2 – Example of a HDC recorded in the ADN. This HDC (courtesy of Dr D. Overington), can be represented by a polar plot showing a clear 'preferred firing direction' towards the North-West of the environment (left). The peak firing rate of the cell is noted in the bottom right of the polar plot, in Hz. Unlike place cells, HDC firing does not show a particular spatial correlate as observed in the spike map (right).

Besides the septal PrS, HDCs have also been shown to exist in several other cortical and subcortical areas. The cortical regions include: retrosplenial cortex (Chen et al., 1994, Cho and Sharp, 2001), MEC (Sargolini et al., 2006) and PaS (Boccara et al., 2010). Subcortically, HDCs are found in: the lateral mammillary nucleus (Blair et al., 1998, Stackman and Taube, 1998) the dorsal tegmental nucleus of Gudden (Sharp et al., 2001) and the anterior thalamic nuclei (Taube, 1995, Tsanov et al., 2011). All of the HDC containing regions are interconnected, with an allothetic sensory and static information stream from cortical areas converging with idiothetic vestibular and motor input arising from thalamic structures (Bassett and Taube, 2005). The converging structures are the dorsal tegmental nucleus and lateral mammillary nucleus, and together they are thought to generate the HDC signal that reaches the anterodorsal nucleus in thalamus (ADN) (Bassett et al., 2007). Subsequently, this thalamic region feeds the head-direction (HD) information into PrS – and to PaS as well (Clark and Taube, 2012) –, as shown by lesion studies in the ADN which abolish HDC activity in the septal PrS, while lesions in the latter structure decrease ADN's HDC accuracy (Goodridge and Taube, 1997). The referred decrease in accuracy is the result of decreased directional firing range of individual HDCs (*i.e.*, the cells maintain their directionality but their preferred directional range increases). This decrease is accompanied by a lower dependence on visual landmarks, as well as an increase of the quality of HDC firing in predicting future HD (Goodridge and Taube, 1997). From the septal PrS, the HDC signal makes its way into the MEC, which then carries it to the HF (Clark and Taube, 2012). This makes the septal PrS and PaS the HD signal gateway into the hippocampal-associated areas of the brain.

Similarly to place cells, HDCs respond to a variety of allothetic cues – allothetic, just as for allocentric, refers to places or locations outside the self. The majority of HDC studies have established that visual cues represent important anchoring stimuli, something that was assessed through cue rotation manipulations (Taube et al., 1990b), with distal cues being favored as potential anchoring landmarks relative to proximal ones (Zugaro et al., 2001). Additional work has also shown that olfactory cues, but not auditory ones, can serve as orienting cues for the HDC network, with rotations of olfactory stimuli triggering

comparable rotational changes to HDC preferred firing direction (Goodridge et al., 1998). Idiothetic cues are also necessary to proper function of the HD system (Yoder et al., 2011). Besides vestibular input (Stackman et al., 2002), motor cues (motor efference copy, motor command signals, and proprioceptive signals) (Taube et al., 1990b, Taube, 1995, Shinder and Taube, 2011), and, in the absence of either of the previous cues, optic flow (Stackman et al., 2003, Shinder and Taube, 2011), are necessary for the proper activity of the HD system.

Unsurprisingly, the HD signal seems to be a necessary component for the stability of the cognitive map. Lesions to dorsal PrS or any HD area upstream of it, lead to place field instability (manifested by poor cue control) (Calton et al., 2003, Goodridge and Taube, 1997) and abolition of grid cell firing (Winter et al., 2015). Additionally, simultaneous recordings of place cells and HDCs have shown that, when animals are disoriented, both cell types will always rotate in unison (Knierim et al., 1995).

HDCs are the most precocious spatial cell type, being recorded dorsal PrS, PaS, and ADN as early as P11/P12, roughly 2/3 days before eye opening (Tan et al., Bjerknes et al.). Even though directional cells can be recorded before the appearance of patterned vision, the signal displays low directional information and directional selectivity (Tan et al., 2015). After eye opening (usually between P14/P15 in the rat), the cells mature quickly in all the recorded structures, becoming stable within trial and across trials (Bjerknes et al., 2015, Tan et al., 2015), and showing adult-like stability and quality by P16 (Wills et al., 2010, Tan et al., 2015, Bjerknes et al., 2015). Before eye opening, HDCs lack directional preference, resulting in drifting of their directional firing within trials. This drift is coherent among the HDC population – the HDCs maintain their firing directions relative to each other, drifting together (Bjerknes et al., 2015). This means that the attractor network that HDCs belong to has directional representation before eye opening, and the emergence of ‘reliable’ visual input may allow the network’s directional selectivity to anchor itself to the real world landmarks. However, local tactile cues, such as boundaries, can stabilize the HDC activity before eye-opening provided that these are in close proximity (Bassett et al., 2018).

2.2.3 – Spatially Modulated Neurons – Boundary Vector Cells

Manipulation of visual cues, as detailed in previous sections, has always proved successful in altering the firing patterns of place fields and directional preference of HDCs. In addition to this, work by O'Keefe and Burgess (1996) showed that the geometry of the environment also plays a role in shaping the receptive field of CA1 place cells. In

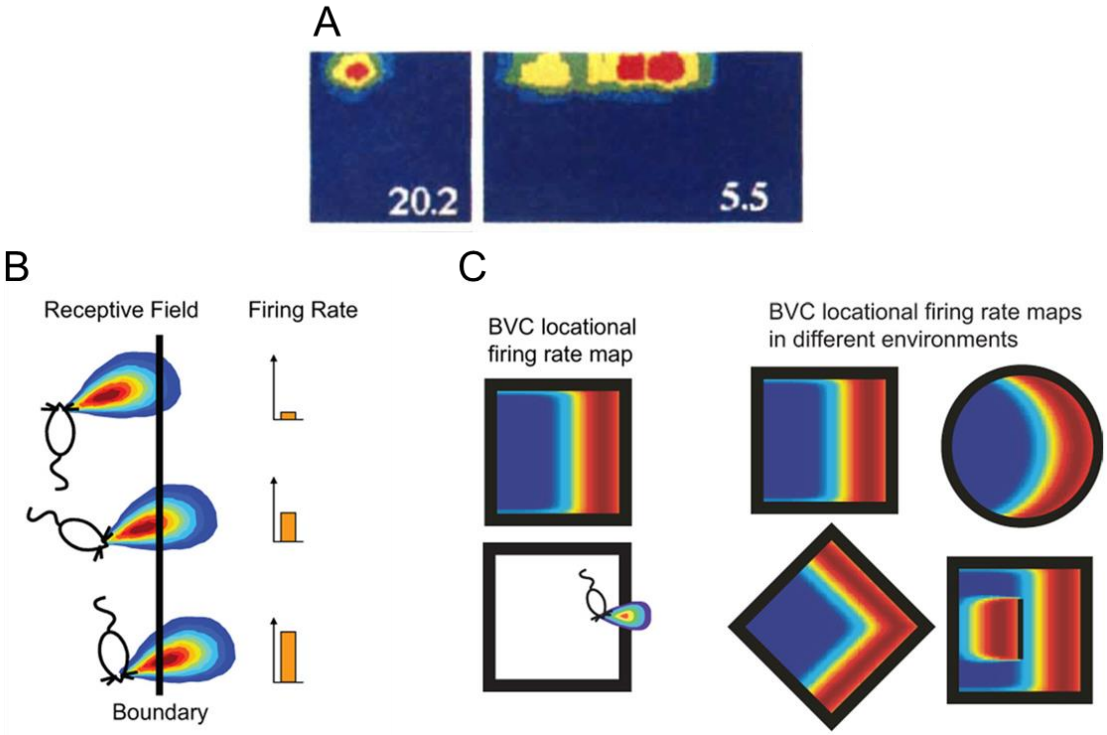

Figure 2.3 – Effect of boundary extension on place cell firing and the boundary-vector model. (A) Example of the rate map of recorded place cell from the work of O'Keefe and Burgess (1996). The place cell was first recorded in a square environment (right) and then recorded in the same environment after wall extension. As a result, the place field of the cell extended parametrically along the extended environmental axis. GCs in the EC also rescale in response to similar environmental manipulations (Barry et al., 2007). (B) Prediction of a BVC receptive field based on the Hartley et al. (2000) model. A BVC receptive field will have a preferred firing distance and allocentric bearing (preferred allocentric firing direction) form any given boundary. As a boundary enters the cell's receptive field, the firing rate of that cell will increase according with the receptive fields preferred tuning distance and bearing. (C) Prediction of the rate maps of a particular BVC in a particular environment (two left panels, with a receptive field shown in the bottom left panel), and the prediction of the of the cells firing across different environments (4 panels on the right). Images B and C are adapted from Lever et al. (2009). The extension of BVC firing observed in A can be explained by the existence of boundary coding neurons with the properties described in B and C.

this experiment, the authors extended the dimension of the recording arena in one of the two possible dimensions, which often resulted in the extension of the place cell's receptive field or revealed a secondary firing location (see Figure 2.3A). This demonstrated that the peak firing rate of recorded place fields was computed relative to the distance to environmental boundaries, such as walls (O'Keefe and Burgess, 1996). These results led the authors to propose that place field formation relied on inputs functionally equivalent to broad Gaussian tuning curves with peaks at specific distances from anchoring cues (O'Keefe and Burgess, 1996, Burgess and O'Keefe, 1996).

Additional evidence for this came from experiments where barriers were introduced into the middle of a recording arena, resulting in the doubling of place fields on either side of the barrier (Barry et al., 2006). Building on this model, Hartley et al. (2000) proposed that a place field could be the result of the thresholded sum of firing rates of neurons tuned to respond to environmental boundaries located at a particular distance and allocentric direction from the rat. These putative neurons were thus called boundary vector cells (BVCs), alluding to their directional and positional properties (Hartley et al., 2000). A boundary, in this context, can be defined as anything that constitutes an obstacle to locomotion, such as a wall, a large obstacle, or a drop on the edges of high standing structure.

Following the previous theoretical work, boundary-responsive cells were then found in the rat MEC (Savelli et al., 2008) and Sub (Barry et al., 2006, Lever et al., 2009). The recorded subicular neurons with boundary-related firing presented typical principal cell waveforms (Lever et al., 2009), although a few short waveform neurons showing BVC-like properties have been recorded since (Stewart et al., 2014). Furthermore, boundary-responsive firing from principal cells was recorded from both bursting and regular-spiking neurons in septal Sub. Bursting BVCs not only presented higher mean firing rates, but showed deeper theta modulation than regular-spiking BVCs (Lever et al., 2009). The original model (Hartley et al., 2000) proposed that BVCs would have continuously variable tuning distances from any given boundary, but the actual *in vivo* data showed that BVCs are biased towards shorter distances (Lever et al., 2009). Further work then showed that the fewer cells with larger fields can also be described as having an inhibition field along a boundary. This type of BVC is thus called 'Boundary-Off Cell' since the cell becomes silent whenever the animal is at the cells' tuning distance (Stewart et al., 2014). Other work has then demonstrated that boundary coding neurons can also be observed in the claustrum, along with other types of spatial neurons (including object cells), meaning that this brain area may receive

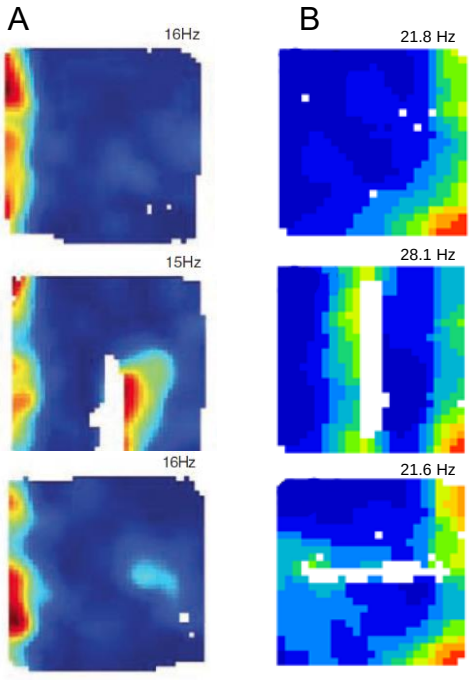

Figure 2.4 – Examples of boundary coding neurons. (A) Example of a border cell recorded from the EC of adult rats (adapted from Solstad et al. (2008). (B) Example of a BVC recorded from the rat Sub by the author. All cells fire along a specific boundary at an allocentric direction (West wall in A and East wall in B), and the firing fields double upon the insertion of a barrier (trials in the second row).

subicular/entorhinal input and then further output it to other cortical regions (Jankowski and O'Mara, 2015).

As predicted, BVC firing fields depend on the distance and allocentric direction from a boundary in the local environment, resulting in the field's long axes taking the curvature of the environment's geometry. Unlike place cells, a BVC's receptive field is independent of the kind of boundary upon which the cell is acting on – changing the boundary from a wall to a drop does not cause BVCs to remap, instead they maintain their firing location. BVC receptive fields are also quite robust across environments, *i.e.* they tend to maintain their preferred tuning distance and direction. Even in the dark, BVCs maintain their firing fields (Lever et al., 2009)– meaning that the visual component is not necessary for their firing –, while place cells in the above-mentioned manipulations tend to remap (Quirk et al., 1990). Another very important prediction of the Hartley et al. (2000) model is that the insertion of second boundary perpendicular to the cells tuning direction will result in the doubling of the BVC firing field. Real BVCs responded exactly as predicted, doubling both when a barrier oriented appropriately is inserted into recording arena, and when a navigable drop between two platforms is created between two previously joined platforms (Lever et al., 2009). Boundary-Off cells, in the presence of the barrier, have their inhibition fields doubled (Stewart et al., 2014).

BVCs are thought to code for the presence of boundaries at a particular allocentric position, but are independent of the animal's heading direction. For instance, a BVC can fire whenever the animal is 5 cm away from a boundary placed in the south of the enclosure, regardless of the direction the animal is facing. Consistent with this, HDCs show higher directional information rates (in bits per second) than BVCs, and mutual information estimates between firing rate and location are also higher than between firing rate and direction (Stewart et al., 2014).

As alluded to, prior to the discovery of subicular BVCs, a subset of boundary coding neurons had already been described in the EC (Savelli et al., 2008, Solstad et al., 2008). These neurons, appropriately called border cells, show quite narrow tuning distances, exhibit field doubling when a barrier is inserted in the environment, and persisted in conditions that usually lead to place cell remapping. Although border neurons can be found throughout all layers of the EC, they make up roughly 10% of total recorded population of neurons (Solstad et al., 2008). Subicular BVCs on the other hand, represent around 24% of the recorded cells in that region (Lever et al., 2009). Given that Sub harbors a larger number BVCs and that Sub projects to the EC, entorhinal border neurons could rely on the subicular input to generate the observed boundary signal.

Considering their potential relevance in stabilizing place cell firing (Hartley et al., 2000), and given that place cells can be recorded in animals as young as P16 (Wills et al., 2010), BVCs ought to mature at similar ages. Recent work on entorhinal border neurons has shown that these can be recorded in animals as young as P16/P17 with adult-like stability (Bjerknes et al., 2014). Moreover, given that before weaning age place cells exhibit more stable and accurate representation of space closer to environmental boundaries, it is possible that border neurons (and possibly BVCs) could be providing anchoring input to CA1 place cells (Muessig et al., 2015). However, nothing is known about early postnatal subicular BVCs. This represents one of the main questions the work in this thesis addresses: 'How early can subicular boundary vector cell activity be detected and how does it develop in young rats?'.

2.2.4 – Spatially Modulated Neurons – Grid Cells

Given that the EC constitutes a major input into the HF, it had been a long standing hypothesis that this brain region would also harbor spatially modulated neurons. Quirk et al. (1992) presented the first report of location tuned neurons in the superficial layers of the MEC, which resembled place cells with weaker spatial modulation. A decade after that, with better technology and systematic approach to MEC recordings, the Moser lab discovered grid cells (GC) in layers II and III of this brain area (Fyhn et al., 2004, Hafting et al., 2005). They defined GCs as having multiple tessellating firing fields, forming a hexagonal grid with a firing field at each vertex (see Figure 2.5). Because of its regularity – the firing fields are equidistant and equiangular –, GCs can be described by the distance between firing peaks (wavelength/grid scale), the angular separation of the firing fields (which is approximately 60°), and the location of the grid vertices within an environment (phase). Within a familiar environment, all of the above-mentioned GC features remain stable. Within the same familiar setting, expansion of the recording environment reveals additional firing fields, meaning that GCs could be representing abstract space and are not confined to a particular geometric enclosure (Hafting et al., 2005). Given their

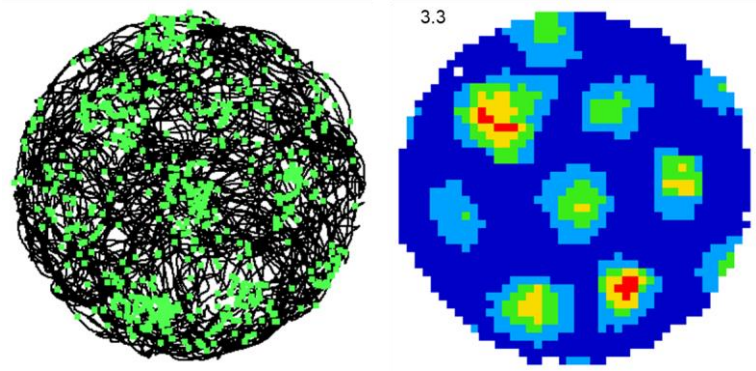

Figure 2.5 – Example of a MEC grid cell. Example of a single GC recorded in the rat MEC by the author. Both the spike map (left) and the rate map (right, with the peak firing rate in Hz on the top left side of this image) show the symmetric organization of the equidistant firing fields of this one cell, which organize a hexagonal grid.

apparent stability and regularity, GCs were thus thought to represent a metric of space (Moser and Moser, 2008), an important component in path-integration-based navigation. In fact, lesion studies showed that the MEC is essential for rodents to successfully complete path-integration tasks (Van Cauter et al., 2013, Jacob et al., 2017). GCs were then found in PrS and PaS (Boccara et al., 2010), while deep layers of the MEC as well as PrS and PaS harbor GCs that also code for direction, called conjunctive cells (Sargolini et al., 2006, Boccara et al., 2010). Anatomically, GCs are thought to be LII principal MEC neurons, both stellate and pyramidal in shape (Domnisoru et al., 2013, Schmidt-Hieber and Hausser, 2013). Additionally, along the MEC dorsomedial-ventrolateral axis, GC properties change: increasingly more ventral MEC areas have GCs with larger firing fields and scale (Hafting et al., 2005). Moreover, this increase is not continuous, as GCs in close proximity (within a module) will share similar properties (except the phase), while non-overlapping GC modules will have distinct scale and orientation, with ventral modules having larger scales than dorsal ones (Barry et al., 2007, Stensola et al., 2012).

Models of grid cell formation theories suggest that these MEC cells integrate speed and direction signals provided by local HDCs (Sargolini et al., 2006) to form the grid-like firing pattern. Sensory information is then used to adjust grid-like firing or correcting the cumulative error which comes from integrating speed (Burgess et al., 2007, Fuhs and Touretzky, 2006, McNaughton et al., 2006, Moser et al., 2008). The existence of border cells (Solstad et al., 2008) and HDCs (Sargolini et al., 2006) in the MEC – border cells being present throughout the MEC, while HDCs occur predominantly in the deep layers – gave further strength to this idea. Given the PP projection to several HF subfields, it was also hypothesized that hippocampal place cell representations could be the product of GC input, with place cell peak representations corresponding to locations where most of contributing GCs are in phase (O'Keefe and Burgess, 2005, Fuhs and Touretzky, 2006, McNaughton et al., 2006, Solstad et al., 2006, Moser et al., 2008). This represented a plausible idea, especially considering the apparent incorruptible geometry of GC firing.

However, further studies that focused on dissecting the role of GCs in wider navigation as well their relationship with other spatially tuned neurons, shed light on the factors underlying the stability and regularity of the grid firing pattern. For instance, drastic changes to the environment where the animal is being tested, lead to the temporary expansion of GC firing fields which lasts days, with cells reversing back when the animal becomes familiar with the environment. Co-recorded place cells also show remapping during the familiarization/grid expansion period (Barry et al., 2012). Moreover, not only

does GC firing rely on theta rhythm imposed by septal input (Brandon et al., 2011, Koenig et al., 2011), but it also requires input from CA1 and ADN, and thus GC firing likely requires both place cell and HDC input, respectively (Bonnevie et al., 2013, Winter et al., 2015). Additionally, MEC lesions (Van Cauter et al., 2008) or inactivation via chemogenetics (Miao et al., 2015) show that place cells, although unstable, do not require GC input.

Developmental studies also corroborate these findings, as GCs emerge only after weaning (P21) (Wills et al., 2010), while place cells, HDCs, and border neurons can be recorded much earlier (Wills et al., 2010, Bjerknes et al., 2014). Unlike place cells, GC firing is much more adult-like from the day they are first recorded and undergo little change from there on after (Wills et al., 2010). Interestingly, the maturation of spatial cell types within the hippocampal formation, with the exception of HDCs, seems to follow the proximal-distal transverse axis organization of the hippocampus, with HF spatial cells maturing first and entorhinal GCs coming online much later. Most of the studies on the maturation of the hippocampus have primarily assessed changes in the electrophysiological properties this brain structure. One of the few studies that explored the molecular modifications associatied with postnatal development, evaluated changes in doublecortin in neurons. Doublecortin is a microtubule-associated protein that is present in neuronal precursors and immature neurons (Gleeson et al., 1999, Nacher et al., 2001). Doublecortin expression is firstly reduced in LII cell at around P14. Then, through neuronal activity, doublecortin negative MEC LII cells lead to the sequential decrease of this protein's expression along the direction of information flow in the hippocampus, *i.e.* DG → CA3 → CA1 → Sub → EC, with the last two regions reducing doublecortin expression at age P26 (Donato et al., 2017). This study thus linked postnatal electrophysiology studies with molecular changes in the whole of hippocampus, showing how sequential neuronal activity may play an important role in establishing proper connectivity and hierarchy within the HF and PHC (Donato et al., 2017, Cacucci et al., 2017). This is the only study thus far that has functionally linked molecular and electrophysiological neuronal changes during postnatal maturation of the hippocampus. The apparent incongruence between the earlier maturation of the EC and late emergence of GCs further demonstrates the potential importance of the functional maturation of hippocampal inputs for GC firing.

The environment's geometry and boundary information are also factors that appear to play a key role GC firing. Besides the existence of MEC boundary coding neurons, recent work demonstrates that boundaries do play a key role in stabilizing GC firing patterns. As GCs integrate speed and direction signals, barriers, similarly as to what has been

hypothesized for place cells, can constitute stable landmarks that help correct for accumulated error along time and distance travelled by an animal (Hardcastle et al., 2015). Moreover, recent work has shown that GCs rely on specific geometric reference points for firing field alignment, and changing an environment's shape into more unusual geometries (trapezoids and sheared squares) leads to GC distortions and asymmetry (Stensola et al., 2015, Krupic et al., 2015). This is in register with previous experiments which have shown that introduction of asymmetries in previously symmetric environments (transforming a square environment into a rectangular one) leads to parametric deformations of grid cell fields (Barry et al., 2007). Moreover, since BVCs are thought to represent important inputs for place cell firing (O'Keefe and Burgess, 1996, Hartley et al., 2000), and that the Sub – the boundary coding center of the hippocampus – gives rise to a major EC afferent, it is possible that GCs require BVC for phase stability and grid alignment. However, the relationship between boundary coding neurons, either entorhinal or subicular, and GCs is poorly understood. This is the second main goal that drove the work presented in this thesis. To put it in simpler terms: 'How does BVC firing inhibition affect GC firing in adult rats?'.

2.2.5 – Other spatial cell types without spatial correlates

In the rhinal cortices, other types of navigation related cells can be found. These are object cells (Deshmukh and Knierim, 2011) and speed cells (Kropff et al., 2015). Neither of these cell types have particular spatial correlates. Object cells, as suggested by the name, respond to the presence of objects in the environment, coding for their location, displacement or novelty (Deshmukh and Knierim, 2011). This particular type of object encoding occurs in both the LEC (Deshmukh and Knierim, 2011) and PER (Deshmukh et al., 2012). Object cells may also display some mnemonic features, as removal of objects after an initial exposition leads to firing of LEC neurons in the locations of the removed objects in subsequent trials (Tsao et al., 2013). The fact LEC and PER appear to be responding to objects present in an environment, it has thus been hypothesized that LEC and MEC are involved in the encoding of different features of the spatial scene: the LEC may encode positional information of elements present in an environment, while the MEC may be involved in the determination of self-position through allothetic cues (Knierim et al., 2014).

Speed cells, as the name suggests, encode the animal's speed by monotonically increasing their firing rate as the animal's speed increases (Kropff et al., 2015). This particular type of neuron was recorded in the MEC of behaving rats, and their firing was not necessarily theta modulated – a surprising finding considering that the amplitude and

frequency of theta oscillations, which are generated in the medial septum, is tightly linked with running speed (Sławińska and Kasicki, 1998). In all recorded speed cells, firing was independent of environmental context and visual input (Kropff et al., 2015). Further work has then proposed that one of the likely origins of entorhinal speed signal is the medial septum, which likely sends locomotion velocity information via glutamatergic projections aimed mostly at pyramidal and stellate cells of the MEC (Justus et al., 2017).

Chapter 3 General aspects of rodent postnatal development

The previous chapter described the components of the spatial cognitive map, as well as its postnatal maturation. Since part of the work of this thesis involved young rats, it is important to understand developmental aspects, both physiological and behavioral, of these animals. Rats are altricial animals, as they are born with rather premature features, and acquire adult-like features and behaviors over a protracted period, lasting until 3 months of age. During this period of time, the spatial cognitive map, as well as other brain regions, also mature until reaching adult-like states/performances. Thus, this chapter aims to briefly describe the developmental timeline and milestones of the hippocampal-dependent behaviors and sensory-motor development in rats. A summary of all the postnatal developments of the traits discussed in this chapter can be found in Figure 3.1.

3.1 General behavior and locomotion

For the first 10 to 14 days, a young rat nurses and sleep in the litter huddle (Bolles and Woods, 1964, Gerrish and Alberts, 1996, Loewen et al., 2005). In this period of time, the animals are only capable of performing relatively simple motor behaviors: righting at P0, *i.e.* rotating back into a quadrupedal position when turned on their backs; pivoting, which is the results of the animal moving its forelimbs while the hindlimbs are inactive; crawling, which can be observed from middle of first week; and walking, which can be observed from P10-P14 initially, fully maturing by P21 (Bolles and Woods, 1964, Altman and Sudarshan, 1975).

Also in the third week (P14-P21), young rats start exhibiting a variety of social behaviors, such as play-fight and social grooming (Bolles and Woods, 1964, Thiels et al., 1990). They also start showing interest in solid food at this stage, but carry on nursing until weaning (Bolles and Woods, 1964, Thiels et al., 1990). In the laboratory environment,

weaning is induced at P21 (Bolles and Woods, 1964, Moye and Rudy, 1985, Schenk, 1985), but this does not reflect the behavior in the wild, as rats can continue to suckle until P34 (Thiels et al., 1990).

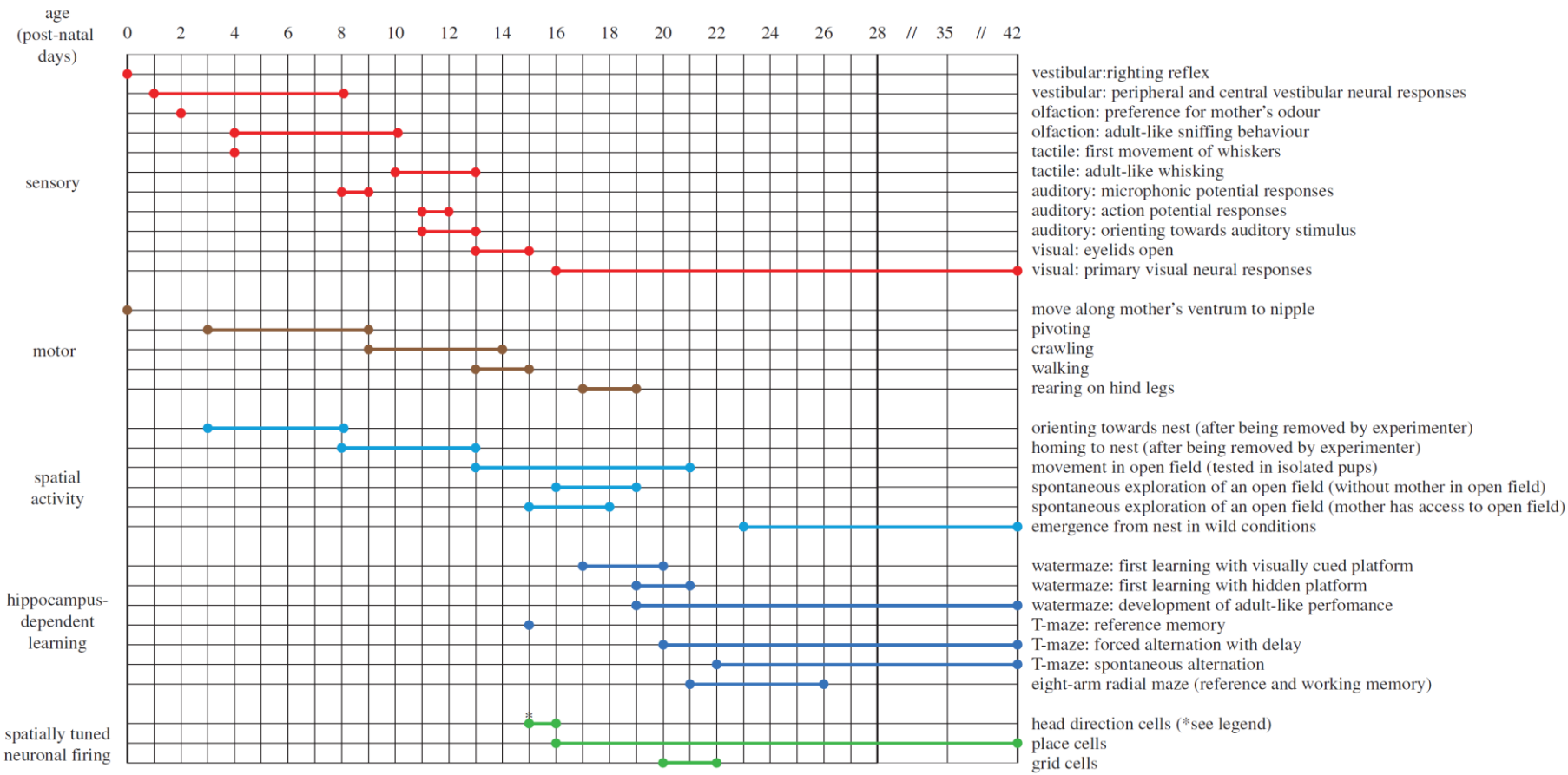

Figure 3.1 – Summary of postnatal developmental milestones of sensory and motor systems, spatial and hippocampus-dependent behaviors, as well as the emergence of spatially tuned neurons. Each horizontal line corresponds to the developmental timeline of a particular trait (indicated on the right) across postnatal days (on top). The bold circles mark the beginning and end of the development of each of the traits. The single circles indicate the existence of the specific trait from a particular age. Different colors group traits belonging to specific category: sensory, motor, spatial behaviors (spatial activity), maze solving (hippocampus-dependent learning), and spatially tuned cells. Image was taken from Wills et al. (2014).

3.2 Olfaction.

The olfactory system is the first sensory system to emerge shortly after birth (P3-P5). At this age, rat pups can discriminate between odors, as shown by an experiment where animals at this age have a clear preference from for nest shavings over other scents (Cornwell-Jones and Sobrian, 1977). If exposure to an odor is accompanied by Lithium-chloride induced nausea, rat pups will show aversion to that odor at P8, indicating that odor discrimination abilities and associative olfactory learning are present early on (Rudy and Cheatle, 1977).

3.3 Somatosensation

Whisking, the result of moving the vibrissae, is an important sensory input for rodents to build mental maps of their surroundings (Zucker and Welker, 1969). In young rats, whisking is first detected around P11-P13, and the frequency and amplitude of whisking movements continuously develops until P28, at which age the movements are more adult-like (Landers and Philip Zeigler, 2006). Contact-dependent whisking gradually matures from P11 to P17 (Grant et al., 2012).

3.4 Auditory perception

The auditory system in rats becomes functional at P8-9, at which state cochlear microphonic potentials can be observed from the round window of the inner ear in response to sound stimulation (Crowley and Hepp-Reymond, 1966, Uziel et al., 1981). At P11-12 action potentials can be recorded from the vestibulocochlear nerve (Uziel et al., 1981), and by P14 rat pups can already discriminate (some) sounds and perform associative auditory learning tasks (Rudy and Hyson, 1984).

3.5 Vision

Vision is the last emerging sensory modality, since eyelid opening occurs around P14-P15 (Altman and Sudarshan, 1975, Bolles and Woods, 1964, Fagiolini et al., 1994, Foreman and Altaha, 1991, Moye and Rudy, 1985, Prevost et al., 2010, Routtenberg et al., 1978). Electrophysiological recordings from rat primary visual cortex (V1) have showed that, 48 hours after eye opening, neurons have spatiotemporal tuning functions to visual gratings similar to adults (Prevost et al., 2010). Recordings from the binocular portion of V1 have also showed that the visual brain areas may undergo protracted maturation: eye optics clear up by P19 (approximately 4-5 days after eye opening); adult-like responsiveness to moving and flashing visual stimuli is reached by P21; visual

orientation selectivity – preferential responses to visual stimuli oriented at specific rotational angles and directions in a moving stimulus – is fully matured by P30; and visual acuity develops quickly between P19-P30, but it reaches adult levels at P40-P45. Additionally, even though young rats can detect visual stimuli after eye opening (and even before (Tan et al., 2015)), it is not until P17-P18 that they can learn the association between a visual cue and an aversive stimulus (Moye and Rudy, 1985).

3.6 Vestibular functions

From birth, young rats display some righting reflexes (Altman and Sudarshan, 1975), which imply that the vestibular system is working at a rudimentary level. Electrophysiological recordings from both peripheral and central vestibular neurons have shown adult-like neuronal responses to body rotations at P8, and weaker responses in P1-P2 animals (Curthoys, 1979, Curthoys, 1982, Lannou et al., 1979). In mice, it appears that optokinetic reflexes – evoked by image motion across the retina, which leads to eye movements in the direction of the visual motion – and vestibulo-ocular reflexes – when, due to head motion, the eyes move in the opposite direction of head movement – are adult-like at P21 (Faulstich et al., 2004). The (not so extensive) evidence regarding the postnatal development of vestibular activity and the emergence of vestibular-related behaviors seems to indicate that, just like the olfactory system, vestibular function is one of the most precocious systems to develop in young rats.

3.7 Hippocampal Associated Spatial Behaviors

3.7.1 – Exploratory Behavior

The first reconnaissance behaviors in young rats are first observed around P14-P16, exploring their surroundings in increasing frequency and duration until the end of the third week, when pups stop huddling (Altman and Sudarshan, 1975, Bolles and Woods, 1964, Gerrish and Alberts, 1996, Loewen et al., 2005). These observations are further reinforced by novelty tasks that show that P19 rats have a strong preference for a novel side of an environment (Goodwin and Yacko, 2004). At P24 they also show preference for novel objects in object recognition tasks, and at P30 they can form memories of the location of novel objects as well (Ainge and Langston, 2012), just like in adult rats (Dix and Aggleton, 1999, Ennaceur and Delacour, 1988). Both novel object tasks are hippocampus-dependent, as shown by cytotoxic lesions to this brain region (Mumby et al., 2002).

3.7.2 – Path Integration

Path integration, also called dead reckoning, is the ability of an animal to home back to a starting location in a straight trajectory after exploration, taking into account only the distance and directions traversed in the excursion (Etienne and Jeffery, 2004), and it requires a working hippocampus (Maaswinkel et al., 1999, Mittelstaedt and Mittelstaedt, 1982, Whishaw and Maaswinkel, 1998, Whishaw and Tomie, 1997). Rats as young as P3, can already successfully orient themselves to the home cage when placed in a circular platform, and at P8 the can physically home towards it (Altman and Sudarshan, 1975). However, this type behavior may be a form of taxis achieved through olfactory and auditory cues coming from the nest – a spatial behavior also designated as piloting (Loewen et al., 2005). Potentially true homing behaviors appear to occur as early as P16 (Loewen et al., 2005).

3.7.3 – Maze Solving

The ability to solve a particular type of maze can inform the experimenter on several aspects of hippocampal function, particularly memory. Different maze types can therefore be used to test different aspects of memory (Olton, 1979). T-mazes consist of a T-shaped narrow arm maze with the starting point located in the stem and two goal arms extending from it. This particular maze type can be used to assess working memory through what is called a spontaneous alternation task or delayed forced choice design. Both tasks assume that the animal starts at the stem and makes a choice between one of the two arms in one trial. The spontaneous spatial alternation task is an unrewarded version were the experimenter measures the rates at which the animal visits both arms across several trials, which should be roughly 50% for each. The delayed forced choice design is different, as in a first trial the animal can only enter one of the arms of the maze and in a second trial the animal is rewarded if it chooses to enter the previously unvisited arm. Varying the delay between the first and second runs allows the assessment of working memory (Deacon and Rawlins, 2006), which is known to be a hippocampus dependent process (Johnson et al., 1977, Olton and Feustle, 1981, Dudchenko et al., 2000). The T-maze can also be used to assess reference memory, which is done by rewarding the animal only when it enters a specific arm during training. When it comes to rat pup behavior in a T-maze, it is known that young animals reach 75% alternation across 20 consecutive trials between P23-P33, with few animals developing this ability much later (Douglas et al., 1973). Spontaneous alternation does appear to be a gradually maturing ability in young rats, lasting until P65 (Douglas et al., 1973) or P80 (Kirkby et al., 1967). When rewarded in either free choice or forced choice versions of the test, P21

rats demonstrate reliable alternation rates of approximately 70% after 20-30 runs (Green and Stanton, 1989). Before then (P15), animals persevere in choosing one side/arm, and do not learn the forced choice aspect of the task (Green and Stanton, 1989).

Another historically relevant maze test was developed by Richard Morris (Morris, 1981), the Morris Water Maze, to assess spatial learning and normal hippocampal function. In a basin of unclear water, animals need to find a submerged platform using a combination of visual cues. Both hippocampal lesions and pharmacological inactivation abolish the animal's ability to solve this maze (*i.e.* they will never learn/remember the location of the hidden platform) (Morris et al., 1982, Riedel et al., 1999). The literature surrounding the emergence of the ability to solve this maze is quite disparate, most likely due to methodological differences in training and/or animal temperature control by the experimenters. Nevertheless, the overall results suggest that young rats are able to solve the hidden platform version of the water maze by either P19-21 (Akers and Hamilton, 2007, Brown and Kraemer, 1997, Brown and Whishaw, 2000, Rudy et al., 1987) or P28 (Schenk, 1985). With a proximal cue pointing at the location of the platform, rat pups can find the platform before P21 (Akers et al., 2011, Rudy et al., 1987, Brown and Whishaw, 2000). This means that, even though not fully matured, the visual acuity of young rats is sufficient to lead them to the hidden platform and escape the maze.

Overall, it appears that maze solving abilities develop concurrently with spatially tuned neurons in the hippocampus. In fact, recent work has shown that the place cell system in young animals is able to pattern separate between different cue combinations of different sensory modalities (Muessig et al., 2016). This 'precocious' ability may be vital to solve difficult spatial tasks. More complex mazes, such as the uncued version of the water maze, may require more complex ego- and allocentric input integration, which is what GCs are thought to add to the spatial cognitive map. Hence, the ability to solve complex spatial tasks emerges later on (in the fourth week in this case).

Preamble Summary and Thesis Goals

At birth, rat pups exhibit poor motor skills, which mature overtime, reaching adult-like levels by the end of the fourth week (Bolles and Woods, 1964, Gerrish and Alberts, 1996). The sensory systems also develop throughout a protracted period, starting with olfaction in the first week (Cornwell-Jones and Sobrian, 1977), and ending with vision at around P45 (Moye and Rudy, 1985). Exploratory behaviors, largely hippocampal-dependent, appear around P15-P16, when all sensory systems, even though not fully mature, are online (Altman and Sudarshan, 1975, Bolles and Woods, 1964). In the fourth week rats fully develop the ability to solve spatial maze tests, which are known to rely on the hippocampus as well (Akers and Hamilton, 2007, Douglas et al., 1973). These abilities also coincide with the maturation of the spatial cognitive map: orientation exists early on in these animals and so do HDCs (Wills et al., 2010, Tan et al., 2015); novel place preference occurs in the middle of the third week, when place cells can be first recorded (Wills et al., 2010); maze solving is only achieved in the fourth week, when GCs are first recorded (Wills et al., 2010, Langston et al., 2010). But where do BVCs fit in this picture?

In this thesis, I provide evidence collected by myself and other colleagues that subicular BVCs can be recorded from age P16 onwards. Additionally, we demonstrate that BVCs' spatial tuning and stability also increases with age, an observation which is in agreement with the protracted maturation of spatially tuned cells in the HF of young rats.

Chapter 4 General Methodology

4.1 Animal Husbandry

All animals used in the work described in this thesis belong to Lister-Hooded strain of *Rattus norvegicus* (Charles River, UK). All adult males used for electrophysiological recordings were initially group-housed until surgery, at which point they were single-housed with enrichment. Similarly, dams were group-housed until the first mating, at which point they were kept single-housed. Litters remained with their mothers until P21 (age of weaning). Dams and litters had *ad libitum* access to food and water.

For breeding, a dam was placed in the cage with another male rat (stud) for 10 days. After this period, the dam was single housed in a cage with bedding (tissue paper, Tork® advance) where she would litter down and nurse the litter until weaning age. The breeding cages were cleaned once a week until the animal seemed heavily pregnant. Daily checks between 5-6pm were performed to determine day of birth (P0). The first cage cleaning after birth happened at/after P10. Large litters were reduced to standard size of 8 animals (all males whenever possible) at P4. Smaller litters were also kept for experimental purposes. All pups remained with their mothers until P21. A total of 13 rat pups received electrode implants in the dorsal subiculum, with implants occurring across the age range of P12-P14, and pups weighing between 24-55g at the day of surgery. This age range allowed the animals to be recorded immediately after eye opening and maximizing sampling time in order to collect data that represented the actual postnatal maturation of subicular BVCs.

All adult rats used in experimental procedures had *ad libitum* access to water and food until one week after surgery. At this point, they were maintained at 90% of their free-feeding weight. All animals were over 3 months of age, weighing between 300-500g at the day of surgery. In total, 4 adult male rats were used as controls for the BVC development experiment (Chapter 5).

Lastly, all animals used in the developmental experiments, which include litters, dams, studs and adult controls, were kept on a 12:12 hour light-dark schedule with lights off at 10:30 am. One adult male used in the second set of experiments was raised in the same light schedule, while the remaining animals were instead kept in a 12:12 hour light-dark cycle with lights off at 10:00 am. All experiments were conducted in accordance with the UK Animals (Scientific Procedures) Act of 1986.

4.2 Microdrive Preparation

Tetrodes used to record neural activity (Recce and O'Keefe, 1989) were held in a vertically movable microdrive (see Figure 4.1A, Axona Ltd, St. Albans, UK). Each tetrode was made of HM-L coated 90%-platinum-10%-iridium wire with 17µm diameter (California Fine Wire; Grover Beach, CA, USA), looped twice and twisted together (approximately 2 turns per mm of wire), resulting in a fine woven strand. The unwoven end was split, and the insulation around the tip of the four loose wires was burned off, allowing each tetrode strand to directly connect to a microdrive wire after the whole tetrode was passed through a cannula of variable length and diameter – which depended on the age of the animal and implant site. Tetrode wires were secured to the microdrive wires with conductive silver paint (Electrolube Ltd, UK), ensuring a strong electrical connection, and then ultimately sealed with nail varnish for protection and insulation. The protruding ends of the tetrodes were then cut to the same length with surgical precision scissors (Fine Science Tools, Germany). Afterwards, tetrode tips were platinum plated in 1:9 0.5%-gelatine:Kohlrausch solution until the impedance on every channel was brought down to 100-200 kΩ at a 2 kHz frequency (Merrill and Ainsworth, 1972). Plating was usually performed between 3 days and 24h before surgery.

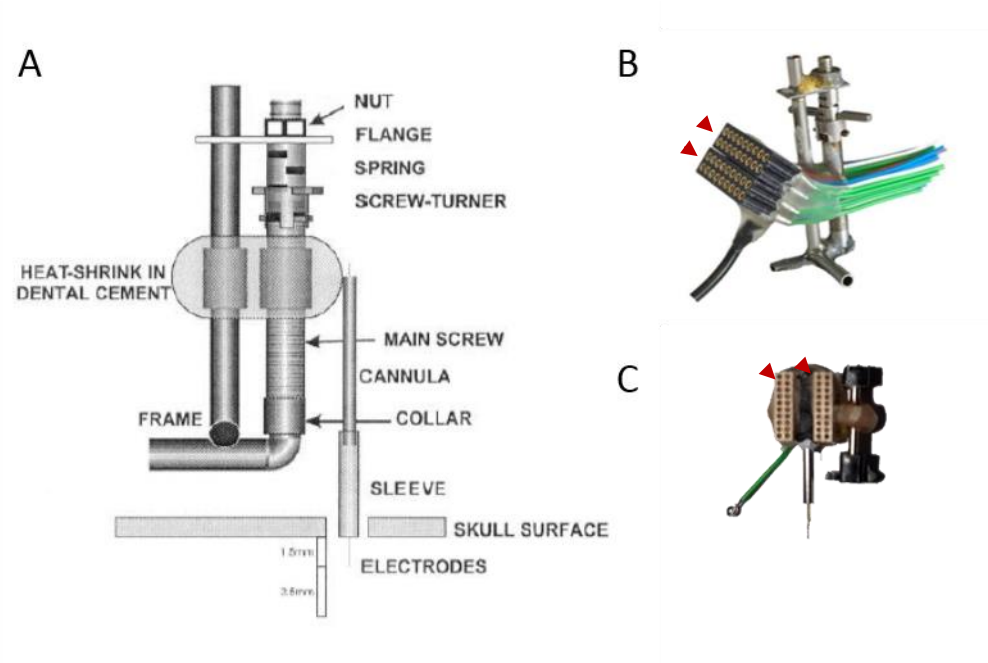

Figure 4.1 – Schematic of tetrode carrying microdrives and photographs of adult 'poor-lady' and pup 'omnetic' microdrives. (A) Schematic of the microdrive, where tetrodes are threaded into the cannula and, once in the brain, protected by a sleeve, while the whole drive is secured to the animal's skull by cementing the frame to the head of the animal. (B) 'Poor lady' microdrive with Mill-Max connectors (red arrow) used to implant adult animals. (C) Microdrive built with Omnetics connectors (red arrows) and similarly designed microdrive mechanism, but smaller and lighter than the one used for adult animals. [Images A and B courtesy of Axona Ltd., St Albans, UK]

The type of microdrive used depended on the age of the animal. Adult animals were implanted with a 'poor-lady' microdrive with Mill-Max connectors (Mill-Max Mfg. Corp., NY, USA), which are bulky and sturdy, allowing an increased stability of the recording electrodes (see Figure 4.1B). For young rats, these same microdrives are too heavy, and so smaller and lighter microdrives with Omnetics connectors (Omnetics Connector Corp., MN, USA) were built especially for rat pups (see Figure 4.1C). The microdrive is built by cementing the connectors as well as a cannula (where the recording tetrodes are housed) to the microdrive mechanism. The mechanism consists of a screw and frame (see Figure 4.1A). The turning of the screw allows movement of the cannula and microdrive upwards or downwards along the frame of the microdrive. The frame of the microdrive is then secured to the skull of the animals using dental cement. The tetrodes, which protrude out of the cannula, are inserted into the brain and, the exposed tetrode region is protected by a loose-fitted sleeve. This sleeve thus constitutes a barrier between the electrode wire and the dental cement, and its loose fitting around the cannula allows the microdrive and recording electrodes to move vertically if the screw is turned.

4.3 Surgeries

The experiments reported in this thesis were performed in 5 different groups of animals, according to the type of experiment being performed. To understand the postnatal maturation of subicular BVCs (Chapter 5) two groups of animals were implanted with 8-tetrode microdrives: 13 rat pups (section 4.3.1 below for pup surgery details); and 4 adult rats.

4.3.1 – Rat pup surgeries

Surgical procedures for pups implanted for the experiments in Chapter 5 were similar to Wills et al. (2010). Approximately 30-50 minutes before surgery, rat pups (aged between P12 and P14) were given a subcutaneous injection of buprenorphine as analgesic (Alstoe Animal Health; York, UK) at a concentration of 0.15µg/g body weight. They were returned to their home until surgery, and then anaesthetized using 3% isoflurane (Abbott; Maidenhead, UK) delivered with O_2 (3L/min). During surgery, the isoflurane concentration was gradually lowered until reaching 0.75-1% half-way through the procedure (approximately two hours). Animals were mounted on a stereotaxic frame (custom made), and an incision was made to expose the skull. The incision aimed to reveal both bregma and lambda so that sufficient space for the insertion of holding screws and microdrive was available. Afterwards, the skull was drilled using a 0.7mm

bur drill (Meisinger, J&S Davies, UK) to allow the placement of the screws. In total 7 jeweler's screws (length, 1.6mm; diameter 0.9mm; AMS-120-1-BIND-SS Antrin Miniature Specialties Inc.; CA, USA) were inserted across the exposed skull to secure the microdrive (2 in the frontal bone plate, 2 in the parietal plate contralateral to the microdrive site, 2 in the inter-parietal plate, and 1 on the parietal plate posterior to microdrive). One of the frontal plate screws served as a ground electrode for the microdrive. For the tetrode insertion, the skull was drilled with a trephine drill bit (1.0mm, Meisinger, J&S Davies, UK) to allow for a clear craniotomy. Just before the insertion of the tetrodes into the brain, the dura was removed with fine forceps (No 5 Dumont, Fine Science Tools, Germany) to allow the smooth implant of the recording wires. After the tetrodes were lowered into the brain, the screws, exposed skull and the feet of the microdrive were covered with dental acrylic (Simplex rapid; Associated Dental Products Ltd.; Swindon, UK), holding the drive in place and closing the animal's head wound. The stereotaxic coordinates used to implant the recording electrodes in the rat pup Sub were calculated by scaling down the adult Sub coordinates (see section 4.3.2.1, page 74) relative to the bregma-lambda distance. In adult rats, this distance is approximately 9.0mm. (Paxinos and Watson, 2006). Thus, for a pup whose bregma-lambda distance is approximately 6.3mm, the Sub stereotaxic coordinates used: -4.4mm AP from bregma; -1.4mm ML from the midline; -2.7mm DV from the dura.

For body temperature control, a water-based heating pad (UNO; Zevenaar, Netherlands) at 38°C was placed underneath the animals during surgery. Surgeries were conducted as fast as possible, never exceeding 2h of anaesthesia.

During recovery, animals were put next to a heat pad (Snugglesafe®; http://www.zooplus.co.uk) inside a warmed enclosure, and were returned to their home cage as soon as awake. To avoid the mother 'attacking' the microdrive or not accepting the pup, a 'mock microdrive' (containing the plug for the headstage, blu-tak® (Bostik, Stafford, UK), dental acrylic and a metal cannula) was put inside the home cage one day before surgery.

4.3.2 – Adult Rat Surgeries

Overall, there are no major differences between young and adult rat surgeries: anesthesia, stereotaxic mounting of the animal, microdrive implant, body temperature control and recovery procedures are identical. For analgesia animals received a subcutaneous injection of caprofen for analgesia (Pfizer; Sandwich, UK) at a concentration of 5µg/g body weight 5-10 minutes before surgery. Postoperative analgesia was administered by providing the animals with a dose of 1 µg/g body weight

of meloxicam (Boehringer Ingelheim; Ingelheim, Germany), for three days after surgery. This aimed to minimize any pain at the implant site so the animal did not scratch, maintaining the proper healing of the area. All animals were chronically implanted with one microdrive with 8 tetrodes of twisted 17µm platinum-iridium wire. Additionally, 6 jeweller's screws (1.6mm width, 3mm length, Slot Cheese Machine Screw DIN 84 A2 ST/S, Precision Technology Supplies Ltd, East Grinstead, United Kingdom), one of which served as a ground electrode for the microdrive. Due to the larger size of the microdrive anchor-screws, a 1.2mm burr drill (Meisinger, J&S Davies, UK) was used for the screw craniotomies, while a 1.4mm trephine drill (Meisinger, J&S Davies, UK) was used for the microdrive implants.

Four adult rats were used as control for the analysis of the postnatal maturation of subicular activity described in Chapter 5. The coordinates used for these implants were: AP 5.4mm posterior to bregma, ML 1.5mm from the midline and DV 2.8mm below the dura (Paxinos and Watson, 2006).

4.4 Data Collection

4.4.1 – General aspects of recording environments

All rats were tested in specific environments according to the type spatial cell type being recorded. Overall, all recording environments consisted of differently shaped wooden enclosures which were raised from the floor. The walls of these environments were 50cm high and painted grey. All environments stood on a 1mm matte acrylic Perspex® sheet (Amari Plastics; Weybridge, UK), supported by top black painted 3mm medium-density fiberboard. Further details on the environments are found in the results chapters.

4.4.1 – Acquisition of electrical signals and positional information

Trial data was recorded using an Axona dacqUSB data acquisition system (Axona Ltd., St. Albans, UK). Single unit signals obtained from the implanted tetrodes were amplified (10-20k) and band-pass filtered between 360Hz-kHz. A spike/unit was recorded whenever a signal across any tetrode channel exceeded 70% of a channel's maximum signal amplitude. Each tetrode channel was sampled at 48kHz, and individual spikes were stored as 50 points across a 200µs pre- and 800µs post-threshold time period. In parallel, LFP signals were recorded at a 250Hz sample rate from at least two channels. The 8-15k amplified LFP signal was band-pass filtered between 0.34-125Hz, and notch filtered at 50Hz frequency. The animal's position, sampled at 50Hz, was recorded via a

camera above the middle of any of the used environments using by detecting the position of two different sized light-emitting diodes (LEDs) attached to the head of the animal. The head orientation was estimated by measuring the relative angular displacement between one LED and the other, the LEDs being at a fixed distance and orientation relative to the animal's head.

4.4.2 – Cell screening procedures

All animals were screened and tested in a foraging task paradigm: animals explored a particular environment while being rewarded with either sweetened milk (rat pups) or sweetened rice (adult rats). Before actual probe trials were performed, all animals were screened for the presence of spatial cells. Cell screening consisted of rewarded exploration of a particular environment at least twice. If spatially tuned cells were detected during these screening trials, the animals were then tested in a specific sequence of environments. The type of environments used in both screening and probe trials differed depending on the type of spatial cell type being recorded: BVCs were screened for and tested in square environments.

Rat pup screening for subicular cells began 1 day after surgery. Tetrodes were lowered ventrally in 62.5 or 125μm increments until typical hippocampal physiological indicators were present, namely the presence of pyramidal cell activity alongside an increase in the amplitude of the recorded LFP. To avoid instability of the recording due to tetrode movements, at least 1h must have elapsed between the last movement of the tetrodes and the start of an experiment. During cell screening sessions (described further in Chapter 5), rat pups were rewarded with sweetened milk while performing the required task. Between screening or test trials, rat pups rested in a holding platform (dimensions: 35x35x30 cm), and the rat pups had a heat pad (Snugglesafe®; www.zooplus.co.uk) that was constantly monitored and replaced with a new one once it became cold to the touch. For pups younger than P18, the duration of screening sessions was kept as short as possible (20-60 min).

Adult rats were always given a 7-day recovery period after surgery before screening started. To collect subicular, the same physiological indicators used in rat pup screening, were applied to determine the moment the tetrodes reached the dorsal Sub. Tetrodes were moved ventrally in 50μm increments once a day, to minimize electrode instability. Between screening and test trials, the animals rested in a holding platform (dimensions: 35x35x30 cm) with some bedding for 10 min.

4.5 Data Analysis

All data analyses were performed using MATLAB R2016b (MathWorks®, Natick, USA), Tint (Axona Ltd., St. Albans, UK), and IBM SPSS Statistics 24 (IBM Corp., Armonk, USA).

4.5.1 – Spike cluster separation

With the exception of recorded GCs, cells recorded on different days or after the tetrodes were lowered were always treated as different cells. The identification and separation of spike clusters belonging to different neurons was achieved by evaluating the different peak-to-trough amplitudes of spikes across the individual tetrode channels. Tetrode data was sorted semi-automatically: spike data was firstly sorted into clusters using Klustakwik (Kadir et al., 2014), and then manually curated to ensure that no over-clustering – the allocation of a set of spikes from the same putative cell into two or more clusters – or any other sorting mistakes had occurred. The tetrode's final cluster space was then saved, and the same procedure was applied to subsequent trials. Spike clusters across trials were matched to ensure the allocation of the same cluster number to the same putative cell.

4.5.2 – Rate maps

To visualize the firing pattern of each recorded neuron, the environment was divided into 2.5cm square bins. The number of spikes in each bin was then divided by the dwell time of the animal in that bin, thus obtaining the firing rate per bin (in Hz). Firing rate maps were then smoothed using a 5x5bin boxcar algorithm, resulting in the value of each bin being the average value of itself plus the surrounding 24 bins. The produced maps are then displayed as false color auto-scaled heat maps, where each bin is assigned to a color band defined by percentage of peak firing rate intervals. In this work, color bands change in 10% increments from the peak firing from cold to progressively warmer colors, (e.g., dark blue corresponds to 0-10% of peak firing rate while red corresponds to 90-100%). Unvisited positions in the environment are represented as white bins. All subsequent analyses were performed on smoothed rate maps.

A potential problem with the generation of rate maps, is the lack of coverage of the testing arena. To accurately evaluate a neuron's firing features, an animal's sampling of the environment ought to be consistent and thorough, although this is not always possible. The use of more complex smoothing filters, like adaptive smoothing, may overcome these problems without substantial signal loss – which boxcar smoothing filters are more

prone to (Eden et al., 2004). However, considering that the overall path lengths and sampling of the testing arena were consistent throughout the tested ages (see Figure 4.2), a simpler boxcar smoothing was chosen for further analyses.

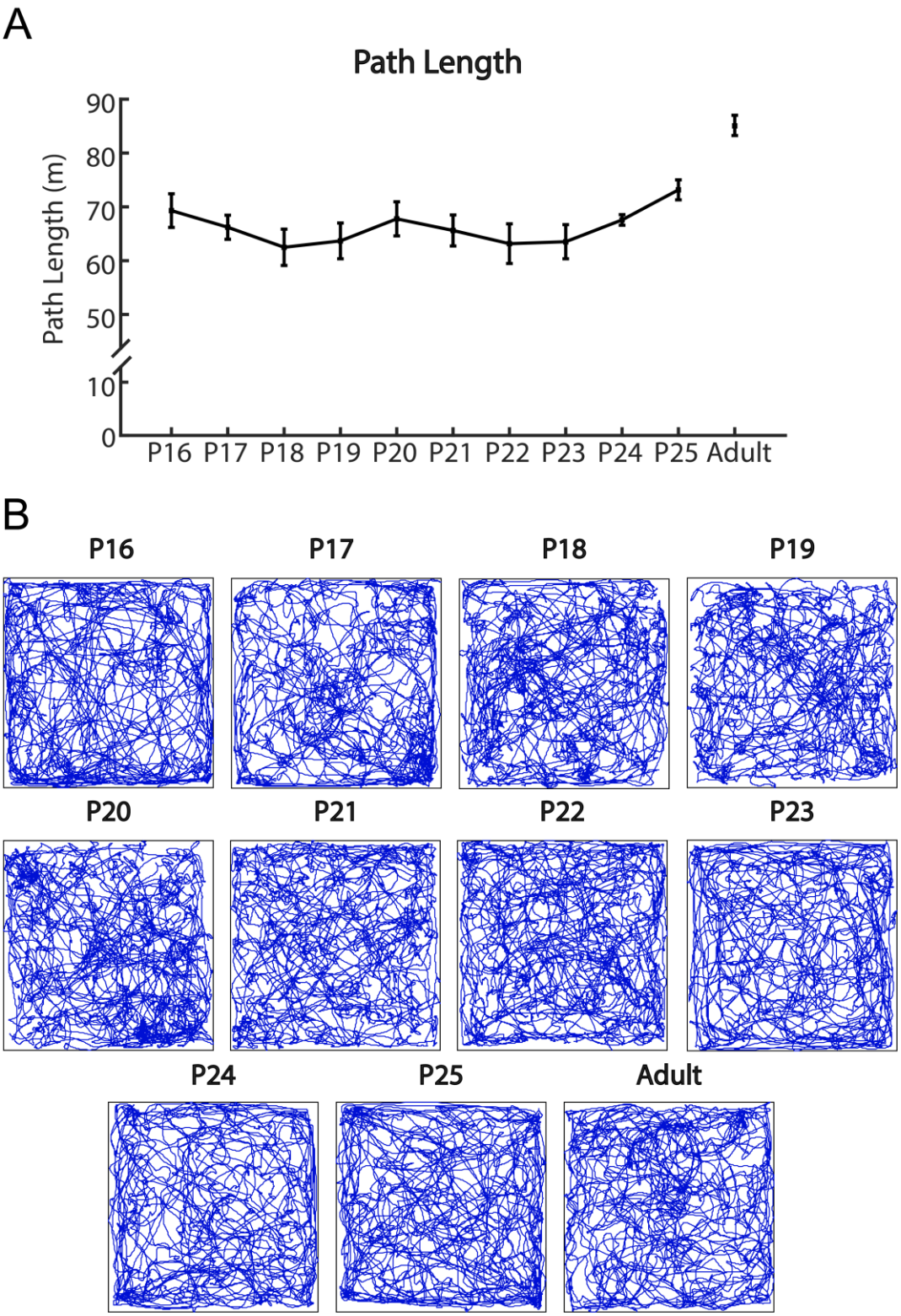

Figure 4.2 – Average path length and coverage of the testing arena across the tested ages. (A) Mean ± standard error of the mean of trial path length for each tested age. (B) Representative examples of the coverage of the testing arena for each tested age. The blue trace corresponds to the position of the animal for the entire duration of the trial.

4.5.3 – Spike shuffling procedure to determine cell inclusion criteria

Cells were defined as spatially tuned according to calculated features of their firing fields. For instance, to determine if a given cell is a GC, the cell's gridness score (calculated as shown in section 4.5.4.5, page 79) is determined. It is then necessary to objectively define a cut-off value/score above which recorded cells can be considered spatially-tuned. To define this cut-off value (or threshold) a population of scores is generated from a population composed of random rate maps obtained by shuffling the spike trains of recorded cells.

The shuffling process involves temporally shifting the spike times of a recorded cell along the duration of the trial. The temporal shift is performed in a user defined number of steps, and in each step the spike train of a given cell is shifted linearly along the trial duration. Thus, at every step of the shuffling procedure, the temporal shift from the original spiking times increases by a pseudorandom amount. Temporally shifting the whole cell's spike train in this manner, maintains the temporal relation of the cell's spikes, but dissociates the cell's firing from the position of the animal (see Figure 4.2). For every step of this shuffling procedure, a new rate map is generated.

For each of these shuffled rate maps, the features being used to assess the spatial-tuning of neurons are calculated, thus producing a distribution of these scores. Then, the cut-off value/threshold is defined as a specific percentile rank from that distribution of values, usually the 95th percentile. Thus, a cell is considered spatially tuned if the feature score being used to assess this, exceeds the value that defines the top 5% of scores present in the shuffled distribution.

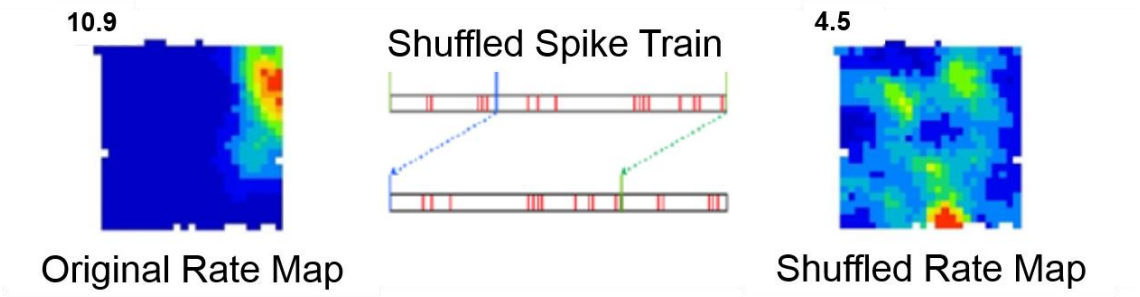

Figure 4.3 – Example of a spike shuffling procedure. The spike train of a particular unit is shifted by a pseudorandom amount along the total length of the trial, resulting in the dissociation between firing of a recorded neuron and the location of the animal in any particular point during the trial. Example adapted from Muessig (2013).

4.5.4 – Individual cell properties

4.5.4.1 – Mean and Peak Firing Rates

The mean firing rate of a neuron in a given trial was obtained by calculating the ratio between total number of spikes of an isolated cell in a given trial and the trial's duration. The peak firing rate corresponds to highest firing rate measured in any of the rate map's bins after smoothing.

4.5.4.2 – Directional Rate Maps and Rayleigh Vector Length

To determine HDC tuning, directional firing rate maps were constructed in an analogous manner to that of the spatial firing rate maps. Firstly, the HD data was divided into 6° bins, with the directional firing rate computed as the number of spikes fired in a bin, divided by the dwell time in that same directional bin. A 5° wide boxcar smoothing filter was applied to the resulting circular distribution. The peak firing rate was determined as the highest rate of this head-direction tuning curve. Lastly, the directionality of the tuning curve was quantified by determining the Rayleigh vector length (RV) using the following formula:

$$RV = \frac{\pi}{n \cdot \sin\left(\frac{\pi}{n}\right)} \cdot \sum_{j=1}^{n} r_{\theta_j} e^{-i\theta_j} \Bigg/ \sum_{j=1}^{n} r_{\theta_j}$$

In this formula, n corresponds to the number of head-direction bins, θ_j is the direction in radians of the jth circular bin ($2\pi j/n$), and r_{θ_j} is the average firing rate for a particular head-direction (Zar, 2010).

4.5.4.3 – Stability

The stability (or similarity) of a cell's firing field was determined by calculating a spatial correlation between two firing rate maps (spatial or directional) in a bin-by-bin fashion (Markus et al., 1994). To achieve this, the Pearson product moment correlation coefficient was calculated between spatially or directionally equivalent bins in two firing rate maps, with unvisited bins excluded from the analysis.

Using this approach, two forms of stability were calculated: within-trials and across trials. The latter corresponds the spatial correlation between two rate maps obtained from separate trials, while the former corresponds to the correlation of the rate maps of the first half and second half of a given trial. For all subsequent statistical analyses, the correlation values were z-transformed in order for these to become normally distributed.

4.5.4.4 – Spatial Information

Spatial information is a measure derived from Information Theory. It quantifies how accurately can each spike predict the animal's position (Skaggs et al., 1993). The obtained value is represented in bits/spike and is calculated using the following formula:

$$I(R|X) \approx \sum_{n} p(\overrightarrow{x_n})\, f(\overrightarrow{x_n})\, log_2\left(\frac{f(\overrightarrow{x_n})}{F}\right)$$

Here, $I(R|X)$ signifies the mutual information between firing rate R and the position X, $p(\overrightarrow{x_n})$ is the probability of the animal being at a location and facing direction $\overrightarrow{x_n}$, $f(\overrightarrow{x_n})$ is the firing rate observed at $\overrightarrow{x_n}$, and F is the overall firing rate of the cell in the trial.

4.5.4.5 – Gridness

For GCs, the determination of their grid properties was performed on the spatial autocorrelograms obtained for each spatial firing rate map (as in Wills et al. (2010)). The autocorrelograms of each map were obtained from the unsmoothed rate maps using the following formula:

$$r(\tau_x, \tau_y) = \frac{n\sum \lambda_1(x,y)\,\lambda_2(x-\tau_x, y-\tau_y) - \sum \lambda_1(x,y)\,\lambda_2(x-\tau_x, y-\tau_y)}{\sqrt{n\sum \lambda_1(x,y)^2 - (\sum \lambda_1(x,y))^2}\cdot\sqrt{n\sum \lambda_2(x-\tau_x, y-\tau_y)^2 - \left(\sum \lambda_2(x-\tau_x, y-\tau_y)\right)^2}}$$

Here, $r(\tau_x, \tau_y)$ represents the autocorrelation between bins with spatial offset of τ_x and τ_y, n corresponds to the number of bins over which the estimate was made, and $\lambda_1(x,y)$ and $\lambda_2(x,y)$ represent the firing rate in bin (x,y). The resulting autocorrelogram was then smoothed using a two-dimensional 5 bin-wide Gaussian kernel. Spatial cross-correlograms were also calculated using this exact same approach, but two different rate maps are used to calculate the correlation instead of the same one.

To determine the cell's gridness, the six central peaks of the autocorrelogram were defined – these being the six local maxima where $r > 0$ and excluding the central peak. Afterwards, a mask centered on the central peak, but excluding the peak itself (where $r > 0.4$) was defined. This mask was bounded by a circle centered on the central peak, and with radius corresponding to the mean distance of the six peaks to the center, multiplied by 1.25. The mask containing the six peaks was then rotated in 30° increments until completing a rotation of 150°. For each 30° step, the Pearson correlation coefficient between the autocorrelogram and the mask was calculated. The gridness score was then calculated as the lowest correlation obtained at either the 60° or 120° rotations (where we expect different grid fields to align perfectly if the cells are indeed GCs), minus

the highest correlation obtained at either the 30°, 90° or 150° rotations (where no alignment is expected).

4.5.4.6 – Grid Scale and Field Size

In order to further characterize GC firing fields, the average distance between firing fields (grid scale or wavelength) as well as the size of each firing field were calculated from the autocorrelograms (Hafting et al., 2005). Grid scale was calculated as the mean distance (in cm) of the central peak to each of the surrounding six peaks. The GC Field size corresponds to the area (in cm^2) of the central peak of the autocorrelogram.

4.6 Histology and Imaging

4.6.1 – Fixation of brain tissue

At the end of each experiment, the animals were anaesthetized and then humanely sacrificed by overdose of barbiturates (Sodium Pentobarbital, Euthatal 1ml/100g, Merial, UK). Upon loss of pedal and corneal reflex, the chest cavity was opened to expose the heart, and a needle was inserted into the left ventricle, while the right atrium was cut open. Transcardial perfusion was initiated by first infusing 0.9% saline (Baxter, UK) at approximately 2mL/min, and when the exsanguinate ran clear, 10% Formalin (Merck, UK) was perfused through the animal's body (about 200mL). For animals where immunohistochemistry was performed, cold 4% paraformaldehyde (Merck, UK) in PBS (Oxoid, UK) was perfused through the animal – approximately 100mL were used per perfusion – instead of formalin. This was done because formalin is known to reduce the binding of antibodies to the tissue (Hancock et al., 1982).

The brain was then carefully removed from the skull, and maintained in 10% formalin at 4°C or at room temperature for subsequent Nissl Staining. For the immunohistochemistry procedure, the post-fixation was performed overnight (less than 16h) at 4°C in 4% paraformaldehyde and then washed in PBS before the subsequent histological processing steps.

4.6.2 – Slicing

After the fixation step, the brains were cryoprotected in 30% sucrose in PBS at 4°C for a minimum of 48h. Afterwards, the brains were embedded on a mold (Peel-A-Way® Disposable Embedding Molds, VWR International Co, PA, USA) filled optimum cutting temperature (OCT) compound (Tissue-Tek, Sakura, UK) and left to freeze. The brains were then mounted on a chilled slicing platform using OCT. The mounted brains were then placed inside the cutting chamber of the cryostat (OTF5000, Bright Instruments,

UK) and left to equilibrate to the cryostat temperature for 30 min (chamber temperature -19°C; specimen holder temperature -16°C). The brain was then cut, and the obtained 30µm slices were placed in multi-well plates containing PBS. The brains of rat pups and adult rat controls used for Sub implants were sectioned coronally. For MEC implanted animals, sagittal sections were obtained, as this plane is better at aiding the visualization of electrode tracks along the dorso-ventral extent of the MEC.

4.6.3 – Nissl Staining for implant tracking

To verify the placement of tetrodes and/or cannula in the brain, the sections were mounted onto gelatin-coated glass slides and stained for the presence of nucleic acids using the Nissl method. Mounted brain slices were air-dried for at least 24h or for 30min on a hot plate. After drying, slides were placed in a 100% Ethanol bath for 1h to remove all fat deposits on slices (coming mostly from glial cells) and thus increasing the contrast provided by the chosen staining method. After this step, slides were then taken through a descending ethanol dilutions series and then left in a cresyl violet solution for 30 min. The cresyl violet acetate solution specifically stains RNA – present in the nucleus and Nissl bodies of neurons. After this step, slides were washed in a water bath, and then taken through an ascending dilution series of ethanol baths until 100%, not only dehydrating the slices, but also removing excess cresyl violet and increasing the differentiation of the staining procedure. The slides were then brought into a clearing agent bath (Histo-Clear, National Diagnostics, USA), and then cover-slipped using DPX mounting medium (Merck, UK). After air-drying overnight or for 1h in the hotplate, the slides were ready to be imaged.

4.6.4 – Immunohistochemistry

For all chemogenetic experiments, immunohistochemistry was performed in order to detect the presence of the virus in the Sub of the experimental animals. The viral construct is engineered to drive expression of mCitrine (a yellow fluorescent reporter with excitation at 515nm, and emission at 530nm) in the host. As mCitrine is a mutated form of green fluorescent protein (GFP) (Griesbeck et al., 2001), it is possible to use polyclonal forms of an anti-GFP antibody (AB) to detect the presence of the mCitrine protein, facilitating the detection of infected cells in a GFP detecting microscope.

With this in mind, immunohistochemical stainings against mCitrine were performed using an anti-GFP AB. To do so, 30µm slices were washed 3 times in PBS with 0.2% Triton-X (Merck, UK), and then blocked for 1h in a 0.25% casein solution in PBS (Dako Protein Block Serum-Free, Agilent, CA, USA) to prevent non-specific binding of the AB.

Afterwards, slices were incubated overnight at 4°C in an incubation solution (PBS with 0.2% Triton-X and Dako Protein Block Solution at a 20µL:1.5mL dilution) containing the anti-GFP AB (Thermo-Fisher Scientific™, MA, USA) raised in chicken in a 1µL:500µL dilution. The following day, slices were washed again in PBS with 0.2% Triton-X for 1h at room temperature. For visualization, the slices were then incubated for 2h at room temperature with a goat-raised secondary AB against chicken Immunoglobulin G, conjugated with the green fluorescence-emitting Alexa Fluor® 488 (Thermo-Fisher Scientific™, MA, USA) in a 1µL:1000µL dilution. After this step, slices were washed in PBS to remove the excess AB (1h room temperature), stained for 5min in a diamidino phenylindole (DAPI) solution (blue fluorescent compound that binds to DNA) to stain the nuclei of neurons in the slices. After washing the excess DAPI in PBS (15 min, 3 times at room temperature), slices were mounted onto positively charged glass slides (Superfrost™, Thermo-Fisher Scientific™, MA, USA), and cover-slipped with anti-fade mounting medium (Dako Fluorescence Mounting Medium, Agilent, CA, USA).

4.6.5 – Imaging

All slides were visualized using a Leica DM5500 B (©Leica Microsystems, Germany). All Nissl stained slices were imaged using a 1.25x objective, while all fluorescent slides were imaged with a 20x objective. For the latter, several images were obtained per slice, and then each image was stitched to create a whole view of the fluorescence pattern in each brain slice. DAPI was imaged using a DAPI filter cube, while mCitrine (and therefore all virus infected neurons expressing $hM4DG_i$) was visualized using an L5 filter cube.

4.7 Statistical Tests

To analyze individual cell properties, both parametric and non-parametric statistical tests were performed. Firstly, the homoscedasticity and normality of the analyzed variables was verified using the Levene's Homogeneity of Variances Test and the Kolmogorov-Smirnov test, respectively. If any of these assumptions was violated, the data was then transformed by calculating the natural logarithm of the variables, and the normality and homoscedasticity of the transformed data verified. If the assumptions were met, parametric tests were performed. ANOVA tests, followed by Tukey post-hoc tests, or repeated measures ANOVA (performed whenever cell properties of the recorded neurons where compared across behavioral or pharmacological/chemogenetic manipulations of cell activity) followed by Bonferroni corrected pairwise comparisons were performed. In order to correct for sphericity violations determined by Mauchly's W test in the repeated measures design, the Greenhouse-Geiser (Greenhouse and

Geisser, 1959) or Huynh-Feldt (Huynh and Feldt, 1976) corrections were applied depending on the estimated epsilon provided by either correction method. For epsilons estimated to be above 0.75, the Huynh-Feldt corrections were applied, otherwise the Greenhouse-Geiser correction was preferred (Girden, 1992).

In the few instances when the parametric assumptions were not met, comparisons between different independent variables were initially made with Kruskal-Wallis median comparison test, followed by Mann-Whitney U tests for pairwise comparisons. For repeated measures designs with low number of subjects, Friedman tests were performed to assess main effects, followed by Bonferroni adjustment Wilcoxon-Signed Ranks tests. The adjustment consisted in dividing the significance level used (0.05) by the number of comparisons performed for that particular test.

For circular data, circular statistical tests were employed using the Circular Statistics Toolbox for MATLAB developed by Philipp Berens. In order to assess the uniformity of the data distribution, the Hodges-Ajne test was computed on circular data. Comparisons between the circular median of groups was carried out using a multi-sample test for equal median directions test (Berens, 2009, Zar, 2010).

.

Chapter 5 The development of Subicular Boundary Representation

5.1 Brief Introduction

Understanding the postnatal timing of the origin of spatial firing and its development constitutes an effective way to dissect not just the development of the spatial cognitive map, but also infer the functional relationship of its elements.

With this idea in mind, much of the research in Francesca Cacucci's research group is focused on characterizing the postnatal development of spatial representations in the brain of rodents. By implanting young animals and testing them in similar behavioral paradigms as those used for adult animals, it is now known that:

- HDCs can be recorded in animals before eye-opening (Tan et al., 2015, Bassett et al., 2018), and that this direction-encoding system is adult-like in rather young animals (Wills et al., 2010, Langston et al., 2010);
- Place cells can be recorded in animals aged P16 onwards, but undergo further maturation of their firing features (stability and spatial information content) until adulthood (Wills et al., 2010, Langston et al., 2010, Muessig et al., 2015, Martin and Berthoz, 2002, Scott et al., 2011);
- GCs can only be recorded from the third week of development (P21) onwards, appearing and maturing quite abruptly (Wills et al., 2010).

Further work on the place cell properties in young animals has shown that the stability of this spatial cell type in locations away from environmental boundaries may require GC input. In fact, adult MEC lesions cause the stability and spatial information content of place cells to decrease (Van Cauter et al., 2008, Brun et al., 2008) regardless of their location. Moreover, before the emergence of GCs, place fields are more stable and more concentrated around the edges/borders of the environment, while centrally, place cells are less stable (Muessig et al., 2015). The increased stability of place cells located closer to environmental edges, along with the influence of environmental boundaries in shaping place fields and determining place cell peak firing location (O'Keefe and Burgess, 1996), suggests that boundaries may act as stabilizing cues for the place cell representation. Altogether, these data strengthen the idea that boundary information may provide important information about the environment, stabilizing the hippocampal spatial representation.

It is known that entorhinal border-encoding neurons (Solstad et al., 2008) can be observed from as early as P16/P17 (Bjerknes et al., 2015). These MEC spatial cells do not undergo much improvement of their firing features during development: their stability and barrier-elicited firing (the formation of a secondary firing field upon the insertion of a barrier into the testing arena) are adult-like from the moment they are first recorded. In adult animals however, it is estimated that less than 10% of recorded MEC principal neurons are coding for the presence of boundaries (Solstad et al., 2008). However, boundary-encoding neurons are also found in the rat Sub (Lever et al., 2009) (see Chapter 2, section 2.2.3, page 56 for more details), and this hippocampal region appears to harbor more boundary-tuned cells (~30%) than the MEC (Lever et al., 2009). Thus, this region is more likely to serve as a hippocampal boundary-encoding hub. However, little is known about the post-natal development of these spatial neurons in Sub. Therefore, understanding the early characteristics of these subicular cells may reveal potential differences between entorhinal and subicular boundary coding.

5.1.1 – Goals of the Experiment

In order to have a more complete picture of the postnatal development of the spatial cognitive map, and to further dissect subicular boundary-coding, we set out to answer two questions:

1. At what age can subicular BVC activity be observed in postnatal rats?
2. Does subicular BVC maturation occur gradually (like place cells) or are they adult-like from the earliest age they can be observed (like MEC border neurons)?

The results presented in this chapter refer to electrophysiological data collected from the Sub of young rats, from ages P16-P25, plus control data from adult animals, designed to answer the questions presented above. As this chapter will show, BVCs can be stably detected from as early as P16. The stability, spatial-tuning, barrier-triggered firing and peak firing rate of the recorded BVCs appears to gradually improve with age (mirroring the development of place cells).

5.2 General Methodology and Analysis

5.2.1 – Behavioral Paradigm

A total of 13 rat pups and 4 adult controls received microdrive implants as described in Chapter 4 (see sections 4.3.1 page 71, and 4.3.2 and 4.3.2.1 on page 72). All implanted animals, pups and adults, were screened in a square environment twice (Baseline Trials)

and then screened in the same environment but with a barrier (Barrier Trials, see Figure 5.1).

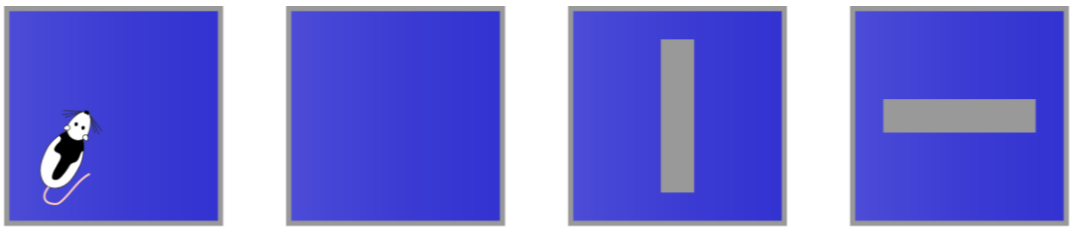

Figure 5.1 – Cell Screening Paradigm for BVC detection. All animals were tested in the same square environment (61.5cm side and 50cm tall) while foraging for sweetened milk (rat pups) or sweetened rice (adults). After two baselines, a barrier (53.5cm x 2.7cm x 49.9cm) was introduced into the center of the environment in a particular orientation (either N-S or W-E), and then rotated by 90° in the following barrier trial to capture BVC doubling along all the boundaries of the environment. The barrier had a N and a S sides for each of the orientations to ensure that textural cues present in the barrier were kept in the same position across different recording sessions and animals.

5.2.1.1 – Baseline Trials

The baseline trials, as well as barrier trials, were performed on a 61.5cm side square wooden enclosure. Surrounding both the holding platform and the baseline environment, several custom-made distal cues (posters with geometric high contrast patterns) were attached to the room walls, with no distinctive polarizing cues inside the recording environment itself. During rat pup screening, for any given litter, the floor of the familiar environment was never completely cleaned between trials, only urine puddles and fecal pellets would be wiped. This was done to ensure the maintenance of olfactory cues and help the animals maintain some degree of familiarity with the testing environment. Once testing was finished for the litter, the floor of the familiar environment was thoroughly cleaned with soapy water. Both adult rats and rat pups were tested in at least two baseline trials before being tested on the barrier probes. Each of the baseline trials lasted 10-15min, with a 10min inter-trial interval for both rat pups and adult rats.

5.2.1.2 – Barrier Probes

Following the baseline trials, if potential BVCs were present, the animals were then tested on at least one barrier trial. The barrier (53.5cm in length, 2.7cm wide, 49.9cm tall) would be oriented along the North-South (NS) axis, and therefore parallel to the East and West walls, or along the West-East axis (WE), parallel to the North and South walls of square environment. The former orientation ought to trigger field doubling for BVCs with receptive fields along the West and East walls (see Figure 5.1), while the latter orientation would cause fields along the North or South boundaries to double along the barrier (Hartley et al., 2000, Lever et al., 2009). The barrier also had North and South sides for each of two barrier orientations, ensuring that whatever textural and olfactory cues present in the barrier were kept in the same position across recording sessions and

animals. Each barrier probe trial lasted 10 minutes. Adult rats were always probed with both barrier orientations. For young rats this was not always possible because it was important not to separate the rat pups from their mothers for long periods of time. Thus, the animals were occasionally tested in one unique barrier probe.

5.3 Data Analysis

A total of 1999 neurons were recorded from the Sub of all rats. For subsequent analyses, neurons had to fire more than 100 spikes in all trials and be recorded in both baseline trials, resulting in a dataset of 1601 neurons. Table 5.1 provides a breakdown of all excluded cells per animal.

Rat No.	Total number of sessions	Cells that fired >100 spikes	Cells not recorded across baselines
R123	2	5	19
R124	2	9	5
R137	6	3	21
R138	5	2	15
R156	7	3	50
R157	3	4	4
R217	8	6	12
R247	7	2	24
R272	5	1	3
R315	7	0	30
R324	5	0	19
R345	8	0	56
R346	5	0	3
R372	11	7	35
R373	3	0	7
R375	7	4	33
R2138	4	1	15

Table 5.1 – Breakdown table of cells excluded from further analyses. Cells were excluded from the analyses depending on whether they were not active (fired less than 100 spikes in any given trial) or whether they were not recorded across consecutive baseline trials.

To assess the developmental changes that occur in Sub, the data was divided into the following age bins: P16-P18 (485 neurons), P19-P21 (409 neurons), P22-P25 (205 neurons), and Adult (575 neurons). The division of the data in this manner allows the comparison of pre-weaning (before P21) and post-weaning (from P22 onwards) animals.

5.3.1 – Detecting BVCs

In order to objectively identify boundary coding neurons, two different methods were used. One of them, the Border Score, is currently the standard method of identifying putative boundary-coding neurons (section 5.3.1.1). It has previously been used to identify border cells in both adult (Solstad et al., 2008) and rat pup electrophysiological recordings (Bjerknes et al., 2014). A novel methodology based on modelled responses presented in Hartley et al. (2000) for boundary coding cells in the hippocampus was developed (section 5.3.1.2, page 92), and its robustness is described for the first time in this chapter.

5.3.1.1 – Method 1: Border Score

Following the methodology currently used in the field, we proceeded to use the Border Score (BS) method (Solstad et al., 2008) to identify potential border cells in the set of recordings obtained in the course of this experiment. This method uses two field parameters to determine the degree of 'borderness' of the cell: the coverage of the field along a boundary in the environment, and the mean distance of the field to the wall weighted by the cell's firing rate.

Firstly, potential border fields were identified as contiguous bins whose firing rate is higher than 30% of the peak firing rate, and spanning through an area of at least 125cm^2. For field identification, these collections of bins do not require to border a wall, in fact, some fields may border more than a single wall; however, if multiple fields are identified, the one with the largest projection along a wall is preferred (Solstad et al., 2008). Once the firing field was identified, its coverage (c_M) along a specific wall measured as maximum spatial extent of the field along any of the walls of the environment. The distance of the field to the wall (d_M) was calculated by averaging distance of the field's bins to the nearest wall, weighted by the firing rate. The firing rate of the field was normalized beforehand by the sum of the in-field firing rates. Then, d_M was normalized to half of the side of the environment – corresponding to the largest possible distance to the edges. The BS was computed as:

$$BS = \frac{c_M - d_M}{c_M + d_M}.$$

The final BS value ranged from -1 for cells firing in central areas in the environment, to 1 for cells whose fields line up completely along one wall.

5.3.1.1.1 – Classifying a cell as a Border Cell

To classify cells, the baseline rate maps of all recorded subicular cells were shuffled as discussed in Chapter 4 (section 4.5.3, page 78). The shuffling procedure was performed 200 times per cell, per baseline trial, and the shuffled maps randomly sampled to obtain 10,000 shuffled rate maps per age group. The age-group matching is necessary to guarantee the computation of unbiased thresholds and exclude any potential developmental effects (Wills et al., 2010, Langston et al., 2010, Muessig et al., 2015). The choice of a relatively small number of shuffled maps per cell, even though relatively liberal, reflected what has already been performed in the current literature (Wills et al., 2010, Langston et al., 2010, Muessig et al., 2015). From this set of age-matched shuffled rate maps, a population of age-matched border scores and spatial information values were obtained. Finally, the thresholds were defined as the 95th percentile values of the age-matched shuffled scores. On their own, each of these percentiles selects a relatively wide range of cells: a BS criterion will select neurons whose firing fields lie in proximity to boundaries of the testing arena, at varying degrees of coverage along walls; while the spatial information criterion will choose neurons with relatively smaller and more restricted fields in any given position (Table 5.2). The combination of these two selection criteria results in a small probability of any given neuron being randomly selected as boundary-responsive, but may also restrict the potential range of variability boundary-responses neurons may exhibit. Using this approach, we followed previously published methodology used to analyze border cells in the MEC of young rats (Bjerknes et al., 2015). A recorded neuron would be considered a border cell if its BS and spatial information, in at least one of the baselines, was higher than the 95th percentile of the respective score in an age-matched population of shuffled scores (see Figure 5.2).

Cells Selected by BS	Cells Selected by SI	Cells Selected by Both
420	324	139
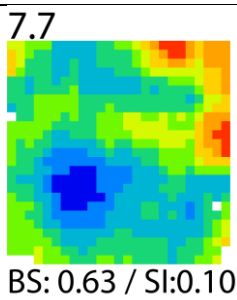	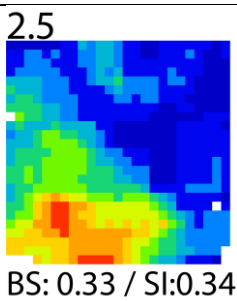	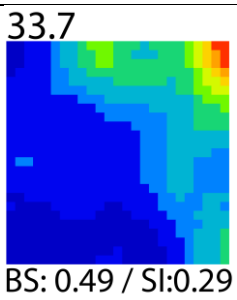

Table 5.2 – Number of cells that pass the cell-matched percentile for BS, SI, and Both, with examples. Overall, the use of both criteria narrows the selection of cells with high BS scores in order to those with narrower/smaller fields. All three examples were taken from the adult dataset. BS, border score, SI, spatial information.

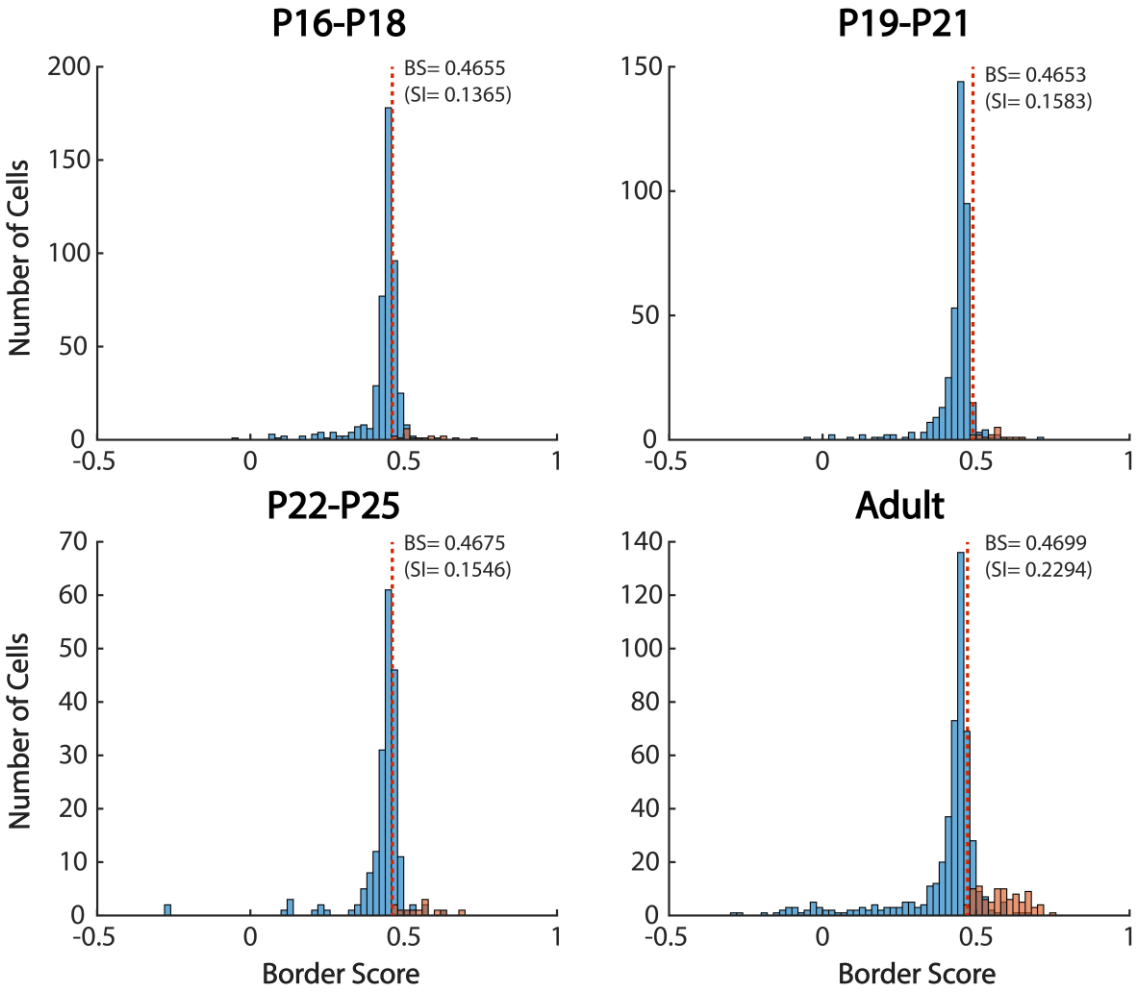

Figure 5.2 – Age-specific cell distribution and respective 95th percentile ranks of the BS (and spatial information) of shuffled rate maps. The histograms show the distribution of cells across the range of BS (bin width of 0.02) included (in orange) and excluded (in blue) from the analyses on the basis of both their BS and spatial information scores from all 4 age-groups. The age specific 95th percentile ranks for both BS and SI are shown at the right of the dashed red line, which represents the BS percentile rank for that age group.

5.3.1.2 – Method 2: BVC Response Model

As mentioned in the introduction to this thesis, work by O'Keefe and Burgess (1996) showed that the shape of place fields in the hippocampus is influenced by the distance to and shape of the boundaries. The putative inputs to place cells that provide the information about distance and allocentric direction from the boundaries were named BVCs (Hartley et al., 2000). According to this idea, BVCs have receptive fields that can be modelled by the product of two Gaussians: one as a function of distance to the boundary, and the other of allocentric direction. These thus represent both the directional and distance tuning of BVCs. Assuming that any BVC receptive field would have constant angular size, according to Hartley et al. (2000), the receptive field g of a BVC i can be written as:

$$g_i(r,\theta) \propto \frac{exp\left[-(r-d_i)^2/2\sigma_{rad}^2(d_i)\right]}{\sqrt{2\pi\sigma_{rad}^2(d_i)}} \times \frac{exp\left[-(\theta-\phi_i)^2/2\sigma_{ang}^2\right]}{\sqrt{2\pi\sigma_{ang}^2}}.$$

In other terms, the receptive field g_i with a preferred tuning distance r and allocentric direction θ, is proportional to a receptive field with a constant angular size σ_{ang} and bearing ϕ_i (second factor of the equation), and preferred tuning distance d_i, and radial extent σ_{rad} (first factor), where σ_{rad} varies with the distance, so that:

$$\sigma_{rad}(d_i) = (d_i/\beta + 1)\sigma_0.$$

In this function, β determines the rate of increase of the radial extent with distance, and σ_0 corresponds to the radial extent of the fields at zero distance.

Hypothetically, a neuron with this type of receptive field could then serve as base input to place cells, thus explaining place field deformations upon changes to the geometry of the recording environment. Place cells could perform a thresholded sum of the inputs of at least two BVCs – assuming that these two cells are strongly active in the location where the peak place response is observed. In this way, BVC input can be used to produce a coherent and boundary-anchored place representation (Hartley et al., 2000).

Using this model as a basis, a method to score putative BVCs from a set of *in vivo* recorded neurons was developed (the original source code was developed by Ben Towse, and further modified by Laurenz Muessig and Tom Wills) to analyze the obtained data.

5.3.1.2.1 – How the Response Model Score works

To define whether any given neuron could be classified as a BVC, we used the equation described above to create rate maps corresponding to a set of possible BVCs, with tuning distances (d) ranging from 1 to 13 bins, with 13 being half of the size of the environment (see Figure 5.3). Half the size of the environment corresponds to the maximum identifiable preferred distance a BVC can exhibit in the box used in this set of experiments (cells with larger preferred distances could not be distinguished from a cell tuned to the opposite boundary). The range of potential bearings (ϕ) in radians varied from 0 to 6.2 rad (355°), every 0.1047 rad (6°). The rate of increase of the radial extent (β) and the radial extent of the fields at zero distance (σ_0) are fixed to a set value of 183cm and 2.2cm, respectively, in line with Hartley et al. (2000). These parameters yielded a set of approximately 1008 model BVCs which were used to identify putative BVCS as well as inferring spatial properties of recorded neurons. The major varying

features of these putative maps were therefore the tuning distances and bearings of the boundary-associated receptive fields.

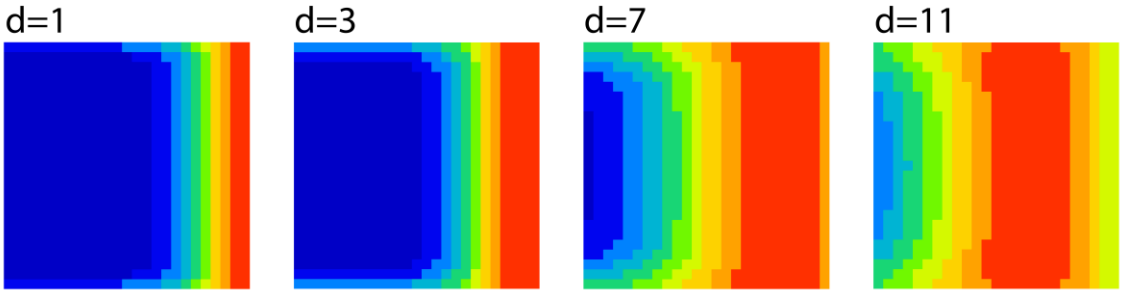

Figure 5.3 – Examples of model maps oriented towards the East wall with varying preferred tuning distances. Each map corresponds to a model response with the same phi, varying tuning distances in bins from the wall.

This set of putative receptive fields (BVC model maps) was then matched to the recorded data: we correlated all of the BVC model maps with the real rate map of the neuron, and defined the putative response which gave the highest correlation as the 'best fit' for the cell (see Figure 5.4). Subsequently, the Pearson correlation scores between the best-fit model map and remaining trials were calculated and stored, along with the respective tuning distances and bearings.

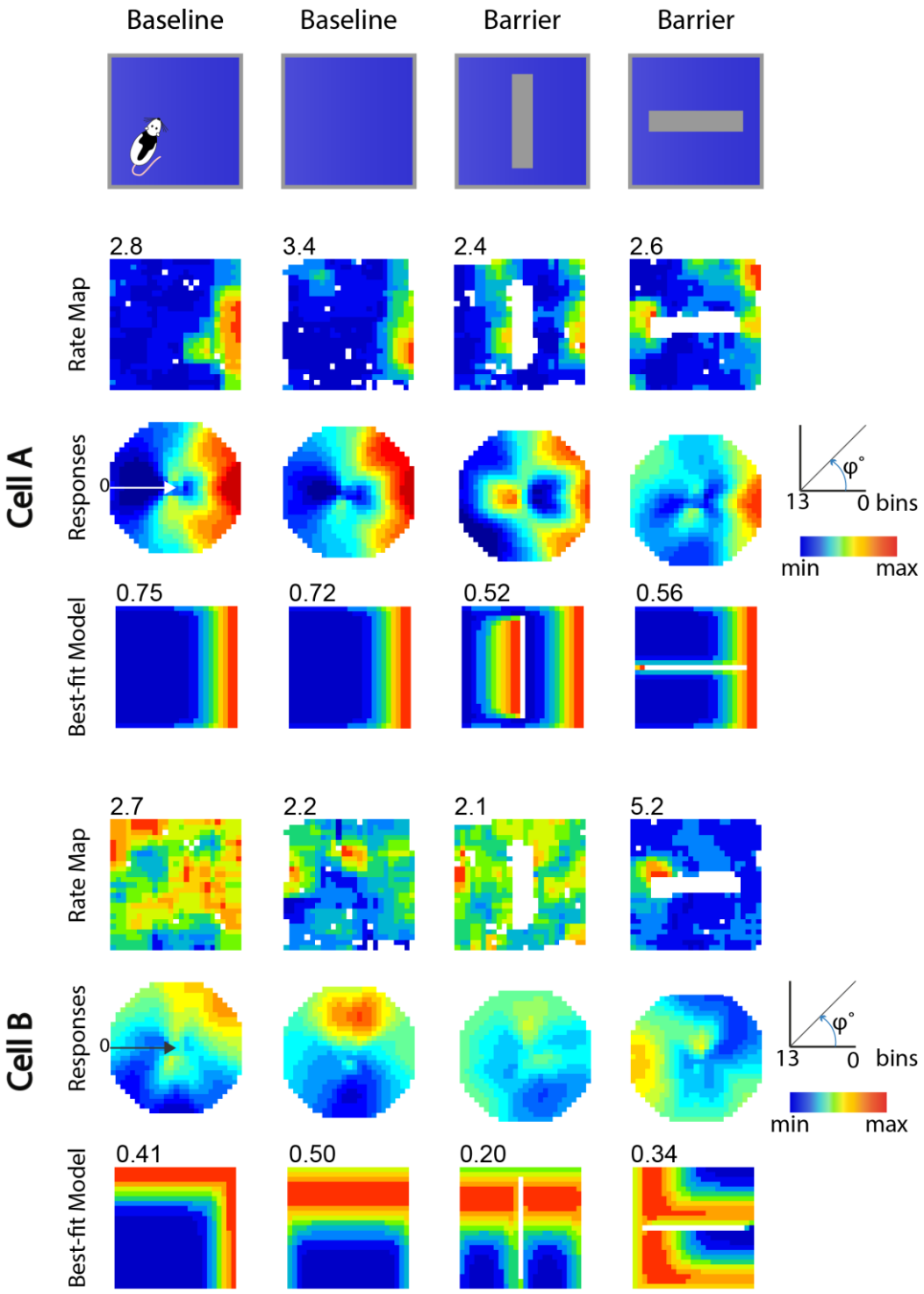

Figure 5.4 – Example of how the Response Model Score works. Two cells from the P22-P25 dataset are illustrated in this figure. For each cell, the top row depicts the real rate maps throughout the trials. The cell's firing rate is indicated on the top left in Hz. Underneath each rate map, each panel consists a false colour representation of r-values of the correlation between the rate map and all 1008 model BVCs generated using this fitting method. Distance is the radial dimension (0 bins at the outside, 13 bins at the centre) and angle is the angular dimension. Points in darker shades of red correspond to the best fit angle and distance from a boundary. The best fit model map for each rate map is then presented on the bottom row, with respective correlation scores presented on the top left corner. The best-fit receptive field for each cell corresponds to the one that results in the highest baseline correlation score (which will be the first response map for cell A, and the second one for cell B). Then, the correlation scores for this max receptive field and remaining trials were calculated. If the correlation scores of both baseline trials with the max receptive field exceeded the 99th percentile of the distribution shuffled correlation scores, the cell was considered a BVC.

5.3.1.2.2 – Defining a cell as boundary-coding

The obtained correlation values, which are the result of the spatial correlation between the best-fit model and real rate maps, can then be used to selectively identify boundary-coding responses. Just as for the BS method, the baseline real maps of all recorded subicular cells were shuffled (section 4.5.3, page 78). The shuffling procedure was performed 200 times per cell, per baseline trial, thus resulting in a minimum of 81,000 shuffled rate maps per age group. For each shuffled rate map, the response model (RM) score method (as described in the previous section) was applied, and the highest model-real map correlation score was stored for each of the shuffled maps. The 99th percentile rank value of these maximal correlation scores was calculated for each of the age groups and used as a threshold to isolate putative BVCs. A cell was thus selected as a BVC if both baseline correlation model scores were higher than the 99th percentile rank value of a population distribution of age-matched baseline shuffled maximum RM scores (Figure 5.5).

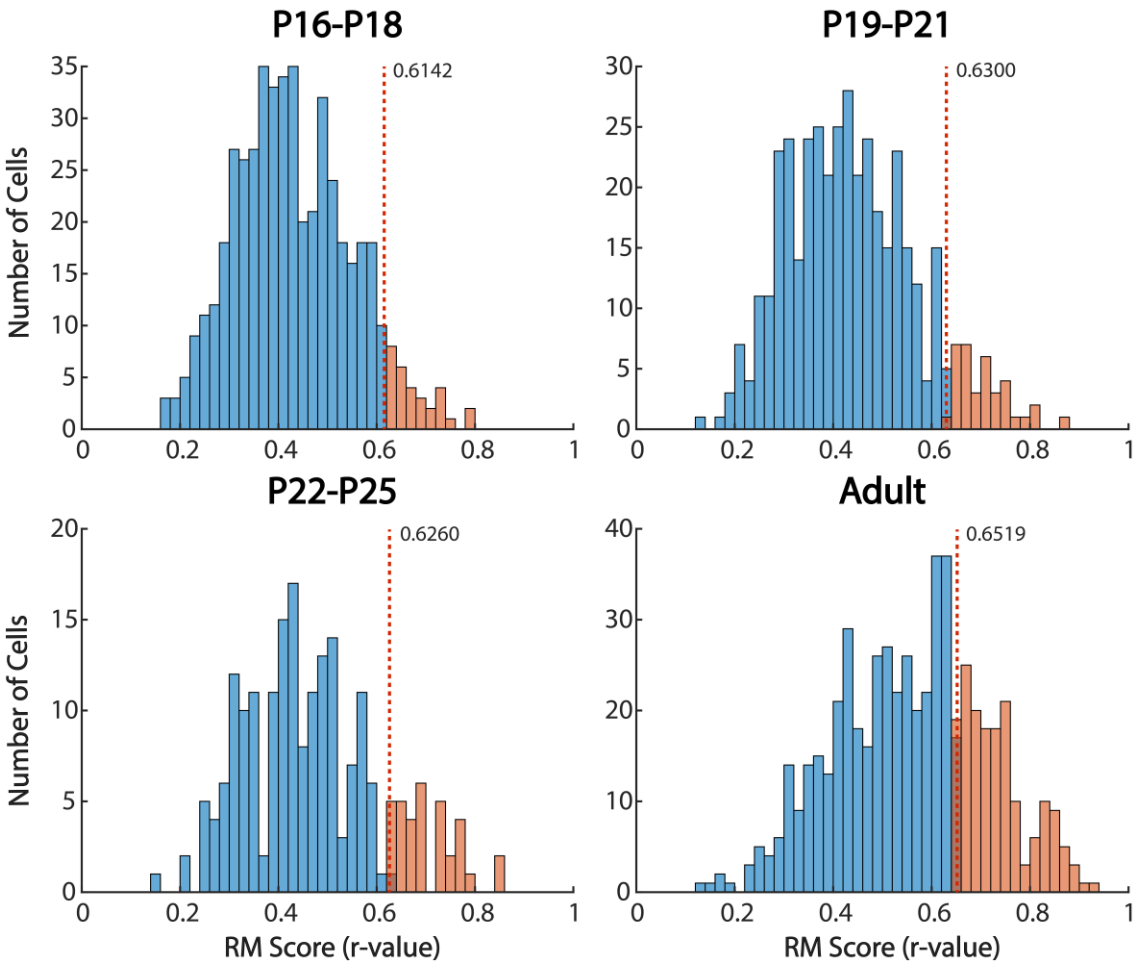

Figure 5.5 – Age-specific cell distribution and respective 99th percentile ranks of the maximum RM scores of shuffled rate maps. The histograms show the distribution of cells across the range of RM scores (bin width of 0.02) included (in orange) and excluded (in blue) from the analyses depending on whether their score surpassed the respective threshold (dashed red line). The age specific 99th percentile ranks are shown at the right of the dashed red line.

5.3.2 – Analyzed features

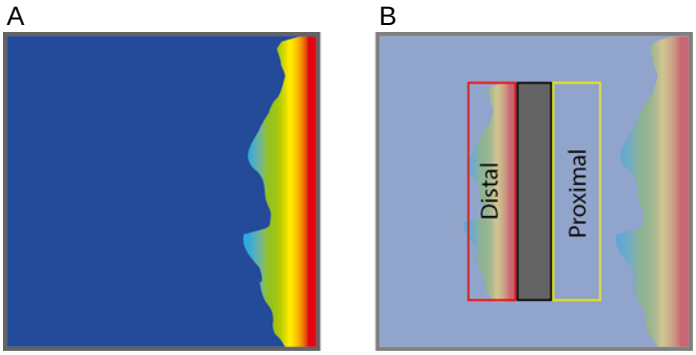

Figure 5.6– Example of region definition for barrier-related firing analysis. In this example, a boundary neuron fires along the East wall (A), and its firing field is expected to double when a barrier, parallel to the wall that the neuron is responding to, is inserted. The area where doubling is expecting is farthest from the firing field, and therefore Distal to it, while the area closest to the field is designated Proximal (B). These firing rate within each of these regions was measured in a baseline trial and corresponding probe, and these values used for subsequent analyses.

Several features of the boundary cell dataset were then evaluated, namely: mean and peak firing rates, within- and across-trial stability, and spatial information.

A feature of BVCs is the barrier-triggered doubling of the firing field. To evaluate if the BVC barrier response also changed during postnatal development, we used a method first introduced in Bjerknes et al. (2015).

Firstly, based on the position of the barrier, a 10cm-wide area along each long side of the barrier (equivalent to a 4bin-wide region from each side of the barrier in the rate map) was generated. Thus, for each barrier probe, two areas were defined in relation to the barrier: in N-S barrier orientation probes, a 10cm area to the right and another to the left of the barrier (see Figure 5.6B); in W-E barrier trials, a 10cm area above the barrier, and a same size area below it. The cell's mean firing rate in each of these areas was calculated in the baseline trials and barrier probes. Subsequently, the position of a cell's firing field in the environment (N, S, W, or E) was determined by finding the boundary closest to the peak firing rate bin in the baseline rate map. In ambiguous situations where the bin with the highest firing was located in an area that could be considered part of two boundaries – for instance, if the bin was located in a NW position and the cell could therefore have responded to either the N and/or W walls –, the mean firing rate of 4bin-wide areas along the length of disputed boundaries was calculated. The location of the field with highest mean firing was then used to determine the position of the firing field. Depending on the location of the maximal firing bin/region, the barrier defined area closest to the firing field – where no increase of firing should be observed – is considered proximal, while the area on the other side of the barrier and farthest from the field – where doubling should occur – is considered distal (see Figure 5.6). The firing rates in these areas were then compared between baseline and barrier probes and across the different age groups.

5.3.3 – Statistical tests

All the characteristics mentioned above were analyzed using parametric statistical methods. To do so, spatial information, mean and peak firing rate values were transformed by calculating the natural logarithm (ln) of each value. This ensured that these data did not violate the assumptions of normality and homoscedasticity of parametric analyses. These variables, as well as within- and across-trial stability, were then compared across the age groups using ANOVA, followed by Tukey-HSD test for post-hoc comparisons.

The barrier-related changes in firing rates were analyzed with a repeated measures ANOVA, and the effect of the trial type (the within-subjects factor) and age (the between-subjects factor) on the firing rate in the distal and proximal barrier regions was determined. The simple main effects were then assessed using Bonferroni corrected post-hoc comparison.

All cell percentages were compared with the aid of Two-Proportion Z-Tests. Differences in preferred tuning distance of putative boundary cells was evaluated with Mann-Whitney U tests. The uniformity of the same selected cells tuning angles was evaluated with the Hodges-Ajne test, while comparisons between methods were carried out with a multi-sample test for equal median directions test.

5.4 Histology

To confirm the position of the recording tetrodes, brain slices from each animal were obtained, stained and imaged as described in section 4.6 (page 79). The most representative histological sections – chosen on the basis of visible electrode tracks – of each of 13 rat pups and 4 adults used in this experiment are shown in Figures 5.7, 5.8, and 5.9.

The coordinates used, according to Paxinos and Watson (2006), would place the majority of the recording electrodes in the anterior portion of septal/dorsal Sub. Given this, it is not unlikely that some of the recording electrodes were closer to CA1 or the transition area between Sub and CA1. Nevertheless, if boundary-associated neurons were recorded in any given tetrode, the data were analyzed with the assumption that the electrodes had reached Sub. If the histological data did not corroborate this assumption, all recordings from that animal would be excluded. This was performed for two rat pups (data not shown) leaving 13 animals where the majority of tetrode tracks were identified to be reaching Sub or in its vicinity. The position of the recording electrodes also varied

along the transverse axis, but the majority of tetrode tracks were found to be in proximal half of the Sub. Given these observations, it is possible that some CA1 activity may have been recorded. In fact, place cells were identified in some of the datasets. But given that histological analysis, as performed here, does not allow for an accurate identification of the placement of individual tetrodes, all electrodes where boundary-coding neurons were observed were included in further analyses.

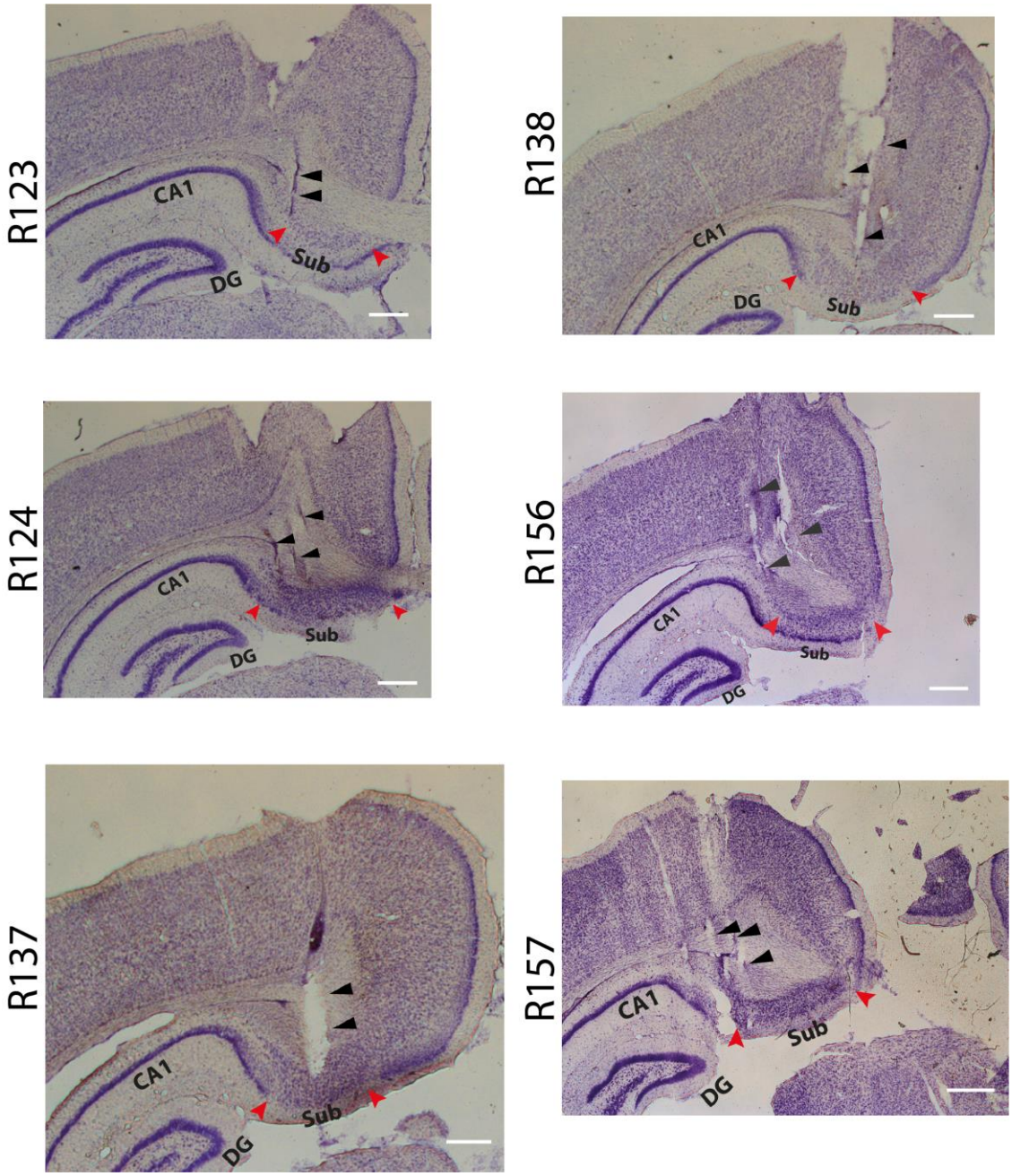

Figure 5.7 – Histological images of the recorded rat pup brains. Each image corresponds to a brain slice from a different animal, and all the images are from rat pups brain slices. The different brain areas (DG, CA1, and Sub are highlighted, with Sub being delineated by the red arrows. The tetrode tracks are highlighted by black arrows. The white bars in the bottom right corners are scaled to 500µm.

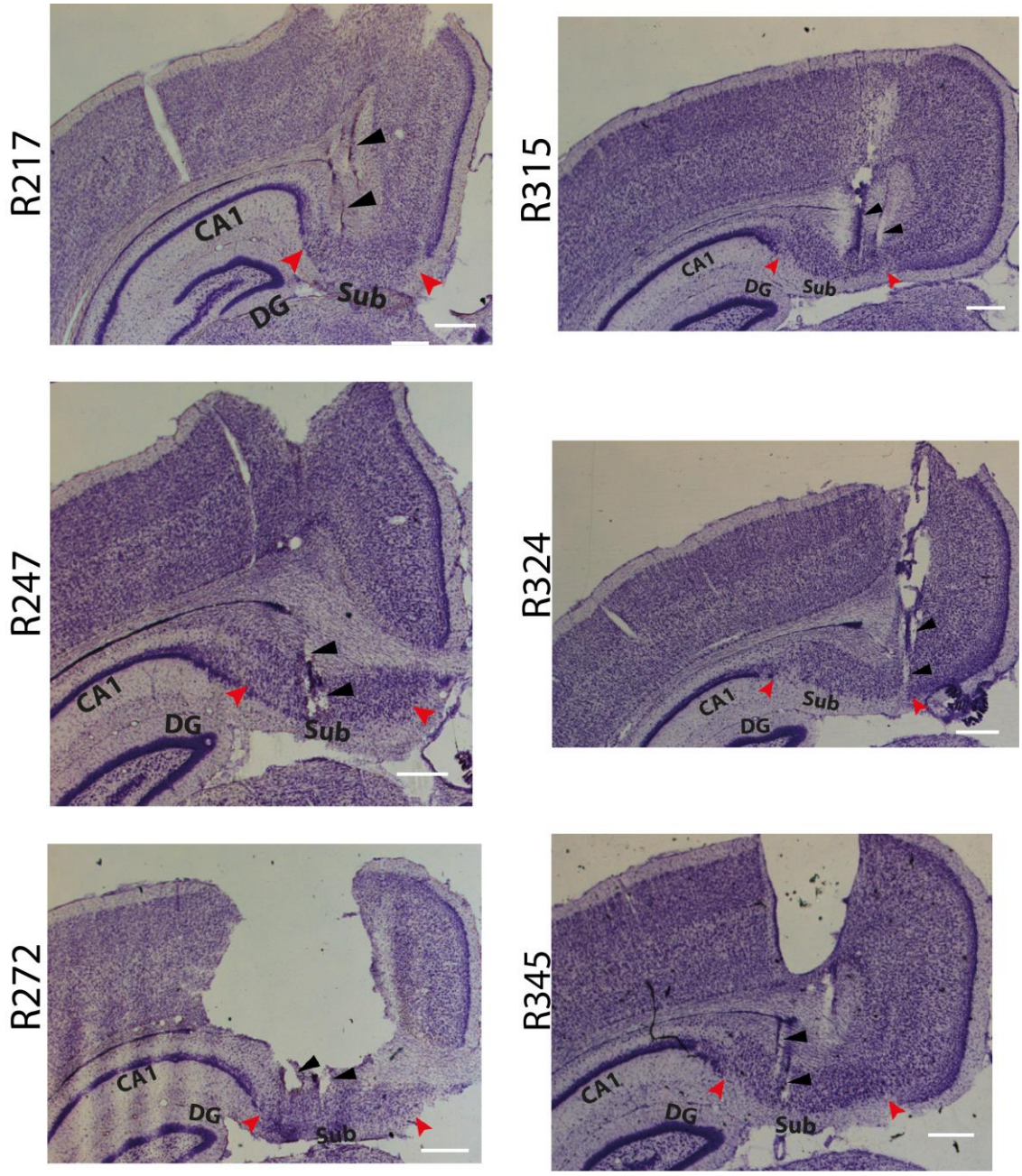

Figure 5.8 – Histological images of the recorded rat pup brains II. Each image corresponds to a brain slice from a different animal, and all the images are from rat pup brain slices. The different brain areas (DG, CA1, and Sub are highlighted, with Sub being delineated by the red arrows. The tetrode tracks are highlighted by black arrows. The white bars in the bottom right corners are scaled to 500µm.

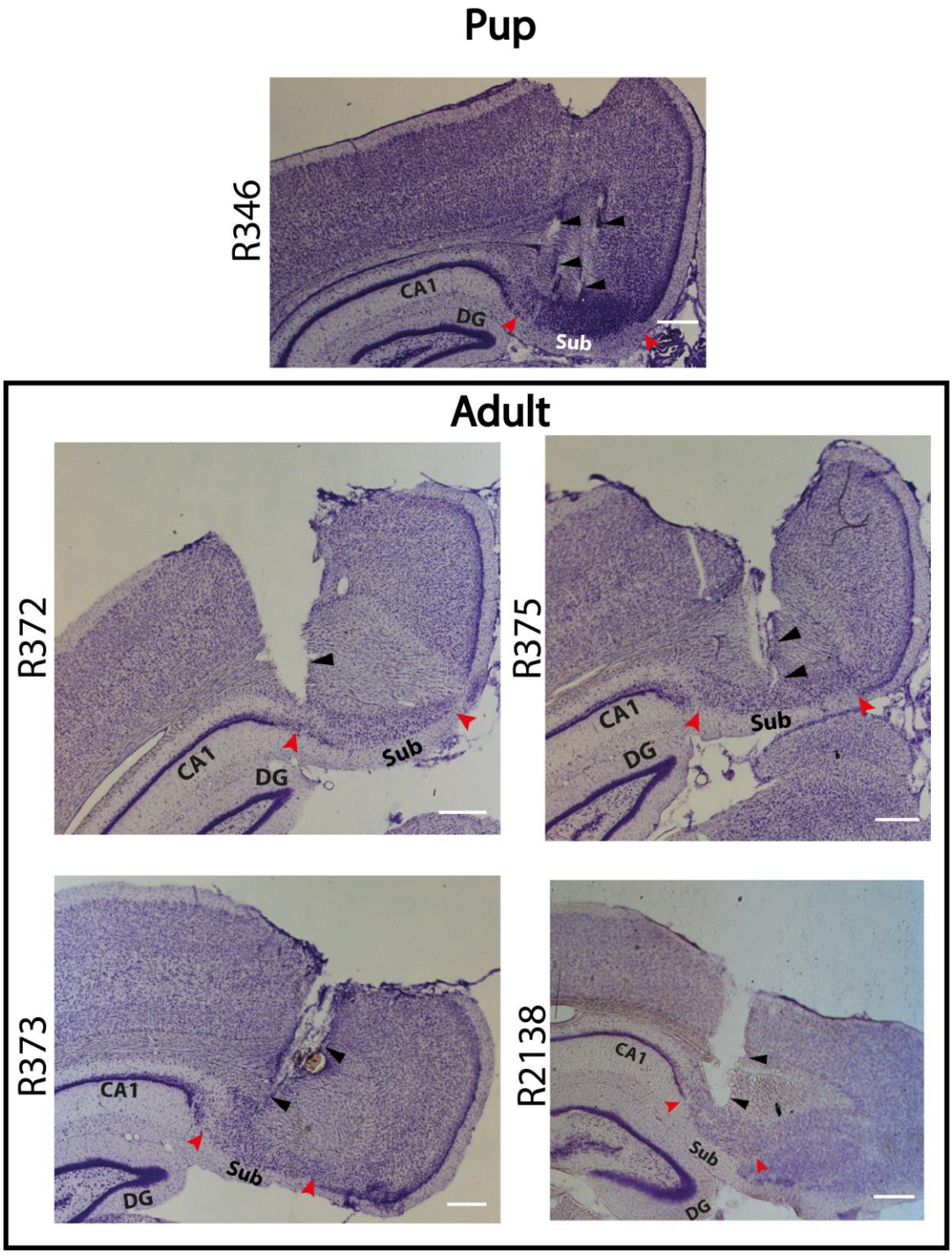

Figure 5.9 – Histological images of the recorded rat pup and adult rat brains. Each image corresponds to a brain slice from a different animal. The adult rat brain slices are contained within the black rectangle, while the pup brain image is not. The different brain areas (DG, CA1, and Sub are highlighted, with Sub being delineated by the red arrows. The tetrode tracks are highlighted by black arrows. The white bars in the bottom right corners are scaled to 500µm.

5.5 – Performance of the BVC Selection Methods

5.5.1 – Putative BVCs according to the Border Score method

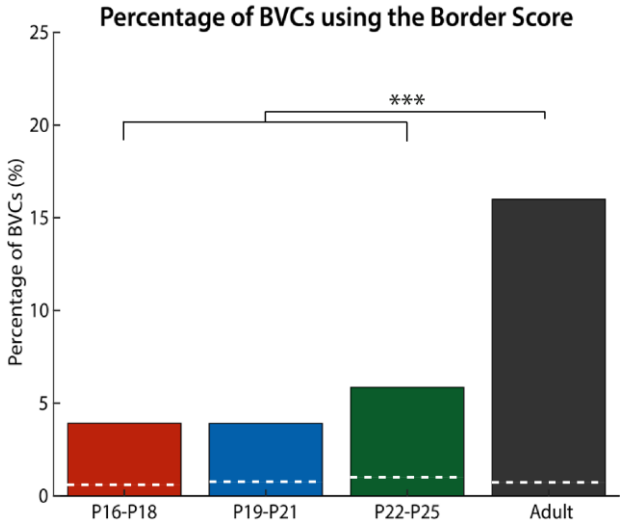

Figure 5.10 – Percentages of selected BVCs using the 95th percentile rank of the BS and spatial information of age matched population shuffled rate maps as a threshold. According to this selection method, only approximately 5% of the recorded cells in rat pup age groups are considered boundary-responsive, compared to approximately 15% in the adult data. The white lines are chance lines, i.e. the percentage of cells from each dataset that would be considered BVCs by chance.

Using the BS selection criteria – BS and spatial information (SI) –border cells were isolated from each age group (for more details, see section 5.3.1.1, page 89). The proportion of selected cells varied between young age groups and adults:

- For the P16-P18 group, 19 out of 485 (3.9%) cells were selected as BVCs
- For the P19-P21, the number was 16 out of 409 (3.9%)
- For the P22-P25, 12 out of 205 (5.9%)
- For the adults, 92 out of 575 (16%)

The disparity in the number potential border cells between the adult dataset and the other young animal age groups is better observed in the percentage bar chart (Figure 5.10). According to this selection criterion, adults have a considerably higher proportion of border cells than young animals. Two-proportion Z-Test confirmed that the proportion of adult border cells is higher than in the remaining age groups (P16-P18, $Z=6.401$, $p<0.001$; P19-P21, $Z=5.978$, $p<0.001$, P22-P25, $Z=3.669$, $p<0.001$). No significant proportion differences are found between young animal age groups (for all comparisons, $Z<1.122$, $p>0.262$).

5.5.1.1– Selected cells

Examples of selected neurons according to this approach are shown in figures 5.11-5.14. As this selection method detects border selective neurons on the basis of both spatial information and border score, cells for each age group were ranked by their mean SI and BS values. As expected by the scoring method, the cells selected across age groups tend to have narrow firing fields aligned along one of the environmental boundaries. This approach might have also led to the inclusion of cells with place-like fields located along the environmental boundaries (for example the 1st cell in Figure 5.10). Additionally, as this method only detects fields in the vicinity of boundaries across

baseline trials, some of the selected cells in young animal age-groups do not display barrier-induced field doubling (Figures 5.11 to 5.13). Nevertheless, boundary responses and respective barrier-related field doubling can be found across all age groups.

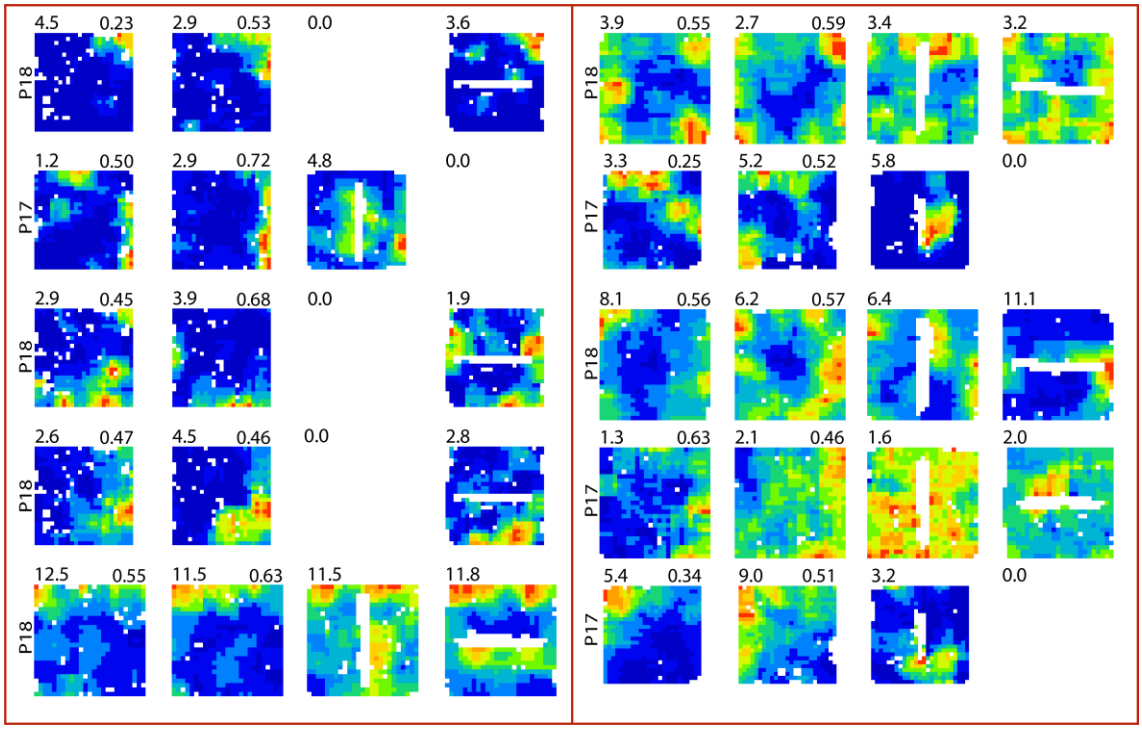

Figure 5.11 – Examples of neurons selected with the Border Score method in the P16-P18 age group. Here, 10 cells from the P16-P18 age group are shown across the four trials the animals were tested on (from left to right: Baseline, Baseline, Barrier, Barrier). Five cells (one per row) are shown in the left half, and other five in the right half. The peak firing rate of the rate map is shown on the top left corner, and its BS is shown on the top right. All these cells have at least one baseline trial whose BS and SI values are higher than the percentile of a population of shuffled scores from all the recorded cells in this age group. The cells were ranked by their mean SI and BS values. The animal's age on the day of recording is shown before the respective rate map sequence.

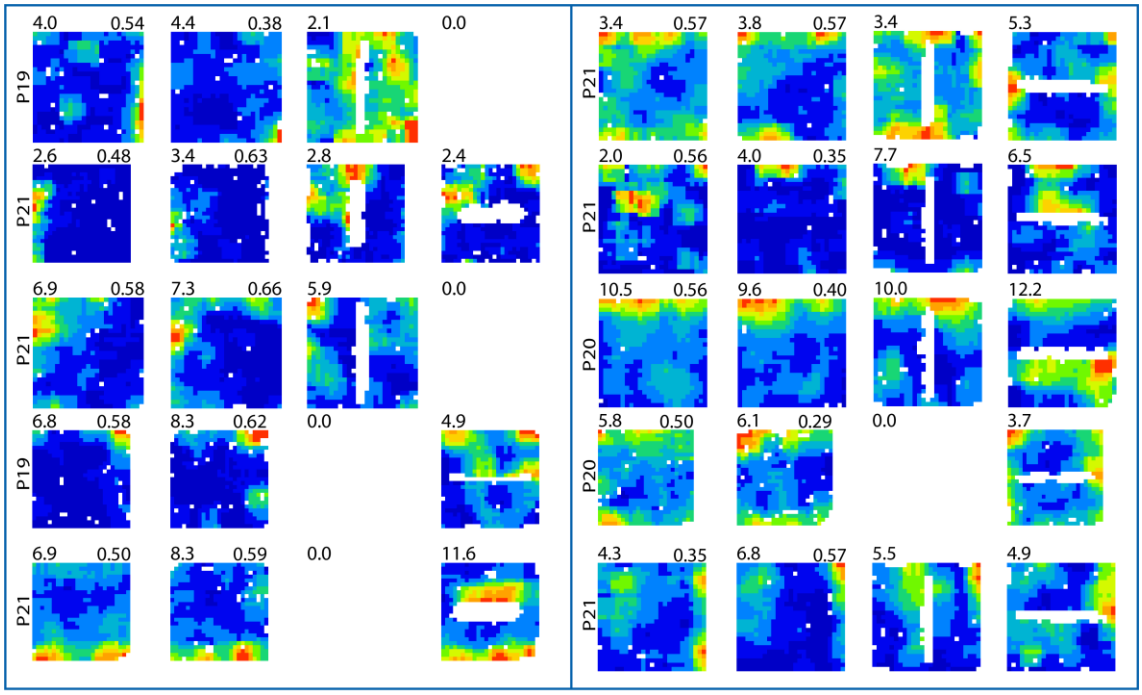

Figure 5.12 – Examples of neurons selected with the Border Score method in the P19-P21 age group. Ten cells from the P19-P21 age group are shown across the four trials the animals were tested on (from left to right: Baseline, Baseline, Barrier, Barrier). The peak firing rate of the rate map is shown on the top left corner, and its BS is shown on the top right. All these cells have at least one baseline trial whose BS and SI values are higher than the percentile of a population of shuffled scores from all the recorded cells in this age group. The cells were ranked by their mean SI and BS values. The animal's age on the day of recording is shown before the respective rate map sequence.

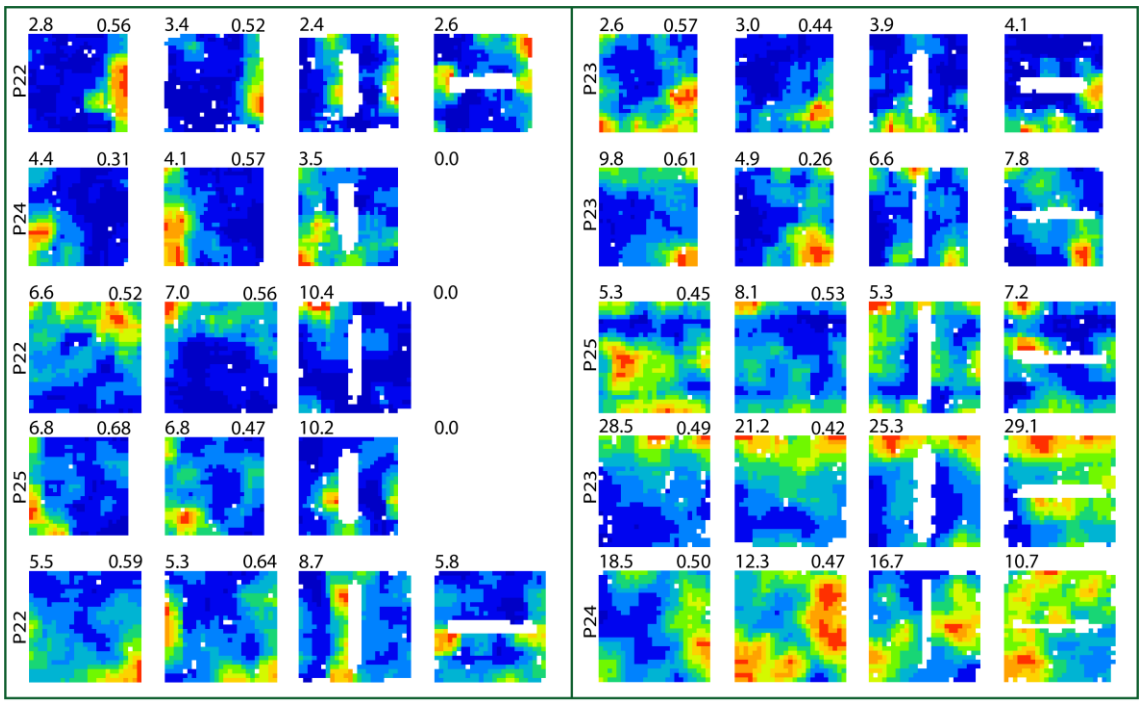

Figure 5.13 – Examples of neurons selected with the Border Score method in the P22-P25 age group. Ten cells from the P22-P25 age group are shown across the four trials the animals were tested on (from left to right: Baseline, Baseline, Barrier, Barrier). The peak firing rate of the rate map is shown on the top left corner, and its BS is shown on the top right. All these cells have at least one baseline trial whose BS and SI values are higher than the percentile of a population of shuffled scores from all the recorded cells in this age group. The cells were ranked by their mean SI and BS values. The animal's age on the day of recording is shown before the respective rate map sequence.

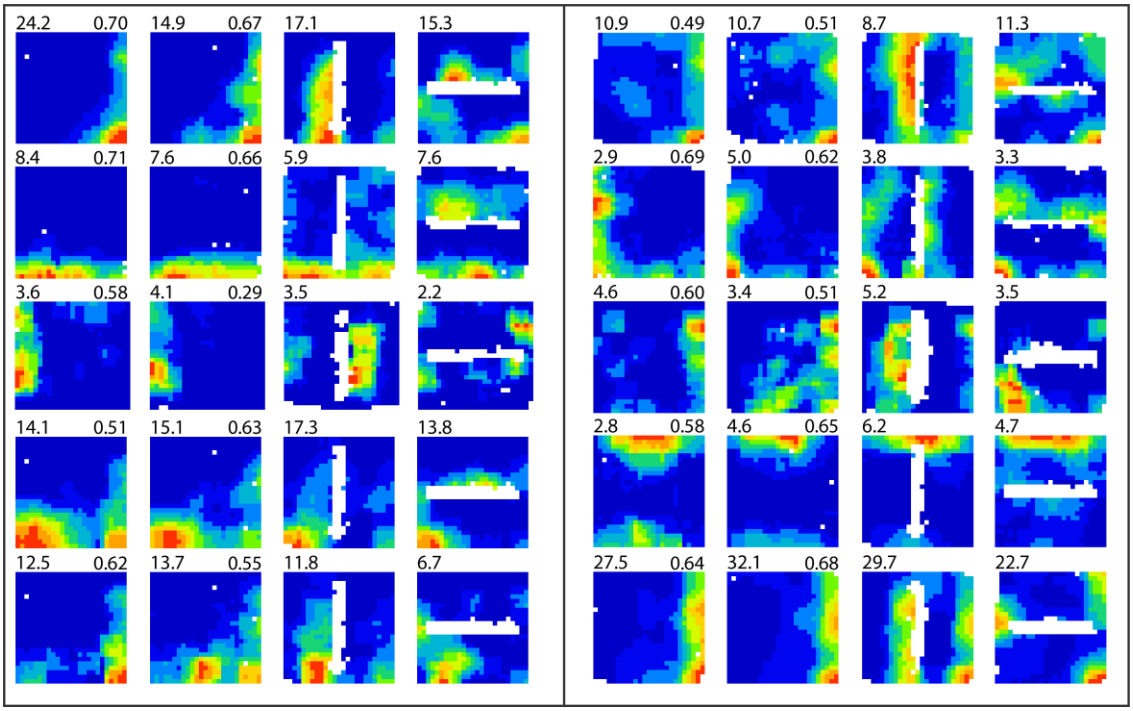

Figure 5.14 – Examples of neurons selected with the Border Score method in adult rats. Ten adult cells are shown across the four trials the animals were tested on (Baseline, Baseline, Barrier, Barrier). The peak firing rate of the rate map is shown on the top left corner, and its BS is shown on the top right. All these cells have at least one baseline trial whose BS and SI values are higher than the percentile of a population of shuffled scores from all the recorded cells in this age group. The cells were ranked by their mean SI and BS values.

5.5.2 – Putative BVCs according to the Response Model method

As an alternative to the BS approach used in the previous section, the BVC Response Model score approach (described in section 5.3.1.2, page 91) was developed and applied to the same data. Following this approach, the numbers of recorded BVCs across the different age groups were as follows:

- 30 out of 485 (6.2%) in the P16-P18 group,
- 36 out of 409 (8.8%) in the P19-P21 age bin,
- 34 out of 205 (16.6%) in the P22-P25 group,
- And 169 out of 575 (29%) in the adult dataset.

The proportions and respective Z-test results are illustrated in Figure 5.15. Overall, just as for the BS approach, the adult dataset contains significantly more cells than young animal age groups (P16-P18, $Z=9.639$, $p<0.001$; P19-P21, $Z=7.838$, $p<0.001$, P22-P25, $Z=3.588$, $p<0.001$). The P22-P25 age group also has a significant higher proportion of cells than the P16-P18 ($Z=4.304$, $p<0.001$) and P19-P21 ($Z=2.862$, $p=0.004$) age groups. No significant differences are found between the P16-P18 and P19-P21 groups ($Z=1.490$, $p=0.136$).

5.5.2.1– Selected cells

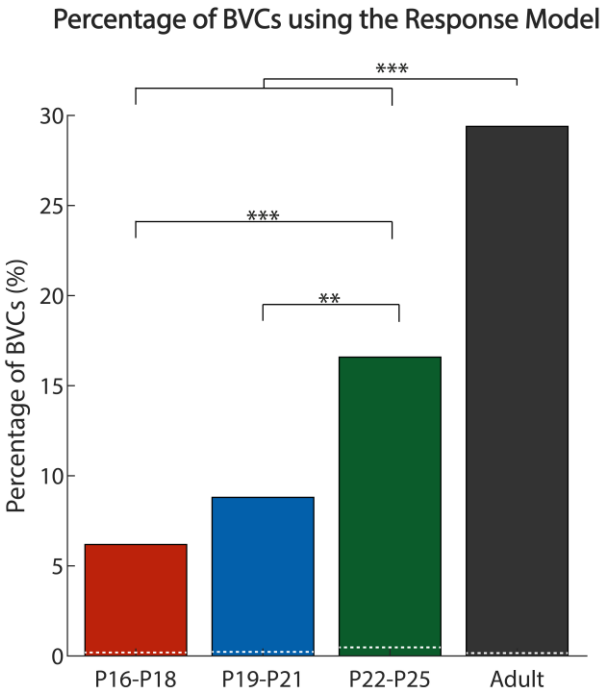

Figure 5.15 – Percentages of selected BVCs using the 99.7th percentile rank of the BVC Model Score of age matched population shuffled rate maps as a threshold. The percentage of BVCs recorded from the rat Sub appears to increase over time. The white lines are chance lines, i.e. the percentage of cells from each dataset that would be considered BVCs by chance.

Examples of cells identified as BVCs using the RM approach are shown throughout Figures 5.16 to 5.19.

Just as with the BS method, some of the cells selected do not show clear field doubling in the barrier trials, particularly in young animal age-groups (6^{th} cell in Figure 5.16 or 2^{nd} cell in Figure 5.18) and some do not even exhibit a BVC-like activity pattern, *i.e.*, no consistent firing along environmental boundaries or field doubling upon barrier insertion (8^{th} and 10^{th} cell in Figure 5.16).

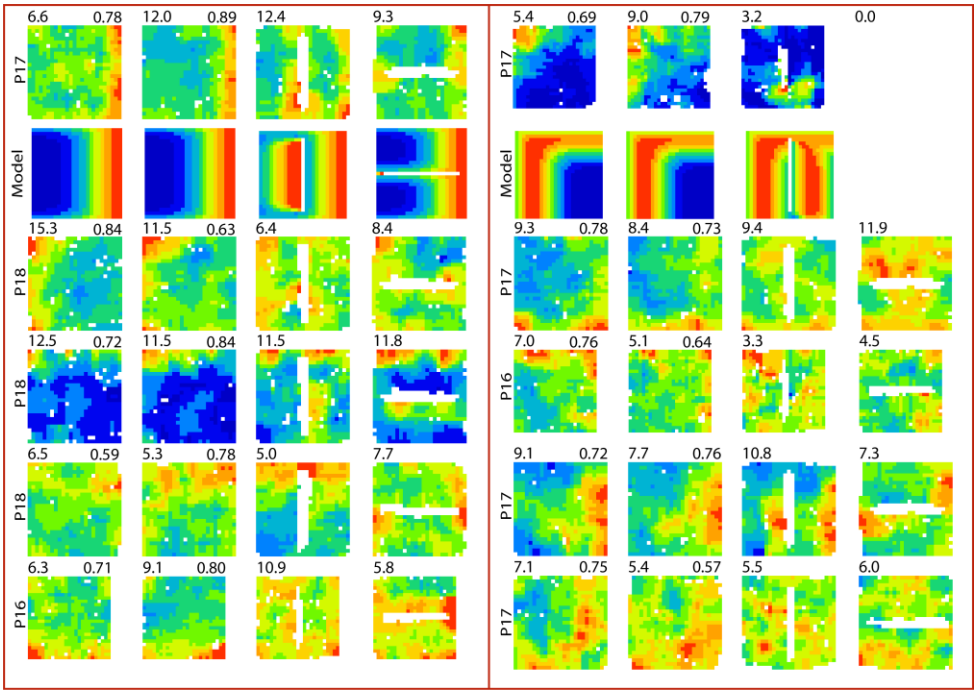

Figure 5.17 – Examples of neurons selected with the Response Model method in the P16-P18 age group. Ten cells from this dataset are shown across four trials the animals were tested on. Five cells (one per row) are shown in the left half, and other five in the right half. The peak firing rate of each map is shown on the top left corner, and its respective RM score is shown on the top right. The highest scoring cell is in the top left side of the figure, while the cells in 5th and 10th ranks are located on the bottom left and right half of the figure, respectively. The animal's age on the day of recording is shown before the respective rate map sequence. The model response for the cells in the top row are presented below them.

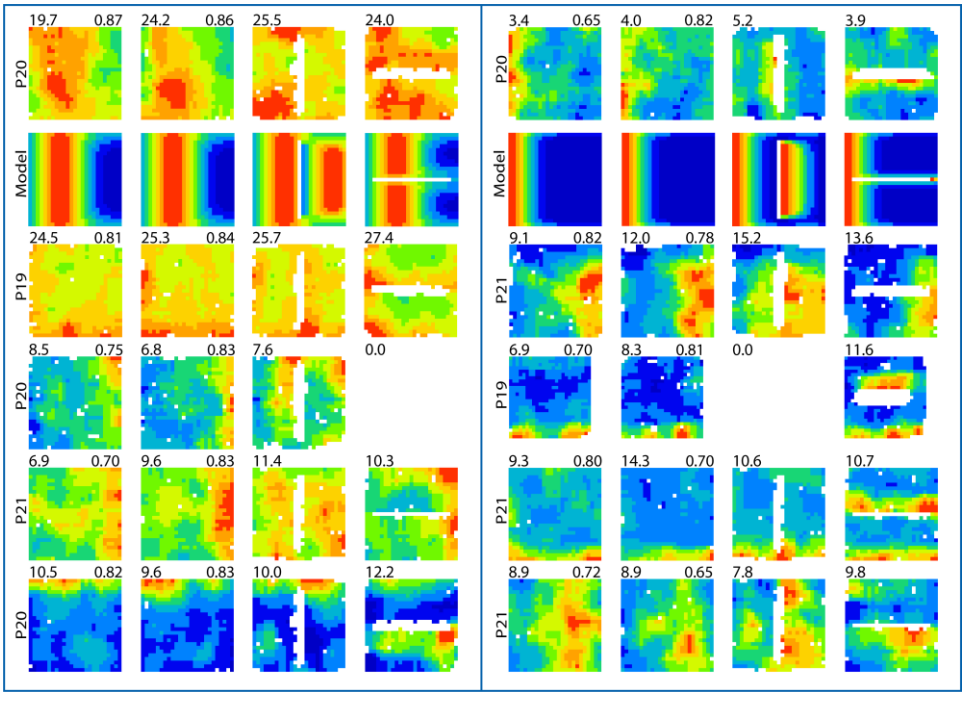

Figure 5.16 – Examples of neurons selected with the Response Model method in the P19-P21 age group. Ten cells from this dataset are shown across the four trials the animals were tested on. Five cells (one per row) are shown in the left half, and other five in the right half. The peak firing rate of each map is shown on the top left corner, and its respective RM score is shown on the top right. The highest scoring cell is in the top left side of the figure, while the cells in 5th and 10th ranks are located on the bottom left and right half of the figure, respectively. The animal's age on the day of recording is shown before the respective rate map sequence. The model response for the cells in the top row are presented below them.

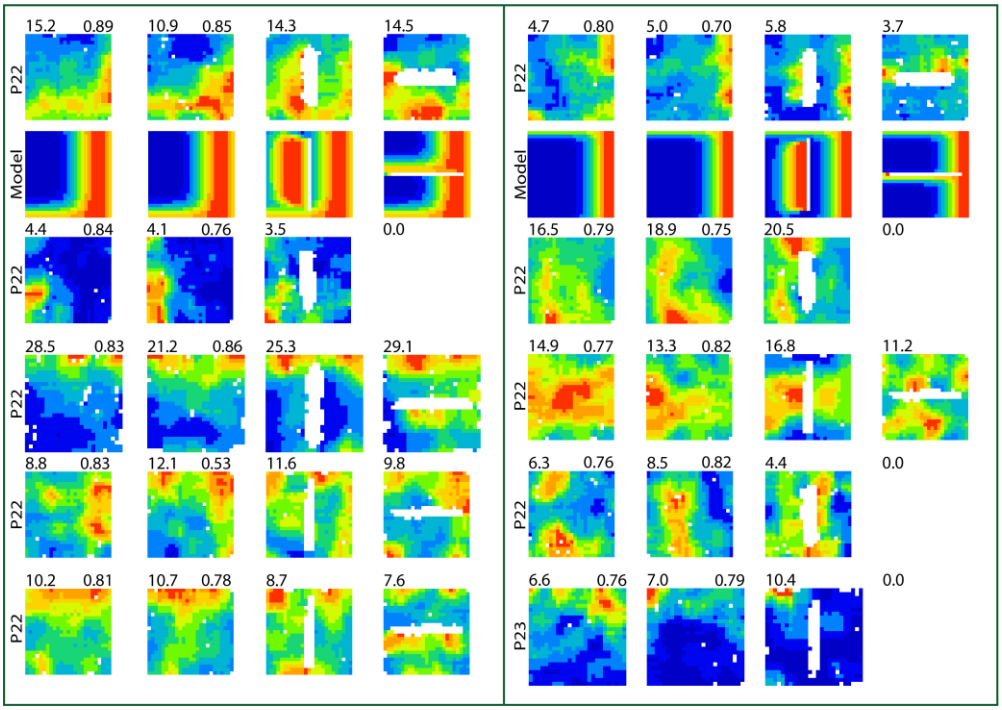

Figure 5.19 – Examples of neurons selected with the Response Model method in the P22-P25 age group. Ten cells from this dataset are shown across the four trials the animals were tested on. Five cells (one per row) are shown in the left half, and other five in the right half. The peak firing rate of each map is shown on the top left corner, and its respective RM score is shown on the top right. The highest scoring cell is in the top left side of the figure, while the cells in 5th and 10th ranks are located on the bottom left and right half of the figure, respectively. The animal's age on the day of recording is shown before the respective rate map sequence. The model response for the cells in the top row are presented below them.

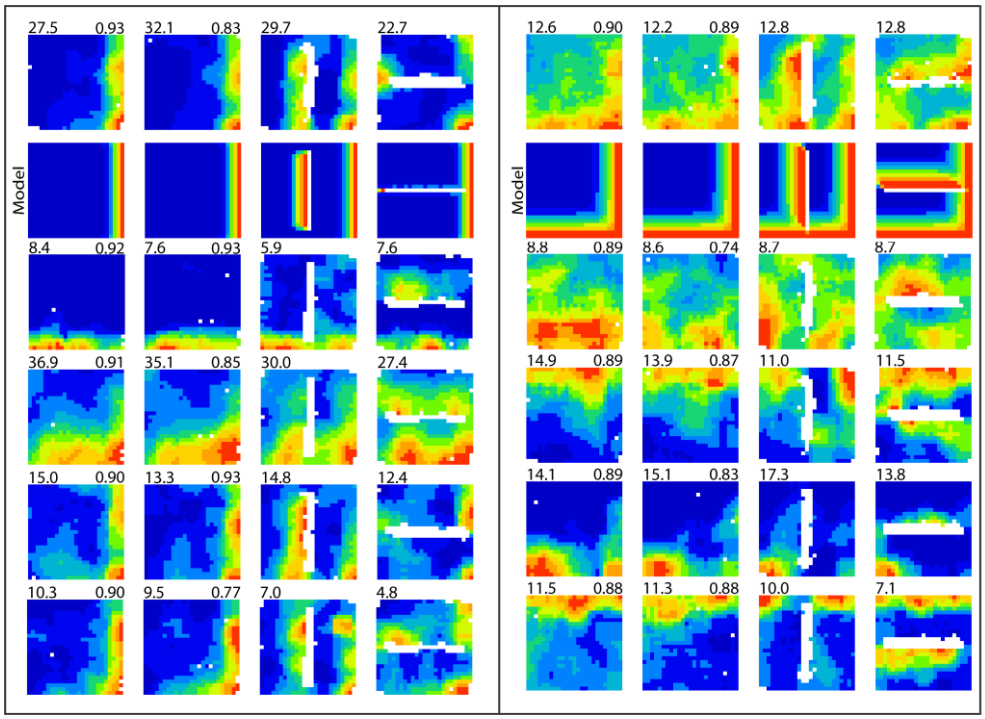

Figure 5.18 – Examples of neurons selected with the Response Model method in the Adult age group. Ten adult cells are shown across the four trials the animals were tested on. Five cells (one per row) are shown in the left half, and other five in the right half. The peak firing rate of each map is shown on the top left corner, and its respective RM score is shown on the top right. The highest scoring cell is in the top left side of the figure, while the cells in 5th and 10th ranks are located on the bottom left and right half of the figure, respectively. The model response for the cells in the top row are presented below them.

5.5.3 – The preferred distance, but not angular tuning of selected cells varies between detection methods

To further compare the effectiveness of both detection methods, the cells selected by both the RM (n=269 cells) and BS (n=139 cells) approaches were compared in terms of their receptive field's tuning distance and bearing. These two features were extracted from each cell's best-fit receptive field, which in turn correspond to the field whose properties generated the maximum correlation score between any of the cells' baseline rate maps and the predicted response map (see section 5.3.1.2.1, page 92 for more details).

Histograms denoting the distribution of preferred tuning distances (in rate-map bins) of boundary-coding cells across the evaluated age groups are shown in Figure 5.20. Overall, the range of preferred tuning distances for BS-selected cells seems to be narrower than that of RM-selected ones. This is expected due to the way the BS is calculated as well as the use of spatial information as an additional threshold for cell isolation. The median distance tuning of putative boundary-coding cells in rate-map bins selected by either the BS or RM methods did not vary for the P16-P18 (BS median=1.5bins, RM median=2.5bins, Mann-Whitney U=235, p=0.302) or the P22-P25 (BS median=2.0bins, RM median=4.5bins, Mann-Whitney U=136.5, p=0.090) age

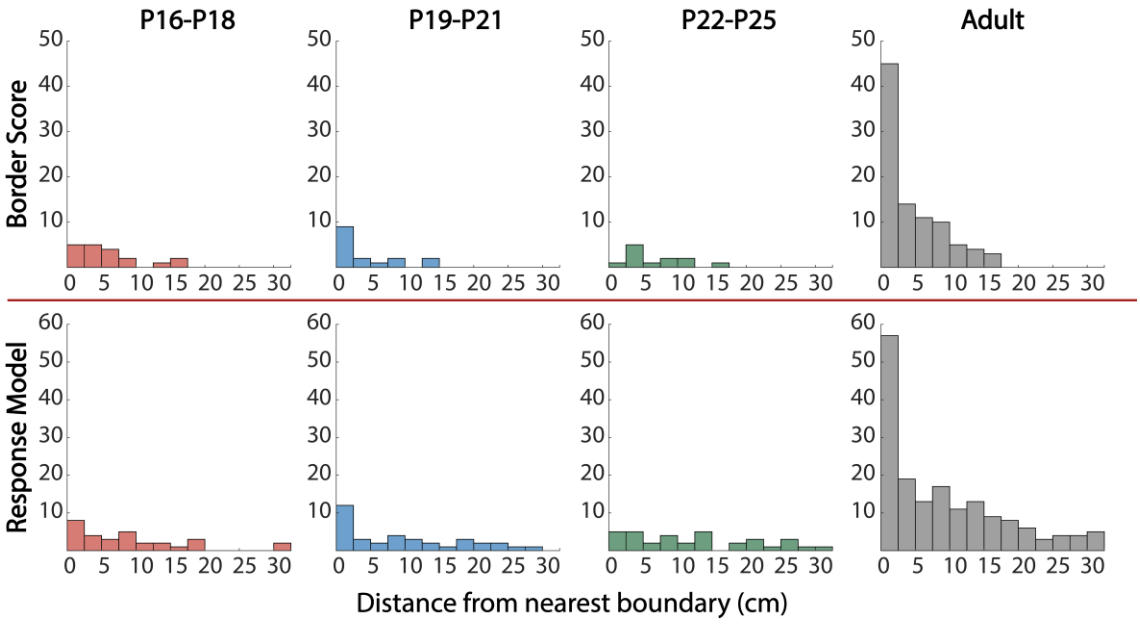

Figure 5.20 – Tuning distance distributions of boundary-coding cells selected by the BS or RM methods across age groups. The figure shows the tuning distance distributions in rate-map bins of putative boundary-coding cells selected by both the BS (top row) and RM (bottom row) methods in histogram form (bar width, 2.5bins) across age groups (organised in columns). Mann-Whitney U tests revealed significant differences in the median tuning distances of cells selected by either method in the P19-P21 (U=182, p=0.032) and Adult (U=5452, p<0.001) groups, but not for the P16-P18 (U=235, p=0.302) or P22-P25 (U=136.5, p=0.090) ones.

groups. However, significant median distance-tuning differences between methods were found in the P19-P21 (BS median=0.25bins, RM median=3.0bins, Mann-Whitney U=182, p=0.032) and Adult (BS median=1.0bins, RM median=2.5bins, Mann-Whitney U=5452, p<0.001) groups. These results are in line with what is expected from both methods. The BS method ought to include cells with shorter tuning distances from boundaries, as cells with fields closer to boundaries will score higher. The RM method reflects a given cell's similarity to a predicted response and not the proximity of its field to a boundary, and thus it seems to include cells with broader tuning distances.

The distribution of receptive field tuning-angles of putative boundary cells selected by either the BS or RM approaches are shown in Figure 5.21. Interestingly, the tuning angles cells selected with the RM approach in the P16-P18 and Adult age groups, as

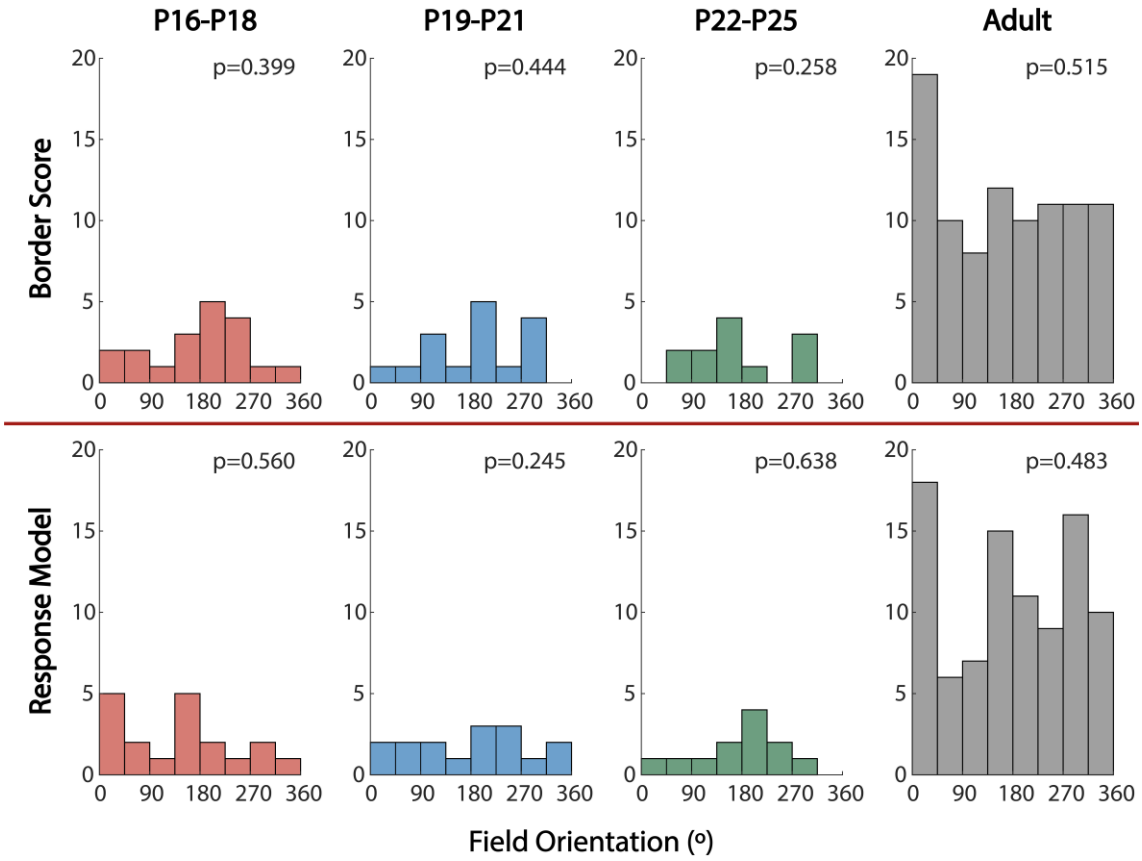

Figure 5.21 – Tuning angle distributions of boundary-coding cells selected by the BS or RM methods across age groups. The figure shows the bearing distributions of putative boundary-coding cells selected by both the BS (top row) and RM (bottom row) methods in histogram form (bar width, 45°) across age groups (organised in columns). The distribution of preferred bearings seems to cluster around cardinal points for Adult and P16-P18 cells selected with the RM method (first and last panels in the bottom row) and for P19-P21 cells selected with the BS (2nd panel, top row). However, Hodges-Ajne tests confirm that the tuning-angles of putative boundary cells selected by either method are uniformly distributed, regardless of age (the respective p-values conducted for each distribution are shown on the top right corner of each panel).

well as P19-P21 cells selected with the BS method, seem to cluster along cardinal points (0°/360°, 90°, 180°, and 270°). This effect could be the result of the geometry of the environment where the animals were tested in (a box). However, Hodges-Ajne tests for

angular uniformity indicated that putative boundary-coding neurons, regardless of selection method or age, may have uniformly distributed preferred bearings (the p-values for each age group and selection method in favor of the null hypothesis that the data is uniformly distributed are shown in the corresponding panel in Figure 5.21). However, it may be that this test is underpowered and may therefore not reveal the actual trends within the data. Further comparisons revealed the absence of significant differences in the circular median of preferred bearings between selection methods (P16-P18, BS median=182.5°, RM median=201.25°, P-statistic=1.830, p=0.176; P19-P21, BS median=182.5°, RM median=263.75°, P-statistic=0.173, p=0.677; P22-P25, BS median=175°, RM median=272.5°, P-statistic=2.310, p=0.129; Adult, BS median=46.25°, RM median=197.5°, P-statistic=1.377, p=0.241).

In summary, neither selection method is biased for putative boundary coding neurons with specific bearings. However, border neurons selected with the BS criterion have shorter median tuning distances than those selected with the RM method. This is due to the BS selection method attributing higher scores to cells with firing fields closer to environmental boundaries, as well as selecting for cells with relatively high spatial information indices. It may therefore result that the BS selection method does not include a larger range of boundary-driven responses. Thus, the RM method may outperform the BS when it comes to including cells with a more diverse range of responses.

5.5.4 – Both selection methods detect high numbers of the same cells in the adult dataset

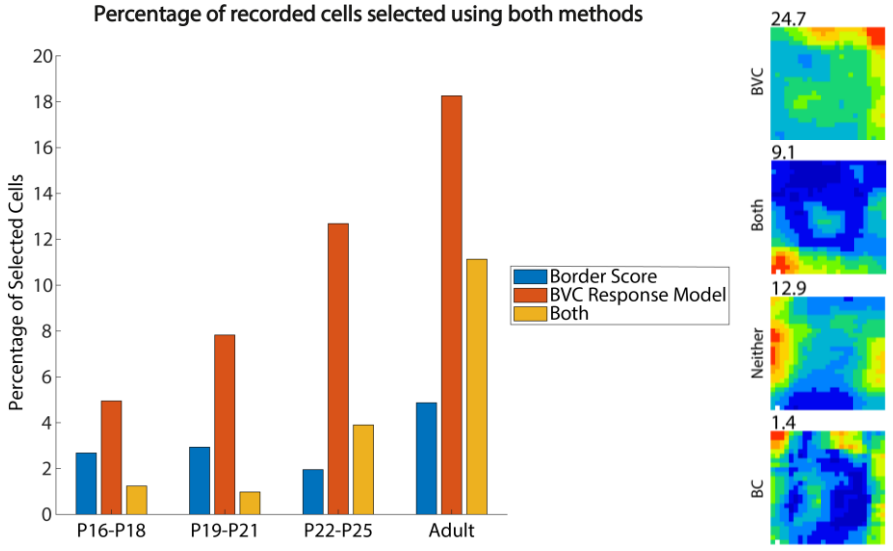

Figure 5.22 – Percentage of cells selected using the BS method, RM method, or both and examples. The percentage of cells selected using the RM fitting method is higher than that of the BS method across all groups, although both approaches fare better in selecting cells from the adult dataset. BC, border cell selected with the BS; BVC, boundary-vector cell selected with the Response Model.

The RM method seemingly identifies a higher number of potential boundary responsive neurons across all age groups. A closer look into the overlap of both detection methods, makes this difference more apparent. For data collected in adult animals, both methods fare relatively well – as indicated in Figure 5.22. The overlap is largest at for this dataset, and in the younger age groups the overlap of both methods is smaller. The smallest difference in the selection capabilities of both approaches is observed at in the P16-P18 age group, but in all other age groups the RM approach does appear to fare better.

Based on these observations, the RM approach seems to be more effective the BS in selecting not only more boundary-responsive neurons, but also including a broader range of boundary cells with varying tuning distances. Therefore, the postnatal maturation of subicular BVCs was primarily assessed using the neuron population obtained with the RM selection approach, but the same trends for the BS-selected data was also evaluated.

5.6 BVCs develop gradually, like their place cell 'neighbors'

5.6.1 – The percentage of recorded BVCs increases with age

Using RM-selected BVCs, and just as reported for place cell data (Wills et al., 2010), it appears that the number of observed BVCs increases throughout the sampled postnatal period (see Figure 5.15, page 105). Before weaning (which in the lab takes place at 21 days of age), boundary responses are observed in less than 10% of all recorded cells (6.2% in P16-P18 aged animals, and 8.8% in P19-P21 ones). After weaning, the number of recorded BVCs roughly doubles, going from 16.6% in P22-P25 animals to 29.4% in the adult Sub. Representative examples of BVCs selected using the model score approach can be found in Figures 5.23 through 5.26.

Based on the observation of the rate maps across each age group, and even across ages, it appears that the quality of the BVC signal improves over time and/or that the accuracy of cells selected with the model score increases. Nevertheless, it appears that subicular boundary coding neurons can be recorded from as early as P16. To objectively quantify the maturation of these neurons, the firing features of the selected cells across the different age groups were analyzed. All of the properties are defined and calculated as described in section 4.5.4 (page 79).

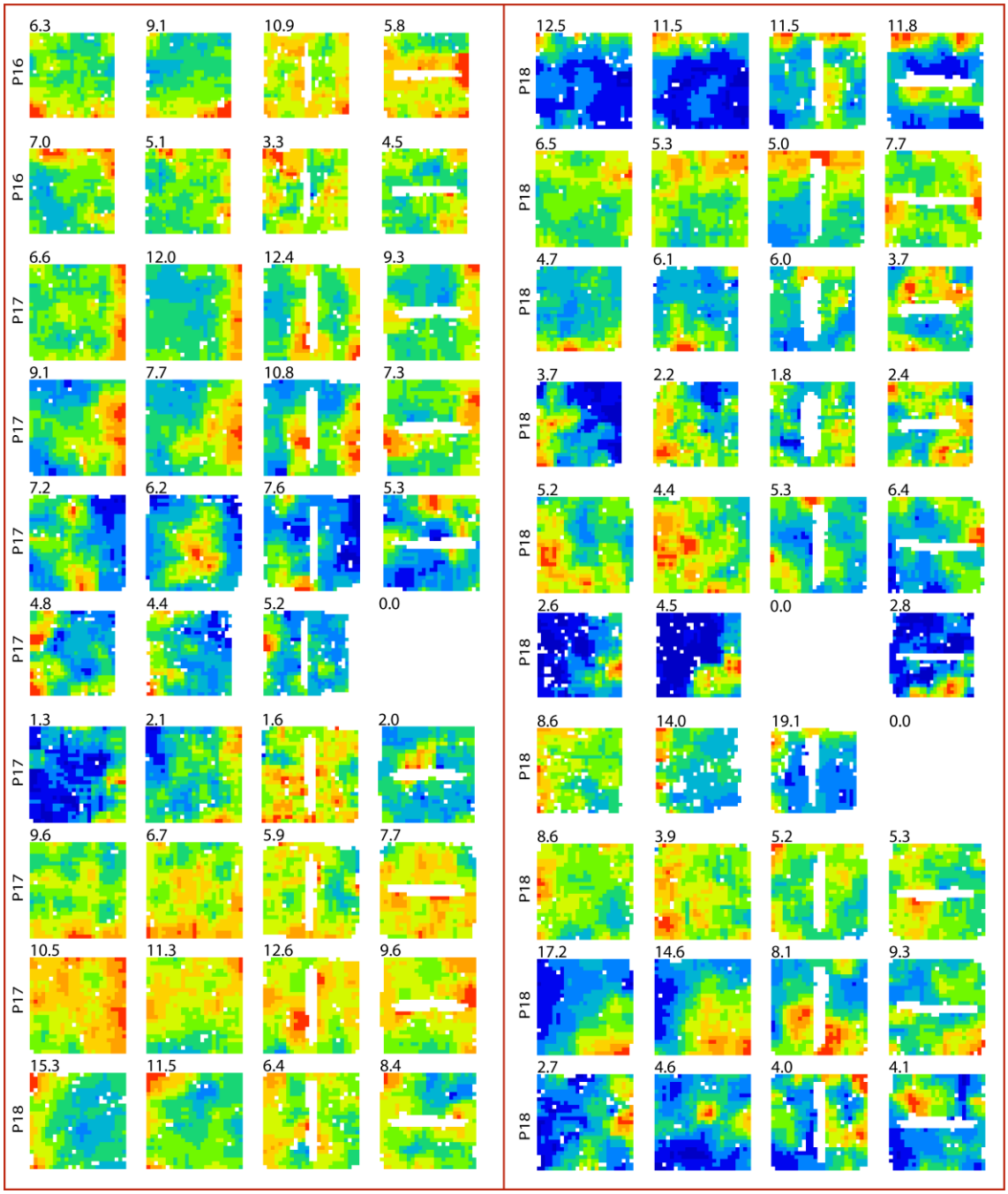

Figure 5.23 – Rate maps of putative BVCs in the P16-P18 age group. The figure shows 20 examples of recorded neurons in the P16-P18 dataset across the four trials the animals were tested on (from left to right: Baseline, Baseline, Barrier, Barrier). Ten cells (one per row) are shown in the left half, and other ten in the right half. The rate maps were then sorted by age (top-down, left to right) in ascending order. The peak firing rate of the rate map is shown in the top left corner. The animal's age on the day of recording is shown before the respective rate map sequence.

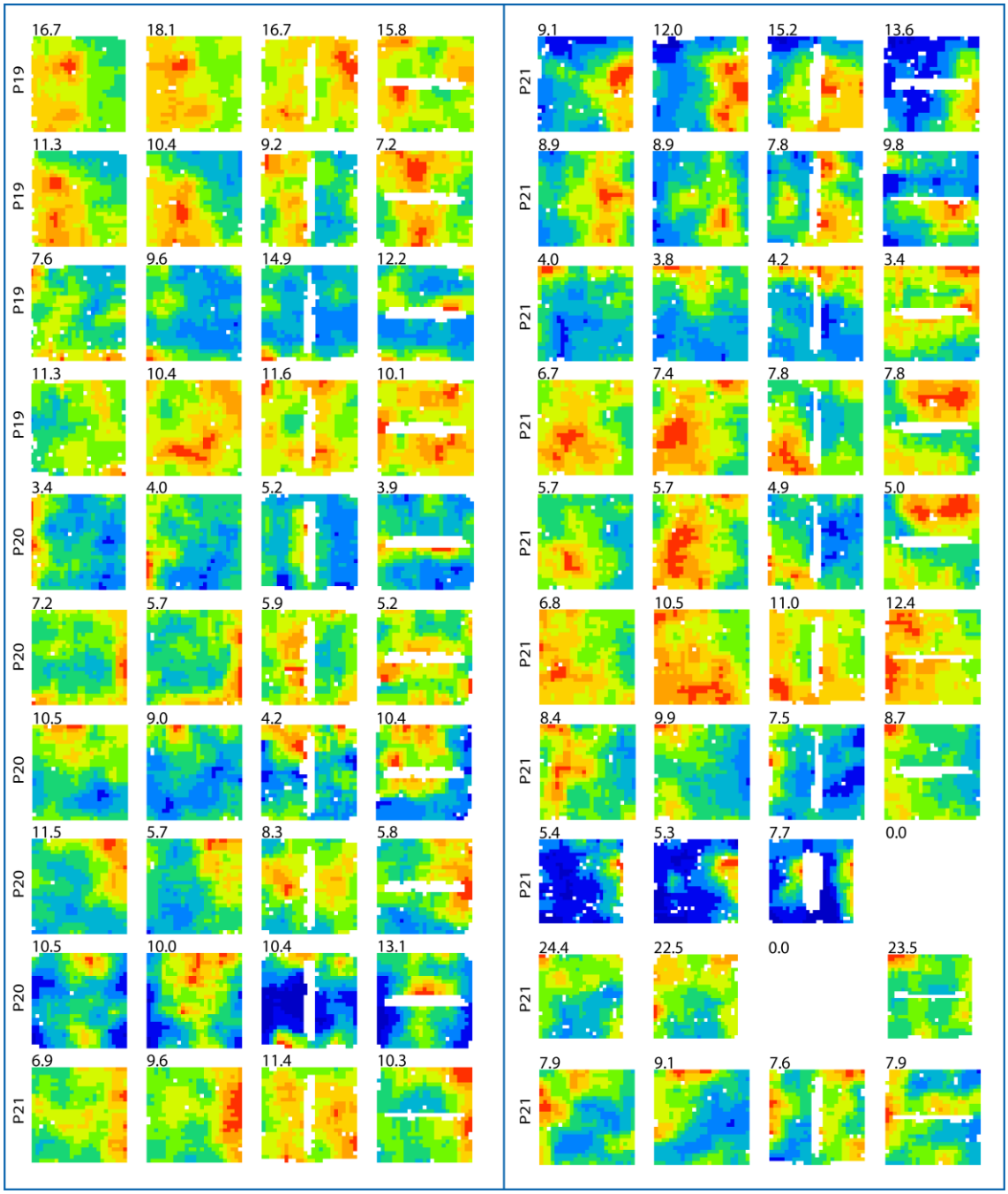

Figure 5.24 – Rate maps of putative BVCs in P19-P21 age group. The figure shows 20 examples of recorded neurons in the P19-P21 dataset across the four trials the animals were tested on (from left to right: Baseline, Baseline, Barrier, Barrier). Ten cells (one per row) are shown in the left half, and other ten in the right half. The rate maps were then sorted by age (top-down, left to right) in ascending order. The peak firing rate of the rate map is shown in the top left corner. The animal's age on the day of recording is shown before the respective rate map sequence.

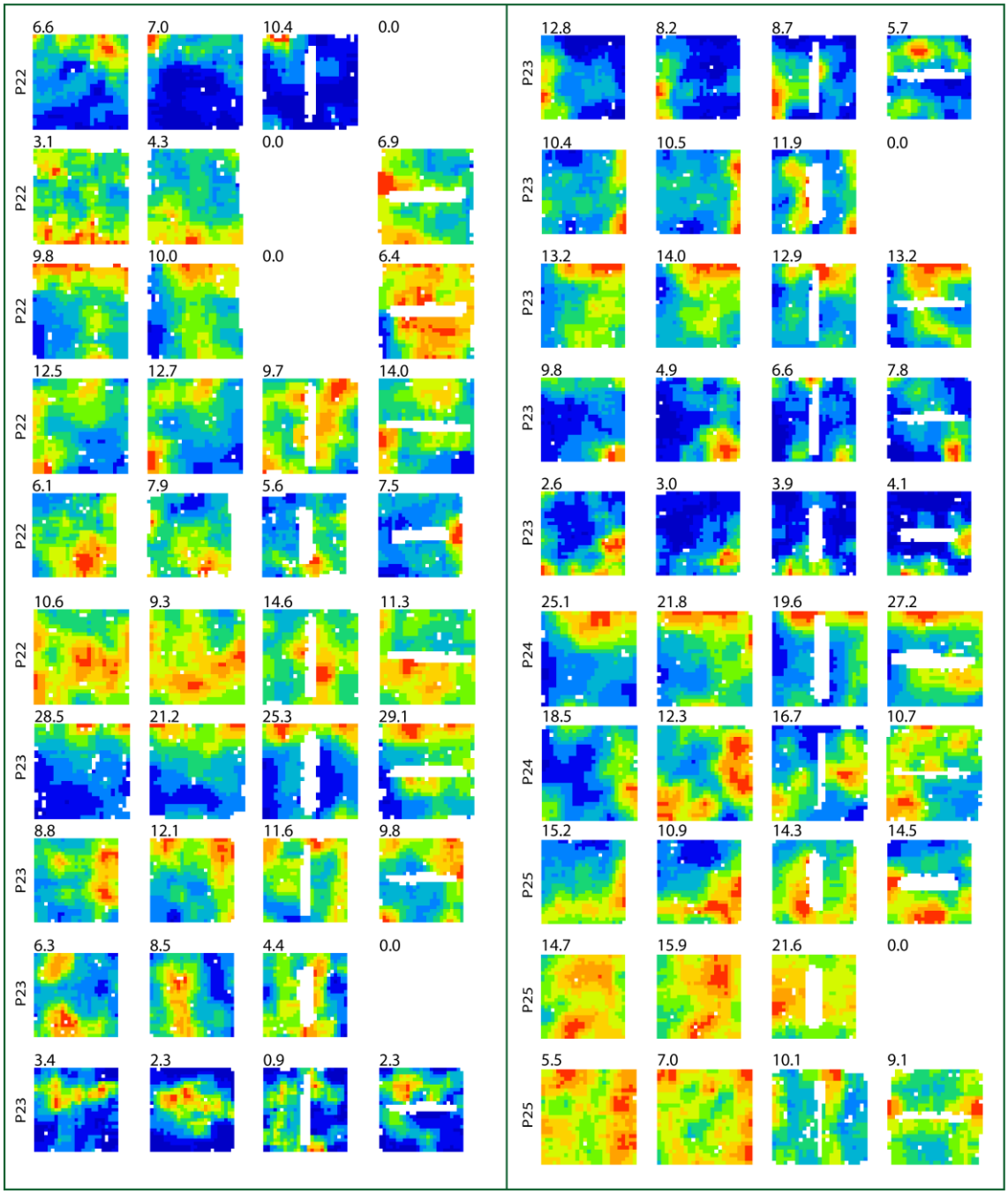

Figure 5.25 – Rate maps of putative BVCs in P22-P25 age group. The figure shows 20 examples of recorded neurons in the P22-P25 dataset across the four trials the animals were tested on (from left to right: Baseline, Baseline, Barrier, Barrier). Ten cells (one per row) are shown in the left half, and other ten in the right half. The rate maps were then sorted by age (top-down, left to right) in ascending order. The peak firing rate of the rate map is shown in the top left corner. The animal's age on the day of recording is shown before the respective rate map sequence.

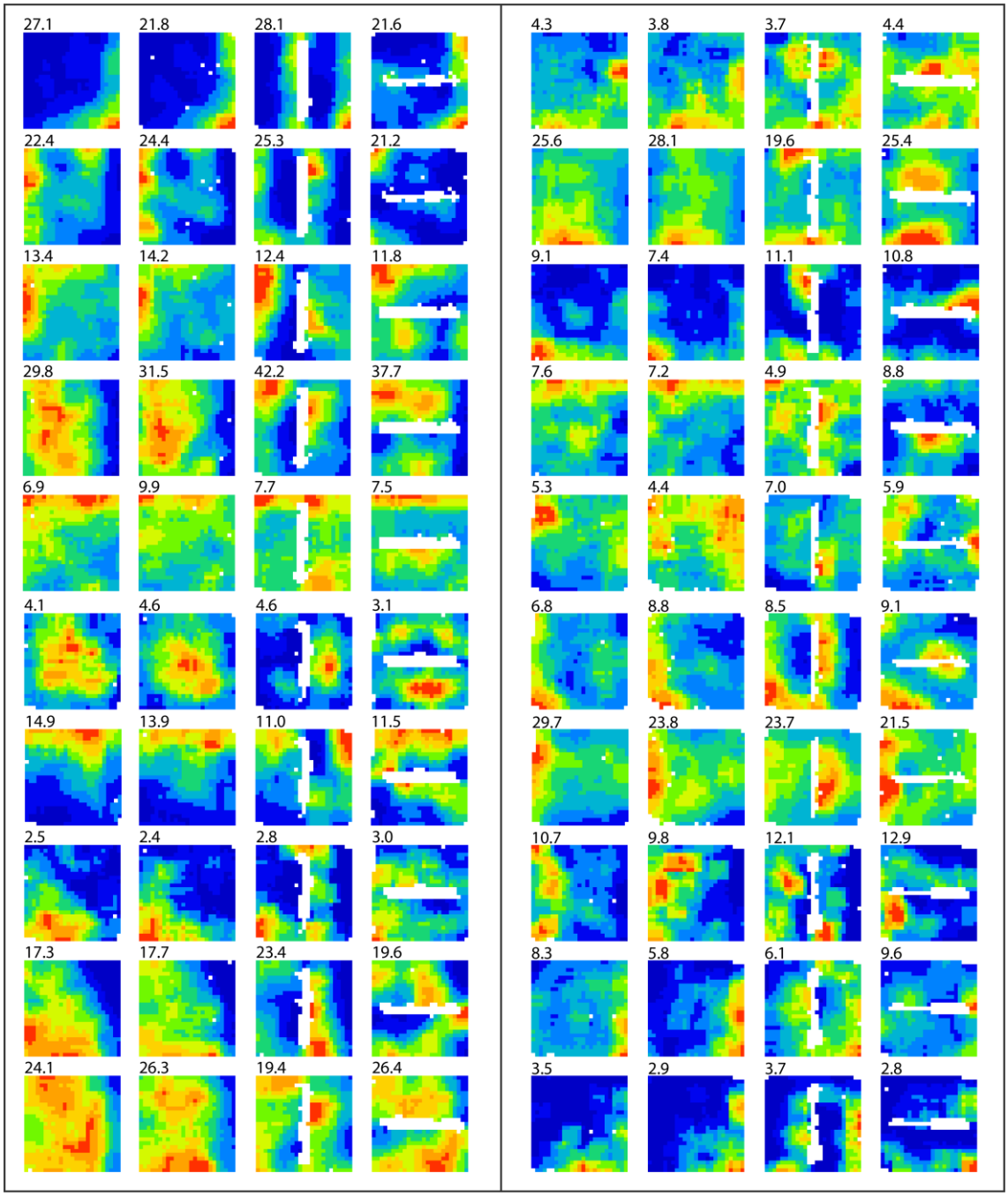

Figure 5.26 – Rate maps of putative BVCs in the Adult dataset. The figure shows 20 examples of recorded neurons in the Adult dataset across the four trials the animals were tested on (from left to right: Baseline, Baseline, Barrier, Barrier). Ten cells (one per row) are shown in the left half, and other ten in the right half. The peak firing rate of the rate map is shown in the top left corner. The animal's age on the day of recording is shown before the respective rate map sequence.

5.6.2 – The peak firing rate of BVCs increases throughout postnatal development

The mean firing rate (see Figure 5.27) of selected BVCs (calculated as described in 4.5.4.1, page 79) does not appear to change throughout postnatal development despite there being a positive trend (ANOVA, $F_{(3,265)}$=2.418, p=0.062), see Table 5.3 for means and standard deviations). However, the BVC peak firing rate (Figure 5.27) was significantly different between age groups (ANOVA, $F_{(3,265)}$=10.696, p<0.001). Post-hoc Tukey-HSD comparisons of the peak rate between age groups further revealed the adult BVC peak firing rates (14.18±9.26Hz, mean and standard deviation) were significantly higher than the peak rates for BVCs in the remaining age groups (P16-P18, 7.18±3.48Hz, p<0.001; P19-P21, 9.28±5.30Hz, p=0.01; P22-P25, 9.79±5.56Hz, p=0.018). No significant differences were found in the P16 to P25 age groups (p>0.401).

Age Groups	Average Mean Firing Rate	Standard Deviation
P16-P18	3.48 Hz	2.02 Hz
P19-P21	4.90 Hz	3.91 Hz
P22-P25	4.54 Hz	2.83 Hz
Adult	6.00 Hz	5.42 Hz

Table 5.3 – Table of means and standard deviations for the mean firing rate per age group.

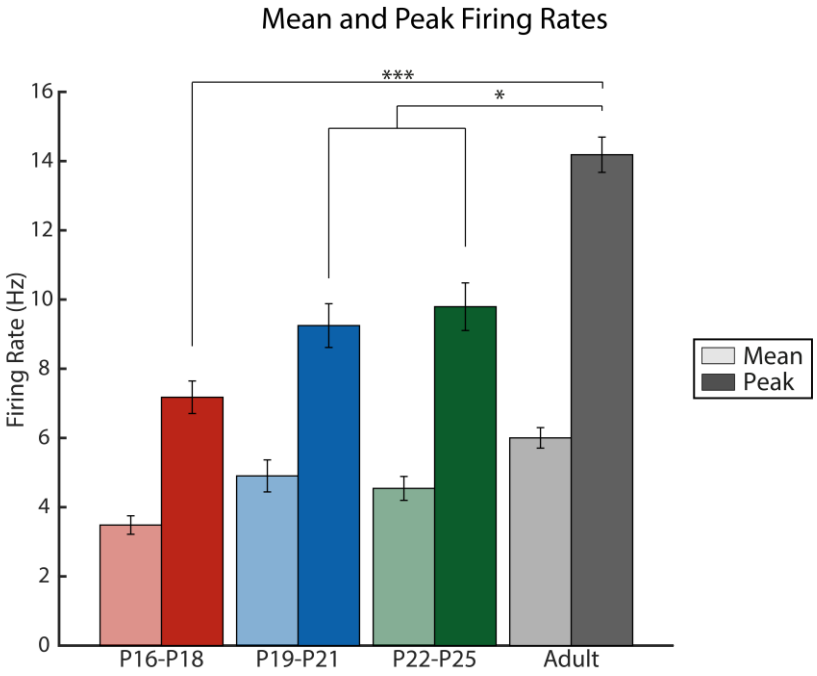

Figure 5.27 – Mean and peak firing rates for selected BVCs across the different age groups. Values are means and the standard error of the means (SEM). The mean firing rates of selected BVCs do not seem to change across the rat's postnatal development. The peak firing on the other hand is significantly different between adult rats and young animals (*, p<0.05; *** p<0.001).

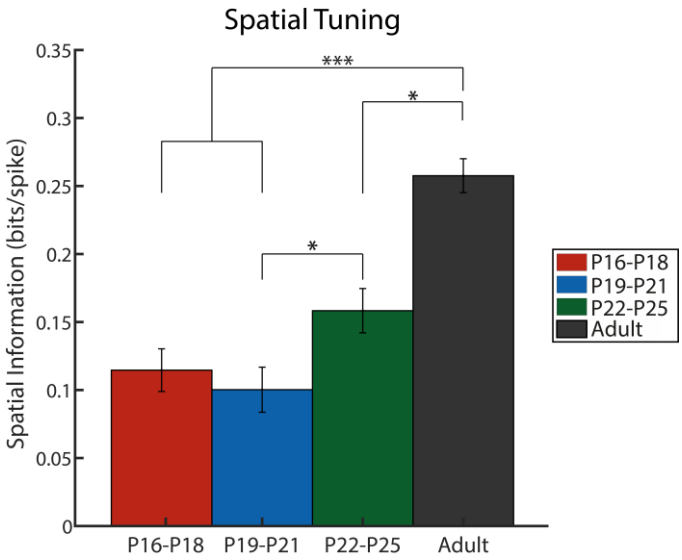

Figure 5.28 – Spatial information of selected BVCs across development. The presented values are the means and SEM of the spatial information indices in the different age groups. Like the peak firing rate, the positional information that can be extracted from one spike increases throughout development. Significant differences are only found between the adult dataset and the remaining age groups (*, p<0.05; ***, p<0.001).

5.6.3 – Spatial information content of adult BVCs is higher than that of younger animals

The spatial tuning of the recorded BVCs (calculated as shown in 4.5.4.4, page 80) also showed significant differences between age groups (ANOVA, $F_{(3,265)}$=17.960, p<0.001). Post-hoc Tukey-HSD tests revealed significant differences between adult (0.26±0.22 bits/spike), and other age groups (P16-P18, 0.11±0.11 bits/spike, p<0.001; P19-P21, 0.10±0.14 bits/spike, p<0.001; P22-P25, 0.16±0.13 bits/spike, p=0.042). The spatial tuning of BVCs in the P22-P25 age group was also significantly higher than the BVCs in the P19-P21 group (p=0.035). Overall, a positive trend in the spatial tuning of BVCs can be observed throughout the rat postnatal development into adulthood (Figure 5.28) just as for the peak firing rate.

5.6.4 – Stability of BVC firing fields also increases with age

The stability of the BVC firing fields (calculated as shown in section 4.5.4.3, page 79) both within and across trials, increases over time (see Figure 5.29, Within Trials, Kruskal-Wallis, $\chi^2_{(3)}$=99.80, p<0.001; Across Trials, Kruskal-Wallis, $\chi^2_{(3)}$=77.446, p<0.001). The means and standard deviations of stability values across age groups can be found in Table 5.4.

The within trial stability of BVCs (Figure 5.29A) in the P16-P18 age group was significantly lower than that of other age groups (P19-P21, Mann-Whitney U=221,

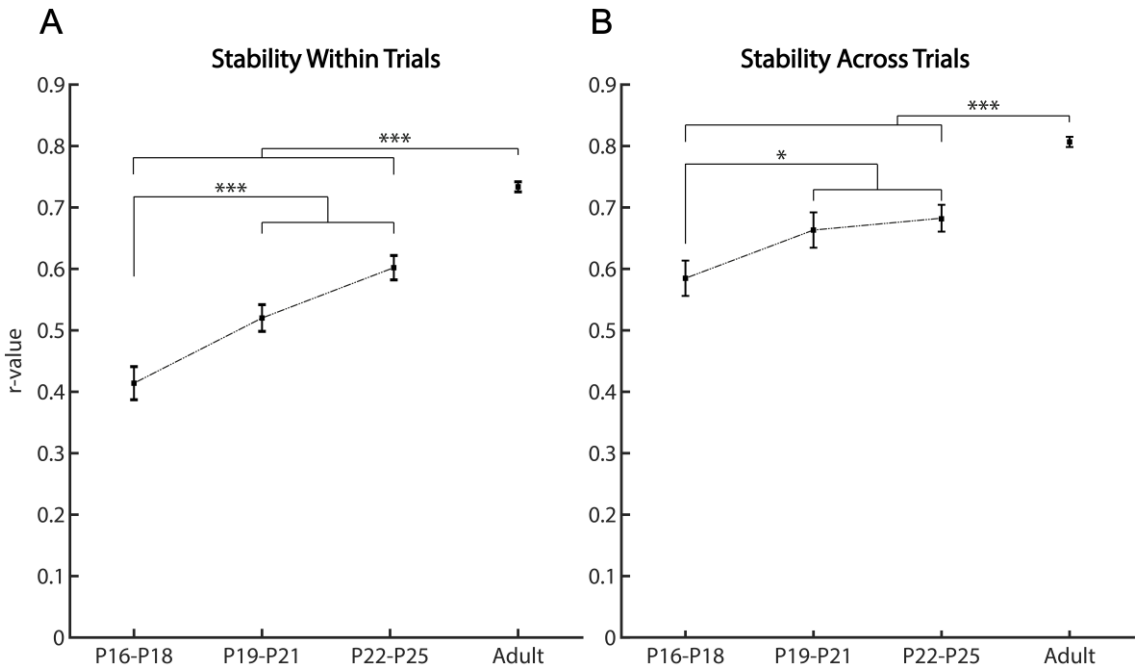

Figure 5.29 – Stability of BVC within and between baseline trials throughout development. Mean and SEM plots for the stability of BVCs within (A) and across (B) trials. In both cases, the stability of the firing fields increases with age (*, p<0.05; ***, p<0.001).

p<0.001; P22-P25, U=180, p<0.001; Adult, U=290, p<0.001). The P19-P21 age group within trial stability was not significantly different (U=555, p=0.503) from that of the P22-P25 group, and both age groups' BVCs had significantly lower stability than that of adult BVCs (P19-P21: Adult, U=1344, p<0.001; P22-P25: Adult, U=1455, p<0.001).

An identical trend was observed for the stability across trials (Figure 5.29B). BVCs in the P16-P18 age group had lower stability between baseline trials than P19-P21 (U=356, p=0.018), P22-P25 (U=327, p=0.014), and Adult (U=647, p<0.001) BVCs. The BVC across trial stability in the P19-P21 age group was not significantly different from those in the P22-P25 bin (U=610, p=0.981), but the BVC between trial stability in both P19-P21 and P22-P25 age groups was significantly lower than adult BVCs (U=1224, p<0.001; and U=1277, p<0.001, respectively).

Age Groups	**Stability Within Trials**		**Stability Across Trials**	
	Mean	Standard Deviation	Mean	Standard Deviation
P16-P18	0.41	0.17	0.58	0.16
P19-P21	0.52	0.16	0.66	0.17
P22-P25	0.60	0.13	0.68	0.13
Adult	0.73	0.13	0.81	0.11

Table 5.4 – Table of means and standard deviations for the stability of BVCs both within and across trials across the different age groups.

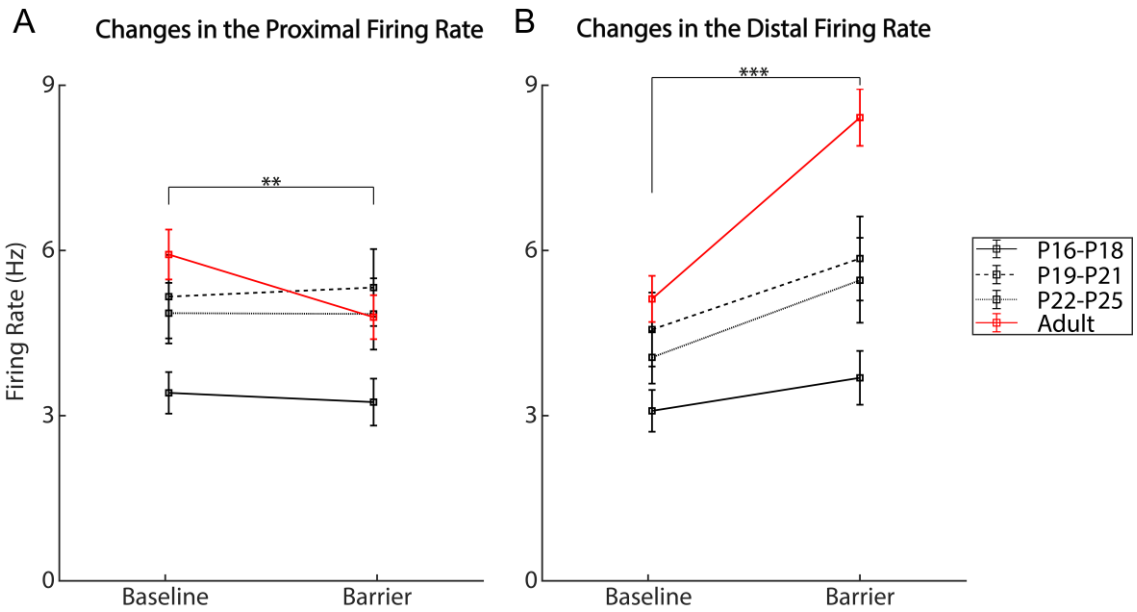

Figure 5.30 – Firing rate in barrier-defined proximal and distal regions across baseline and barrier trials per age group. Both plots are the means and SEMs of the mean firing rates in the proximal (A) and distal (B) regions in the baseline and barrier trials. There was a significant effect of the trial type in the firing rate in both the proximal and distal areas of the barrier. The insertion of the barrier lead to a significant increase in the mean firing rate in the distal region ($p<0.001$), as well as a significant interaction ($p<0.001$) between the age and trial type (B). Significant firing rate differences were also found between ages when a barrier is inserted into the recording environment ($p=0.011$). There was also a significant effect ($p=0.004$) of the insertion of the barrier in the proximal region of the field (A), as well as a significant interaction between age and trial type ($p=0.001$). (**, $p<0.01$; ***, $p<0.001$).

5.6.5 – Barrier-triggered changes in firing rate

The analysis of field doubling in the barrier probes were performed as described in 5.3.2 (page 96). A 10cm region on each long side of the barrier was taken, and the mean firing rates were measured in both barrier and baseline trials. The region closest to the BVCs' firing field was designated as proximal, while the region on the opposite side of the barrier (where an increase in the firing rate is expected) was designated as distal. The firing rates in these regions were then plotted (Figure 5.30), and their ln-transformed values analyzed by performing a two-way repeated measures ANOVA, using the trial type (Baseline and Barrier) as a within-subjects factor, and the age groups as between-subjects factor. The means and standard deviations of both distal and proximal firing rates, for each trial and age group are shown in Tables 5.5 and 5.6, respectively.

The results show that there was a significant main effect of the trial type in the firing in the distal region of the barrier (Figure 5.30B, $F_{(1,265)}=49.168$, $p<0.001$), with a significant interaction between the trial and the age of the animal (repeated measures ANOVA, $F_{(3,265)}=2.227$, $p<0.001$). With the exception of the P16-P18 age group, there was a significant simple main effect of the insertion of the barrier and firing on the distal region of the environment (P16-P18, $p=0.291$; P19-P21, $p=0.002$; P22-P25, $p=0.034$; Adult,

p<0.001). Significant differences were also found between the different age groups ($F_{(3,265)}$=5.882, p=0.011). Tukey-HSD post-hoc tests demonstrated that the P16-P18 age group firing was lower than adult firing rate in both the proximal and distal regions.

A significant effect of the barrier insertion was also found in the proximal region of the environment (Figure 5.30A, $F_{(1,265)}$=8.233 p=0.004), as well as a significant interaction between trial and age ($F_{(3,265)}$=5.752, p=0.001), with no differences between age groups ($F_{(3,265)}$=0.933, p=0.425). Simple main effects assessment showed that only Adult BVCs have a significantly different proximal firing rate upon the insertion of the barrier (Bonferroni correction, p<0.001), while the other groups showed no significant differences between trials (P16-P18, p=0.178; P19-P21, p=0.477; P22-P25, p=0.279).

Distal Firing Rate				
Age Groups	**Baseline**		**Barrier**	
	Mean	Standard Deviation	Mean	Standard Deviation
P16-P18	3.09 Hz	2.08 Hz	3.69 Hz	2.68 Hz
P19-P21	4.56 Hz	4.03 Hz	5.85 Hz	4.58 Hz
P22-P25	4.06 Hz	2.78 Hz	5.46 Hz	4.50 Hz
Adult	5.12 Hz	5.45 Hz	8.41 Hz	6.68 Hz

Table 5.5 – Table of means and standard deviations for the firing rate of BVCs in the distal region across the different age groups and trials.

Proximal Firing Rate				
Age Groups	**Baseline**		**Barrier**	
	Mean	Standard Deviation	Mean	Standard Deviation
P16-P18	3.41 Hz	2.07 Hz	3.25 Hz	2.34 Hz
P19-P21	5.16 Hz	4.55 Hz	5.33 Hz	4.19 Hz
P22-P25	4.86 Hz	3.21 Hz	4.85 Hz	3.77 Hz
Adult	5.93 Hz	5.89 Hz	4.79 Hz	5.19 Hz

Table 5.6 – Table of means and standard deviations for the firing rate of BVCs in the distal region across the different age groups and trials.

The changes in barrier related firing rate are expected of BVCs, particularly in the distal area. This effect is observed significantly in all age groups except the P16-P18. The changes in firing along the proximal regions are in the opposite direction: the firing rate in the proximal areas tends to decrease from the baseline. However, the effect of the barrier insertion appears to be significant solely for the adult BVC dataset.

5.6.6 – Subicular cells selected with the BS method also show protracted maturation

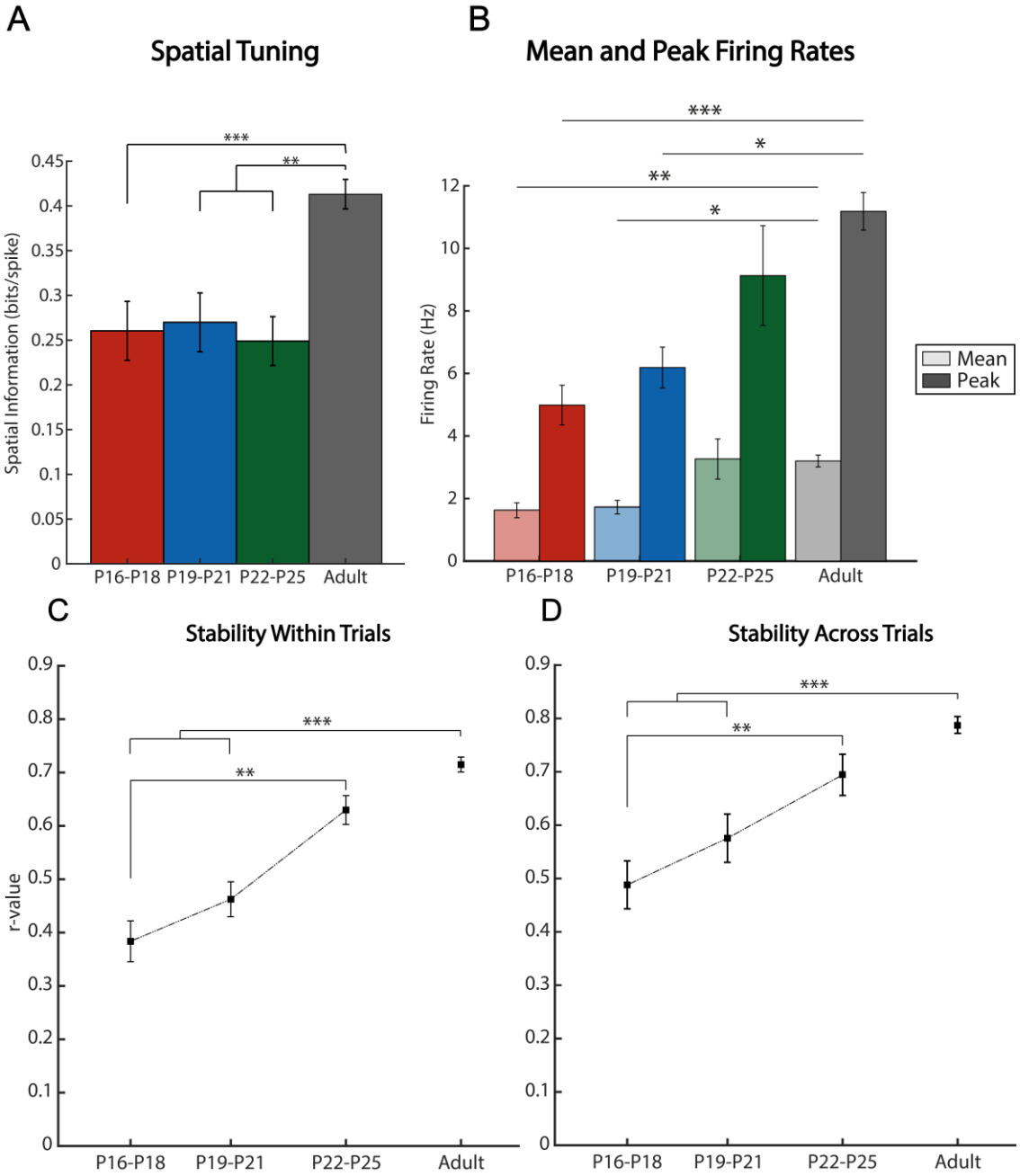

Figure 5.31 – Subicular cells selected with the BS method also show protracted maturation of their spatial tuning, firing, and stability. (A) Spatial tuning, (B) mean and peak firing rates, and BVC stability (C) within and (D) across trials. Age. Just as for the RM method, BS-selected cells also exhibit developmental trends. Both mean and peak firing rates, as well as the stability, gradually attain adult-like firing characteristics. A similar trend is not observed for the spatial tuning, potentially because this feature is used as additional selection criterion. (*, $p<0.05$; **, $p<0.01$; ***, $p<0.001$).

The set of cells selected with the BS method (Bjerknes et al., 2014), were also analysed in terms of their mean spatial information (Figure 5.31A), mean and peak firing rates (Figure 5.31B), and stability within (Figure 5.31C) and between trials (Figure 5.31D).

The spatial tuning of selected cells (Figure 5.31A) varied between age groups (ANOVA, $F_{(3,135)}$=12.563, p<0.001), with Tukey-HSD comparisons exhibiting only significant differences between adult neurons (mean ± standard deviation [sd], 0.41±0.21 bits/spike) and those of young animal age groups (P16-P18 mean ± sd, 0.26±0.19 bits/spike, p<0.001; 19-21 mean ± sd, 0.27±0.18 bits/spike, p=0.002; 22-25 mean ± sd, 0.25±0.13 bits/spike, p=0.003). The lack of differences in the young animal age groups can be attributed to the use of a spatial information threshold to select putative boundary responses. In fact, the RM-selected cells show a positive increase in spatial tuning throughout the sampled postnatal period.

The mean firing (Figure 5.31B, translucent bars) and peak firing rates (Figure 5.31B, opaque bars) of BS-selected cells also changed throughout the sampled ages (mean firing rate ANOVA, $F_{(3,135)}$=6.754, p<0.001; peak firing rate ANOVA, $F_{(3,135)}$=9.907, p<0.001). The mean firing rate of adult neurons (mean ± sd, 3.20±2.55 Hz) was significantly higher than that of P16-P18 (mean ± sd, 1.62±1.44 Hz, p=0.002) and P19-P21 (mean ± sd, 1.72±1.25 Hz, p=0.014) cells, but not compared to the ones in the P22-P25 age group (mean ± sd, 3.26±3.20 Hz, p=0.969). Similarly, the peak firing rate of adult cells (mean ± sd, 11.18±8.03 Hz) was significantly higher than that of P16-P18 (mean ± sd, 4.99±3.88 Hz, p<0.001) and P19-P21 cells (mean ± sd, 6.19±3.67 Hz, p=0.013), but not than P22-P25 ones (mean ± sd, 9.13±7.80 Hz, p=0.527). For both parameters, no significant differences were found between young animal age groups, although both the mean and peak firing rates tended to increase with age.

Just as for the RM-selected cells, both the stability within (Figure 5.31C) and between (Figure 5.31D) trials of BS-selected neurons tended to increase with the animals age, a trend which was significant for both parameters (stability within trials ANOVA, $F_{(3,135)}$=26.487, p<0.001; stability across trials ANOVA, $F_{(3,135)}$= 23.299, p<0.001). The within-trial stability (C) of adult neurons (mean ± sd, 0.71±0.17) was significantly higher than that of cells in the P16-P18 (mean ± sd, 0.38±0.20, p<0.001) and P19-P21 (mean ± sd, 0.46±0.17, p<0.001) age groups. Also, the within trial stability of cells in the P22-P25 age group (mean ± sd, 0.63±0.13) was significantly higher than that of cells in the P16-P18 age group (p=0.001). The stability between trials followed a similar pattern: adult across-trial stability (mean ± sd, 0.79±0.15) was higher than that of the two youngest age groups (P16-P18 mean ± sd, 0.49±0.20, p<0.001; P19-P21 mean ± sd, 0.58±0.18, p<0.001), and the stability between trials of cells in the P22-P25 group (mean ± sd, 0.69±0.13) was higher than that of neurons in the P16-P18 age group (p=0.003).

Overall, subicular cells selected with the BS method appear to progressively acquire adult-like firing characteristics, just like putative BVCs selected with the RM approach. This set of results further strengthens the developmental trends detected with the RM approach. Thus, unlike entorhinal border cells, subicular BVCs appear to mature throughout a protracted period. This may imply that both types of boundary-responsive neurons may have different functions within the hippocampal spatial cognitive map.

5.7 Chapter Discussion

In summary, the main findings of the work presented in this chapter are as follows:

- The BS method, initially developed for MEC border cells, is not as effective as the RM method in detecting subicular boundary coding neurons throughout the rat's postnatal development;
- Subicular BVCs may be observed from age P16 onwards;
- Subicular BVCs, unlike entorhinal border cells, gradually attain adult firing characteristics, much like place cells.

5.7.1 – Boundary coding in the MEC of young rats

Boundary coding neurons in the rat MEC were described by (Savelli et al., 2008), and (Solstad et al., 2008). In the latter work, the authors developed a quantitative method to determine the degree of 'border responsiveness' of neurons called the border score (BS). The BS uses two particular features of boundary-coding spatial cells: the mean distance at which the neurons fire from any given boundary/border, and the coverage of the field along that particular boundary/border. Each neuron is scored on the basis of these two features, namely by normalizing the difference between the coverage of the field along the boundary and the average distance of the field to the boundary by the sum of these values. This scoring/detection method was first employed in entorhinal boundary coding cells of adult rats (Solstad et al., 2008), where border cells were identified as cells whose BS was higher than 0.5 and stable across trials (with an across trial correlation score higher than 0.5 as well). In the same publication, the authors describe some variety of boundary coding responses: cells responding to one border, to more than one border, cells that respond to all borders, as well as boundary-off cells – cells that fire in the center of the environment and not around any borders. However, most of the presented border neurons appear to have shorter tuning distances, meaning that they fire when the animal is in close proximity to the wall (see Figure 5.14, page 104).

A similar response pattern was also observed in younger animals (Bjerknes et al., 2015). However, the detection of border cells in these experiments also involved a spatial information threshold. Thus, a cell was considered boundary coding if its BS and spatial information scores were higher than the respective 95th percentiles of cell matched shuffled distributions. This approach led to the inclusion of cells that fire more closely to the boundaries of the environment. The spatial information threshold may have also led to inclusion of cells with smaller and better-defined fields. As this index measures the mutual information between spikes and position (Skaggs et al., 1993), a single action potential from cells with lower spatial information indices, and likely larger firing fields, will hold less information about the animal's position. It is therefore possible that if the EC contains boundary coding neurons with large response fields, these will not be detected using this scoring method. In fact, as shown in section 5.5.3, (page 108), when applied to subicular recordings, the BS approach led to the inclusion of cells with relatively short median tuning distances from boundaries. Thus, it is possible that our current knowledge of entorhinal border cells is not comprehensive and representative of its entire population.

Regardless of the potential issues with the BS method – namely the preference of short-tuned boundary-dependent responses –, when applied to subicular data, it also revealed the existence of developmental trends similar to those seen with the RM method: gradual increase of boundary cell stability, within and across trials; increased spatial tuning in adults; and increase of mean and peak firing rates throughout the early postnatal period. This means that despite its strictness, the BS method does not exclude developmental trends, and reinforces the results obtained with the RM approach. Furthermore, the RM approach also has some caveats. The method is more liberal than the BS in the definition of boundary responses, but it is based on comparisons with a pre-defined collection of putative boundary responses artificially generated. These boundary responses may not accurately the diversity of boundary-driven responses that can be observed in the rat Sub. In fact, some particular types of boundary responses (including boundary-off cells or cells that fire along all boundaries) can be recorded, but are not included by this approach. Thus, even though the RM selects more putative boundary coding neurons than the BS, it may not be representative of the nature of subicular boundary responses.

5.7.2 – Postnatal maturation of boundary coding in the Sub appears to mirror that of hippocampal place cells

The spatial features of BVCs presented here appear to improve throughout an animal's early postnatal life, as shown by the improvement of their spatial tuning and stability. This

pattern of maturation mirrors place cell postnatal development as well (Wills et al., 2010, Langston et al., 2010). The observed protracted maturation is also in agreement with the overall extended development of the hippocampus and associated spatial exploration behaviors (Wills et al., 2014, Wills et al., 2010, Langston et al., 2010, Altman and Sudarshan, 1975, Loewen et al., 2005, Douglas et al., 1973, Akers and Hamilton, 2007, Schenk, 1985). The analysis of the barrier-triggered firing (section 5.6.5, page 119) revealed another of BVCs which are seemingly not shared by their entorhinal counterparts. Both border cell and BVCs have increased firing rate in the distal region after insertion of the barrier in the environment, a response that is expected from boundary coding neurons. On the other hand, entorhinal border cell firing in the area proximal to the firing field does not significantly decrease after the insertion of the barrier in the environment (Bjerknes et al., 2014), whereas BVC firing does. In these proximal regions, BVCs appear to have decreased firing rates compared to the baseline, an effect which occurs only in adult animals.

The gradual development of BVCs and place cells also may constitute a common aspect of spatially tuned neuron development within the HF. These functional observations are also in register with recent work that looked at maturation of hippocampal networks using molecular/developmental markers (Donato et al., 2017). The results of these experiments suggested that the maturation of hippocampal networks is activity dependent. Interestingly, the progression of hippocampal network maturation observed through molecular markers does not directly correlate with the progression of the maturation of hippocampal spatial representation: CA1 and Sub mature later than the EC, observed by the later loss of doublecortin expression – a microtubule-associated protein present in immature neurons (Gleeson et al., 1999) – in the two latter regions, despite the fact that entorhinal GCs emerge later than CA1 place cells (Wills et al., 2010, Langston et al., 2010) and Subicular BVCs. Nevertheless, CA1 and Sub ‘co-maturation’ is observed both at the level of spatial representation and loss of doublecortin. Thus, it would be interesting to further dissect this relationship by evaluating if CA1 input is required for BVC activity.

5.7.3 – Comparing entorhinal and subicular boundary coding

The differences observed in postnatal development between entorhinal border neurons and subicular BVCs point to potential differences in the functional aspects of both boundary coding cell types. Given the narrower firing fields/shorter tuning distances of entorhinal border cells, these may be computing boundary information in the environment. Because the EC is known to project to the Sub via the PP (see section

1.2.2.3, page 38), it is possible that entorhinal boundary information is transmitted to subicular excitatory neurons. The decreased firing in the barrier-defined proximal region (likely potentiated by increased inhibition) substantiates this idea. The insertion of the barrier into the recording arena can be interpreted as dividing the environment into two compartments. When this 'compartmentalization' occurs, the firing field of BVCs can scale relative to the new size of the compartments (Sharp, 2006), thus explaining the decreased firing rate observed in the barrier-defined proximal areas. Therefore, it may be possible that the radial extent of a BVCs' receptive field depends not solely on the distance from one single boundary, but may be integrating distances from all barriers to locomotion, explaining the scaling upon the insertion of the barrier.

It may be that subicular and entorhinal boundary coding are not analogous: border cells may strictly carry boundary location information, which explains their short-tuning while BVCs use this information to perform distance estimations based on boundaries. However, some caution is necessary when making this assumption, because the RM score method is yet to be applied to developmental entorhinal border neurons. It is thus possible that the EC harbors boundary-coding neurons with similar features to subicular BVCs. Furthermore, the use of the BS method with subicular data showed that, just as the RM approach, and unlike entorhinal border cells, subicular boundary cells tend to mature over a protracted period of time. This attests to the possibility that subicular and entorhinal boundary-tuned neurons are functionally different. Further work should aim to apply the RM method to datasets obtained from the entorhinal cortex of young animals to prove that the MEC border cells are/are not different from subicular BVCs.

Chapter 6 General Discussion

The work laid out in this thesis aimed to answer the following questions:

1. Can subicular BVCs be recorded as early their entorhinal counterparts?
2. Do subicular BVCs undergo functional maturation during the first postnatal weeks of a rat's life (like place cells) or are they adult-like from the earliest age they are observed (like HDCs and entorhinal border cells)?
3. Given the strong connectivity between Sub and MEC, what is the relationship between subicular excitatory cell activity and GC firing?

Ultimately, these experiments aimed to deepen our understanding of spatial firing in Sub and its relation to other elements of the spatial cognitive map, particularly GCs in the entorhinal cortex. The results of the experiments described in the previous chapters provide answers to the first two questions. The last question still remains unanswered, as the data collected to answer it does not provide enough evidence to understand relationship between subicular activity and GC firing.

6.1 Subicular BVCs can be recorded from P16 onwards and gradually attain adult-like firing characteristics

To further understand the functional development of subicular BVCs, young rats were implanted in Sub with tetrode-carrying microdrives. Subicular units were found in animals as young as P16 onwards as they foraged for sweetened milk in a rectangular environment. To probe for the existence of boundary coding neurons in these animals, a barrier was inserted into the recording arena to prompt doubling of BVC firing fields. The data obtained from young animals was then compared to the data collected in adult rats, thus allowing to determine if BVCs undergo functional maturation of their firing properties throughout the rat's juvenility. Through this approach, boundary coding neurons in Sub were first observed in P16 animals, and recorded also in all subsequent ages. Given that place cells and entorhinal border cells can be recorded in animals at this same age (Wills et al., 2010, Langston et al., 2010, Muessig et al., 2015, Bjerknes et al., 2015), this finding is not unexpected.

Even though boundary responses were subjectively observed in P16 animals, to overcome experimenter bias, an objective method to detect boundary coding responses needed to be applied to the dataset. Therefore, and as explained in Chapter 5, two different detection methods were employed: the Border Score method (Solstad et al.,

2008), and the Response Model Score method based on the Hartley BVC Model (Hartley et al., 2000).

6.1.1 – Border Score vs Response Model Score

Both the Border Score and Response Model Score are reliable methods to detect boundary responsive neurons, but they use different aspects of boundary coding.

The BS method scores each recorded neuron on the basis of its preferred firing distance from a boundary (the location of the firing field relative to the closest boundary), and the field's coverage along that same boundary (see more details on section 5.3.1.1, page 90). Ultimately, short-distanced tuned neurons that cover most of a boundary will be given a score of 1, while those whose activity is more prevalent in off-boundary locations will be given a lower or negative score (Solstad et al., 2008, Savelli et al., 2008). This approach has been used to identify entorhinal boundary coding neurons in the postnatal rat brain (Bjerknes et al., 2014). To do so, Bjerknes et al. (2014) attempted to identify boundary coding neurons not solely on the basis of their border score, but also on their spatial tuning. The result uncovered sharply tuned boundary coding neurons in the MEC which are adult-like from the age of first recording.

Based on the BVC computational model set forward in Hartley et al. (2000), the work featured in this thesis uses a an alternative scoring method. The Response Model score uses the proposed properties of BVCs to determine the match a putative receptive field with each trial of each recorded cell. The 'best-fit' receptive field for the neuron in question is the one that generates the maximum correlation score between a given response and one of the baseline rate maps. Afterwards, the neuron's best-fit response is correlated with both baseline trials. Then, if the neuron's baseline correlation scores were higher than the 99^{th} percentile of an age-matched distribution of maximum correlation score values generated via spike shuffling, the cell would be considered a BVC (more details in section 5.3.1.2, page 92). This selection procedure, resulted in not just the selection of more cells, but also cells exhibiting larger tuning distances from environmental boundaries.

The difference in the efficacy of the number and type of cells selected using the RM score over the BS can be explained as follows. The former takes into consideration the variability of a cell's tuning distance (shorter or longer) as well as its preferred firing direction. Because of its flexibility, the type of boundary responses selected with the RM more accurately characterizes the spatial properties of neurons in Sub. The BS, as discussed, is a stricter scoring criterion, only selecting cells with shorter tuning distances

from the boundaries of the environment (see section 5.5.3, page 108). The latter cell type may be observed less frequently in the maturing Sub because, as shown, the tuning of cells within the Sub increases with age, just as what is observed in CA1 place cells (Wills et al., 2010).

Despite their different efficacy, the developmental trends observed using either method are similar (trends for RM and BS-selected BVCs can be found throughout section 5.6, page 110). Both BS- or RM-selected cells show that during development, subicular boundary-responsive cells gradually mature.

6.1.2 – Spatial cells within the HF obtain adult-like firing characteristics throughout a protracted period

Regarding subicular boundary coding, it appears that an increasing proportion of BVCs is present throughout the animal's development. In pre-weaning animals (younger than P21), the proportion of recorded BVCs is between 6-8%. It then doubles after weaning (between P22-P25), and continues to increase until adulthood, where BVCs correspond to roughly 30% of recorded cells, which is in agreement with previously published work (Lever et al., 2009, Stewart et al., 2014).

The recorded neurons were subsequently analyzed in terms of their firing rate, SI, stability, and barrier related firing. All of these parameters, unlike what was observed for entorhinal border cells (Bjerknes et al., 2015), exhibit developmental trends. Overall, the peak firing rate (but not the mean firing rate), the SI content and stability (both within and across trials) increase throughout the animal's postnatal development until adulthood. The observed increase in proportion of recorded BVCs, as well the increase in the cells' spatial firing accuracy, are similar to what has been described for CA1 place cells (Wills et al., 2010, Langston et al., 2010, Muessig, 2013). This similarity in the postnatal maturation of two different spatial cell types can be attributed to the overall protracted postnatal maturation of the HF. Given the anatomical proximity of Sub and CA1, it is probable that Sub can develop at a similar if not slower rate than CA1. Furthermore, recent work has also shown that subicular neurons lose expression of doublecortin (a protein present in immature neurons) later than CA1 neurons, and that this maturation is activity-dependent (Donato et al., 2017). This suggests that maturation of CA1 activity may precede the maturation of Sub. In fact, CA1 activity may be required for the proper maturation of subicular neurons.

As the output structure of the hippocampus, it is not surprising to find that subicular spatial activity maturation resembles that of CA1. Just as for place cells (Wills et al.,

2010), the percentage of recorded BVCs increases following weaning, which also corresponds to age when GCs emerge in MEC (Wills et al., 2010). This points to a likely role of GC activity in stabilizing spatial firing fields within the HF, as already hypothesized by (Muessig et al., 2015). However, recent work has shown that geometric cues play a role in stabilizing HDC tuning and directionality in pre-visual animals (Bassett et al., 2018). HDCs recorded in the ADN of pre-visual animals, previously observed not to have directionality (Tan et al., 2015), were shown to have stronger directional tuning and provide more directional information when the animals were recorded in a small environment (20cm square box) (Bassett et al., 2018). Further analyses showed that HDC activity in regular recording environments (62.5cm square box) closely followed changes in angular head velocity when the animals were closer to the corners of the environments. Thus, the proximity of local cues (boundaries) may allow these to act as a multisensory supervisory stimulus that anchors the representation of space in the absence of the more dominant visual cues.

Considering these findings, it is possible that boundary-responsive neurons can anchor the spatial representation of other spatially-tuned cells in the absence of more dominant sensory stimuli. Therefore, in an environment where local cues are closer to each other, subicular BVCs and/or entorhinal border cells may provide the necessary input for a more adult-like spatial representation in the HF of rodents. However, testing this hypothesis in pre-visual animals may not be feasible, as the recording of clear firing fields requires active environment exploration, which only emerges at around P14-P16 (Altman and Sudarshan, 1975, Bolles and Woods, 1964, Gerrish and Alberts, 1996, Loewen et al., 2005). Nevertheless, and in line with work outlined in this thesis, it would be of interest to further asses the role of boundaries and their relative distance in stabilizing spatial representation within the HF in pre-weaning animals (i.e. before the emergence of GCs). Since smaller environments allow an increase in HDC spatial tuning in pre-visual animals, similar-sized recording arenas may also increase the positional information and stability of both BVCs and place cells in the HF. The same may also be true for GCs. As previously hypothesized, boundaries are thought to error-correct the activity of entorhinal GCs (Hardcastle et al., 2015) and align grid cells along particular orientations (Stensola et al., 2015). Therefore, in the absence of dominant visual stimuli, the proximity of boundaries to locomotion may be sufficient to support the activity of spatially-tuned neurons.

In summary, the work outlined in Chapter 5, and further discussed in this and previous sections, has deepened our understanding of the development of spatially tuned neurons in the HF. The protracted maturation of subicular BVCs compared to the precocious

adult-like activity of entorhinal border cells, may also underlie functional differences between both types of boundary-tuned neurons.

6.2 – Fitting BVCs in the spatial cognitive map

Given that both subicular (as shown in this thesis) and entorhinal (Bjerknes et al., 2014) boundary coding cells can be recorded as early as P16, and that geometric cues may act as an anchoring cue for place cells (O'Keefe and Burgess, 1996) and HDCs in the thalamus (Bassett et al., 2018), it is possible that boundaries can act as landmarks that stabilize the hippocampal spatial map. The relatively early emergence of BVCs lends support to this idea, as cells that are the base of hippocampal-mediated navigation are likely to emerge earlier in postnatal maturation of the HF. For instance, HDCs, the first cells to be recorded with adult-like stability in young rats (Wills et al., 2010, Langston et al., Tan et al., 2015), have been shown to be necessary for the proper activity of other spatial cells (Goodridge and Taube, 1997, Calton et al., 2003, Winter et al., 2015). The presence of boundary-dependent firing in both the Sub and the MEC can thus indicate a probable role of boundaries in anchoring the activity of the spatial cognitive map. Moreover, previous experimental work has shown that irregular boundary configurations lead to asymmetric GC firing (Stensola et al., 2015, Krupic et al., 2015). This further supports the hypothesis that boundary-coding cell activity may be necessary to maintain GC properties in the rodent MEC. The work outlined in chapters 5 and 6 aimed at addressing this issue.

As discussed by Hartley et al. (2000), BVC firing fields have preferred tuning distances and allocentric bearings to environmental boundaries. In consequence, BVC activity may be used to make estimations of self-position based on environmental boundaries. Assuming entorhinal border cell is conveying information about boundary location and that its activity remains unchanged following subicular inactivation, boundary location information is still fed into the hippocampal cognitive map via the PP. Thus, through subicular inactivation, distance-to-boundary estimation, but not information regarding its location, may be impaired. To offset for this, GCs – thought to be the distance estimation/path integration building blocks of the spatial cognitive map (Fuhs and Touretzky, 2006, Donato et al., 2017) – may change their activity pattern. An increase in gridness, which is underlain by the decrease in field size and distance between fields, could allow for more accurate distance-to-boundary estimations in the absence of BVC input.

6.3 – Boundaries and navigation

In summary, the overall role of subicular BVCs in spatial cognitive map is still to be determined. The developmental evidence presented in this thesis suggests that this spatial cell type may be different from entorhinal border neurons: BVCs gradually increase in numbers, and gradually increase in stability and positional information content; border neurons emerge as early as subicular BVCs, but have adult-like firing characteristics from the earliest time they are found. This difference in maturation can tentatively underscore different functions between these cell types: subicular BVCs, whose firing fields have been predicted to have varying tuning distances from a boundary, can be more involved in distance-to-boundary estimations (just as discussed in the previous section); entorhinal border neurons, whose firing is seemingly confined to regions adjacent to barriers to locomotion, may be providing the HF and PHR with information on boundary location along an allocentric bearing (Savelli et al., 2008, Solstad et al., 2008). As discussed in Chapter 5 (section 5.7.3, page 123), due to the nature of the selection criteria used to defined border cells (namely the BS method), there is still the possibility that the boundary-dependent activity recorded in both Sub and MEC is similar. Nevertheless, barriers to locomotion constitute prominent environmental features encoded by spatial neurons in the rodent brain, which may then be used by other spatial cell types to anchor their representation (Stensola et al., 2015, Bassett et al., 2018). Boundary information may also be important in correcting the error in entorhinal GC spiking activity relative to the nearest GC field center, which accumulate over time and distance travelled (Hardcastle et al., 2015). But what sensory input(s) define boundaries?

Visual information is perhaps the dominant sensory stimulus: place cells (Quirk et al., 1990, Markus et al., 1994, Save et al., 2000) and HDCs (Taube et al., 1990b, Zugaro et al., 2001) use visual stimuli as landmarks which can then be used as allothetic reference points to generate a mental representation of an environment; and visual input in mice (Chen et al., 2016, Perez-Escobar et al., 2016), but not in rats (Hafting et al., 2005) is necessary for proper generation of grid-like activity in the MEC. Interestingly, subicular BVC activity is unchanged in absence of visual input (Lever et al., 2009). It is therefore possible that boundary-encoding relies on the configuration of other sensory modalities, such as somatosensory/tactile input and/or olfactory information. However, it has also been shown that BVC activity is impervious to changes in boundary types, as testing the animals in wall-less environments does not elicit BVC field remapping – while CA1 place field were shown to remap in the same circumstances (Lever et al., 2009). Therefore,

drastic tactile changes were also not sufficient to alter border-coding information in the rat Sub. It is therefore likely that a configuration of sensory stimuli and limitations to movement (by either walls or drops) generate conceptual notions of boundaries.

A promising and unexplored approach is observing subicular BVC activity in head-restrained mice during virtual navigation of open arenas (Chen et al., 2018). Recent work from our group has shown that BVCs can be recorded from the mouse Sub (unpublished), thus making it possible to test the activity of this cell type in virtual environments. Besides self-motion cues, the major sensory stimulus the animals can use to navigate these simulated environments is vision. In these conditions, mouse place and grid cells have been shown to not carry as much positional information compared to when recorded in the real environment (Chen et al., 2018). This occurs because the grid and place fields of the recorded cells expand in the computer-generated environment – the opposite of what was expected from the pharmacological and pharmacogenetic inactivation of Sub experiments. It is therefore possible that, in this task, visual information alone is not sufficient to generate a strong boundary-cue that anchors the activity of other spatial cell types. As a result, solely visual-based distance estimations to boundaries may have lead to larger firing fields. Building on this, subicular recordings from mice in these conditions may show altered BVC activity, whereby: possibly fewer BVCs will be detectable in the simulated versus real world conditions, as these will have less sensory stimuli to generate boundary signals; or recorded BVCs will have larger firing fields, also associated with larger error in estimating distance to boundaries. If true, the latter point can further support the premise that not all BVCs encode solely boundary location, but may use this information to compute distance to boundary estimations.

Subicular cells, which are not simply hippocampal output cells, may encode boundary information using combinations of sensory cues. These potential differences were already observed when the two different selection methods were applied to the same dataset, which resulted in the selection of potentially distinct types of BVCs. Moreover, the Sub (and perhaps the MEC) may display a range of different boundary-related activity, ranging from neurons that purely code for their location, to neurons that generate barrier mnemonic representations (personal communication), and/or distance to boundary computations. Future studies should focus on ascertaining the potential diversity in boundary-dependent activity that the Sub may harbor and understanding their role within the hippocampal spatial map.

References

AGSTER, K. L. & BURWELL, R. D. 2009. Cortical efferents of the perirhinal, postrhinal, and entorhinal cortices of the rat. *Hippocampus,* 19**,** 1159-86.

AINGE, J. A. & LANGSTON, R. F. 2012. Ontogeny of neural circuits underlying spatial memory in the rat. *Front Neural Circuits,* 6**,** 8.

AKERS, K. G., CANDELARIA-COOK, F. T., RICE, J. P., JOHNSON, T. E. & HAMILTON, D. A. 2011. Cued platform training reveals early development of directional responding among preweanling rats in the Morris water task. *Dev Psychobiol,* 53**,** 1-12.

AKERS, K. G. & HAMILTON, D. A. 2007. Comparison of developmental trajectories for place and cued navigation in the Morris water task. *Dev Psychobiol,* 49**,** 553-64.

ALONSO, A. & KOHLER, C. 1984. A study of the reciprocal connections between the septum and the entorhinal area using anterograde and retrograde axonal transport methods in the rat brain. *J Comp Neurol,* 225**,** 327-43.

ALTMAN, J. 1966. Proliferation and migration of undifferentiated precursor cells in the rat during postnatal gliogenesis. *Exp Neurol,* 16**,** 263-78.

ALTMAN, J. & BAYER, S. A. 1990a. Migration and distribution of two populations of hippocampal granule cell precursors during the perinatal and postnatal periods. *J Comp Neurol,* 301**,** 365-81.

ALTMAN, J. & BAYER, S. A. 1990b. Mosaic organization of the hippocampal neuroepithelium and the multiple germinal sources of dentate granule cells. *J Comp Neurol,* 301**,** 325-42.

ALTMAN, J. & DAS, G. D. 1966. Autoradiographic and histological studies of postnatal neurogenesis. I. A longitudinal investigation of the kinetics, migration and transformation of cells incorporating tritiated thymidine in neonate rats, with special reference to postnatal neurogenesis in some brain regions. *J Comp Neurol,* 126**,** 337-89.

ALTMAN, J. & SUDARSHAN, K. 1975. Postnatal development of locomotion in the laboratory rat. *Anim Behav,* 23**,** 896-920.

AMARAL, D. G. 1978. A Golgi study of cell types in the hilar region of the hippocampus in the rat. *J Comp Neurol,* 182**,** 851-914.

AMARAL, D. G. & DENT, J. A. 1981. Development of the mossy fibers of the dentate gyrus: I. A light and electron microscopic study of the mossy fibers and their expansions. *J Comp Neurol,* 195**,** 51-86.

AMARAL, D. G., DOLORFO, C. & ALVAREZ-ROYO, P. 1991. Organization of CA1 projections to the subiculum: a PHA-L analysis in the rat. *Hippocampus,* 1**,** 415-35.

AMARAL, D. G. & KURZ, J. 1985a. An analysis of the origins of the cholinergic and noncholinergic septal projections to the hippocampal formation of the rat. *J Comp Neurol,* 240**,** 37-59.

AMARAL, D. G. & KURZ, J. 1985b. The time of origin of cells demonstrating glutamic acid decarboxylase-like immunoreactivity in the hippocampal formation of the rat. *Neurosci Lett,* 59**,** 33-9.

AMARAL, D. G. & WITTER, M. P. 1989. The three-dimensional organization of the hippocampal formation: a review of anatomical data. *Neuroscience,* 31**,** 571-91.

ANDERSEN, P., BLISS, T. V. P. & SKREDE, K. K. 1971. Lamellar Organization of Hippocampal Excitatory Pathways. *Experimental Brain Research,* 13**,** 222-&.

ANDERSEN, P., MORRIS, R., AMARAL, D., BLISS, T. & O'KEEFE, J. 2007. *The Hippocampus Book,* New York, Oxford University Press, USA.

ANDERSON, M. I. & O'MARA, S. M. 2004. Responses of dorsal subicular neurons of rats during object exploration in an extended environment. *Exp Brain Res,* 159**,** 519-29.

ANDERSON, S. A. 1997. Interneuron Migration from Basal Forebrain to Neocortex: Dependence on Dlx Genes. *Science,* 278**,** 474-476.

ANGEVINE JR, J. B. 1965. Time of neuron origin in the hippocampal region: An autoradiographic study in the mouse. *Experimental Neurology,* 11, Supplement**,** 1-39.

BARRY, C., GINZBERG, L. L., O'KEEFE, J. & BURGESS, N. 2012. Grid cell firing patterns signal environmental novelty by expansion. *Proc Natl Acad Sci U S A,* 109**,** 17687-92.

BARRY, C., HAYMAN, R., BURGESS, N. & JEFFERY, K. J. 2007. Experience-dependent rescaling of entorhinal grids. *Nat Neurosci,* 10**,** 682-4.

BARRY, C., LEVER, C., HAYMAN, R., HARTLEY, T., BURTON, S., O'KEEFE, J., JEFFERY, K. & BURGESS, N. 2006. The boundary vector cell model of place cell firing and spatial memory. *Rev Neurosci,* 17**,** 71-97.

BASSETT, J. P. & TAUBE, J. S. 2005. Head direction signal generation: ascending and descending information streams. *In:* WIENER, S. I. & TAUBE, J. S. (eds.) *Head Direction Cells and the Neural Mechanisms of Spatial.* Cambridge, MA: MIT Press.

BASSETT, J. P., TULLMAN, M. L. & TAUBE, J. S. 2007. Lesions of the tegmentomammillary circuit in the head direction system disrupt the head direction signal in the anterior thalamus. *J Neurosci,* 27**,** 7564-77.

BASSETT, J. P., WILLS, T. J. & CACUCCI, F. 2018. Self-Organized Attractor Dynamics in the Developing Head Direction Circuit. *Curr Biol,* 28**,** 609-615 e3.

BAYER, S. A. 1980a. Development of the hippocampal region in the rat. I. Neurogenesis examined with 3H-thymidine autoradiography. *J Comp Neurol,* 190**,** 87-114.

BAYER, S. A. 1980b. Development of the hippocampal region in the rat. II. Morphogenesis during embryonic and early postnatal life. *J Comp Neurol,* 190**,** 115-34.

BECKSTEAD, R. M. 1978. Afferent connections of the entorhinal area in the rat as demonstrated by retrograde cell-labeling with horseradish peroxidase. *Brain Research,* 152**,** 249-264.

BECKSTEAD, R. M. 1979. An autoradiographic examination of corticocortical and subcortical projections of the mediodorsal-projection (prefrontal) cortex in the rat. *J Comp Neurol,* 184**,** 43-62.

BEHAN, M. & HABERLY, L. B. 1999. Intrinsic and efferent connections of the endopiriform nucleus in rat. *J Comp Neurol,* 408**,** 532-48.

BERENS, P. 2009. CircStat: A MATLAB Toolbox for Circular Statistics. *Journal of Statistical Software,* 31.

BIENKOWSKI, M. S., BOWMAN, I., SONG, M. Y., GOU, L., ARD, T., COTTER, K., ZHU, M., BENAVIDEZ, N. L., YAMASHITA, S., ABU-JABER, J., AZAM, S., LO, D., FOSTER, N. N., HINTIRYAN, H. & DONG, H. W. 2018. Integration of gene expression and brain-

wide connectivity reveals the multiscale organization of mouse hippocampal networks. *Nat Neurosci,* 21**,** 1628-1643.

BINGMAN, V. P., SIEGEL, J. J., GAGLIARDO, A. & ERICHSEN, J. T. 2006. Representing the richness of avian spatial cognition: properties of a lateralized homing pigeon hippocampus. *Rev Neurosci,* 17**,** 17-28.

BJERKNES, T. L., LANGSTON, R. F., KRUGE, I. U., MOSER, E. I. & MOSER, M. B. 2015. Coherence among head direction cells before eye opening in rat pups. *Curr Biol,* 25**,** 103-8.

BJERKNES, T. L., MOSER, E. I. & MOSER, M. B. 2014. Representation of geometric borders in the developing rat. *Neuron,* 82**,** 71-8.

BLACKSTAD, T. W. 1956. Commissural Connections of the Hippocampal Region in the Rat, with Special Reference to Their Mode of Termination. *Journal of Comparative Neurology,* 105**,** 417-537.

BLAIR, H. T., CHO, J. & SHARP, P. E. 1998. Role of the lateral mammillary nucleus in the rat head direction circuit: a combined single unit recording and lesion study. *Neuron,* 21**,** 1387-97.

BOCCARA, C. N., KJONIGSEN, L. J., HAMMER, I. M., BJAALIE, J. G., LEERGAARD, T. B. & WITTER, M. P. 2015. A three-plane architectonic atlas of the rat hippocampal region. *Hippocampus,* 25**,** 838-57.

BOCCARA, C. N., SARGOLINI, F., THORESEN, V. H., SOLSTAD, T., WITTER, M. P., MOSER, E. I. & MOSER, M. B. 2010. Grid cells in pre- and parasubiculum. *Nat Neurosci,* 13**,** 987-94.

BOLLES, R. C. & WOODS, P. J. 1964. The ontogeny of behaviour in the albino rat. *Animal Behaviour,* 12**,** 427-441.

BONNEVIE, T., DUNN, B., FYHN, M., HAFTING, T., DERDIKMAN, D., KUBIE, J. L., ROUDI, Y., MOSER, E. I. & MOSER, M. B. 2013. Grid cells require excitatory drive from the hippocampus. *Nat Neurosci,* 16**,** 309-17.

BOSTOCK, E., MULLER, R. U. & KUBIE, J. L. 1991. Experience-dependent modifications of hippocampal place cell firing. *Hippocampus,* 1**,** 193-205.

BRANDON, M. P., BOGAARD, A. R., LIBBY, C. P., CONNERNEY, M. A., GUPTA, K. & HASSELMO, M. E. 2011. Reduction of theta rhythm dissociates grid cell spatial periodicity from directional tuning. *Science,* 332**,** 595-9.

BRODMANN, K. 1909. *Vergleichende Lokalisationslehre der Grosshirnrinde in ihren Prinzipien dargestellt auf Grund des Zellenbaues*, Barth.

BROWN, R. W. & KRAEMER, P. J. 1997. Ontogenetic differences in retention of spatial learning tested with the Morris water maze. *Dev Psychobiol,* 30**,** 329-41.

BROWN, R. W. & WHISHAW, I. Q. 2000. Similarities in the development of place and cue navigation by rats in a swimming pool. *Dev Psychobiol,* 37**,** 238-45.

BRUN, V. H., LEUTGEB, S., WU, H. Q., SCHWARCZ, R., WITTER, M. P., MOSER, E. I. & MOSER, M. B. 2008. Impaired spatial representation in CA1 after lesion of direct input from entorhinal cortex. *Neuron,* 57**,** 290-302.

BURDACH, K. F. 1826. *Vom Baue und Leben des Gehirns*, Dyk.

BURGESS, N., BARRY, C. & O'KEEFE, J. 2007. An oscillatory interference model of grid cell firing. *Hippocampus,* 17**,** 801-12.

BURGESS, N. & O'KEEFE, J. 1996. Neuronal computations underlying the firing of place cells and their role in navigation. *Hippocampus,* 6**,** 749-762.

BURWELL, R. D. 2001. Borders and cytoarchitecture of the perirhinal and postrhinal cortices in the rat. *J Comp Neurol,* 437**,** 17-41.

BURWELL, R. D. & AMARAL, D. G. 1998a. Cortical afferents of the perirhinal, postrhinal, and entorhinal cortices of the rat. *J Comp Neurol,* 398**,** 179-205.

BURWELL, R. D. & AMARAL, D. G. 1998b. Perirhinal and postrhinal cortices of the rat: interconnectivity and connections with the entorhinal cortex. *J Comp Neurol,* 391**,** 293-321.

BURWELL, R. D., WITTER, M. P. & AMARAL, D. G. 1995. Perirhinal and postrhinal cortices of the rat: a review of the neuroanatomical literature and comparison with findings from the monkey brain. *Hippocampus,* 5**,** 390-408.

BUZSAKI, G. 1986. Hippocampal Sharp Waves - Their Origin and Significance. *Brain Research,* 398**,** 242-252.

BUZSAKI, G. 2002. Theta oscillations in the hippocampus. *Neuron,* 33**,** 325-40.

BUZSAKI, G., ANASTASSIOU, C. A. & KOCH, C. 2012. The origin of extracellular fields and currents--EEG, ECoG, LFP and spikes. *Nat Rev Neurosci,* 13**,** 407-20.

BUZSAKI, G., HORVATH, Z., URIOSTE, R., HETKE, J. & WISE, K. 1992. High-frequency network oscillation in the hippocampus. *Science,* 256**,** 1025-7.

BUZSAKI, G., LEUNG, L. W. & VANDERWOLF, C. H. 1983. Cellular bases of hippocampal EEG in the behaving rat. *Brain Res,* 287**,** 139-71.

CACUCCI, F., SALINAS, P. & WILLS, T. J. 2017. Hippocampus: Activity-Driven Maturation of Neural Circuits for Navigation. *Curr Biol,* 27**,** R428-R430.

CALTON, J. L., STACKMAN, R. W., GOODRIDGE, J. P., ARCHEY, W. B., DUDCHENKO, P. A. & TAUBE, J. S. 2003. Hippocampal place cell instability after lesions of the head direction cell network. *J Neurosci,* 23**,** 9719-31.

CANTERAS, N. S., SIMERLY, R. B. & SWANSON, L. W. 1994. Organization of projections from the ventromedial nucleus of the hypothalamus: a Phaseolus vulgaris-leucoagglutinin study in the rat. *J Comp Neurol,* 348**,** 41-79.

CANTERAS, N. S. & SWANSON, L. W. 1992. Projections of the ventral subiculum to the amygdala, septum, and hypothalamus: a PHAL anterograde tract-tracing study in the rat. *J Comp Neurol,* 324**,** 180-94.

CANTO, C. B. & WITTER, M. P. 2012a. Cellular properties of principal neurons in the rat entorhinal cortex. I. The lateral entorhinal cortex. *Hippocampus,* 22**,** 1256-76.

CANTO, C. B. & WITTER, M. P. 2012b. Cellular properties of principal neurons in the rat entorhinal cortex. II. The medial entorhinal cortex. *Hippocampus,* 22**,** 1277-99.

CAPPAERT, N. L. M., VAN STRIEN, N. M. & WITTER, M. P. 2015. Chapter 20 - Hippocampal Formation A2 - Paxinos, George. *The Rat Nervous System (Fourth Edition).* San Diego: Academic Press.

CEMBROWSKI, M. S., PHILLIPS, M. G., DILISIO, S. F., SHIELDS, B. C., WINNUBST, J., CHANDRASHEKAR, J., BAS, E. & SPRUSTON, N. 2018. Dissociable Structural and Functional Hippocampal Outputs via Distinct Subiculum Cell Classes. *Cell,* 173**,** 1280-1292 e18.

CENQUIZCA, L. A. & SWANSON, L. W. 2006. Analysis of direct hippocampal cortical field CA1 axonal projections to diencephalon in the rat. *J Comp Neurol,* 497**,** 101-14.

CERANIK, K., DENG, J., HEIMRICH, B., LUBKE, J., ZHAO, S., FORSTER, E. & FROTSCHER, M. 1999. Hippocampal Cajal-Retzius cells project to the entorhinal cortex: retrograde tracing and intracellular labelling studies. *Eur J Neurosci,* 11**,** 4278-90.

CHEN, G., KING, J. A., LU, Y., CACUCCI, F. & BURGESS, N. 2018. Spatial cell firing during virtual navigation of open arenas by head-restrained mice. *Elife,* 7.

CHEN, G., MANSON, D., CACUCCI, F. & WILLS, T. J. 2016. Absence of Visual Input Results in the Disruption of Grid Cell Firing in the Mouse. *Curr Biol,* 26**,** 2335-42.

CHEN, L. L., LIN, L.-H., GREEN, E. J., BARNES, C. A. & MCNAUGHTON, B. L. 1994. Head-direction cells in the rat posterior cortex. *Experimental Brain Research,* 101**,** 8-23.

CHO, J. & SHARP, P. E. 2001. Head direction, place, and movement correlates for cells in the rat retrosplenial cortex. *Behav Neurosci,* 115**,** 3-25.

CLARK, B. J. & TAUBE, J. S. 2012. Vestibular and attractor network basis of the head direction cell signal in subcortical circuits. *Front Neural Circuits,* 6**,** 7.

CONRAD, L. C., LEONARD, C. M. & PFAFF, D. W. 1974. Connections of the median and dorsal raphe nuclei in the rat: an autoradiographic and degeneration study. *J Comp Neurol,* 156**,** 179-205.

CORKIN, S. 2002. What's new with the amnesic patient H.M.? *Nat Rev Neurosci,* 3**,** 153-60.

CORKIN, S. 2013. *Permanent Present Tense: The man with no memory, and what he taught the world*, Penguin.

CORKIN, S., AMARAL, D. G., GONZÁLEZ, R. G., JOHNSON, K. A. & HYMAN, B. T. 1997. H. M.'s Medial Temporal Lobe Lesion: Findings from Magnetic Resonance Imaging. *The Journal of Neuroscience,* 17**,** 3964-3979.

CORNWELL-JONES, C. & SOBRIAN, S. K. 1977. Development of odor-guided behavior in Wistar and Spraque-Dawley rat pups. *Physiology & Behavior,* 19**,** 685-688.

CROWLEY, D. E. & HEPP-REYMOND, M. C. 1966. Development of cochlear function in the ear of the infant rat. *Journal of Comparative & Physiological Psychology,* 62**,** 427-432.

CURTHOYS, I. S. 1979. The development of function of horizontal semicircular canal primary neurons in the rat. *Brain Res,* 167**,** 41-52.

CURTHOYS, I. S. 1982. The response of primary horizontal semicircular canal neurons in the rat and guinea pig to angular acceleration. *Exp Brain Res,* 47**,** 286-94.

D'ARCANGELO, G., MIAO, G. G., CHEN, S. C., SOARES, H. D., MORGAN, J. I. & CURRAN, T. 1995. A protein related to extracellular matrix proteins deleted in the mouse mutant reeler. *Nature,* 374**,** 719-23.

DAMÁSIO, A. R. 1994. *Descartes' error: emotion, reason, and the human brain*, Quill.

DE LA ROSA-PRIETO, C., UBEDA-BANON, I., MOHEDANO-MORIANO, A., PRO-SISTIAGA, P., SAIZ-SANCHEZ, D., INSAUSTI, R. & MARTINEZ-MARCOS, A. 2009. Subicular and CA1 hippocampal projections to the accessory olfactory bulb. *Hippocampus,* 19**,** 124-9.

DEACON, R. M. & RAWLINS, J. N. 2006. T-maze alternation in the rodent. *Nat Protoc,* 1**,** 7-12.

DELLER, T., ADELMANN, G., NITSCH, R. & FROTSCHER, M. 1996. The alvear pathway of the rat hippocampus. *Cell Tissue Res,* 286**,** 293-303.

DESHMUKH, S. S., JOHNSON, J. L. & KNIERIM, J. J. 2012. Perirhinal cortex represents nonspatial, but not spatial, information in rats foraging in the presence of objects: comparison with lateral entorhinal cortex. *Hippocampus,* 22**,** 2045-58.

DESHMUKH, S. S. & KNIERIM, J. J. 2011. Representation of non-spatial and spatial information in the lateral entorhinal cortex. *Front Behav Neurosci,* 5**,** 69.

DESMOND, N. L., SCOTT, C. A., JANE, J. A., JR. & LEVY, W. B. 1994. Ultrastructural identification of entorhinal cortical synapses in CA1 stratum lacunosum-moleculare of the rat. *Hippocampus,* 4**,** 594-600.

DIX, S. L. & AGGLETON, J. P. 1999. Extending the spontaneous preference test of recognition: evidence of object-location and object-context recognition. *Behav Brain Res,* 99**,** 191-200.

DOLORFO, C. L. & AMARAL, D. G. 1998. Entorhinal cortex of the rat: organization of intrinsic connections. *J Comp Neurol,* 398**,** 49-82.

DOMNISORU, C., KINKHABWALA, A. A. & TANK, D. W. 2013. Membrane potential dynamics of grid cells. *Nature,* 495**,** 199-204.

DONATO, F., JACOBSEN, R. I., MOSER, M. B. & MOSER, E. I. 2017. Stellate cells drive maturation of the entorhinal-hippocampal circuit. *Science,* 355.

DOUGLAS, R. J., PETERSON, J. J. & DOUGLAS, D. P. 1973. The ontogeny of a hippocampus-dependent response in two rodent species. *Behav Biol,* 8**,** 27-37.

DUDAI, Y. 2012. The restless engram: consolidations never end. *Annu Rev Neurosci,* 35**,** 227-47.

DUDCHENKO, P. A., WOOD, E. R. & EICHENBAUM, H. 2000. Neurotoxic hippocampal lesions have no effect on odor span and little effect on odor recognition memory but produce significant impairments on spatial span, recognition, and alternation. *Journal of Neuroscience,* 20**,** 2964-2977.

DUGLADZE, T., HEINEMANN, U. & GLOVELI, T. 2001. Entorhinal cortex projection cells to the hippocampal formation in vitro. *Brain Res,* 905**,** 224-31.

EDEN, U. T., FRANK, L. M., BARBIERI, R., SOLO, V. & BROWN, E. N. 2004. Dynamic analysis of neural encoding by point process adaptive filtering. *Neural Comput,* 16**,** 971-98.

EKSTROM, A. D., KAHANA, M. J., CAPLAN, J. B., FIELDS, T. A., ISHAM, E. A., NEWMAN, E. L. & FRIED, I. 2003. Cellular networks underlying human spatial navigation. *Nature,* 425**,** 184-188.

ENNACEUR, A. & DELACOUR, J. 1988. A new one-trial test for neurobiological studies of memory in rats. 1: Behavioral data. *Behav Brain Res,* 31**,** 47-59.

ERIKSSON, P. S., PERFILIEVA, E., BJORK-ERIKSSON, T., ALBORN, A. M., NORDBORG, C., PETERSON, D. A. & GAGE, F. H. 1998. Neurogenesis in the adult human hippocampus. *Nat Med,* 4**,** 1313-7.

ETIENNE, A. S. & JEFFERY, K. J. 2004. Path integration in mammals. *Hippocampus,* 14**,** 180-92.

FAGIOLINI, M., PIZZORUSSO, T., BERARDI, N., DOMENICI, L. & MAFFEI, L. 1994. Functional postnatal development of the rat primary visual cortex and the role of visual experience: dark rearing and monocular deprivation. *Vision Res,* 34**,** 709-20.

FALLON, J. H., KOZIELL, D. A. & MOORE, R. Y. 1978. Catecholamine innervation of the basal forebrain. II. Amygdala, suprarhinal cortex and entorhinal cortex. *J Comp Neurol,* 180**,** 509-32.

FAULSTICH, B. M., ONORI, K. A. & DU LAC, S. 2004. Comparison of plasticity and development of mouse optokinetic and vestibulo-ocular reflexes suggests differential gain control mechanisms. *Vision Res,* 44**,** 3419-27.

FENTON, A. A., CSIZMADIA, G. & MULLER, R. U. 2000. Conjoint Control of Hippocampal Place Cell Firing by Two Visual Stimuli. *The Journal of General Physiology,* 116**,** 191-210.

FENTON, A. A., KAO, H. Y., NEYMOTIN, S. A., OLYPHER, A., VAYNTRUB, Y., LYTTON, W. W. & LUDVIG, N. 2008. Unmasking the CA1 ensemble place code by exposures to small and large environments: more place cells and multiple, irregularly arranged, and expanded place fields in the larger space. *J Neurosci,* 28**,** 11250-62.

FINCH, D. M., NOWLIN, N. L. & BABB, T. L. 1983. Demonstration of axonal projections of neurons in the rat hippocampus and subiculum by intracellular injection of HRP. *Brain Res,* 271**,** 201-16.

FOREMAN, N. & ALTAHA, M. 1991. The development of exploration and spontaneous alternation in hooded rat pups: effects of unusually early eyelid opening. *Dev Psychobiol,* 24**,** 521-37.

FORSTER, E., KALTSCHMIDT, C., DENG, J., CREMER, H., DELLER, T. & FROTSCHER, M. 1998. Lamina-specific cell adhesion on living slices of hippocampus. *Development,* 125**,** 3399-410.

FOX, S. E. & RANCK, J. B., JR. 1975. Localization and anatomical identification of theta and complex spike cells in dorsal hippocampal formation of rats. *Exp Neurol,* 49**,** 299-313.

FREUND, T. F. & ANTAL, M. 1988. GABA-containing neurons in the septum control inhibitory interneurons in the hippocampus. *Nature,* 336**,** 170-3.

FREUND, T. F., GULYAS, A. I., ACSADY, L., GORCS, T. & TOTH, K. 1990. Serotonergic control of the hippocampus via local inhibitory interneurons. *Proc Natl Acad Sci U S A,* 87**,** 8501-5.

FRICKE, R. & COWAN, W. M. 1977. An autoradiographic study of the development of the entorhinal and commissural afferents to the dentate gyrus of the rat. *J Comp Neurol,* 173**,** 231-50.

FROTSCHER, M. 1997. Dual role of Cajal-Retzius cells and reelin in cortical development. *Cell Tissue Res,* 290**,** 315-22.

FROTSCHER, M. 1998. Cajal-Retzius cells, Reelin, and the formation of layers. *Curr Opin Neurobiol,* 8**,** 570-5.

FUHS, M. C. & TOURETZKY, D. S. 2006. A spin glass model of path integration in rat medial entorhinal cortex. *J Neurosci,* 26**,** 4266-76.

FUNAHASHI, M. & STEWART, M. 1997. Presubicular and parasubicular cortical neurons of the rat: functional separation of deep and superficial neurons in vitro. *J Physiol,* 501 (Pt 2)**,** 387-403.

FURTAK, S. C., MOYER, J. R., JR. & BROWN, T. H. 2007a. Morphology and ontogeny of rat perirhinal cortical neurons. *J Comp Neurol,* 505**,** 493-510.

FURTAK, S. C., WEI, S. M., AGSTER, K. L. & BURWELL, R. D. 2007b. Functional neuroanatomy of the parahippocampal region in the rat: the perirhinal and postrhinal cortices. *Hippocampus,* 17**,** 709-22.

FYHN, M., MOLDEN, S., WITTER, M. P., MOSER, E. I. & MOSER, M. B. 2004. Spatial representation in the entorhinal cortex. *Science,* 305**,** 1258-64.

GAARSKJAER, F. B. 1978. Organization of the mossy fiber system of the rat studied in extended hippocampi. I. Terminal area related to number of granule and pyramidal cells. *J Comp Neurol,* 178**,** 49-72.

GATOME, C. W., SLOMIANKA, L., LIPP, H. P. & AMREIN, I. 2010. Number estimates of neuronal phenotypes in layer II of the medial entorhinal cortex of rat and mouse. *Neuroscience,* 170**,** 156-65.

GERRISH, C. J. & ALBERTS, J. R. 1996. Environmental temperature modulates onset of independent feeding: Warmer is sooner. *Developmental Psychobiology,* 29**,** 483-495.

GIRDEN, E. R. 1992. *ANOVA: Repeated measures,* Newbury Park, CA, Sage.

GLEESON, J. G., LIN, P. T., FLANAGAN, L. A. & WALSH, C. A. 1999. Doublecortin is a microtubule-associated protein and is expressed widely by migrating neurons. *Neuron,* 23**,** 257-271.

GLOVELI, T., DUGLADZE, T., SCHMITZ, D. & HEINEMANN, U. 2001. Properties of entorhinal cortex deep layer neurons projecting to the rat dentate gyrus. *Eur J Neurosci,* 13**,** 413-20.

GOLDING, N. L., JUNG, H. Y., MICKUS, T. & SPRUSTON, N. 1999. Dendritic calcium spike initiation and repolarization are controlled by distinct potassium channel subtypes in CA1 pyramidal neurons. *J Neurosci,* 19**,** 8789-98.

GOLGI, C. 1885. *Sulla fina anatomia degli organi centrali del sistema nervoso*, S. Calderini.

GOLGI, C., BENTIVOGLIO, M. & SWANSON, L. 2001. On the fine structure of the pes Hippocampi major (with plates XIII-XXIII). 1886. *Brain Res Bull,* 54**,** 461-83.

GOODRIDGE, J. P., DUDCHENKO, P. A., WORBOYS, K. A., GOLOB, E. J. & TAUBE, J. S. 1998. Cue control and head direction cells. *Behav Neurosci,* 112**,** 749-61.

GOODRIDGE, J. P. & TAUBE, J. S. 1997. Interaction between the postsubiculum and anterior thalamus in the generation of head direction cell activity. *Journal of Neuroscience,* 17**,** 9315-9330.

GOODWIN, G. A. & YACKO, H. 2004. Emergence of the exploratory motive in rats. *Dev Psychobiol,* 45**,** 34-48.

GRANT, R. A., MITCHINSON, B. & PRESCOTT, T. J. 2012. The development of whisker control in rats in relation to locomotion. *Dev Psychobiol,* 54**,** 151-68.

GRAVES, A. R., MOORE, S. J., BLOSS, E. B., MENSH, B. D., KATH, W. L. & SPRUSTON, N. 2012. Hippocampal Pyramidal Neurons Comprise Two Distinct Cell Types that Are Countermodulated by Metabotropic Receptors. *Neuron,* 76**,** 776-789.

GRAVES, A. R., MOORE, S. J., SPRUSTON, N., TRYBA, A. K. & KACZOROWSKI, C. C. 2016. Brain-derived neurotrophic factor differentially modulates excitability of two classes of hippocampal output neurons. *J Neurophysiol,* 116**,** 466-71.

GREEN, R. J. & STANTON, M. E. 1989. Differential ontogeny of working memory and reference memory in the rat. *Behav Neurosci,* 103**,** 98-105.

GREENE, J. R. & MASON, A. 1996. Neuronal diversity in the subiculum: correlations with the effects of somatostatin on intrinsic properties and on GABA-mediated IPSPs in vitro. *J Neurophysiol,* 76**,** 1657-66.

GREENE, J. R. & TOTTERDELL, S. 1997. Morphology and distribution of electrophysiologically defined classes of pyramidal and nonpyramidal neurons in rat ventral subiculum in vitro. *J Comp Neurol,* 380**,** 395-408.

GREENE, J. R. T., LIN, H., MASON, A. J. R., JOHNSON, L. R. & TOTTERDELL, S. 1997. Differential expression of NADPH-diaphorase between electrophysiologically-defined classes of pyramidal neurons in rat ventral subiculum, in vitro. *Neuroscience,* 80**,** 95-104.

GREENHOUSE, S. W. & GEISSER, S. 1959. On methods in the analysis of profile data. *Psychometrika,* 24**,** 95–112.

GRIESBECK, O., BAIRD, G. S., CAMPBELL, R. E., ZACHARIAS, D. A. & TSIEN, R. Y. 2001. Reducing the Environmental Sensitivity of Yellow Fluorescent Protein: MECHANISM AND APPLICATIONS. *Journal of Biological Chemistry,* 276**,** 29188-29194.

GROENEWEGEN, H. J., DER ZEE, E. V.-V., TE KORTSCHOT, A. & WITTER, M. P. 1987. Organization of the projections from the subiculum to the ventral striatum in the rat. A study using anterograde transport of Phaseolus vulgaris leucoagglutinin. *Neuroscience,* 23**,** 103-120.

GULYAS, A. I. & FREUND, T. F. 1996. Pyramidal cell dendrites are the primary targets of calbindin D28k-immunoreactive interneurons in the hippocampus. *Hippocampus,* 6**,** 525-34.

GULYAS, A. I., GORCS, T. J. & FREUND, T. F. 1990. Innervation of different peptide-containing neurons in the hippocampus by GABAergic septal afferents. *Neuroscience,* 37**,** 31-44.

HABERLY, L. B. & PRICE, J. L. 1978. Association and commissural fiber systems of the olfactory cortex of the rat. *J Comp Neurol,* 178**,** 711-40.

HAFTING, T., FYHN, M., MOLDEN, S., MOSER, M. B. & MOSER, E. I. 2005. Microstructure of a spatial map in the entorhinal cortex. *Nature,* 436**,** 801-6.

HAGLUND, L., SWANSON, L. W. & KOHLER, C. 1984. The projection of the supramammillary nucleus to the hippocampal formation: an immunohistochemical and anterograde transport study with the lectin PHA-L in the rat. *J Comp Neurol,* 229**,** 171-85.

HAMAM, B. N., KENNEDY, T. E., ALONSO, A. & AMARAL, D. G. 2000. Morphological and electrophysiological characteristics of layer V neurons of the rat medial entorhinal cortex. *J Comp Neurol,* 418**,** 457-72.

HAN, Z.-S., BUHL, E. H., LÖRINCZI, Z. & SOMOGYI, P. 1993. A High Degree of Spatial Selectivity in the Axonal and Dendritic Domains of Physiologically Identified Local-circuit Neurons in the Dentate Gyms of the Rat Hippocampus. *European Journal of Neuroscience,* 5**,** 395-410.

HANCOCK, W. W., BECKER, G. J. & ATKINS, R. C. 1982. A Comparison of Fixatives and Immunohistochemical Technics for Use with Monoclonal Antibodies to Cell Surface Antigens. *American Journal of Clinical Pathology,* 78**,** 825-831.

HARDCASTLE, K., GANGULI, S. & GIOCOMO, L. M. 2015. Environmental boundaries as an error correction mechanism for grid cells. *Neuron,* 86**,** 827-39.

HARRIS, E., WITTER, M. P., WEINSTEIN, G. & STEWART, M. 2001a. Intrinsic connectivity of the rat subiculum: I. Dendritic morphology and patterns of axonal arborization by pyramidal neurons. *J Comp Neurol,* 435**,** 490-505.

HARRIS, K. D., HIRASE, H., LEINEKUGEL, X., HENZE, D. A. & BUZSAKI, G. 2001b. Temporal interaction between single spikes and complex spike bursts in hippocampal pyramidal cells. *Neuron,* 32**,** 141-149.

HARTLEY, T., BURGESS, N., LEVER, C., CACUCCI, F. & O'KEEFE, J. 2000. Modeling place fields in terms of the cortical inputs to the hippocampus. *Hippocampus,* 10**,** 369-79.

HAYMAN, R. M., CHAKRABORTY, S., ANDERSON, M. I. & JEFFERY, K. J. 2003. Context-specific acquisition of location discrimination by hippocampal place cells. *Eur J Neurosci,* 18**,** 2825-34.

HAZLETT, J. C., JR. & FARKAS, N. 1978. Short axon molecular layer neurons in the opossum fascia dentata: a Golgi study. *Brain Res,* 143**,** 355-60.

HENZE, D. A., BORHEGYI, Z., CSICSVARI, J., MAMIYA, A., HARRIS, K. D. & BUZSAKI, G. 2000. Intracellular features predicted by extracellular recordings in the hippocampus in vivo. *J Neurophysiol,* 84**,** 390-400.

HERKENHAM, M. 1978. The connections of the nucleus reuniens thalami: evidence for a direct thalamo-hippocampal pathway in the rat. *J Comp Neurol,* 177**,** 589-610.

HETHERINGTON, P. A. & SHAPIRO, M. L. 1997. Hippocampal place fields are altered by the removal of single visual cues in a distance-dependent manner. *Behav Neurosci,* 111**,** 20-34.

HIROTSUNE, S., TAKAHARA, T., SASAKI, N., HIROSE, K., YOSHIKI, A., OHASHI, T., KUSAKABE, M., MURAKAMI, Y., MURAMATSU, M., WATANABE, S., NAKAO, K., KATSUKI, M. & HAYASHIZAKI, Y. 1995. The reeler gene encodes a protein with an EGF-like motif expressed by pioneer neurons. *Nat Genet,* 10**,** 77-83.

HJORTH-SIMONSEN, A. & JEUNE, B. 1972. Origin and termination of the hippocampal perforant path in the rat studied by silver impregnation. *J Comp Neurol,* 144**,** 215-32.

HOLLUP, S. A., MOLDEN, S., DONNETT, J. G., MOSER, M. B. & MOSER, E. I. 2001. Accumulation of hippocampal place fields at the goal location in an annular watermaze task. *Journal of Neuroscience,* 21**,** 1635-1644.

HONDA, Y., FURUTA, T., KANEKO, T., SHIBATA, H. & SASAKI, H. 2011. Patterns of axonal collateralization of single layer V cortical projection neurons in the rat presubiculum. *J Comp Neurol,* 519**,** 1395-412.

HONDA, Y. & ISHIZUKA, N. 2004. Organization of connectivity of the rat presubiculum: I. Efferent projections to the medial entorhinal cortex. *J Comp Neurol,* 473**,** 463-84.

HUNSAKER, M. R. & KESNER, R. P. 2013. The operation of pattern separation and pattern completion processes associated with different attributes or domains of memory. *Neurosci Biobehav Rev,* 37**,** 36-58.

HUXTER, J., BURGESS, N. & O'KEEFE, J. 2003. Independent rate and temporal coding in hippocampal pyramidal cells. *Nature,* 425**,** 828-32.

HUYNH, H. & FELDT, L. S. 1976. Estimation of the Box correction for degrees of freedom from sample data in randomised block and split-plot designs. *Journal of Educational Statistics,* 1**,** 69-82.

INSAUSTI, R., HERRERO, M. T. & WITTER, M. P. 1997. Entorhinal cortex of the rat: cytoarchitectonic subdivisions and the origin and distribution of cortical efferents. *Hippocampus,* 7**,** 146-83.

ISHIZUKA, N., COWAN, W. M. & AMARAL, D. G. 1995. A quantitative analysis of the dendritic organization of pyramidal cells in the rat hippocampus. *J Comp Neurol,* 362**,** 17-45.

ISHIZUKA, N., WEBER, J. & AMARAL, D. G. 1990. Organization of intrahippocampal projections originating from CA3 pyramidal cells in the rat. *J Comp Neurol,* 295**,** 580-623.

ITO, H. T., ZHANG, S. J., WITTER, M. P., MOSER, E. I. & MOSER, M. B. 2015. A prefrontal-thalamo-hippocampal circuit for goal-directed spatial navigation. *Nature,* 522**,** 50-5.

JACKSON, J., AMILHON, B., GOUTAGNY, R., BOTT, J.-B., MANSEAU, F., KORTLEVEN, C., BRESSLER, S. L. & WILLIAMS, S. 2014. Reversal of theta rhythm flow through intact hippocampal circuits. *Nature Neuroscience,* 17**,** 1362.

JACOB, P.-Y., GORDILLO-SALAS, M., FACCHINI, J., POUCET, B., SAVE, E. & SARGOLINI, F. 2017. Medial entorhinal cortex and medial septum contribute to self-motion-based linear distance estimation. *Brain Structure and Function***,** 1-16.

JANKOWSKI, M. M. & O'MARA, S. M. 2015. Dynamics of place, boundary and object encoding in rat anterior claustrum. *Front Behav Neurosci,* 9**,** 250.

JARSKY, T., MADY, R., KENNEDY, B. & SPRUSTON, N. 2008. Distribution of bursting neurons in the CA1 region and the subiculum of the rat hippocampus. *J Comp Neurol,* 506**,** 535-47.

JAY, T. M., GLOWINSKI, J. & THIERRY, A. M. 1989. Selectivity of the hippocampal projection to the prelimbic area of the prefrontal cortex in the rat. *Brain Res,* 505**,** 337-40.

JAY, T. M. & WITTER, M. P. 1991. Distribution of hippocampal CA1 and subicular efferents in the prefrontal cortex of the rat studied by means of anterograde transport of Phaseolus vulgaris-leucoagglutinin. *J Comp Neurol,* 313**,** 574-86.

JOHNSON, C. T., OLTON, D. S., GAGE, F. H., 3RD & JENKO, P. G. 1977. Damage to hippocampus and hippocampal connections: effects on DRL and spontaneous alternation. *J Comp Physiol Psychol,* 91**,** 508-22.

JONES, M. W. & MCHUGH, T. J. 2011. Updating hippocampal representations: CA2 joins the circuit. *Trends Neurosci,* 34**,** 526-35.

JUNG, H. Y., STAFF, N. P. & SPRUSTON, N. 2001. Action potential bursting in subicular pyramidal neurons is driven by a calcium tail current. *Journal of Neuroscience,* 21**,** 3312-3321.

JUNG, M. W. & MCNAUGHTON, B. L. 1993. Spatial selectivity of unit activity in the hippocampal granular layer. *Hippocampus,* 3**,** 165-82.

JUSTUS, D., DALUGGE, D., BOTHE, S., FUHRMANN, F., HANNES, C., KANEKO, H., FRIEDRICHS, D., SOSULINA, L., SCHWARZ, I., ELLIOTT, D. A., SCHOCH, S., BRADKE, F., SCHWARZ, M. K. & REMY, S. 2017. Glutamatergic synaptic integration of locomotion speed via septoentorhinal projections. *Nat Neurosci,* 20**,** 16-19.

KADIR, S. N., GOODMAN, D. F. & HARRIS, K. D. 2014. High-dimensional cluster analysis with the masked EM algorithm. *Neural Comput,* 26**,** 2379-94.

KARLSSON, K. A., MOHNS, E. J., DI PRISCO, G. V. & BLUMBERG, M. S. 2006. On the co-occurrence of startles and hippocampal sharp waves in newborn rats. *Hippocampus,* 16**,** 959-65.

KEMPERMANN, G., KUHN, H. G. & GAGE, F. H. 1997. More hippocampal neurons in adult mice living in an enriched environment. *Nature,* 386**,** 493-5.

KERR, K. M., AGSTER, K. L., FURTAK, S. C. & BURWELL, R. D. 2007. Functional neuroanatomy of the parahippocampal region: the lateral and medial entorhinal areas. *Hippocampus,* 17**,** 697-708.

KIM, Y. & SPRUSTON, N. 2012. Target-specific output patterns are predicted by the distribution of regular-spiking and bursting pyramidal neurons in the subiculum. *Hippocampus,* 22**,** 693-706.

KIRKBY, R. J., STEIN, D. G., KIMBLE, R. J. & KIMBLE, D. P. 1967. Effects of hippocampal lesions and duration of sensory input on spontaneous alternation. *J Comp Physiol Psychol,* 64**,** 342-5.

KLINK, R. & ALONSO, A. 1997. Morphological characteristics of layer II projection neurons in the rat medial entorhinal cortex. *Hippocampus,* 7**,** 571-83.

KLOOSTERMAN, F., WITTER, M. P. & VAN HAEFTEN, T. 2003. Topographical and laminar organization of subicular projections to the parahippocampal region of the rat. *J Comp Neurol,* 455**,** 156-71.

KNIERIM, J. J. 2002. Dynamic interactions between local surface cues, distal landmarks, and intrinsic circuitry in hippocampal place cells. *Journal of Neuroscience,* 22**,** 6254-6264.

KNIERIM, J. J., KUDRIMOTI, H. S. & MCNAUGHTON, B. L. 1995. Place cells, head direction cells, and the learning of landmark stability. *J Neurosci,* 15**,** 1648-59.

KNIERIM, J. J., NEUNUEBEL, J. P. & DESHMUKH, S. S. 2014. Functional correlates of the lateral and medial entorhinal cortex: objects, path integration and local-global reference frames. *Philos Trans R Soc Lond B Biol Sci,* 369**,** 20130369.

KOENIG, J., LINDER, A. N., LEUTGEB, J. K. & LEUTGEB, S. 2011. The spatial periodicity of grid cells is not sustained during reduced theta oscillations. *Science,* 332**,** 592-5.

KOHARA, K., PIGNATELLI, M., RIVEST, A. J., JUNG, H. Y., KITAMURA, T., SUH, J., FRANK, D., KAJIKAWA, K., MISE, N., OBATA, Y., WICKERSHAM, I. R. & TONEGAWA, S. 2014. Cell type-specific genetic and optogenetic tools reveal hippocampal CA2 circuits. *Nat Neurosci,* 17**,** 269-79.

KOHLER, C. 1986. Intrinsic connections of the retrohippocampal region in the rat brain. II. The medial entorhinal area. *J Comp Neurol,* 246**,** 149-69.

KOHLER, C. 1988. Intrinsic connections of the retrohippocampal region in the rat brain: III. The lateral entorhinal area. *J Comp Neurol,* 271**,** 208-28.

KÖHLER, C. 1985. Intrinsic projections of the retrohippocampal region in the rat brain. I. The subicular complex. *J Comp Neurol,* 236**,** 504-22.

KÖHLER, C., CHAN-PALAY, V. & STEINBUSCH, H. 1981. The distribution and orientation of serotonin fibers in the entorhinal and other retrohippocampal areas. *Anatomy and Embryology,* 161**,** 237-264.

KOHLER, C., CHAN-PALAY, V. & WU, J. Y. 1984. Septal neurons containing glutamic acid decarboxylase immunoreactivity project to the hippocampal region in the rat brain. *Anat Embryol (Berl),* 169**,** 41-4.

KOSEL, K. C., VAN HOESEN, G. W. & WEST, J. R. 1981. Olfactory bulb projections to the parahippocampal area of the rat. *J Comp Neurol,* 198**,** 467-82.

KRETTEK, J. E. & PRICE, J. L. 1977. The cortical projections of the mediodorsal nucleus and adjacent thalamic nuclei in the rat. *J Comp Neurol,* 171**,** 157-91.

KROPFF, E., CARMICHAEL, J. E., MOSER, M. B. & MOSER, E. I. 2015. Speed cells in the medial entorhinal cortex. *Nature,* 523**,** 419-24.

KRUPIC, J., BAUZA, M., BURTON, S., BARRY, C. & O'KEEFE, J. 2015. Grid cell symmetry is shaped by environmental geometry. *Nature,* 518**,** 232-5.

LACAILLE, J. C., MUELLER, A. L., KUNKEL, D. D. & SCHWARTZKROIN, P. A. 1987. Local Circuit Interactions between Oriens-Alveus Interneurons and Ca1 Pyramidal Cells in Hippocampal Slices - Electrophysiology and Morphology. *Journal of Neuroscience,* 7**,** 1979-1993.

LANDERS, M. & PHILIP ZEIGLER, H. 2006. Development of rodent whisking: trigeminal input and central pattern generation. *Somatosens Mot Res,* 23**,** 1-10.

LANG, U. & FROTSCHER, M. 1990. Postnatal development of nonpyramidal neurons in the rat hippocampus (areas CA1 and CA3): a combined Golgi/electron microscope study. *Anat Embryol (Berl),* 181**,** 533-45.

LANGSTON, R. F., AINGE, J. A., COUEY, J. J., CANTO, C. B., BJERKNES, T. L., WITTER, M. P., MOSER, E. I. & MOSER, M. B. 2010. Development of the spatial representation system in the rat. *Science,* 328**,** 1576-80.

LANNOU, J., PRECHT, W. & CAZIN, L. 1979. The postnatal development of functional properties of central vestibular neurons in the rat. *Brain Research,* 175**,** 219-232.

LAWSON, V. H. & BLAND, B. H. 1993. The role of the septohippocampal pathway in the regulation of hippocampal field activity and behavior: analysis by the intraseptal microinfusion of carbachol, atropine, and procaine. *Exp Neurol,* 120**,** 132-44.

LEBLANC, M. O. & BLAND, B. H. 1979. Developmental aspects of hippocampal electrical activity and motor behavior in the rat. *Exp Neurol,* 66**,** 220-37.

LEIN, E. S., CALLAWAY, E. M., ALBRIGHT, T. D. & GAGE, F. H. 2005. Redefining the boundaries of the hippocampal CA2 subfield in the mouse using gene expression and 3-dimensional reconstruction. *J Comp Neurol,* 485**,** 1-10.

LEINEKUGEL, X., KHAZIPOV, R., CANNON, R., HIRASE, H., BEN-ARI, Y. & BUZSAKI, G. 2002. Correlated bursts of activity in the neonatal hippocampus in vivo. *Science,* 296**,** 2049-52.

LEUTGEB, J. K., LEUTGEB, S., MOSER, M. B. & MOSER, E. I. 2007. Pattern separation in the dentate gyrus and CA3 of the hippocampus. *Science,* 315**,** 961-6.

LEUTGEB, S. & LEUTGEB, J. K. 2007. Pattern separation, pattern completion, and new neuronal codes within a continuous CA3 map. *Learn Mem,* 14**,** 745-57.

LEUTGEB, S., LEUTGEB, J. K., BARNES, C. A., MOSER, E. I., MCNAUGHTON, B. L. & MOSER, M. B. 2005. Independent codes for spatial and episodic memory in hippocampal neuronal ensembles. *Science,* 309**,** 619-23.

LEVER, C., BURTON, S., JEEWAJEE, A., O'KEEFE, J. & BURGESS, N. 2009. Boundary vector cells in the subiculum of the hippocampal formation. *J Neurosci,* 29**,** 9771-7.

LI, X. G., SOMOGYI, P., YLINEN, A. & BUZSAKI, G. 1994. The hippocampal CA3 network: an in vivo intracellular labeling study. *J Comp Neurol,* 339**,** 181-208.

LINGENHOHL, K. & FINCH, D. M. 1991. Morphological characterization of rat entorhinal neurons in vivo: soma-dendritic structure and axonal domains. *Exp Brain Res,* 84**,** 57-74.

LOEWEN, I., WALLACE, D. G. & WHISHAW, I. Q. 2005. The development of spatial capacity in piloting and dead reckoning by infant rats: use of the huddle as a home base for spatial navigation. *Dev Psychobiol,* 46**,** 350-61.

LORENTE DE NÓ, R. 1934. Studies on the structure of the cerebral cortex. II. Continuation of the study of the ammonic system. *Journal für Psychologie und Neurologie,* 46**,** 113-177.

LOY, R., LYNCH, G. & COTMAN, C. W. 1977. Development of afferent lamination in the fascia dentata of the rat. *Brain Res,* 121**,** 229-43.

MAASWINKEL, H., JARRARD, L. E. & WHISHAW, I. Q. 1999. Hippocampectomized rats are impaired in homing by path integration. *Hippocampus,* 9**,** 553-61.

MAGUIRE, E. A., NANNERY, R. & SPIERS, H. J. 2006. Navigation around London by a taxi driver with bilateral hippocampal lesions. *Brain,* 129**,** 2894-907.

MARIN, O. & RUBENSTEIN, J. L. 2001. A long, remarkable journey: tangential migration in the telencephalon. *Nat Rev Neurosci,* 2**,** 780-90.

MARKUS, E. J., BARNES, C. A., MCNAUGHTON, B. L., GLADDEN, V. L. & SKAGGS, W. E. 1994. Spatial information content and reliability of hippocampal CA1 neurons: effects of visual input. *Hippocampus,* 4**,** 410-21.

MARR, D. 1971. Simple Memory: A Theory for Archicortex. *Philosophical Transactions of the Royal Society of London. B, Biological Sciences,* 262**,** 23-81.

MARTIN, P. D. & BERTHOZ, A. 2002. Development of spatial firing in the hippocampus of young rats. *Hippocampus,* 12**,** 465-480.

MARTINEZ, A., LUBKE, J., DEL RIO, J. A., SORIANO, E. & FROTSCHER, M. 1996. Regional variability and postsynaptic targets of chandelier cells in the hippocampal formation of the rat. *J Comp Neurol,* 376**,** 28-44.

MCNAUGHTON, B. L., BATTAGLIA, F. P., JENSEN, O., MOSER, E. I. & MOSER, M. B. 2006. Path integration and the neural basis of the 'cognitive map'. *Nat Rev Neurosci,* 7**,** 663-78.

MCNAUGHTON, B. L., O'KEEFE, J. & BARNES, C. A. 1983. The Stereotrode - a New Technique for Simultaneous Isolation of Several Single Units in the Central Nervous-System from Multiple Unit Records. *Journal of Neuroscience Methods,* 8**,** 391-397.

MELZER, S., MICHAEL, M., CAPUTI, A., ELIAVA, M., FUCHS, E. C., WHITTINGTON, M. A. & MONYER, H. 2012. Long-range-projecting GABAergic neurons modulate inhibition in hippocampus and entorhinal cortex. *Science,* 335**,** 1506-10.

MERRILL, E. G. & AINSWORTH, A. 1972. Glass-coated platinum-plated tungsten microelectrodes. *Med Biol Eng,* 10**,** 662-72.

MIAO, C., CAO, Q., ITO, H. T., YAMAHACHI, H., WITTER, M. P., MOSER, M. B. & MOSER, E. I. 2015. Hippocampal Remapping after Partial Inactivation of the Medial Entorhinal Cortex. *Neuron,* 88**,** 590-603.

MIETTINEN, M., PITKANEN, A. & MIETTINEN, R. 1997. Distribution of calretinin-immunoreactivity in the rat entorhinal cortex: coexistence with GABA. *J Comp Neurol,* 378**,** 363-78.

MILNER, B. & PENFIELD, W. 1955. The effect of hippocampal lesions on recent memory. *Trans Am Neurol Assoc***,** 42-8.

MITCHELL, S. J. & RANCK JR, J. B. 1980. Generation of theta rhythm in medial entorhinal cortex of freely moving rats. *Brain Research,* 189**,** 49-66.

MITTELSTAEDT, H. & MITTELSTAEDT, M. L. 1982. Homing by Path Integration. *In:* PAPI, F. & WALLRAFF, H. G. (eds.) *Avian Navigation: International Symposium on Avian Navigation (ISAN) held at Tirrenia (Pisa), September 11–14, 1981.* Berlin, Heidelberg: Springer Berlin Heidelberg.

MOHNS, E. J., KARLSSON, K. A. & BLUMBERG, M. S. 2007. Developmental emergence of transient and persistent hippocampal events and oscillations and their association with infant seizure susceptibility. *Eur J Neurosci,* 26**,** 2719-30.

MOITA, M. A., ROSIS, S., ZHOU, Y., LEDOUX, J. E. & BLAIR, H. T. 2004. Putting fear in its place: remapping of hippocampal place cells during fear conditioning. *J Neurosci,* 24**,** 7015-23.

MORRIS, R. G., GARRUD, P., RAWLINS, J. N. & O'KEEFE, J. 1982. Place navigation impaired in rats with hippocampal lesions. *Nature,* 297**,** 681-3.

MORRIS, R. G. M. 1981. Spatial localization does not require the presence of local cues. *Learning and Motivation,* 12**,** 239-260.

MOSER, E. I., KROPFF, E. & MOSER, M. B. 2008. Place cells, grid cells, and the brain's spatial representation system. *Annu Rev Neurosci,* 31**,** 69-89.

MOSER, E. I. & MOSER, M. B. 2008. A metric for space. *Hippocampus,* 18**,** 1142-56.

MOSER, M. B., ROWLAND, D. C. & MOSER, E. I. 2015. Place cells, grid cells, and memory. *Cold Spring Harb Perspect Biol,* 7**,** a021808.

MOSKO, S., LYNCH, G. & COTMAN, C. W. 1973. The distribution of septal projections to the hippocampus of the rat. *J Comp Neurol,* 152**,** 163-74.

MOYE, T. B. & RUDY, J. W. 1985. Ontogenesis of learning: VI. Learned and unlearned responses to visual stimulation in the infant hooded rat. *Dev Psychobiol,* 18**,** 395-409.

MUESSIG, L. 2013. *Sensory integration in the hippocampal formation of pre- and post-weanling rats.* Doctor of Philosophy, UCL.

MUESSIG, L., HAUSER, J., WILLS, T. J. & CACUCCI, F. 2015. A Developmental Switch in Place Cell Accuracy Coincides with Grid Cell Maturation. *Neuron,* 86**,** 1167-73.

MUESSIG, L., HAUSER, J., WILLS, T. J. & CACUCCI, F. 2016. Place Cell Networks in Pre-weanling Rats Show Associative Memory Properties from the Onset of Exploratory Behavior. *Cerebral Cortex,* 26**,** 3627-3636.

MULLER, R. 1996. A quarter of a century of place cells. *Neuron,* 17**,** 813-22.

MULLER, R. & KUBIE, J. 1987. The effects of changes in the environment on the spatial firing of hippocampal complex-spike cells. *The Journal of Neuroscience,* 7**,** 1951-1968.

MULLER, R. U., BOSTOCK, E., TAUBE, J. S. & KUBIE, J. L. 1994. On the directional firing properties of hippocampal place cells. *J Neurosci,* 14**,** 7235-51.

MULLER, R. U., KUBIE, J. L. & RANCK, J. B., JR. 1987. Spatial firing patterns of hippocampal complex-spike cells in a fixed environment. *J Neurosci,* 7**,** 1935-50.

MUMBY, D. G., GASKIN, S., GLENN, M. J., SCHRAMEK, T. E. & LEHMANN, H. 2002. Hippocampal damage and exploratory preferences in rats: memory for objects, places, and contexts. *Learn Mem,* 9**,** 49-57.

NABER, P. A., DA SILVA, F. H. L. & WITTER, M. P. 2001. Reciprocal connections between the entorhinal cortex and hippocampal fields CA1 and the subiculum are in register with the projections from CA1 to the subiculum. *Hippocampus,* 11**,** 99-104.

NABER, P. A. & WITTER, M. P. 1998. Subicular efferents are organized mostly as parallel projections: A double-labeling, retrograde-tracing study in the rat. *The Journal of Comparative Neurology,* 393**,** 284-297.

NABER, P. A., WITTER, M. P. & DA SILVA, F. H. L. 1999. Perirhinal cortex input to the hippocampus in the rat: evidence for parallel pathways, both direct and indirect. A combined physiological and anatomical study. *European Journal of Neuroscience,* 11**,** 4119-4133.

NABER, P. A., WITTER, M. P. & LOPES DA SILVA, F. H. 2000. Networks of the Hippocampal Memory System of the Rat: The Pivotal Role of the Subiculuma. *Annals of the New York Academy of Sciences,* 911**,** 392-403.

NACHER, J., CRESPO, C. & MCEWEN, B. S. 2001. Doublecortin expression in the adult rat telencephalon. *Eur J Neurosci,* 14**,** 629-44.

NAFSTAD, P. H. J. 1967. An electron microscope study on the termination of the perforant path fibres in the hippocampus and the fascia dentata. *Zeitschrift für Zellforschung und Mikroskopische Anatomie,* 76**,** 532-542.

NYAKAS, C., LUITEN, P. G., SPENCER, D. G. & TRABER, J. 1987. Detailed projection patterns of septal and diagonal band efferents to the hippocampus in the rat with emphasis on innervation of CA1 and dentate gyrus. *Brain Res Bull,* 18**,** 533-45.

O'KEEFE, J. 1976. Place units in the hippocampus of the freely moving rat. *Exp Neurol,* 51**,** 78-109.

O'KEEFE, J. & BURGESS, N. 1996. Geometric determinants of the place fields of hippocampal neurons. *Nature,* 381**,** 425-8.

O'KEEFE, J. & BURGESS, N. 2005. Dual phase and rate coding in hippocampal place cells: theoretical significance and relationship to entorhinal grid cells. *Hippocampus,* 15**,** 853-66.

O'KEEFE, J. & CONWAY, D. H. 1978. Hippocampal place units in the freely moving rat: Why they fire where they fire. *Experimental Brain Research,* 31**,** 573-590.

O'KEEFE, J. & DOSTROVSKY, J. 1971. The hippocampus as a spatial map. Preliminary evidence from unit activity in the freely-moving rat. *Brain Research,* 34**,** 171-175.

O'KEEFE, J. & NADEL, L. 1978. *The Hippocampus as a Cognitive Map*, Oxford University Press.

O'KEEFE, J., NADEL, L., KEIGHTLEY, S. & KILL, D. 1975. Fornix lesions selectively abolish place learning in the rat. *Exp Neurol,* 48**,** 152-66.

O'KEEFE, J. & RECCE, M. L. 1993. Phase relationship between hippocampal place units and the EEG theta rhythm. *Hippocampus,* 3**,** 317-30.

O'MARA, S. M., COMMINS, S., ANDERSON, M. & GIGG, J. 2001. The subiculum: a review of form, physiology and function. *Prog Neurobiol,* 64**,** 129-55.

O'REILLY, K. C., GULDEN DAHL, A., ULSAKER KRUGE, I. & WITTER, M. P. 2013. Subicular-parahippocampal projections revisited: development of a complex topography in the rat. *J Comp Neurol,* 521**,** 4284-99.

OLIVA, A., FERNANDEZ-RUIZ, A., BUZSAKI, G. & BERENYI, A. 2016. Role of Hippocampal CA2 Region in Triggering Sharp-Wave Ripples. *Neuron,* 91**,** 1342-55.

OLSEN, G. M., OHARA, S., IIJIMA, T. & WITTER, M. P. 2017. Parahippocampal and retrosplenial connections of rat posterior parietal cortex. *Hippocampus,* 27**,** 335-358.

OLTON, D. S. 1979. Mazes, maps, and memory. *Am Psychol,* 34**,** 583-96.

OLTON, D. S. & FEUSTLE, W. A. 1981. Hippocampal function required for nonspatial working memory. *Exp Brain Res,* 41**,** 380-9.

OVERINGTON, D. 2017. *Resolution of spatial ambiguity by the hippocampal place system.* PhD, University College London.

PAXINOS, G. & WATSON, C. 2006. *The rat brain in stereotaxic coordinates,* San Diego, Academic Press.

PEREZ-ESCOBAR, J. A., KORNIENKO, O., LATUSKE, P., KOHLER, L. & ALLEN, K. 2016. Visual landmarks sharpen grid cell metric and confer context specificity to neurons of the medial entorhinal cortex. *Elife,* 5.

PICKEL, V. M., SEGAL, M. & BLOOM, F. E. 1974. A radioautographic study of the efferent pathways of the nucleus locus coeruleus. *J Comp Neurol,* 155**,** 15-42.

PIKKARAINEN, M., RONKKO, S., SAVANDER, V., INSAUSTI, R. & PITKANEN, A. 1999. Projections from the lateral, basal, and accessory basal nuclei of the amygdala to the hippocampal formation in rat. *J Comp Neurol,* 403**,** 229-60.

PITKANEN, A., PIKKARAINEN, M., NURMINEN, N. & YLINEN, A. 2000. Reciprocal connections between the amygdala and the hippocampal formation, perirhinal cortex, and postrhinal cortex in rat - A review. *Parahippocampal Region,* 911**,** 369-391.

PLEASURE, S. J., ANDERSON, S., HEVNER, R., BAGRI, A., MARIN, O., LOWENSTEIN, D. H. & RUBENSTEIN, J. L. R. 2000. Cell migration from the ganglionic eminences is required for the development of hippocampal GABAergic interneurons. *Neuron,* 28**,** 727-740.

POKORNÝ, J. & YAMAMOTO, T. 1981. Postnatal ontogenesis of hippocampal CA1 area in rats. I. Development of dendritic arborisation in pyramidal neurons. *Brain Research Bulletin,* 7**,** 113-120.

PREVOST, F., LEPORE, F. & GUILLEMOT, J. P. 2010. Cortical development of the visual system of the rat. *Neuroreport,* 21**,** 50-4.

QUIRK, G., MULLER, R. & KUBIE, J. 1990. The firing of hippocampal place cells in the dark depends on the rat's recent experience. *The Journal of Neuroscience,* 10**,** 2008-2017.

QUIRK, G., MULLER, R., KUBIE, J. & RANCK, J. 1992. The positional firing properties of medial entorhinal neurons: description and comparison with hippocampal place cells. *The Journal of Neuroscience,* 12**,** 1945-1963.

RAMÓN Y CAJAL, S. 1893. *Estructura del asta de ammon y fascia dentata*, tip. de Fortanet.

RAMÓN Y CAJAL, S. 1909. Histologie du Systeme Nerveux de l'Homme et des Vertebres Maloine. Paris.

RANCK, J. B. 1973. Studies on single neurons in dorsal hippocampal formation and septum in unrestrained rats. *Experimental Neurology,* 41**,** 462-531.

RANCK JR, J. Head direction cells in the deep cell layer of dorsal presubiculum in freely moving rats. Soc Neurosci Abstr, 1984.

RECCE, M. & O'KEEFE, J. The tetrode: a new technique for multi-unit extracellular recording. Soc. Neurosci. Abstr., 1989. 1250.

RENAUDINEAU, S., POUCET, B. & SAVE, E. 2007. Flexible use of proximal objects and distal cues by hippocampal place cells. *Hippocampus,* 17**,** 381-95.

RIBAK, C. E. & SERESS, L. 1983. Five types of basket cell in the hippocampal dentate gyrus: a combined Golgi and electron microscopic study. *J Neurocytol,* 12**,** 577-97.

RIBAK, C. E. & SHAPIRO, L. A. 2007. Ultrastructure and synaptic connectivity of cell types in the adult rat dentate gyrus. *In:* HELEN, E. S. (ed.) *Progress in Brain Research.* Elsevier.

RIEDEL, G., MICHEAU, J., LAM, A. G., ROLOFF, E. L., MARTIN, S. J., BRIDGE, H., DE HOZ, L., POESCHEL, B., MCCULLOCH, J. & MORRIS, R. G. 1999. Reversible neural inactivation reveals hippocampal participation in several memory processes. *Nat Neurosci,* 2**,** 898-905.

ROLLS, E. T. 1996. A theory of hippocampal function in memory. *Hippocampus,* 6**,** 601-20.

ROUTTENBERG, A., STROP, M. & JERDAN, J. 1978. Response of the infant rat to light prior to eyelid opening: mediation by the superior colliculus. *Dev Psychobiol,* 11**,** 469-78.

RUDY, J. W. & CHEATLE, M. D. 1977. Odor-aversion learning in neonatal rats. *Science,* 198**,** 845-6.

RUDY, J. W. & HYSON, R. L. 1984. Ontogenesis of learning: III. Variation in the rat's differential reflexive and learned responses to sound frequencies. *Dev Psychobiol,* 17**,** 285-300.

RUDY, J. W., STADLER-MORRIS, S. & ALBERT, P. 1987. Ontogeny of spatial navigation behaviors in the rat: dissociation of "proximal"- and "distal"-cue-based behaviors. *Behav Neurosci,* 101**,** 62-73.

RUTH, R. E., COLLIER, T. J. & ROUTTENBERG, A. 1982. Topography between the entorhinal cortex and the dentate septotemporal axis in rats: I. Medial and intermediate entorhinal projecting cells. *J Comp Neurol,* 209**,** 69-78.

RUTH, R. E., COLLIER, T. J. & ROUTTENBERG, A. 1988. Topographical relationship between the entorhinal cortex and the septotemporal axis of the dentate gyrus in rats: II. Cells projecting from lateral entorhinal subdivisions. *J Comp Neurol,* 270**,** 506-16.

SARGOLINI, F., FYHN, M., HAFTING, T., MCNAUGHTON, B. L., WITTER, M. P., MOSER, M. B. & MOSER, E. I. 2006. Conjunctive representation of position, direction, and velocity in entorhinal cortex. *Science,* 312**,** 758-62.

SAVE, E., NERAD, L. & POUCET, B. 2000. Contribution of multiple sensory information to place field stability in hippocampal place cells. *Hippocampus,* 10**,** 64-76.

SAVELLI, F., YOGANARASIMHA, D. & KNIERIM, J. J. 2008. Influence of boundary removal on the spatial representations of the medial entorhinal cortex. *Hippocampus,* 18**,** 1270-82.

SCHENK, F. 1985. Development of place navigation in rats from weaning to puberty. *Behav Neural Biol,* 43**,** 69-85.

SCHMIDT-HIEBER, C. & HAUSSER, M. 2013. Cellular mechanisms of spatial navigation in the medial entorhinal cortex. *Nat Neurosci,* 16**,** 325-31.

SCOTT, R. C., RICHARD, G. R., HOLMES, G. L. & LENCK-SANTINI, P.-P. 2011. Maturational dynamics of hippocampal place cells in immature rats. *Hippocampus,* 21**,** 347-353.

SCOVILLE, W. B. & MILNER, B. 1957. Loss of recent memory after bilateral hippocampal lesions. *J Neurol Neurosurg Psychiatry,* 20**,** 11-21.

SEKI, M. & ZYO, K. 1984. Anterior thalamic afferents from the mamillary body and the limbic cortex in the rat. *J Comp Neurol,* 229**,** 242-56.

SERESS, L. 1977. The postnatal development of rat dentate gyrus and the effect of early thyroid hormone treatment. *Anatomy and Embryology,* 151**,** 335-339.

SHARP, P. E. 2006. Subicular place cells generate the same "map" for different environments: comparison with hippocampal cells. *Behav Brain Res,* 174**,** 206-14.

SHARP, P. E. & GREEN, C. 1994. Spatial Correlates of Firing Patterns of Single Cells in the Subiculum of the Freely Moving Rat. *Journal of Neuroscience,* 14**,** 2339-2356.

SHARP, P. E., TINKELMAN, A. & CHO, J. 2001. Angular velocity and head direction signals recorded from the dorsal tegmental nucleus of gudden in the rat: implications for path integration in the head direction cell circuit. *Behavioral neuroscience,* 115**,** 571-588.

SHIBATA, H. 1989. Descending projections to the mammillary nuclei in the rat, as studied by retrograde and anterograde transport of wheat germ agglutinin-horseradish peroxidase. *J Comp Neurol,* 285**,** 436-52.

SHIBATA, H. 1993. Direct projections from the anterior thalamic nuclei to the retrohippocampal region in the rat. *J Comp Neurol,* 337**,** 431-45.

SHINDER, M. E. & TAUBE, J. S. 2011. Active and passive movement are encoded equally by head direction cells in the anterodorsal thalamus. *J Neurophysiol,* 106**,** 788-800.

SILLS, J. B., CONNORS, B. W. & BURWELL, R. D. 2012. Electrophysiological and morphological properties of neurons in layer 5 of the rat postrhinal cortex. *Hippocampus,* 22**,** 1912-22.

SKAGGS, W., MCNAUGHTON, B., GOTHARD, K. & MARKUS, E. An information-theoretic approach to deciphering the hippocampal code. Advances in neural information processing systems, 1993. 1030-1037.

SKAGGS, W. E. & MCNAUGHTON, B. L. 1998. Spatial firing properties of hippocampal CA1 populations in an environment containing two visually identical regions. *J Neurosci,* 18**,** 8455-66.

SKUTELLA, T. & NITSCH, R. 2001. New molecules for hippocampal development. *Trends Neurosci,* 24**,** 107-13.

SŁAWIŃSKA, U. & KASICKI, S. 1998. The frequency of rat's hippocampal theta rhythm is related to the speed of locomotion. *Brain Research,* 796**,** 327-331.

SOLSTAD, T., BOCCARA, C. N., KROPFF, E., MOSER, M. B. & MOSER, E. I. 2008. Representation of geometric borders in the entorhinal cortex. *Science,* 322**,** 1865-8.

SOLSTAD, T., MOSER, E. I. & EINEVOLL, G. T. 2006. From grid cells to place cells: a mathematical model. *Hippocampus,* 16**,** 1026-31.

SOMOGYI, P. & KLAUSBERGER, T. 2005. Defined types of cortical interneurone structure space and spike timing in the hippocampus. *J Physiol,* 562**,** 9-26.

STACKMAN, R. W., CLARK, A. S. & TAUBE, J. S. 2002. Hippocampal spatial representations require vestibular input. *Hippocampus,* 12**,** 291-303.

STACKMAN, R. W., GOLOB, E. J., BASSETT, J. P. & TAUBE, J. S. 2003. Passive transport disrupts directional path integration by rat head direction cells. *J Neurophysiol,* 90**,** 2862-74.

STACKMAN, R. W. & TAUBE, J. S. 1998. Firing properties of rat lateral mammillary single units: head direction, head pitch, and angular head velocity. *J Neurosci,* 18**,** 9020-37.

STANFIELD, B. B. & COWAN, W. M. 1979. The development of the hippocampus and dentate gyrus in normal and reeler mice. *J Comp Neurol,* 185**,** 423-59.

STENSOLA, H., STENSOLA, T., SOLSTAD, T., FROLAND, K., MOSER, M. B. & MOSER, E. I. 2012. The entorhinal grid map is discretized. *Nature,* 492**,** 72-8.

STENSOLA, T., STENSOLA, H., MOSER, M. B. & MOSER, E. I. 2015. Shearing-induced asymmetry in entorhinal grid cells. *Nature,* 518**,** 207-12.

STEPHAN, H. 1975. Allocortex. Handbuch der mikroskopischen Anatomie des Menschen. Vol. IV/9. Berlin: Springer.

STEWARD, O. & SCOVILLE, S. A. 1976. Cells of origin of entorhinal cortical afferents to the hippocampus and fascia dentata of the rat. *J Comp Neurol,* 169**,** 347-70.

STEWART, S., JEEWAJEE, A., WILLS, T. J., BURGESS, N. & LEVER, C. 2014. Boundary coding in the rat subiculum. *Philos Trans R Soc Lond B Biol Sci,* 369**,** 20120514.

SUGAR, J. & WITTER, M. P. 2016. Postnatal development of retrosplenial projections to the parahippocampal region of the rat. *Elife,* 5**,** e13925.

SUN, Y., NGUYEN, A. Q., NGUYEN, J. P., LE, L., SAUR, D., CHOI, J., CALLAWAY, E. M. & XU, X. 2014. Cell-type-specific circuit connectivity of hippocampal CA1 revealed through Cre-dependent rabies tracing. *Cell Rep,* 7**,** 269-80.

SUN, Y., NITZ, D. A., HOLMES, T. C. & XU, X. 2018. Opposing and Complementary Topographic Connectivity Gradients Revealed by Quantitative Analysis of Canonical and Noncanonical Hippocampal CA1 Inputs. *eNeuro,* 5**,** ENEURO.0322-17.2018.

SUPER, H., MARTINEZ, A., DEL RIO, J. A. & SORIANO, E. 1998. Involvement of distinct pioneer neurons in the formation of layer-specific connections in the hippocampus. *J Neurosci,* 18**,** 4616-26.

SUPER, H. & SORIANO, E. 1994. The organization of the embryonic and early postnatal murine hippocampus. II. Development of entorhinal, commissural, and septal connections studied with the lipophilic tracer DiI. *J Comp Neurol,* 344**,** 101-20.

SWANSON, L. & COWAN, W. 1975. Hippocampo-hypothalamic connections: origin in subicular cortex, not ammon's horn. *Science,* 189**,** 303-304.

SWANSON, L., SAWCHENKO, P. & COWAN, W. 1980. Evidence that the commissural, associational and septal projections of the regio inferior of the hippocampus arise from the same neurons. *Brain research,* 197**,** 207-212.

SWANSON, L. W. 1981. A direct projection from Ammon's horn to prefrontal cortex in the rat. *Brain Research,* 217**,** 150-154.

SWANSON, L. W. & COWAN, W. M. 1977. An autoradiographic study of the organization of the efferet connections of the hippocampal formation in the rat. *The Journal of Comparative Neurology,* 172**,** 49-84.

SWANSON, L. W., WYSS, J. M. & COWAN, W. M. 1978. An autoradiographic study of the organization of intrahippocampal association pathways in the rat. *The Journal of Comparative Neurology,* 181**,** 681-715.

TAHVILDARI, B. & ALONSO, A. 2005. Morphological and electrophysiological properties of lateral entorhinal cortex layers II and III principal neurons. *J Comp Neurol,* 491**,** 123-40.

TAMAMAKI, N. & NOJYO, Y. 1993. Projection of the entorhinal layer II neurons in the rat as revealed by intracellular pressure-injection of neurobiotin. *Hippocampus,* 3**,** 471-80.

TAN, H. M., BASSETT, J. P., O'KEEFE, J., CACUCCI, F. & WILLS, T. J. 2015. The development of the head direction system before eye opening in the rat. *Curr Biol,* 25**,** 479-83.

TAUBE, J. 1995. Head direction cells recorded in the anterior thalamic nuclei of freely moving rats. *The Journal of Neuroscience,* 15**,** 70-86.

TAUBE, J. S. 1993. Electrophysiological properties of neurons in the rat subiculum in vitro. *Exp Brain Res,* 96**,** 304-18.

TAUBE, J. S. 2007. The head direction signal: origins and sensory-motor integration. *Annu Rev Neurosci,* 30**,** 181-207.

TAUBE, J. S., MULLER, R. U. & RANCK, J. B. 1990a. Head-Direction Cells Recorded from the Postsubiculum in Freely Moving Rats .1. Description and Quantitative-Analysis. *Journal of Neuroscience,* 10**,** 420-435.

TAUBE, J. S., MULLER, R. U. & RANCK, J. B. 1990b. Head-Direction Cells Recorded from the Postsubiculum in Freely Moving Rats .2. Effects of Environmental Manipulations. *Journal of Neuroscience,* 10**,** 436-447.

THIELS, E., ALBERTS, J. R. & CRAMER, C. P. 1990. Weaning in rats: II. Pup behavior patterns. *Dev Psychobiol,* 23**,** 495-510.

TOLMAN, E. C. 1948. Cognitive maps in rats and men. *Psychol Rev,* 55**,** 189-208.

TOLMAN, E. C. & HONZIK, C. H. 1930. Degrees of hunger, reward and non-reward, and maze learning in rats. *University of California Publications in Psychology,* 4**,** 241-256.

TOLMAN, E. C., RITCHIE, B. F. & KALISH, D. 1946a. Studies in spatial learning. II. Place learning versus response learning. *Journal of Experimental Psychology,* 36**,** 221-229.

TOLMAN, E. C., RITCHIE, B. F. & KALISH, D. 1946b. Studies in spatial learning: Orientation and the short-cut. *J Exp Psychol,* 36**,** 13-24.

TÓTH, K. & FREUND, T. F. 1992. Calbindin D28k-containing nonpyramidal cells in the rat hippocampus: Their immunoreactivity for GABA and projection to the medial septum. *Neuroscience,* 49**,** 793-805.

TSANOV, M., CHAH, E., VANN, S. D., REILLY, R. B., ERICHSEN, J. T., AGGLETON, J. P. & O'MARA, S. M. 2011. Theta-modulated head direction cells in the rat anterior thalamus. *J Neurosci,* 31**,** 9489-502.

TSAO, A., MOSER, M. B. & MOSER, E. I. 2013. Traces of experience in the lateral entorhinal cortex. *Curr Biol,* 23**,** 399-405.

ULANOVSKY, N. & MOSS, C. F. 2007. Hippocampal cellular and network activity in freely moving echolocating bats. *Nat Neurosci,* 10**,** 224-33.

UZIEL, A., ROMAND, R. & MAROT, M. 1981. Development of cochlear potentials in rats. *Audiology,* 20**,** 89-100.

VAN CAUTER, T., CAMON, J., ALVERNHE, A., ELDUAYEN, C., SARGOLINI, F. & SAVE, E. 2013. Distinct roles of medial and lateral entorhinal cortex in spatial cognition. *Cereb Cortex,* 23**,** 451-9.

VAN CAUTER, T., POUCET, B. & SAVE, E. 2008. Unstable CA1 place cell representation in rats with entorhinal cortex lesions. *Eur J Neurosci,* 27**,** 1933-46.

VAN GROEN, T. & WYSS, J. M. 1990a. The connections of presubiculum and parasubiculum in the rat. *Brain Res,* 518**,** 227-43.

VAN GROEN, T. & WYSS, J. M. 1990b. Extrinsic projections from area CA1 of the rat hippocampus: olfactory, cortical, subcortical, and bilateral hippocampal formation projections. *J Comp Neurol,* 302**,** 515-28.

VAN GROEN, T. & WYSS, J. M. 1990c. The postsubicular cortex in the rat: characterization of the fourth region of the subicular cortex and its connections. *Brain Res,* 529**,** 165-77.

VAN GROEN, T. & WYSS, J. M. 1995. Projections from the anterodorsal and anteroventral nucleus of the thalamus to the limbic cortex in the rat. *J Comp Neurol,* 358**,** 584-604.

VAN HAEFTEN, T., BAKS-TE-BULTE, L., GOEDE, P. H., WOUTERLOOD, F. G. & WITTER, M. P. 2003. Morphological and numerical analysis of synaptic interactions between neurons in deep and superficial layers of the entorhinal cortex of the rat. *Hippocampus,* 13**,** 943-52.

VAN STRIEN, N. M., CAPPAERT, N. L. & WITTER, M. P. 2009. The anatomy of memory: an interactive overview of the parahippocampal-hippocampal network. *Nat Rev Neurosci,* 10**,** 272-82.

VANDERWOLF, C. H. 1969. Hippocampal electrical activity and voluntary movement in the rat. *Electroencephalography and Clinical Neurophysiology,* 26**,** 407-418.

VERTES, R. P., FORTIN, W. J. & CRANE, A. M. 1999. Projections of the median raphe nucleus in the rat. *The Journal of Comparative Neurology,* 407**,** 555-582.

VERWER, R. W. H., MEIJER, R. J., VAN UUM, H. F. M. & WITTER, M. P. 1997. Collateral projections from the rat hippocampal formation to the lateral and medial prefrontal cortex. *Hippocampus,* 7**,** 397-402.

VOGT, B. A. & MILLER, M. W. 1983. Cortical connections between rat cingulate cortex and visual, motor, and postsubicular cortices. *The Journal of Comparative Neurology,* 216**,** 192-210.

WANG, X.-J. 2009. Attractor Network Models.

WHISHAW, I. Q. & MAASWINKEL, H. 1998. Rats with fimbria-fornix lesions are impaired in path integration: A role for the hippocampus in "sense of direction". *Journal of Neuroscience,* 18**,** 3050-3058.

WHISHAW, I. Q. & TOMIE, J. 1997. Piloting and dead reckoning dissociated by fimbria-fornix lesions in a rat food carrying task. *Behav Brain Res,* 89**,** 87-97.

WHISHAW, I. Q. & VANDERWOLF, C. H. 1973. Hippocampal EEG and behavior: Change in amplitude and frequency of RSA (Theta rhythm) associated with spontaneous and learned movement patterns in rats and cats. *Behavioral Biology,* 8**,** 461-484.

WHITE, T. D., TAN, A. M. & FINCH, D. M. 1990. Functional reciprocal connections of the rat entorhinal cortex and subicular complex with the medial frontal cortex: an in vivo intracellular study. *Brain Research,* 533**,** 95-106.

WILLS, T. J. & CACUCCI, F. 2014. The development of the hippocampal neural representation of space. *Curr Opin Neurobiol,* 24**,** 111-9.

WILLS, T. J., CACUCCI, F., BURGESS, N. & O'KEEFE, J. 2010. Development of the hippocampal cognitive map in preweanling rats. *Science,* 328**,** 1573-6.

WILLS, T. J., LEVER, C., CACUCCI, F., BURGESS, N. & O'KEEFE, J. 2005. Attractor dynamics in the hippocampal representation of the local environment. *Science,* 308**,** 873-6.

WILLS, T. J., MUESSIG, L. & CACUCCI, F. 2014. The development of spatial behaviour and the hippocampal neural representation of space. *Philos Trans R Soc Lond B Biol Sci,* 369**,** 20130409.

WINTER, S. S., CLARK, B. J. & TAUBE, J. S. 2015. Disruption of the head direction cell network impairs the parahippocampal grid cell signal. *Science,* 347**,** 870-4.

WITTER, M. P. 2006. Connections of the subiculum of the rat: topography in relation to columnar and laminar organization. *Behav Brain Res,* 174**,** 251-64.

WITTER, M. P., GROENEWEGEN, H. J., LOPES DA SILVA, F. H. & LOHMAN, A. H. 1989. Functional organization of the extrinsic and intrinsic circuitry of the parahippocampal region. *Prog Neurobiol,* 33**,** 161-253.

WITTER, M. P., NABER, P. A., VAN HAEFTEN, T., MACHIELSEN, W. C., ROMBOUTS, S. A., BARKHOF, F., SCHELTENS, P. & LOPES DA SILVA, F. H. 2000. Cortico-hippocampal communication by way of parallel parahippocampal-subicular pathways. *Hippocampus,* 10**,** 398-410.

WITTER, M. P., OSTENDORF, R. H. & GROENEWEGEN, H. J. 1990. Heterogeneity in the Dorsal Subiculum of the Rat. Distinct Neuronal Zones Project to Different Cortical and Subcortical Targets. *Eur J Neurosci,* 2**,** 718-725.

WONDERS, C. P. & ANDERSON, S. A. 2006. The origin and specification of cortical interneurons. *Nat Rev Neurosci,* 7**,** 687-96.

WOUTERLOOD, F. G., HARTIG, W., BRUCKNER, G. & WITTER, M. P. 1995. Parvalbumin-immunoreactive neurons in the entorhinal cortex of the rat: localization, morphology, connectivity and ultrastructure. *J Neurocytol,* 24**,** 135-53.

WOUTERLOOD, F. G. & POTHUIZEN, H. 2000. Sparse colocalization of somatostatin- and GABA-immunoreactivity in the entorhinal cortex of the rat. *Hippocampus,* 10**,** 77-86.

WOUTERLOOD, F. G., SALDANA, E. & WITTER, M. P. 1990. Projection from the nucleus reuniens thalami to the hippocampal region: light and electron microscopic tracing study in the rat with the anterograde tracer Phaseolus vulgaris-leucoagglutinin. *J Comp Neurol,* 296**,** 179-203.

WRIGHT, N. F., ERICHSEN, J. T., VANN, S. D., O'MARA, S. M. & AGGLETON, J. P. 2010. Parallel but separate inputs from limbic cortices to the mammillary bodies and anterior thalamic nuclei in the rat. *J Comp Neurol,* 518**,** 2334-54.

WYSS, J. M., SWANSON, L. W. & COWAN, W. M. 1979. A study of subcortical afferents to the hippocampal formation in the rat. *Neuroscience,* 4**,** 463-476.

YARTSEV, M. M. & ULANOVSKY, N. 2013. Representation of three-dimensional space in the hippocampus of flying bats. *Science,* 340**,** 367-72.

YASSA, M. A. & STARK, C. E. 2011. Pattern separation in the hippocampus. *Trends Neurosci,* 34**,** 515-25.

YODER, R. M., CLARK, B. J., BROWN, J. E., LAMIA, M. V., VALERIO, S., SHINDER, M. E. & TAUBE, J. S. 2011. Both visual and idiothetic cues contribute to head direction cell stability during navigation along complex routes. *J Neurophysiol,* 105**,** 2989-3001.

ZAR, J. H. 2010. *Biostatistical Analysis*, Prentice Hall.

ZIPP, F., NITSCH, R., SORIANO, E. & FROTSCHER, M. 1989. Entorhinal fibers form synaptic contacts on parvalbumin-immunoreactive neurons in the rat fascia dentata. *Brain Research,* 495**,** 161-166.

ZIV, Y., BURNS, L. D., COCKER, E. D., HAMEL, E. O., GHOSH, K. K., KITCH, L. J., EL GAMAL, A. & SCHNITZER, M. J. 2013. Long-term dynamics of CA1 hippocampal place codes. *Nat Neurosci,* 16**,** 264-6.

ZUCKER, E. & WELKER, W. I. 1969. Coding of somatic sensory input by vibrissae neurons in the rat's trigeminal ganglion. *Brain Res,* 12**,** 138-56.

ZUGARO, M. B., BERTHOZ, A. & WIENER, S. I. 2001. Background, but not foreground, spatial cues are taken as references for head direction responses by rat anterodorsal thalamus neurons. *The Journal of Neuroscience,* 21**,** RC154.